

A Progress Report To "Made available under NASA sponsorship
in the interest of early and wide dis-
semination of Earth Resources Survey
Program information and without liability
for any use made thereof."

NATIONAL AERONAUTICS AND SPACE ADMINISTRATION

Office of University Affairs

Washington, D.C. 20546

7.8-10028
CR-155253

(E78-10028) ON MULTIDISCIPLINARY RESEARCH
ON THE APPLICATION OF REMOTE SENSING TO
WATER RESOURCES PROBLEMS Progress Report,
1976 - 1977 (Wisconsin Univ.) 384 p
HC A17/MF A01

N78-13504

Unclas
00028

CSCS 08H G3/43

On Multidisciplinary Research On The
Application of Remote Sensing To
Water Resources Problems

Original photography may be purchased from:
EROS Data Center

Sioux Falls, SD

ORIGINAL CONTAINS
COLOR ILLUSTRATIONS

Research Funded Under Grant #NGL 50-002-127

et

1976-1977

from

James L. Clapp, Project Leader
Institute for Environmental Studies
The University of Wisconsin
Madison, Wisconsin 53705





INSTITUTE FOR ENVIRONMENTAL STUDIES
Environmental Monitoring and Data Acquisition Group

University of Wisconsin—Madison
1063 WARF Building, 610 Walnut
Madison, Wisconsin 53706
Telephone 608-263-4789

11 November 1977

NASA Scientific and Technical Information Facility
P.O. Box 8757
Baltimore/Washington International Airport
Maryland 21240

Dear Sir or Madam:

Enclosed please find two (2) copies of our 1976-1977 Progress Report for research funded under grant NGL 50-002-127 entitled "Multidisciplinary Research on the Application of Remote Sensing to Water Resources Problems."

We have also enclosed two (2) copies of each of our recent publications which have emerged from this research. If additional copies of the Progress Report or the publications are desired, please contact us.

Sincerely,

James L. Clapp
Director
Environmental Monitoring and
Data Acquisition Group

JLC/ljq
Enclosures

TABLE OF CONTENTS

	<u>Page</u>
I. INTRODUCTION	1
A. Overview	1
B. Relationship with DNR and Other Agencies	1
C. Summary of Significant Applications	2
II. CONTINUING PROJECTS	4
A. Introduction	5
B. Multidate LANDSAT Classification of Inland Lake Trophic Status -- Progress Toward an Operational Statewide System	5
1. Background	5
2. Specifications for the Operational System	6
a. Preliminary Ground Verification	6
b. Preliminary Plans for the Data Extraction Process	6
c. Calibration Methods	7
d. File Structures	8
e. Data Extraction Programs	8
3. Results and Status -- October 1977	13
C. The Lake Eutrophication Manual	15
III. NON-POINT SOURCE POLLUTION	17
A. Background	20
B. Approach	21
C. Sources of Sediment Group	22
1. Introduction	22
2. Application of Remote Sensing to Quantification of Sediment Transport Processes	23
3. Imagery Currently Available for Analysis	24
4. The Pheasant Branch Data Bank	25
5. Universal Soil Loss Equation Analysis	38
6. Hydrologic Source Area Identification	38
7. Involvement with Sediment Runoff Experiment (July 1977)	41
8. Coordination with Involved Agencies	41

	<u>Page</u>
D. Sedimentation Concentration Group	43
1. Theoretical Models	43
2. Equipment and Methods	44
a. Imagery	44
b. Scattering and Extinction Measurements	45
3. Data Acquisition and Preliminary Discussion of Results	46
a. Imagery	47
b. Meteorological Data	47
c. Water Measurements	47
4. Proposed Analysis	48
E. Mixing and Water Chemistry	48
1. Vertical Mixing of Sediments	48
a. Background	48
b. Field Studies	49
c. Laboratory Studies	49
2. Water Chemistry	50
a. Introduction	50
b. Methods	50
c. Results	52
d. Discussion	52
e. Future Plans	53
F. Data Acquisition and Storage for Field Operations	53
IV. THE SEDIMENT RUNOFF EXPERIMENT	55
A. Operational Planning for the Sediment Runoff Experiment	55
1. Test Site	55
2. Boats and Instrumentation	56
3. Location Control	56
4. Communications	56
5. Flight Planning	56
B. Preliminary Attempts	58
C. 16-17 July 1977	58
D. 18 July 1977	58
E. 19 July 1977	59
F. 20 July 1977	61
G. 21 July 1977	63
H. 22 and 23 July 1977	64

	<u>Page</u>
V. OTHER APPLICATIONS	65
A. Introduction	65
B. Airborne Thermal Scanning of Rooftops	66
C. Remote Sensing and the Energy Extension Service	68
D. Spruce Budworm Defoliation Mapping Using LANDSAT	69
E. Thermal Monitoring of Heated Discharges from Electric Power Plants and Paper Mills	70
1. Ground Truth	70
2. Routine Monitoring	70
3. River Monitoring	71
4. Thermal Standards	71
F. Remote Sensing Data Center	71
G. LANDSAT Land Cover Classification of Watersheds - with USGS	72
H. Corn Yield from Digitized Low Altitude Airphotos	73
I. Land Cover Determined from Digital Interpretation of High Altitude Aerial Imagery	73

LIST OF FIGURES

<u>Figure</u>		<u>Page</u>
1	A typical control point picture from Program CONTROL (Pewaukee Lake, near Milwaukee)	10
2	Control point distribution and row/column residuals for a single LANDSAT file from Program SATNAV	11
3	Control point tabulation and residuals for a typical LANDSAT file from program SATNAV	12
4	Output from Program EXTRACT	14
5	Pheasant Branch Watershed with one hectare grid superimposed	26
6	Computer-generated map showing the 6136 one-hectare cells and identifying "non-contributing" areas.	27
7	Computer-generated map showing topographic slope	30
8	Computer-generated map showing Soil Loss "K" Value	31
9	Computer-generated map showing Predominant Land Cover Type interpreted from 1:120,000 CIR airphoto	32
10	Computer-generated map showing amount of Impervious Surface in each cell interpreted from 1:120,000 CIR airphoto	33
11	Computer-generated map showing amount of Forest Cover in each cell interpreted from 1:120,000 CIR airphoto	34
12	Computer-generated map showing amount of Forest Cover in each cell extracted from USGS topographic map	35
13	Sampling Strategy	51
14	Sediment Runoff Experiment Site	57
15	The sediment plume at 9 A.M., 19 July 1977	60

LIST OF TABLES

<u>Table</u>		<u>Page</u>
I	Predominant Land Cover Classification System	36
II	Data Derived from USGS Topographic Maps	36
III	Data Based on USDA-SCS Soil Survey Information	36
IV	Data Based on Interpretations of RB-57 Photography	37
V	Variable Classification System for Figures 7 to 12	37
VI	Factor Value Information to be Collected	39
VII	Land Use Comparison in Pheasant Branch Watershed	39
VIII	Key for Land Use Identification	40
IX	Crop Identification Key	40
X	Chronology of Aircraft Passes on 19 July 1977	62

LIST OF APPENDICES

Appendix

- I A DNR Evaluation of the LANDSAT
 Lake Classification Program
- II Assessment of Aquatic Environments by
 Remote Sensing
- III Radiative Transfer Model Including
 Air-Water Interface
- IV Letter from WPL to Janesville Gazette
- V Letter from UW-Parkside Physical Plant indicating
 positive use of thermal imagery for heat loss monitoring
- VI Digital Analysis of LANDSAT Data in the
 Detection in Mapping of Spruce Budworm
 Infestation in Northern Wisconsin

I. INTRODUCTION

A. Overview

This project report to NASA's Office of University Affairs describes progress during 1976-1977 on research entitled "Multidisciplinary Research on the Application of Remote Sensing to Water Resources Problems," conducted under NASA Grant NGL 50-002-127 in cooperation with the Wisconsin Department of Natural Resources (DNR).

Section II discusses two research projects which have been active for several years and have now matured. One of the projects has resulted in a manual entitled "The Assessment of Aquatic Environments by Means of Remote Sensing" which is a compendium of research results obtained over the past five years. A final printed version of this manual is included in this report. The other project is closely related work on development of an operational statewide system for classification of 3000 Wisconsin lakes by trophic status. This project is now being implemented by DNR.

Section III describes the past year's research efforts which have been focused upon the problem of non-point source pollution detection and monitoring. This includes discussion of the sediment sources and transport, detection of sediments by remote sensing, the role of sediments as carriers of chemical pollutants, and their hydrological behavior.

Section IV describes the coordinated experiment, called the Sediment Runoff Experiment, devised to obtain data to answer the interdisciplinary questions posed by the approach described in Section III. This experiment focused efforts on a specific watershed. Remote sensing and in situ measurements were closely coordinated to acquire data simultaneously.

Section V briefly discusses a variety of "spin off" projects which deal with a broad spectrum of problems and agencies. Although these projects were not funded by NASA Grant NGL 50-002-127, they would not have been possible without the core of instrumentation and personnel made possible by the NASA Grant.

B. Relationship with DNR and Other Agencies

Our research has focused closely on projects of concern to the Wisconsin Department of Natural Resources (DNR). DNR investigators have participated in virtually every aspect of the work, and excellent working arrangements between University and DNR people have evolved.

Research on water quality assessment relates directly to DNR requirements to monitor and report upon water quality in inland lakes. In a state with as many lakes as Wisconsin, conventional sampling procedures are prohibitively expensive, so interest in remote sensing techniques, especially using LANDSAT data, is high. An operational procedure for semi-automatic lake classification has been developed with DNR, and DNR people are working

closely with the University to implement it. Among other things, DNR has provided ground truth data gathering and water sample analysis. DNR has committed several thousand dollars for tapes and computer time, and has two people working on implementation and testing of the analysis methods.

In the area of thermal scanning of heated water discharges data has been cooperatively gathered using DNR aircraft and crews, and the results of the analysis have provided the agency with information needed for rule-making and setting of standards. DNR crews are now prepared to manage the entire system on an operational basis.

Other agencies have cooperated with the University and benefitted from research under this grant. We are working with the International Joint Commission (IJC) on an investigation of non-point source pollution of Lake Michigan. We have just completed a small project with the U.S. Forest Service to map insect infestation in a forest area using LANDSAT data. The U.S. Geological Survey is working with us to model surface runoff characteristics of Wisconsin watersheds. We are working with a private firm in developing remote sensing techniques using low altitude airphotos to predict corn yields.

We have been involved in using remote sensing in energy conservation with a Wisconsin utility. Wisconsin Power and Light provided funds for an airborne thermal scan of two cities and personnel for dissemination of the imagery. The U.W. Extension and the Wisconsin Office of Planning and Energy are using our remote sensing expertise and personnel to aid in training energy auditors.

C. Summary of Significant Applications

- (1) The manual "The Assessment of Aquatic Environments by Means of Remote Sensing" is completed, culminating five years of research. This should be valuable to a wide range of users.
- (2) An operational set of programs for lake quality classification is being absorbed and tested by DNR.
- (3) The field portion of a sediment runoff experiment was successfully completed. Researchers from the various disciplines involved are now digesting the large quantity of data obtained during this event.
- (4) Analysis of power plant heated water discharges has provided DNR with data needed for rule making and standards setting.
- (5) Operational use of thermal scanning by DNR is now available.
- (6) Computer analysis of remotely sensed data for a wide range of research or application needs is now possible.
- (7) Photographic and satellite data are being used in a variety of small, short-term applications. These include water quality planning studies, mapping of forest insect infestation, and crop yield prediction.

- (8) Energy auditors are being trained in the use and limitations of thermal scanning applied to energy conservation.
- (9) Thermal scanning was successful in stimulating public awareness regarding home energy conservation.

II. CONTINUING PROJECTS

Principal Investigators

Michael S. Adams, Associate Professor, Department of Botany

Lawrence T. Fisher, Remote Sensing Project Coordinator, Institute for Environmental Studies

Frank L. Scarpace, Assistant Professor, Department of Civil and Environmental Engineering, and Institute for Environmental Studies

James P. Scherz, Professor, Department of Civil and Environmental Engineering

Francis H. Schraufnagel, Chief, Bureau of Standards and Surveys, Department of Natural Resources

William J. Woelkerling, Le Trobe University, Bundoura, Victoria, Australia

Research Assistants

Kenneth Holmquist, Department of Civil and Environmental Engineering

ABSTRACT

Two projects which have been active for several years are:

- (1) the development of an operational statewide system for the classification of 3000 lakes by trophic status; and
- (2) the development and publication of a manual, "The Assessment of Aquatic Environments by Means of Remote Sensing."

The development of an operational system for the classification of lakes has progressed significantly. Computer files and programs have been completed to obtain navigation control points, navigate scenes to provide latitude/longitude to row/column conversion (and vice versa) and to automatically extract data for all lakes on a LANDSAT scene. Analysis and classification programs are operating but more work is being done to refine algorithms. Atmospheric correction techniques and multirate analysis methods have been developed and applied to large-scale experiments in southern and southeast Wisconsin. DNR is committing several thousand dollars for tapes and computer time, and now has two people working on the project. One is the graduate student who has worked with us for three years.

In Section C, the final draft of the lake eutrophication manual is discussed. The manual, authored by Scherz, Woelkerling, Adams and Scarpace, is a compendium of five years of research.

A. Introduction

Some of our past research has largely reached maturity. These projects, while not part of our current research thrust, have been supported to allow them to reach the implementation stage. First, considerable work has been done to deliver an operational system for classification of the trophic status of inland lakes using LANDSAT. Computer software has been developed to allow automatic data extraction from LANDSAT scenes for 3,000 Wisconsin lakes. Classification and analysis programs are being developed to incorporate atmospheric corrections and multitime LANDSAT scenes. The following section gives details of progress in this work. Section C briefly discusses progress on the lake eutrophication manual.

B. Multitime LANDSAT Classification of Inland Lake Trophic Status -- Progress Toward an Operational Statewide System

1. Background

Since 1974, UW-Madison researchers have been working with Department of Natural Resources personnel to apply remote sensing and, in particular, LANDSAT to help monitor and classify water quality of inland lakes. Under provisions of the Federal Water Pollution Control Act Amendments of 1972, PL92-500, reports must be filed with the Environmental Protection Agency (EPA) classifying all lakes in each state. With about 3,000 lakes greater than 20 acres in the state of Wisconsin, the difficulty and expense of traditional monitoring methods using boats to obtain water samples is formidable. Remote sensing offered attractive alternatives.

Early studies [1,2] correlated water turbidity with film density using both 7-inch and 70mm film products provided by the EROS Data Center. Radiometric quality of the 7-inch imagery was inadequate, but sufficient correlations were obtained with the 70mm film to warrant further research.

The next step was to computerize the procedure, using interactive computing techniques in which operators identified lakes from a crude "picture" generated on an interactive graphics terminal by their general appearance and location, and then used a terminal cursor to identify particular points from which data were extracted for analysis. In this process, only Band 5 (red) data were inspected, only a single date was used, and no atmospheric corrections were applied. Data from 1974 LANDSAT scenes were extracted in this fashion for all lakes over 20 acres and deeper than 8 feet, as listed by the DNR in a brochure entitled "Wisconsin Lakes," which tabulates all lakes in each of Wisconsin's 72 counties. About 3,000 lakes were included. From the extracted data, tabulations by county and district were prepared, ranking lakes in order of increasing Band 5 value and thus nominally in terms of increasing turbidity. These were delivered to the DNR in early 1975 and formed the basis for an initial report to EPA.

Several shortcomings of this approach were evident. First, substantial human interpretation was needed. We felt that a large portion could be

automated. In addition to easing personnel time requirements, this would allow overnight or weekend batch computation at rates considerably less than the premium paid for interactive computing. Second, only a few selected data points were taken for each lake. This process was subject to the risk that data points might, for example, be taken directly in an algae bloom, badly skewing the results. Third, only a single date per season was analyzed. Finally, no correction process was used to provide correction for atmospheric degradation.

2. Specifications for the Operational System

a. Preliminary Ground Verification

In late 1975 and early 1976, preliminary plans for an operational classification procedure were drawn up. First, a better evaluation of the quality and potential of LANDSAT for lake quality classification had to be done. Therefore, an extensive ground verification effort was begun by DNR and UW-Madison personnel during the summer of 1975 and continued during the summer of 1976. Water samples and turbidity measurements were taken in 10 lakes in southeastern Wisconsin within a day of a LANDSAT pass. After tapes had been obtained for three dates in 1975, LANDSAT data from all bands were correlated with the ground measurements. Several conclusions were drawn from these early studies. First, there was sufficiently good correlation to warrant a substantial commitment to the project. Second, it appeared that data from Bands 4, 5 and 6 were all useful and needed, especially if atmospheric corrections could be provided. Third, we concluded that the most necessary data were mean values in those three bands for all data points within each lake, together with the corresponding variance-covariance matrix data. Extracting these values rather than storing all data points for the lakes would have the effect of dramatically reducing the size of the needed archival information, and would reduce all data sets, no matter the size of the lake, to the same number of archived values.

b. Preliminary Plans for the Data Extraction Process

To locate the lakes with a minimum of human intervention, some mechanism was needed to identify and locate the lakes. After several potential approaches had been considered, it was decided to construct a statewide file containing latitude/longitude coordinates of all lakes to be analyzed. Using the largest available scale topographic maps, a polygon with up to 10 apexes was drawn around each lake. Sufficient shoreline was included so that navigation procedures to convert from latitude/longitude to LANDSAT coordinates and vice versa could err by several rows or columns or seconds without causing the lakes to be missed. These polygons and the corners of the maps were digitized to a nominal precision of .005 inches under contract with the University of Wisconsin-Madison Cartographic Laboratory. Computer software necessary to calculate latitudes and longitudes from the digitized coordinates was also developed by the Cartographic Lab. Editing and error correction programs were also made available.

In addition to the lake polygons, one prominent point per map-sheet was selected in a water body -- a peninsula, island or similar feature -- and digitized. The latitude and longitudes of these points were made available in a separate format to serve as "control points" for scene navigation procedures.

The digitizing effort occupied much of the winter and spring of 1976 and 1977, and yielded recorded information for all lakes to be included in the procedure. It was a difficult, expensive and time-consuming process, but it needed to be done only once. It is now complete except for occasional editing of errors or omissions which will inevitably come to light.

Once the lake polygon positions had been defined, definite planning was begun for the file structures and programs to utilize them.

c. Calibration Methods

Atmospheric variability manifests itself in two distinct ways with LANDSAT. Light reflected from the ground can be absorbed, or it can be scattered. Correction can be obtained to a large degree if two constants can be obtained. First, if a very dark area can be located, a measure of scattered light can be obtained by noting its brightness in each of the LANDSAT wavelengths. Following Scherz et al. [3], we sought the most oligotrophic lake in a scene as our best available "dark body." Average values from such lakes are subtracted from all those for all other lakes on a LANDSAT scene. Second, some consistently bright object of uniform contrast from scene to scene was needed to normalize effects of atmospheric absorption. Major airports are sufficiently common and offer large areas of concrete whose reflectance is high and not subject to seasonal variation, so we selected these as our second calibration tool. Airport values are extracted from each scene. Therefore the change of this difference ($Airport_i^j - Clear\ Lake_i^j$, i = the band, j = the day) from day to day must be due to differing atmospheric absorption. In the present scheme, the normalization factor is A_{ij} .

$$A_{ij} = \frac{\alpha \text{ clear day}}{\alpha \text{ day}_j} = \frac{Airport_i^{CD} - CL_i^{CD}}{Airport_i^j - CL_i^j}$$

Therefore, the portion of the recorded signal due to the reflectance of the matter present in the water, the value upon which the classification should be based is

$$G_{ij} = (lake_i^j - CL_i^j) \left(\frac{Airport_i^{CD} - CL_i^{CD}}{Airport_i^j - CL_i^j} \right)$$

Fortunately, the corrections which are needed by our procedures need not be applied pixel by pixel. Instead, we can obtain statistical information in the form of mean values for each band and variances and covariances for all points within a lake. Similar figures can be obtained for the calibration points (the nearest large airport and the most oligotrophic lake). Then we

correct the statistics instead of the individual raw data values. This is so because the statistics performed act as linear transformations on the data as a whole. The analysis is substantially simplified because raw data can be extracted and statistically processed.

d. File Structures

Three major mass storage files were needed. One provides a set of points of known latitude and longitude which could be easily identified on crude "pictures" produced from LANDSAT tapes. These are to be used to correlate latitude/longitude and row/column coordinate systems to "navigate" scenes, providing necessary "tie points" between the two coordinate systems. The second, a much larger file, provides a compact and efficient means of identifying all lakes to be considered. The third, DATA-FILE, provides a mechanism to store extracted data for later classification.

CONTROL-PT is the name of the first of these files. It presently consists of 335 islands, peninsulas and points in lakes and rivers around the state. An average of one point from each topographic map quadrangle in Wisconsin with latitude/longitude coordinates determined by digitization from those maps is included. These coordinates are specified as number of seconds north of 40° and west of 85° , an arbitrary point selected sufficiently southeast of Wisconsin that no LANDSAT scene would encompass the point and part of Wisconsin.

ACCESS is the second file. It contains lake name, identification number (keyed to Wisconsin's 72 counties), and coordinates of the bounding polygon (again using the seconds north of 40° and west of 85° system), for each of about 3,000 lakes. There is also a system of "pointers" in the file, so that we can easily obtain (1) the first lake on a given 15 minute quadrangle, (2) the next lake on a quadrangle; (3) the first or next lake in a specified county; or (4) the next lake in alphabetical sequence within a county. FORTRAN-V subroutines accompany this file to facilitate extraction of its data, or to edit or regenerate it.

DATA-FILE is the third file in the system. It is keyed to ACCESS, and provides a compact place to store statistical data for each lake considered. These statistics are used by the classification program once three sets of data acquired over the course of a season are stored, and after appropriate calibration data have been obtained.

e. Data Extraction Programs

Three steps, each with its own large program, comprise the data extraction process for a single LANDSAT scene. First, a dozen or so well-distributed points must be found for each of the four "quarter scene" files of a LANDSAT computer-compatible tape so that latitude/longitude to row/column transformations can be

found. This is done by means of program CONTROL, which uses nominal scene geometry and scene-center coordinates to produce (row/column) coordinates of points from the control point file, CONTROL-PT. It produces pictures such as Figure 1 on printer output or, preferably, microfiche of the areas surrounding each predicted control point position within the scene. These "pictures" clearly show water features as well as clouds, cloud shadows, and major cultural features such as highways. Usually, control points can be identified from these pictures, and precise row/column coordinates can be interpolated by an operator. If the points are missed, the program can rerun for selected points with "offsets" introduced. Usually, after at most two or three "runs," enough control points have been located to provide a sufficient number of sets of row/column and latitude/longitude coordinates for use by the next program, SATNAV.

SATNAV accepts operator-interpreted coordinates in row/column form for selected control points. It retrieves latitude/longitude coordinates for these points from CONTROL-PT, and uses non-linear regression analysis procedures to determine a set of models which best fit the two coordinate systems. Heuristically, the models have been chosen as follows, where r and c are LANDSAT row and column coordinates, and ζ and θ are latitude and longitude in our local system of seconds north of 40° and west of 85°

$$r = a_{11} + a_{12}\theta + a_{13}\zeta + a_{14}\zeta^2 + a_{15}\zeta^3$$

$$c = a_{21} + a_{22}\theta + a_{23}\zeta + a_{24}\zeta^2 + a_{25}\theta^2$$

$$\zeta = a_{31} + a_{32}c + a_{33}r + a_{34}r^2 + a_{35}r^3$$

$$\theta = a_{41} + a_{42}c + a_{43}r + a_{44}r^2 + a_{45}c^2$$

SATNAV's role is to calculate the a_{ij} 's, called the navigation parameters, so that mean square errors between measured and calculated coordinates are minimized. It uses the calculated parameters to predict rows and columns from measured latitudes and longitudes (supplied by CONTROL-PT) and to predict latitude and longitude from measured rows and columns (supplied by operator interpretation). These predicted values are compared with their corresponding "actual" values and tabulated. Graphical displays of resulting errors or "residuals" are presented, such as those of Figures 2 and 3. Its main purpose, though (provided the operator approves of the residuals), is to file the navigation parameters in a small mass-storage file where the next program, EXTRACT, can use them.

EXTRACT concerns itself with extraction of multispectral data from each file, or quarter-scene, of a LANDSAT tape. First, it uses the navigation parameters computed by SATNAV to calculate latitudes and longitudes of extremities of the scene. This identifies all 15 minute quadrangles encompassed by the extremities, some of which do not intersect the scene itself. A subroutine, INTSCT, tells whether two polygons actually intersect (and which gives coordinates of the resulting intersection polygon, if they

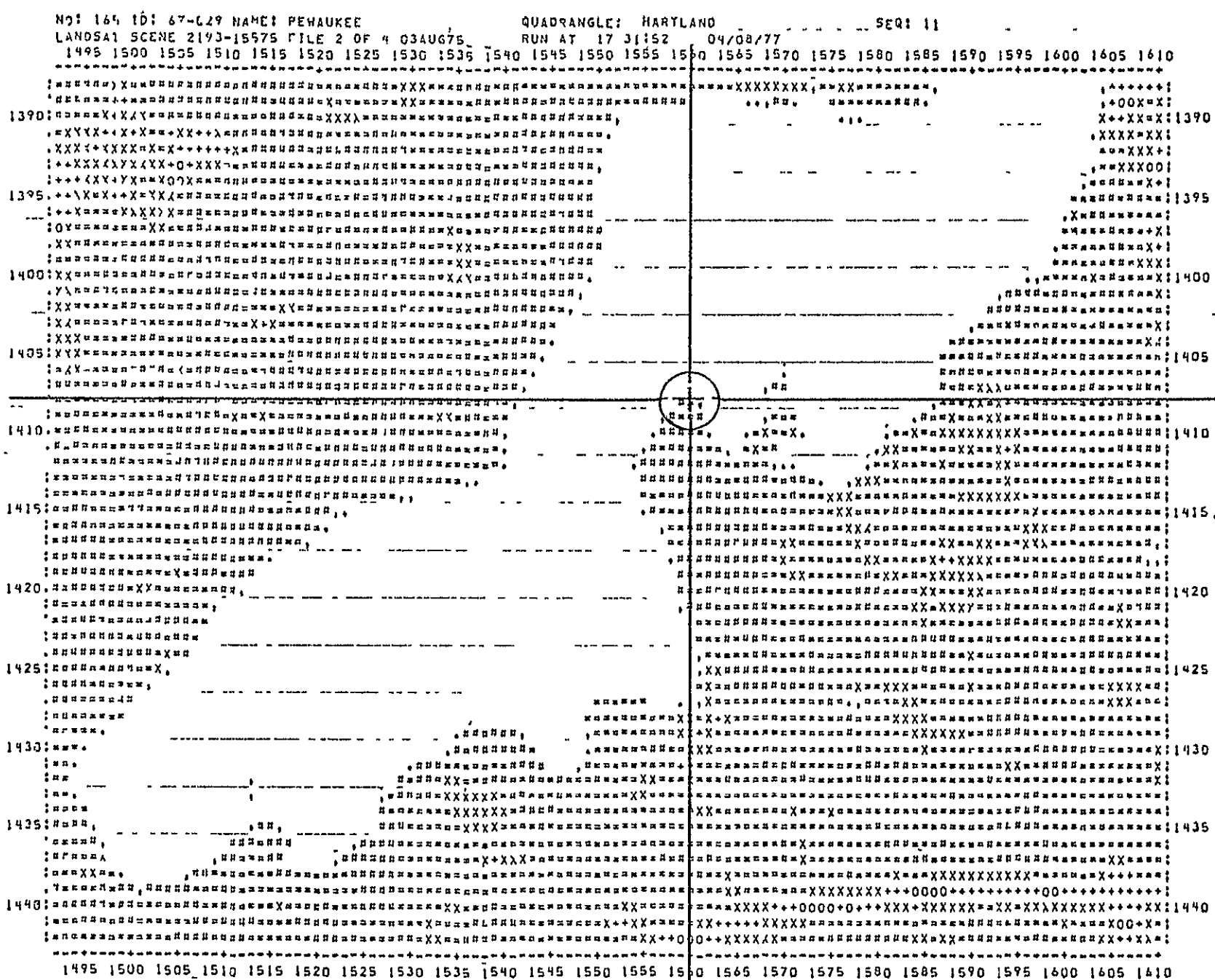


FIGURE 1. A typical control point picture from
Program CONTROL (Pewaukee Lake, near Milwaukee).

CONTROL DISTRIBUTION AND ROW/COL ERRORS--<ACTUAL - PREDICTED>
 ROW

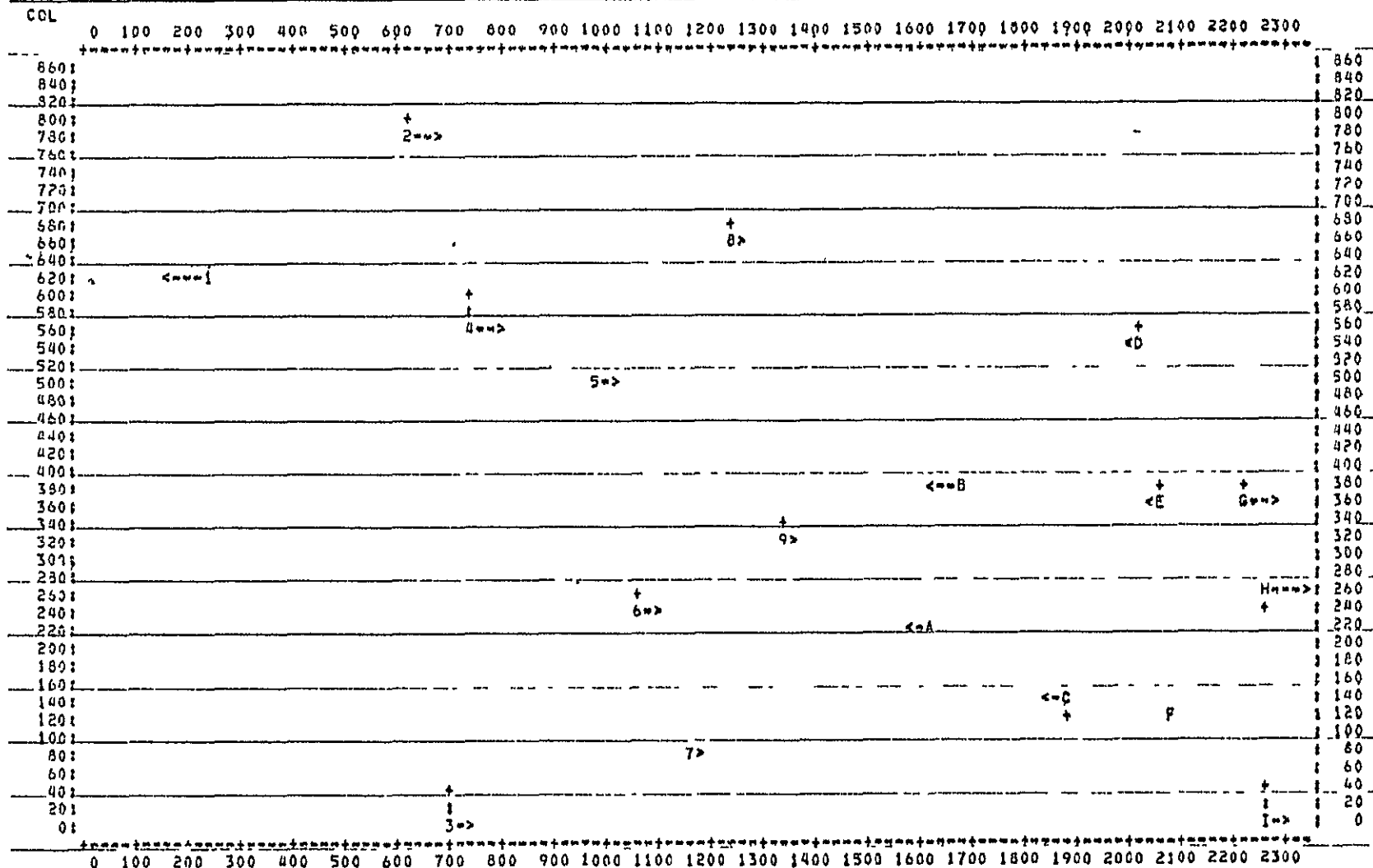


FIGURE 2. Control Point distribution and row/column residuals for a single Landsat file from Program SATNAV.

ORIGINAL PAGE 11
 OF POOR QUALITY

PROGRAM <SATNAV>=VERSION 2.0=5 OCT. 1977
 RUN AT 00151105 10/07/77

NO PREVIOUS DATA IN FILE 18

INPUT OPTIONS:

SCENE 1757 16110

NONE

CONTROL POINTS USED FOR LANDSAT SCENE 1757-16110 FILE 1 OF 4:

NO.	POINT	ID	NAME	QUADRANGLE	SCALE	LAT/LONG	
1	327		BAD RIVER DELTA	ODANAH	62500	N 46-38'21"	W 90-39' 6"
2	320	02-021	LOON	MFLLEN	62500	N 46-21' 1"	W 90-38'46"
3	322	04-146	STAR LAKE	GRANDVIEW	48000	N 46-23'12"	W 91-13'25"
4	321	02-024	MINFRAL	MARENGO	62500	N 46-17'45"	W 90-49'44"
5	311	57-069	LOHER CLAM	CLAM LAKE	48000	N 46- 8'23"	W 90-56'17"
6	312	57-067	LOST LAND	NAMEKAGON	48000	N 46- 6'29"	W 91- 8'27"
7	313	57-121	UPPER THIN (TIGER)	HAYWARD	48000	N 46- 3'44"	W 91-16'59"
8	297	57-010	BLAISDELL	DRAPER	48000	N 45-56'31"	W 90-53'38"
9	298	57-091	POKEGAMA	RADISSON	48000	N 45-54'17"	W 91- 9'52"
10	252	57-122	WEIRGOR	WEIPGOR	24000	N 45-43'48"	W 91-18'35"
11	251	57-126	WINDFALL	EXELAND	48000	N 45-39'41"	W 91-12'49"
12	253	54-042	AUDIE	BUCKS LAKE	24000	N 45-33'10"	W 91-25'52"
13	218	54-037	THORNAPPLE FLOW	LADYSMITH	48000	N 45-24'41"	W 91-10'52"
14	219	54-001	AMACDY	BUCE	24000	N 45-24' 4"	W 91-18'55"
15	222	54-003	BASS	WEYERHAUSER	24000	N 45-25'33"	W 91-29'40"
16	220	54-034	SAND	FIRESIDE LAKES	24000	N 45-17'56"	W 91-21'15"
17	221	09-007	CHAIN	CHAIN LAKE	24000	N 45-16'58"	W 91-26'17"
18	223	03-016	CHETEK	CHETEK	62500	N 45-18'38"	W 91-37'36"

SYM, NO, POINT			MEASURED		PREDICTED		ERRORS		MEASURED		PREDICTED		ERROR (SEC)	
			ROW	COL	ROW	COL	ROW	COL	LAT	LONG	LAT	LONG	LAT	LONG
1	1	327	247.0	632.0	251	632	-4.0	.0	46-38'21"	90-39' 6"	46-38'20"	90-39' 9"	-1	-3
2	2	320	640.0	779.5	637	779	3.0	.5	46-21' 1"	90-38'46"	46-21' 2"	90-38'47"	-1	-1
3	3	322	709.0	16.5	707	15	2.0	1.5	46-23'12"	91-13'25"	46-23'10"	91-13'13"	2	12
4	4	321	751.5	573.0	749	571	2.5	2.0	46-17'45"	90-49'44"	46-17'44"	90-49'42"	1	2
5	5	311	988.0	506.0	986	506	2.0	.0	46- 8'23"	90-56'17"	46- 8'23"	90-56'20"	0	-3
6	6	312	1073.0	259.0	1071	258	2.0	1.0	46- 6'29"	91- 8'27"	46- 6'28"	91- 8'26"	1	1
7	7	313	1164.5	95.0	1164	95	.5	.0	46- 3'44"	91-16'59"	46- 3'44"	91-16'58"	0	1
8	8	297	1250.0	660.0	1249	659	1.0	1.0	45-56'31"	90-53'38"	45-56'30"	90-53'37"	1	1
9	9	298	1358.0	327.0	1357	326	1.0	1.0	45-54'17"	91- 9'52"	45-54'13"	91- 9'54"	4	-2
A	10	252	1626.0	221.0	1628	221	-2.0	.0	45-43'48"	91-18'35"	45-43'48"	91-18'38"	0	-3
B	11	251	1700.0	381.0	1703	381	-3.0	.0	45-39'41"	91-12'49"	45-39'41"	91-12'49"	0	0
C	12	253	1894.0	147.5	1896	148	-2.0	.5	45-33'10"	91-25'52"	45-33'11"	91-25'55"	-1	-3
D	13	218	2036.0	546.0	2037	545	-1.0	1.0	45-24'41"	91-10'52"	45-24'41"	91-10'43"	0	-9
E	14	219	2078.0	375.0	2079	374	-1.0	1.0	45-24' 4"	91-18'55"	45-24' 4"	91-18'51"	0	4
F	15	222	2082.0	126.0	2082	126	.0	.0	45-25'33"	91-29'40"	45-25'32"	91-29'44"	1	-4
G	16	220	2227.0	374.0	2224	373	3.0	1.0	45-17'56"	91-21'15"	45-17'54"	91-21' 9"	2	6
H	17	221	2267.0	269.0	2263	270	4.0	-1.0	45-16'58"	91-26'17"	45-16'56"	91-26'20"	2	-3
I	18	223	2267.0	8.0	2265	6	2.0	2.0	45-18'38"	91-37'36"	45-18'39"	91-37'38"	-1	-2

FIGURE 3. Control Point Tabulation and residuals for a typical Landsat file from Program SATNAV.

do). With this aid, EXTRACT systematically inspects each quadrangle of possible interest, starting at the northwest corner of the scene. If the quadrangle does not intersect the LANDSAT scene, the program passes to the next quadrangle east, or next row south when a row is finished. If, however, it is found that the quadrangle and the scene intersect, then ACCESS is asked to return (latitude/longitude) coordinates of the first lake in that quadrangle, if any. The lake polygon is then tested for intersection with the LANDSAT scene. If it does not intersect, then the next lake in the quadrangle is called, if there is one, or else the next quadrangle is inspected. If the lake polygon does intersect the scene, then a search for "water-like" points within the lake polygon is initiated. To do this, the polygon is converted, by the navigation parameters, to row/column form. The LANDSAT tape is moved to the beginning row, and data is transferred into high-speed memory. Our "interior points of polygons" subroutine is called to ascertain which columns lie inside the lake polygon, and each of these points is inspected in turn. If Band 7 values are below a preset threshold, an interior point is declared "water-like", and its Band 4, 5 and 6 values are extracted and filed in fast memory. After all points within the lake polygon have been inspected, a statistics program is called to calculate mean values for each band, and the "variance-covariance matrix" for all water-like points. This information is filed with date and scene identification in the output storage area, DATA-FILE. EXTRACT also produces a picture such as Figure 4, usually on microfiche, showing each lake polygon and indicating all water-like points by 0's. This provides a check of the navigation and extraction and allows appropriate reruns if data are unsuitable.

Data for "darkest lake in the scene" and for a suitable airport in each scene are also extracted and filed. At present, rather crude manual interactive techniques are used to obtain statistics for the airports, but programs have been partially modified to automatically extract this data.

Several weeks of work may be required to complete operation of the data extraction process for three dates in a season for a large area. During this time, DATA-FILE is gradually built up. When it has sufficient data, the classification procedures can be performed. The program CLASSIFY is still in a state of flux, but it is small enough that various versions can be applied to DATA-FILE at very moderate cost. Present versions apply heuristically determined weighting coefficients to the mean values for Bands 4, 5 and 6 and to variances for these bands to produce a "Trophic Status Index Number" of 1 to 7. The weighting factors have been determined by regression techniques to best agree with ground measurements and with assessments of lakes in southeastern Wisconsin made by DNR district limnologists. Experiments to choose the best set of weights are continuing.

3. Results and Status -- October 1977

All of the files have been generated at this time; inevitable errors are being located and corrected. The data extraction programs are running and have been used successfully to extract data for all lakes

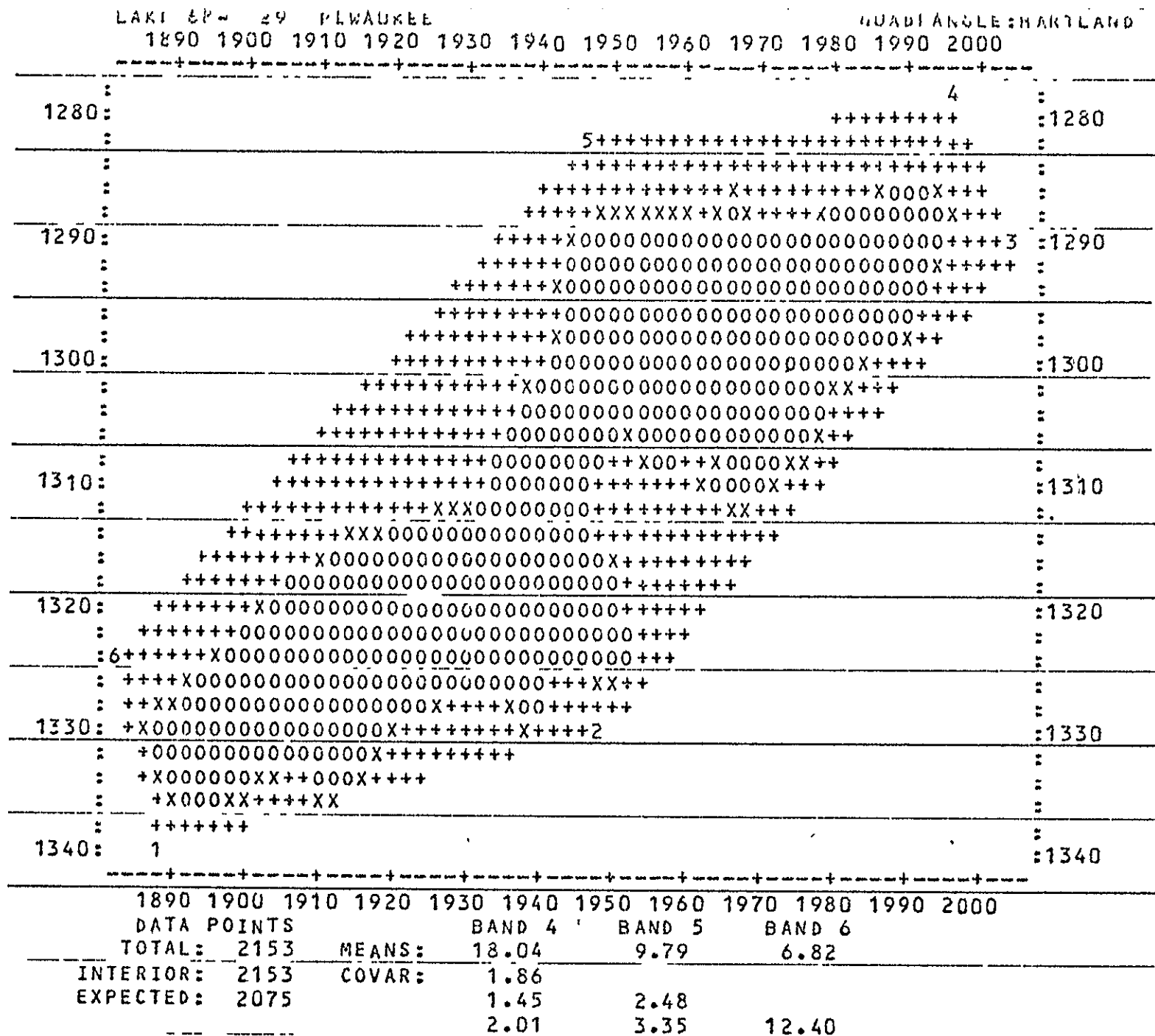


FIGURE 4. Output from Program EXTRACT
 0's are "waterlike" pixels (low band 7 values)
 X's are waterlike "edge" pixels
 +'s are inside the navigated lake polygon but are not "waterlike".

in southeast Wisconsin using LANDSAT data from 1975. An experiment is underway in the same area using 1976 data, although we are still awaiting delivery of the last of the 1976 tapes for the Madison area. Classifications of southeastern Wisconsin lakes has been done for 1975 and partially completed for 1976. Correlations have been performed against both our own ground calibration data, based on in situ measurements and on DNR evaluations of a selected subset of lakes. Weights have been selected to combine mean values and variances to best correlate with the different forms of ground verification. The best fit equation for the relationship between satellite data and lake turbidity was determined. An R^2 value of 83% is associated with this equation. This means that 83% of the variability in the data is accounted for by the regression equation. A large part of the unaccounted for variability may be due to the difference in time between satellite overflight and ground sampling time. This difference varied between one and nine days for the actual data used. The best relationship between the satellite data and the known trophic status numbers provided by DNR personnel had an R^2 value of 76.8%. This equation has been used to classify all lakes in the southeastern section of the state.

The DNR will provide LANDSAT tapes for 1977 for southern and southeast Wisconsin. Data for a test area in northern Wisconsin, where lakes are both plentiful and unfamiliar to our personnel, will provide a stern test to the programs and procedures. DNR has hired Mr. Holmquist, who did much of the ground verification and who has participated in the project since its inception, as a full-time employee to coordinate University-Agency efforts during the next few months. DNR has also provided part-time services of Mr. Ron Martin to work with us. Funds for full-scale, state-wide implementation of the procedure are being sought for the next fiscal year. Appendix I is an evaluation by DNR of the LANDSAT lake classification program.

C. The Lake Eutrophication Manual

Final draft of the manual, "The Assessment of Aquatic Environments by Means of Remote Sensing," was completed by Scherz, Woelkerling, Adams and Scarpace in early 1977. The authors decided to seek outside publication, so a several month review was done by the University of Wisconsin Press. They decided its projected sales would not justify hard-cover publication, however, so pre-publication editing was resumed by the Institute for Environmental Studies Publications Office. This editing was completed in August 1977. Printing and collating is scheduled by the end of October 1977. The manual will be ready for general circulation in November 1977, and is included as Appendix II.

References

1. Scarpace, F.L., L.T. Fisher and R. Wade, "Trophic Status of Inland Lakes from ERTS." Proceedings, Fall ASP Meeting, 1974.

2. Fisher, L.T. and F.L. Scarpace, "Classification of Inland Lakes from LANDSAT." Proceedings, NASA Symposium, June 1975.
3. Scherz, J.P., et al., 1976. "The Assessment of Aquatic Environments by Means of Remote Sensing " Unpublished at this time.

III. NON-POINT SOURCE POLLUTION

Principal Investigators

Anders W. Andren, Assistant Professor, Department of Civil and Environmental Engineering, and Water Chemistry Program, UW-Madison.

Kenneth L. Beghin, Chief, Aeronautics Section, Wisconsin Department of Natural Resources

John M. Cain, Chief, Water Quality Planning Section, Wisconsin Department of Natural Resources

James L. Clapp, Professor, Civil and Environmental Engineering, and Director, Environmental Monitoring and Data Acquisition Group

Donald P. Cox, Associate Professor, Department of Physics, UW-Madison

Lawrence T. Fisher, Remote Sensing Project Coordinator, Environmental Monitoring and Data Acquisition Group, UW-Madison

Theodore Green III, Professor, Department of Civil and Environmental Engineering, and Meteorology Department, UW-Madison

John A. Hoopes, Professor, Department of Civil and Environmental Engineering, UW-Madison

Ralph W. Kiefer, Professor, Department of Civil and Environmental Engineering, UW-Madison

John G. Konrad, Supervisor, Special Studies, Wisconsin Department of Natural Resources, and Assistant Professor, Department of Soil Science, UW-Madison

Robert P. Madding, Project Associate, Marine Studies Center, and Environmental Monitoring and Data Acquisition Group, UW-Madison

Frederick W. Madison, Jr., Specialist, Department of Soil Science, UW-Madison

Jerome R. McKersie, Chief, Water Quality Evaluation Section, Wisconsin Department of Natural Resources

Frank L. Scarpace, Assistant Professor, Institute for Environmental Studies, and Department of Civil and Environmental Engineering, UW-Madison

James P. Weinman, Professor, Department of Meteorology, UW-Madison

Donald R. Winter, Acting Director, Office of Inland Lake Renewal, Wisconsin Department of Natural Resources

Research Assistants

Linda Kalman, Department of Civil and Environmental Engineering

Donald Morris-Jones, Environmental Monitoring Degree Program,
Institute for Environmental Studies

Ananta Nath, Department of Civil and Environmental Engineering
(1/4 time for 1 semester only)

John Schettle, Department of Civil and Environmental Engineering

Barry Verdegan, Department of Civil and Environmental Engineering

ABSTRACT

The non-point source pollution problem is being approached through several avenues. There are three groups addressing sediment sources and transport, remote sensing of sediment concentration, and sediment mixing and water chemistry. These groups have been studying a specific watershed (Pheasant Branch) and working closely to each provide a piece of the puzzle for an integrated solution to the overall problem. This section deals with the individual group's approach to each facet. Preliminary research, data collection during the sediment runoff experiment, preliminary results and future analyses are discussed. The following paragraphs abstract each group's efforts.

The sources of sediment group is under the direction of Professors R.W. Kiefer and F.L. Scarpace. This group also includes work on sediment transport directed by Professor J.A. Hoopes. Graduate students are D. Morris-Jones and A. Nath. Work on investigating the sources of sediment in the Pheasant Branch Watershed has proceeded on several fronts. Existing remote sensing imagery of the watershed has been inventoried and new aerial photography has been obtained. A computer-based data bank containing 6136 one hectare cells has been developed for the Pheasant Branch Watershed. Data from several sources, including topographic maps, soils maps, and aerial photography, have been encoded into the data bank. The application of the Universal Soil Loss Equation to estimate potential sediment loss in the watershed has been initiated. The application of remote sensing to quantification of sediment transport through the watershed is being investigated. Coordination of research efforts with involved political bodies and governmental agencies continues.

The sedimentation concentration group is under the direction of Professors J.A. Weinman and F.L. Scarpace. The graduate student working on the project is L. Kalman. The proposed study of determining sediment concentrations in water using multiband aerial photography has progressed significantly. A mathematical model which can predict exposures produced on the film by sediment laden water has been developed. Imagery of a runoff event has been obtained along with extensive ground truth. The ground truth is being analyzed to determine the spectral characteristics of the sediment, water and atmosphere. These data will be used as input to the model when analyzing the film.

The water mixing group is directed by Professor T. Green with graduate student J. Schettle. Their research aims toward developing field measurements complementing remote sensing imagery in order to infer vertical and bottom sediment distribution. Specifically, attempts were made to observe the "mud fingering" phenomenon in the field and to generate this phenomenon in the laboratory. "Mud fingering" has been generated in the laboratory: conditions necessary for occurrence are being parameterized. The lab studies indicated poor conditions for field observation of "mud fingering" during the sediment runoff experiment. The phenomenon has not yet been observed outside the laboratory.

The water chemistry group is directed by Professor A. Andren with graduate student B. Verdegan. Water samples were collected during the sediment runoff experiment. Analyses have been completed for eight parameters including turbidity, suspended solids, conductivity, chloride, and four forms of phosphorous. A technique has been developed to obtain particle size from a given water sample. Results indicate a decrease in suspended solids and phosphorous forms with increasing distance from the mouth of the creek. Conductivity and chloride tend to increase with distance into the lake from the creek mouth. It was discovered that a major source of resuspension of sediments was, in addition to current and wave action, turbulence created by the boat propellers. One form of phosphorous was probably affected by sample preservation techniques. Improvements in sample collection and preservation are planned for future runoff events.

The proposed work on data acquisition and storage for field operations has been shelved due to lack of time, funds and necessity. Conventional methods proved to be quite adequate.

A. Background

Since the passage of Public Law 92-500 (the 1972 amendments to the Water Pollution Control Act) increasing interest has focused upon pollution sources other than those derived from specific point locations. Federal agencies, University investigators and the DNR are aware that non-point source pollution is a major contributor to water quality degradation and have become interested in locating and monitoring it.

Non-point source pollution is caused by materials originating from land use activities. These materials, carried into waters by erosional runoff processes, impair water quality and create pollution problems. Potential sources of non-point source pollution include urban storm water runoff, construction site erosion, agricultural runoff and sediment loss, land disturbance caused by mining or timbering activities, and other diffuse natural or man-made phenomena. Major non-point pollutants are generally considered to be sediment particles, nutrients (both natural and those added to enhance agricultural productivity), and in some cases toxic materials such as heavy metals, pesticides and oxygen-demanding substances.

The institutional framework established within the DNR to evaluate non-point source pollution consists of three sections within the Bureau of Water Quality, as well as the district offices. A Non-Point Source Program has been formulated under the Special Studies Section to complete major portions of this program element. This Section provides guidance and advice for monitoring studies done within the State and serves as the focal point for instituting remedial measures. The Section will analyze and define "Best Management Practices" (BMP). It will evaluate the capability of each BMP to meet the needs of the State and the capability of each to be instituted. Special Studies also coordinates DNR activities in the International Joint Commission (IJC) Study on the Menomonee River Basin and in the Washington County Project funded under Section 108 of 92-500.

The Water Quality Evaluation Section serves as the stream data collection agency within the Bureau. This Section coordinates district non-point source monitoring. Data management and field report organization are the primary responsibilities of this Section in the Non-Point Source Program, with subsequent interpretation and evaluation of the data an integral result.

Requirements of PL 92-500 have imposed a heavy data gathering burden on the DNR, both for planning purposes and to meet reporting requirements. Present data sources (primarily reporting services of the Soil Conservation Service) lack badly needed detail and currency. One prime objective of this research is to provide more detailed and current information by remote sensing means.

B. Approach

To obtain a synoptic view of sediments, their detection by remote sensing, their sources, their role as carriers of chemical pollutants, and their hydrologic behavior, a coordinated data gathering experiment, called the Sediment Runoff Experiment, was devised. Plans were made to await a heavy runoff-producing rainstorm. Then water sampling boats would be quickly deployed and a variety of in situ measurements performed while simultaneously acquiring aerial photographs and on-land measurements and samples. In mid-July 1977, a splendid opportunity to conduct this experiment presented itself. Advance planning and coordination allowed us to capitalize on this opportunity.

The following questions were posed, and the planning for the experiment was begun to attempt to answer them:

- (1) How does sediment in a river or a lake affect air photos? What are the scattering properties of sediment, and what are the spectral characteristics of sediment-laden water?
- (2) What film/filter combinations can best be used to quantify sediments?
- (3) How does the surface concentration of sediment relate to concentrations at depth? What particular mechanisms govern vertical mixing?
- (4) How can aircraft or spacecraft remote sensing best be used to quantitatively assess source areas for sediments?
- (5) What sorts of measurements can best be used to calibrate remotely sensed imagery?
- (6) How does sedimentation affect chemical properties of waters?

During the winter and spring of 1977, investigators met frequently to discuss and plan for the Sediment Runoff Experiment. During this period, operational procedures evolved and clearer estimates were developed about what data were needed by each of the various groups

- (1) Hydrologic Source Areas: Essential data in the watershed were color and color infrared aerial photographs acquired before, during and after a major storm event, to allow determination of extent of bare soils and nature and extent of ground cover throughout the watershed; rainfall measurements at a network of points throughout the watershed; and ground samples of runoff water taken during or soon after the storm. Stream discharge figures, acquired by the U.S. Geological Survey, were also deemed necessary.
- (2) Optical Characteristics of Sediments: Researchers involved in this aspect of the research needed spectral measurements of transmitted and scattered light, obtained during the experiment, and narrow band aerial photography of the test area. Laboratory and field experiments indicated that narrow band filters with center wavelengths of 4800, 5500, 6000 and 6500 angstroms (A)

and pass bands of 100 Å were needed. These were procured to fit our Hasselblad 80mm lenses. Test flights were made to evaluate the suitability of Kodak Type 2424 black-and-white infrared film, but with the 100 Å pass bands of the narrow band filters, exposure times were found to be too long for aerial photography. Exposures in excess of 1/125 second would have been needed, even with "pushed" film processing and maximal lens apertures. Therefore, it was decided to use only Kodak Type 2403 TRI-X film. With its very high speed and with "push processing," exposures times of 1/250 second were found to be suitable, fast enough that image blurring would not be a major problem. The inevitable graininess of "push processed" film was considered acceptable, and a necessary degradation.

- (3) **Mixing and Water Chemistry:** This group needed a procedure for sampling water quality within a sediment plume at known locations and at a variety of depths. Other data could be acquired by sediment traps located at various locations, sampled at intervals bracketing the major storm event. Conventional sampling techniques using boats deployed during the storm event were deemed suitable, provided some method was available to monitor location. In addition to gaining information on vertical mixing of sediments from the boat samples, plans were made for divers to obtain underwater photography to evaluate sediment concentrations and patterns. Laboratory studies were begun to investigate the mechanisms and characteristics of environmental conditions which affect vertical mixing and lead to (or permit) instabilities such as "mud fingering."

This section details the specific work done by each of these groups in preparation for the sediment runoff experiment, data collection procedures during the experiment, preliminary data analyses, and plans for further analysis and research. Section IV details the operations and coordination of the sediment runoff experiment.

C. Sources of Sediment Group

1. Introduction

Remote sensing of hydrologically active source areas has been one of the activities studied under past NASA support. This theoretical work is being applied to extend source area mapping techniques to the problems of remote detection and mapping of sources of sediment moving from a watershed into a lake. The investigation includes a cost-effectiveness comparison between computer analysis of remotely sensed imagery and human photo interpretation and field sampling methods. It complements research on non-point source pollutants in the Menomonee River Watershed, Detroit Metropolitan area, and elsewhere, being funded by the International Joint Commission. Non-point pollution refers to the pollution of water from diffuse sources, such as urban or agricultural runoff. Since sediment is itself a non-point pollutant, and many other non-point source pollutants contained in runoff are attached to suspended sediment particles, it is useful to concentrate efforts on monitoring sediments.

This group is also responsible for outreach between the Pheasant Branch project and potential user groups, the various political entities and governmental bodies concerned with land management within the Pheasant Branch Watershed.

2. Application of Remote Sensing to Quantification of Sediment Transport Processes

Computer models are frequently used to describe sediment transport processes in watersheds. To function, these models require different types of geographically referenced environmental data. Since land use or land cover information is usually a necessary input, remote sensing techniques can make an important contribution to sediment transport modeling. The land cover information required for sediment transport modeling varies for urban and agricultural watersheds. In urban watersheds the quantity and location of land covered with impervious surfaces is the most critical variable. However, crop types, crop management practices and soil conservation practices are the most important land cover factors in agricultural watersheds. While these are the most critical factors, gross land use or cover classifications are usually required for the entire watershed in both urban and agricultural sediment transport modeling.

The Dane County Regional Planning Commission (RPC) estimate of the soil loss from the Pheasant Branch Creek Watershed, using the Universal Soil Loss Equation (USLE) with data from "representative" subareas (1/4 sections) of the watershed (constituting about 28% of the watershed) for 1971-72 conditions, was reviewed. The USLE was developed for 20 year average annual soil loss estimates, hence its use for individual storms is questionable. In addition, use of USLE requires specification of a sediment delivery ratio (fraction of detached soil leaving basin) which, for a basin with varying land use and physiographic characteristics (as Pheasant Branch), should reflect these features as well as the channel system. In practice a constant value for a whole basin is used. Using aerial imagery throughout the year with basin topography and soils maps, the land use and basin physiography can be delineated for use in soil loss determinations from individual storms throughout the year. This work points to the need for a transport model approach for estimating soil loss to the lake from individual storms. The model would employ relations for soil detachment and transport by rainfall, overland runoff and channel flow along with information on land use and soil condition at the time of the storm. Relations for soil detachment and transport by rainfall and overland flow, based upon studies of small, homogeneous land parcels, are available. For a large, heterogeneous basin such relations would be applied to homogeneous subareas and coupled to a water runoff model, based either on the hydrologic source area concept or a traditional basin runoff model (e.g. SCS-TR20), such that the sediment loss from each subarea was routed to the basin outlet. Some work on simplifying Ishaq's hydrologic source area runoff model has been initiated.

Rainfall and channel flow data, which have been and are being collected by the Dane County RPC, USGS and SCE, have been obtained. This information will be used in the water and sediment runoff modeling effort.

It has already been used to estimate travel times for the surface runoff from the basin: 2-3 hours from the upper reaches of the basin to Highway 12, and 8-12 hours from Highway 12 to Lake Mendota.

Two subbasins in the northern and western portions of the watershed were identified for detailed sampling and analysis of precipitation and runoff (sediment and water). The northern basin was instrumented in late spring with a daily average and a continuously recording rain gauge. For several significant rain storms in late spring and early summer, sediment sampling and flow gear were used to gauge runoff from the two subbasins. As an example, on 30 July 1977 2.5 cm of rain fell in 1 hour (about 6 AM-7 AM) as recorded on the northern subbasin. However, no runoff occurred from the northern basin (about 400 hectare area). There was significant runoff from the western basin (about 600 hectare area). Sampling one hour after the rain ended gave a flow of about 0.14 m³/sec and a sediment concentration of about 1.4 g/liter. Through the City of Middleton there was a significant (5-fold) increase in sediment concentration (i.e. from Highway 12 to Century Avenue), probably due to channel erosion in the large channel drop through the city.

3. Imagery Currently Available for Analysis

The following imagery is or will be available for use in analysis of the land resource and land cover characteristics of the Pheasant Branch Watershed:

a. U.S. Soil Conservation Service Photography

Dates: 1962 and 1968

Scale: 1:20,000

Imagery Characteristics: black-and-white prints (9"x9")

b. NASA RB-57 High Altitude Imagery

1) Date: 4 July 1972

Scales: 1:60,000 and 1:120,000

Imagery Characteristics: Color infrared positive transparencies (9"x9")

2) Date: 31 July 1974

Scale: 1:120,000

Imagery Characteristics: Color infrared positive transparencies (9"x9")

c. Project Imagery

Dates: 3 September 1976

26 September 1976

28 April 1977

18-19 July 1977

15 August 1977

3 October 1977

6-13 November 1977 (scheduled)

1978 (as appropriate)

Scale: 1:60,000

Imagery Characteristics: color and color infrared positive transparencies (70mm)

d. LANDSAT Digital Data and Imagery

Several dates of imagery and digital tapes are available on campus. Additional data are available from the EROS Data Center.

4. The Pheasant Branch Data Bank

The Pheasant Branch Data Bank has been developed to store and manipulate the physiographic, soil, land cover, agricultural, and other information necessary for sediment yield and sediment transport modeling. Figure 5 shows the outline of the Pheasant Branch Watershed with a one-hectare grid superimposed. The basic grid cell for the data bank is one hectare, based on the UTM system, and the watershed contains 6,136 one-hectare grid cells. As shown in Figure 6, there are 969 hectares of "non-contributing areas", depressions in the landscape where runoff percolates into the ground, feeding the ground water, rather than flowing over land into the channels of the Pheasant Branch drainage system. The net area of the Pheasant Branch Watershed which drains into Lake Mendota (subtracting out the non-contributing areas) is 5,167 hectare (all cells shown as dots in Figure 6 contribute to the Pheasant Branch surface drainage).

The capabilities of the Pheasant Branch Data Bank must be considered before data collection efforts are begun. The computer can store only one value per grid cell for each individual data variable. However, there is no practical limit to the number of individual data variables which can be stored in the computer file. Consequently, data concerning an individual terrain characteristic, such as topographic slope, can be encoded in a variety of ways if desired.

For data collection purposes, transparent overlays of the grid cell network can be placed on either base maps or aerial photographs. Data collection proceeds on a cell-by-cell basis. Data can be recorded in terms of predominant type within a cell, percent of cell of a particular type, or average value within a cell. The data values for each data variable must be encoded into one of not more than ten classes (stored in the computer as 0 through 9). The data collection methods and the data encoding system both reduce data complexity in order to facilitate more efficient computer calculations. The computer can produce grid cell map for each variable printed in either numeric or computer overprint form. With the computer overprint system, each encoded value is automatically printed as a symbol of a particular density. Very dense overprint symbols correspond to high encoded values. Both manual photo interpretation and computer interpretation techniques have been and/or will be utilized in analysis of the available imagery.

Two land/water classification systems were developed to provide a mechanism for gathering land cover information on a basic and expanded level. When the basic land/water classification system is used, the

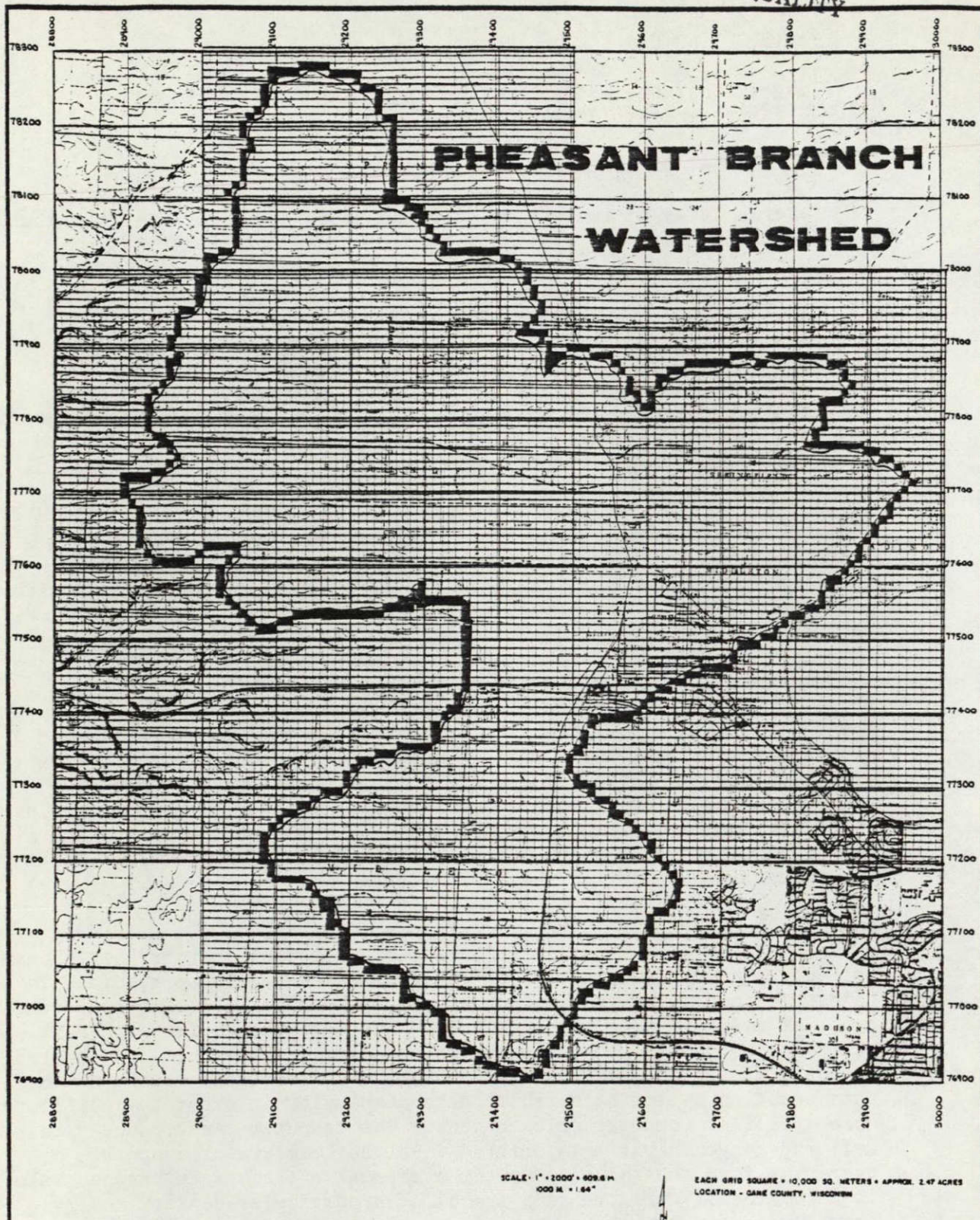
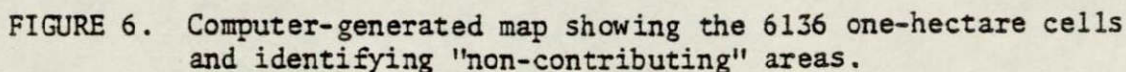


FIGURE 5. Pheasant Branch Watershed with one hectare grid superimposed.

VARIABLE NO.	VARIABLE NAME	NO OF CELLS FOUND	CONVERTED TO ACRES	JJOGEMENT	REVERSED
28	NONCONTRIBUTING AREAS	4-136	15.155-32		



following five interpretations are made and recorded for each grid cell:

- (1) Predominant cover within a cell;
- (2) Percent of cell which is open water;
- (3) Percent of cell which is forested lands;
- (4) Percent of cell which is open lands;
- (5) Percent of cell which is impervious surfaces.

The predominant cover interpretations are coded according to the system shown in Table I.

The predominant cover classification system is designed to make effective use of the capabilities of the Pheasant Branch Data System, i.e. an individual computer overprint map can include up to ten classes. The specific classifications utilized in the above system are comprehensive and not subject to seasonal change.

The expanded land/water classification system is designed to permit detailed classification of land cover specific to the time of overflight. When the expanded land/water classification system is used, percent of cell in all categories is recorded. The following classes are included in the expanded land/water classification system:

- (1) Open Water
 - a. open water
- (2) Forested Lands
 - a. forested lands
- (3) Open Lands
 - a. non-forested wetlands
 - b. grassland
 - c. lawns
 - d. gravel pits
 - e. quarries
 - f. bare soil
 - g. row crops
 - 1) corn
 - 2) peas
 - 3) soybeans, etc., as needed

h. small grain

- 1) oats
- 2) barley
- 3) wheat, etc., as needed

i. legumes/rotation meadow

- 1) permanent hay
- 2) rotation meadow

j. fallow

(4) Structured or Built-Up Lands

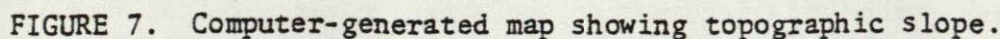
- a. bare soil
- b. farm buildings
- c. single family residential
- d. multiple family residential
- e. commercial
- f. institutional
- g. industrial
- h. unpaved roads, etc.
- i. paved roads, etc.
- j. railroad tracks

The expanded land/water classification system can be used to develop overprint maps in each of the four major land cover categories, i.e. open water, forested lands, open lands and built-up lands.

The data items (or "variables") presently (October 1977) stored in the Pheasant Branch Data Bank are listed below (see Tables II through IV). A considerable number of additional data items will be added during 1977-78, especially interpretations of land cover and other data using photographic and satellite data sources.

Figures 7 through 12 illustrate some of the data items in the Pheasant Branch Data Bank. Table V lists the value of the data item corresponding to each code number printed out in Figures 7 through 12. Figure 7, for example, shows the percent slope in each cell of the data bank, classified into one of 10 levels (0-9). Level 0 represents a 0 percent slope and is shown by the symbol ".", level 1 represents a 1-2 percent slope and is shown by the symbol ",", level 2 represents a 3-4 percent slope and is shown by the symbol "+", and so on, for a total of 10 levels. Note that data from three sources are shown in these figures. The data source for Figures 7 and 12 is USGS topographic maps, the data source for Figure 8 is USDA-SCS soil maps, and the data source for Figures 9, 10 and 11 is interpretations using RB-57 color infrared photography.

Since interpretations are formatted in the data bank, it will be possible to readily compare data extraction by various means. For example, a CROSSTAB program can be run on the computer to compare on a cell-by-cell basis information about tree cover obtained from USGS topographic maps (Figure 12) with information about tree cover interpreted from 1:120,000 RB-57 photographs (Figure 11). In a like manner, variables 37 (tree cover from 1:60,000) and 38 (tree cover from

[illegible]

ORIGINAL PAGE IS
OF POOR QUALITY

FIGURE 8. Computer-generated map showing Soil Loss "K" Value.

VARIABLE NO.	VARIABLE NAME	NO OF CELLS FOUND	CONVERTED TO ACRES	JJGEMENT	REVERSED
14	PREDOMINANT COVER 12000	8.136	15.158-22		

[illegible]

ORIGINAL PAGE IS
OF POOR QUALITY

FRQUENCY	27.03	106.00	118.00	612.00	23.00	4830.00	97.00	11.00	56.33	33.00	.00
*****	*****	*****	*****	*****	*****	*****	*****	*****	*****	*****	*****
*****	*****	*****	*****	*****	*****	*****	*****	*****	*****	*****	*****
*****	*****	*****	*****	*****	*****	*****	*****	*****	*****	*****	*****
*****	*****	*****	*****	*****	*****	*****	*****	*****	*****	*****	*****
*****	*****	*****	*****	*****	*****	*****	*****	*****	*****	*****	*****
SUM RANGE	7.03	1.33	2.00	3.00	4.00	5.00	6.00	7.00	8.00	9.00	10.00

FIGURE 9. Computer-generated map showing Predominant Land Cover Type interpreted from 1:120,000 CIR airphoto.

TEST OF NEW FORM OF PHEASANT BRANCH DATA AREA

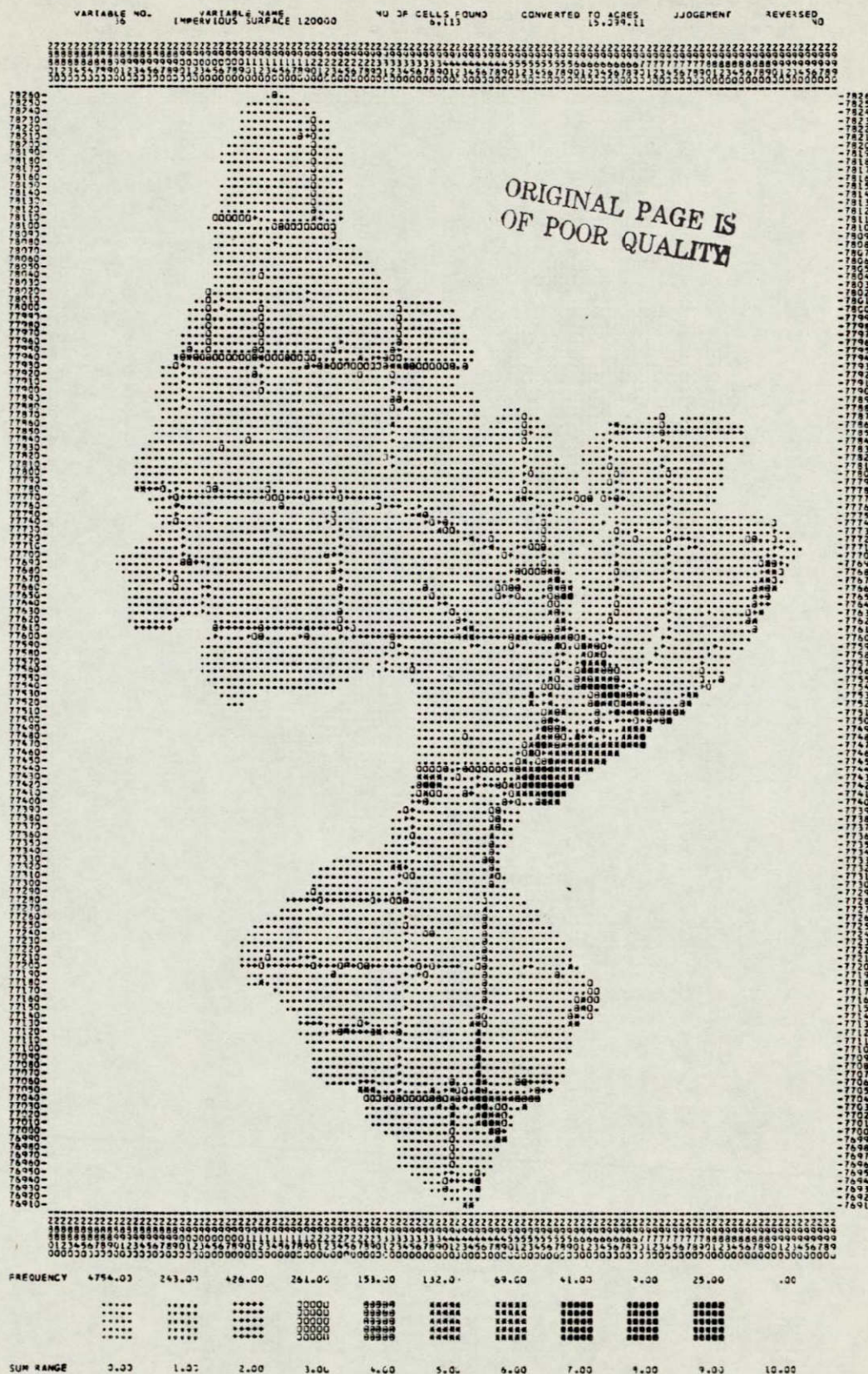


FIGURE 10. Computer-generated map showing amount of Impervious Surface in each cell interpreted from 1:120,000 CIR airphoto.

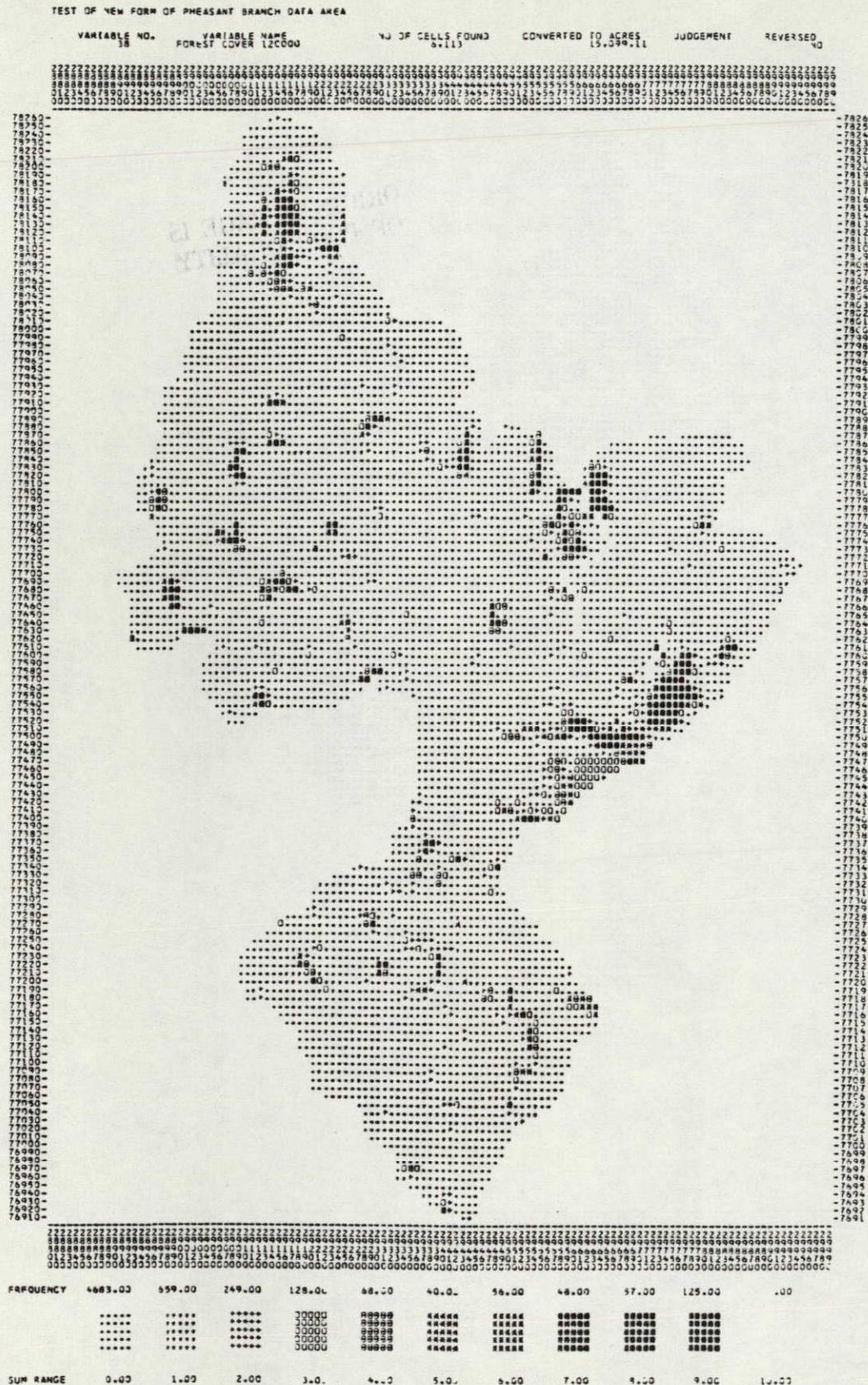


FIGURE 11. Computer-generated map showing amount of Forest Cover in each cell interpreted from 1:120,000 CIR airphoto.

TEST OF NEW FORM OF PHEASANT BRANCH DATA AREA

VARIABLE NO.	VARIABLE NAME	NO OF CELLS FOUND	CONVERTED TO ACRES	JUDGEMENT	REVERSED
33	TREE COVER U.S.-G.S.	2,113	15,239.11		40

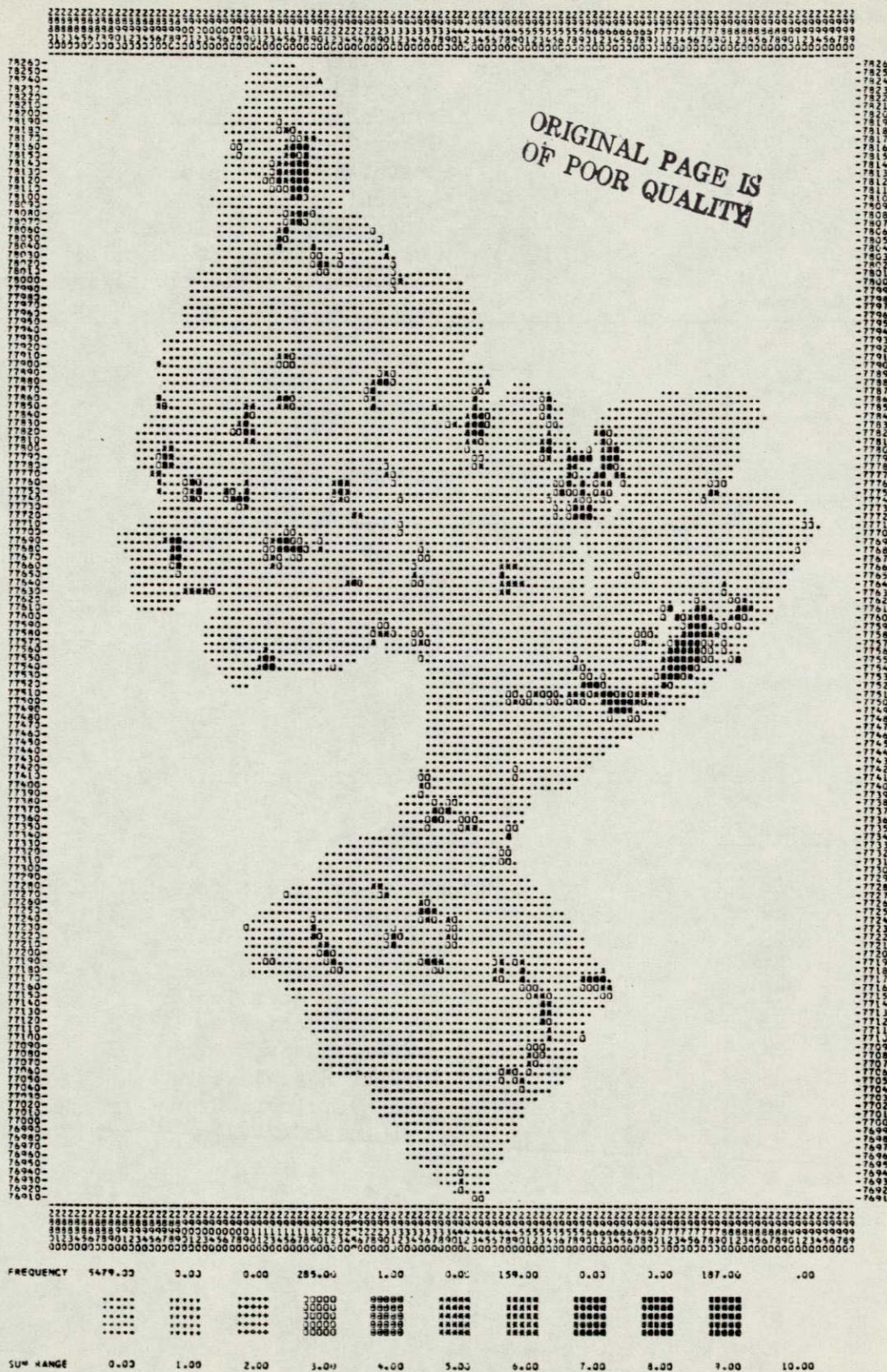


FIGURE 12. Computer-generated map showing amount of Forest Cover in each cell extracted from USGS topographic map (green overprint).

TABLE I. Predominant Land Cover Classification System.

<u>Code Number</u>	<u>Land/Water Class</u>
0	Open Water
1	Forested Lands
2	Non-Forested Lands
3	Other Open Lands
4	Gravel Pits/Quarries
5	Agricultural Lands
6	Single Family Residential
7	Multiple Family Residential
8	Commercial/Institutional/Industrial Development
9	Roads and Parking Lots

TABLE II. Data Derived from USGS Topographic Maps.

Variable 28: Non-Contributing Areas
 Variable 39: Tree Cover (green overprint)
 Variable 40: Watershed Boundary
 Variable 42: Topographic Slope

TABLE III. Data Based on USDA-SCS Soil Survey Information.

<u>Variable</u>	<u>Class</u>
18	USCS Soil Class (at 150cm depth)
19	Depth to Bedrock
20	Flood Hazard
21	Soil Drainage Class
22	Depth to Water Table
23	Corn Productivity
24	Hay Productivity
25	Surface Soil Texture
26	Soil Hydrologic Group
27	Soil Loss "K" Value

1:120,000) can be readily compared and evaluated.

5. Universal Soil Loss Equation Analysis

The Universal Soil Loss Equation (USLE) can be used to assess the soil erosion potential of agricultural watersheds. Traditionally, extensive field studies are required in order to use the USLE. As a consequence, soil erosion potential of watersheds is infrequently assessed and trends over time are inadequately understood. Many sediment transport models for agricultural watersheds use the USLE as a subroutine. Cooperative research was conducted with Ken Morgan, Ph.D. student in Land Resources at the University of Wisconsin-Madison, to develop a methodology for utilizing the USLE with remote sensing as a primary data source. Table VI lists the various factors in the USLE and the method of data collection utilized in our experimental methodology. Remote sensing is used to monitor and/or provide a basis for determining crop types, crop management practices, soil conservation practices and land use.

In 1975 the Dane County Soil and Water Conservation District and the Dane County Regional Planning Commission conducted a detailed study of the Pheasant Branch Watershed using traditional USLE methods. In this study randomly selected quarter sections within the Pheasant Branch Watershed were ground-truthed extensively and statistical methods were used to estimate land uses in the total watershed. For comparative purposes, we used manual photo interpretation techniques, RB-57 imagery and project imagery to monitor land uses in the previously sampled quarter sections and statistically estimate total land use for the watershed. Table VII summarizes the results of this comparison. In addition, a simple selective key was prepared for the USLE land use classification system. Table VIII shows this key. —

Crop types growing in the Pheasant Branch Watershed were ground-truthed during the spring and summer of 1977. A simple crop identification key was prepared after analysis of project imagery and ground truth information. This key is shown in Table IX.

Manual photo interpretation techniques using imagery of the most appropriate data and film type were used to identify the percent of each cell in corn, oats and permanent hay. This information is not yet in the data bank. Consequently, no comparison with the 1975 USLE study has been done to date. This comparison will be completed in the future. Photo interpretation techniques and computer interpretation techniques will be explored further to determine if the number of overflights necessary to accurately monitor crops can be reduced.

Soil conservation practices, i.e. contour tillage, strip cropping, grass waterways, etc., are easily monitored because of their characteristic patterns. A key is in preparation.

6. Hydrologic Source Area Identification

Using the criteria developed by Ishaq, aerial color infrared imagery from 4 July 1972 was examined with a spot microdensitometer to

TABLE VI. Factor Value Information to be Collected.

Factor	Information	Collection Method	Data of Photography
K	Soils	Soil Survey	Not applicable
LS	Topography	Topo Maps	Not applicable
C	Tillage	Remote Sensing	Spring
	Rotation		Summer
	Plowing		Late Fall
	Residue		Late Fall
P	Contour	Remote Sensing	Summer
	Strip		
	Terracing		
	Grass Waterways etc.		

TABLE VII. Land Use Comparison in Pheasant Branch Watershed
Values Expressed as a Percent (%).

Land Use	1972 RB-57 1:120,000	1975 RPC Inventory	1977 Low Alt. Color 1:60,000	Relative Change
Cropland	79.6	78.1	78.9	(-)
Forestland	5.9	3.5	4.5	(-)
Rangeland	8.9	7.7	7.4	(-)
Urban Land	4.1	6.9	7.2	(+)
Misc.	1.5	3.8	2.0	

ORIGINAL PAGE IS
OF POOR QUALITY

TABLE VIII. Key for Land Use Identification.

Land Use	Characteristics	Spectral Response	
		1972--CIR	1977--Color
Cropland	Cultivated fields used for crops	Square fields, bluish or bright red color	Square fields, shades of greens, yellows
Forestland	Abundance of tree canopy	Reddish clumps, Coarse texture	Green clumps, Coarse texture
Rangeland	Wildlife and pasture areas	Purplish tones, often irregular shape	Light greens, irreg. boundaries
Urban Land	Subdivisions, stores, etc.	Distinctive light & dark tones from roofs	Distinctive tones from roofs
Misc.	Roads, farmlots, etc.	Recognized by tones & shapes	Recognized by tones & shapes

TABLE IX. Crop Identification Key.

Crop Type	Tone	Date/Film Type
Corn	dull blue-green	15 August 1977/color positive transparencies
Oats	yellow	July 1977/color positive transparencies
Permanent Hay	bright red	28 April 1977/color infrared positive transparencies
Hay	bright green	15 August 1977/color positive transparencies

determine the presence of source areas. Areas chosen for examination were suspected source areas, based upon soil properties and topography. Although it had not rained for several days prior to the imagery, most of the areas examined would be "potential" source areas based upon Ishaq's criteria. Further work is needed to correlate source areas to soil properties, land cover and use, and topography and to delineate the hydraulic connection of these potential source areas to the stream channel.

7. Involvement with Sediment Runoff Experiment (July 1977)

To provide advance warning for when the sediment runoff experiment (SRE) could occur, 24 hour precipitation forecasts were obtained from a student in the Meteorology Department and from local weather stations. Plans were made to monitor, cooperatively with the USGS, water and sediment runoff at several locations within the basin and at the stream outlet into Lake Mendota. To delineate the hydrologic source areas and land cover, it was decided to obtain color IR and color aerial imagery on the day of the SRE storm and 1-2 days afterwards.

Measurements of sediment concentration and water flow were obtained at various locations within the basin and at the basin outlet during the SRE and the following days. Continuous measurements of flow and sediment concentration were obtained at Highway 12 by the USGS. Periodic samples of flow and sediment concentration were obtained by the USGS and our group at the creek outlet into Lake Mendota, at the Century Avenue Bridge (prior to entering the marsh), on the north and south branches of the creek above Highway 12, and on the outlets from the northern and western subbasins mentioned above. A continuous record of the precipitation was obtained. Aerial imagery for the watershed was obtained at the time of the SRE.

The above data, after suitable reduction, needs to be analyzed to determine: sediment and water discharges within and from the watershed throughout the runoff period, and hydrologic source areas (from the imagery). Subsequently, attempts will be made to correlate the sediment discharge to land and water runoff conditions; the concept of sediment source areas will be examined. Finally modelling of the sediment and water runoff for the SRE conditions will be attempted, along the lines discussed above and in the 1977-78 proposal.

8. Coordination with Involved Agencies

As detailed below, various political bodies and governmental agencies concerned with non-point source pollution planning and land management in the Pheasant Branch Watershed have been identified. Those groups presently conducting research in the watershed were contacted early in the study to determine if any coordination was appropriate. The USGS Surface Water Branch and the City of Middleton are jointly funding research in the Pheasant Branch Watershed. This group will utilize our land cover information and provide useful information to the Pheasant Branch project in return. All groups contacted were interested in the results of the research. Another round of contacts will be

made in the near future to keep groups informed of interim results.

The following agencies have been contacted

- (1) United States Geological Survey, Surface Water Branch,
City of Middleton Water Resources Council

The USGS-Surface Water Branch and the City of Middleton Water Resources Council are involved in a joint study of non-point source pollution within the Pheasant Branch watershed and stream channel erosion processes within the Pheasant Branch River. The purpose of this study is to aid the City of Middleton in assessing the impacts of alternative land management and planning policies. A cooperative relationship has developed between this study group and the Remote Sensing Program research group. For example, Remote Sensing Program researchers will gather land cover information needed by the USGS/City of Middleton researchers will provide information to the Remote Sensing Program researchers regarding subwatersheds within the watershed and will also provide some flow/sediment information from USGS monitoring stations.

- (2) United States Soil Conservation Service

The SCS provides technical assistance to farmers on request. The SCS is interested in Remote Sensing Program research. The imagery and land cover information are of potential utility for SCS purposes.

- (3) Wisconsin Department of Natural Resources

The DNR has completed a simple sediment transport model of the Pheasant Branch watershed as part of a larger study of non-point pollution in the Lake Mendota drainage basin. DNR is interested in using the more detailed data being gathered by the Remote Sensing Program researchers.

- (4) Wisconsin Soil and Water Conservation Districts

These agencies are interested in the educational value of the Remote Sensing Program research being conducted in the Pheasant Branch watershed.

- (5) University of Wisconsin Extension Resource Agent

University of Wisconsin Extension Resource Agents provide technical assistance and education in support of better community planning. The Dane County Resource Agent is interested in the educational value of the imagery collected and research conducted by the Remote Sensing Program.

- (6) Dane County Water Quality Planning Agency, Dane County
Regional Planning Agency

The Dane County Regional Planning Commission and the Dane County Water Quality Planning Agency are involved in research and planning activities regarding non-point pollution mandated by Section 208 of Public Law 92-500. Ground sampling methods developed by the

U.S. Soil Conservation Service were utilized to gather land resource information needed for input into the Universal Soil Loss Equation. Staff planners expressed strong interest in the land cover information which will be gathered by Remote Sensing Program researchers. At present, staff planners use statistical techniques to project land cover data from limited ground sampling data. Staff planners are also interested in reviewing other information and research conducted by Remote Sensing Program researchers.

The following agencies will also be contacted

- (a) Dane County Board of Soil and Water Conservation Districts
- (b) City of Middleton
- (c) Town of Middleton
- (d) Town of Springfield

D. Sedimentation Concentration Group

The goal of this portion of the research is to determine how photographic imagery is affected by various types and concentrations of sediment in lake water. Light penetrating the water undergoes absorption and scattering by the water itself, as well as by particles within the water. Detection of sediment in the water is accomplished by observation of the light scattered back to the camera by the sediment particles.

The scattering and absorption of light by water or sediment particles are wavelength dependent processes. Shorter wavelengths (blue and green) penetrate farther into the water, yet are scattered more highly by the water itself than the longer wavelengths. Sediment particles scatter all wavelengths much more highly than water. Therefore, the exposure produced by silt-laden water will be higher than that produced by clear water, particularly in the red wavelengths.

Due to the high absorption in the red wavelengths by water, the back-scattered red light detected by the camera will have come from the surface or near surface water. By observing the backscattered green and blue wavelengths it may be possible to obtain information concerning sediment deeper in the water. It must be noted, however, that the atmosphere is a source of scattering also, particularly for the shorter wavelengths. Thus exposures obtained in the shorter wavelengths will be increased by the backscattered skylight. Exposures obtained in the longer wavelengths will be at least affected by atmospheric scattering.

1. Theoretical Models

To glean useful information from photographic imagery, it is necessary to understand the interactions of light with air, water, and sediment. Personnel in the Meteorology Department have considerable experience

in developing models of the passage of light through the atmospheric hazes [1,2]. The scattering and absorption processes involved are generally similar to those occurring in the water. A model has been developed to include the water and air layers, with appropriate changes to account for the air-water interface. Using this model and incorporating the appropriate air and water parameters measured during the event, it is possible to compute the intensity in a spectral band coming from the lake, and eventually incident on the camera lens. Appendix III gives mathematical details.

2. Equipment and Methods

a. Imagery

The effects of air, water and sediment on exposure can best be explored and untangled from each other by observing the back-scattered light in several bands centered at advantageous wavelengths. The wavelengths were chosen to (1) obtain maximum penetration of light in clear water (480 nm), (2) to detect light scattered by algae (550 nm), and (3) to detect light scattered by sediment on or near the surface (600 nm and 650 nm). Narrow band interference filters (10 nm bandwidth) centered at the above wavelengths were obtained for use with four 80mm lenses on the Hasselblad camera system. The cameras were mounted to view the same scene, so simultaneous exposures in the four wavelength bands could be made.

To obtain accurate exposure data, the radiometric properties of the lenses, filters and film must be known. Black-and-white Tri-X film (2043) was chosen for its speed and stability. The radiometric properties of the film are well known. Step wedges are used to calibrate the film during the developing process (done by Precision Photo Inc., Dayton, Ohio). Using data supplied by Precision Photo Inc., absolute exposures can be calculated for the film densities. The lenses themselves also affect the exposure. This effect, known as lens falloff, is generally assumed to vary as $1/\cos^3\theta$ (θ is the angular displacement from the optical axis). The actual falloff will be measured at Johnson Spacecraft Center in the near future, and incorporated into the exposure calculations. The filter transmission characteristics also affect the exposure. Spectral transmission curves have been obtained for the filters, and will be employed in the exposure calculations.

One goal of the project is to determine the spatial extent of the sediment-laden water, and produce contour maps of sediment concentration. Thus it is necessary that the cameras be calibrated for photogrammetric calculations. Fiducial marks were filed into the magazines, and are imaged onto every frame. The distance between these marks will be measured accurately so they can serve as control points on the image.

b. Scattering and Extinction Measurements

During the development of the model, it became evident which parameters must be measured. These parameters are the water and air scattering and extinction of light as a function of wavelength and concentration or type of suspended particles. The atmospheric attenuation was to be measured using a calibrated pyroheliometer and a flux photometer to observe the direct sunlight and diffuse skylight incident on the ground. Grey panels of known reflectance were also to be placed in the water during the event. These panels and grey areas on shore -- such as rooftops and streets -- were to be photographed at low altitudes at the beginning of the data acquisition. From this the reflectance of the rooftops and streets would be calculated. Then the rooftops and streets would be used as secondary "reflectance panels" for the higher altitude imagery (since the panels would be too small to be imaged). These features of known reflectance can later be used to deduce the light intensity incident on the water surface. The LIDAR system in the Meteorology Department was also to be used to obtain profiles of the haze in the atmosphere, revealing the elevation of a haze layer or stratus deck. The data can then be used to deduce information about the scattering properties of the atmosphere.

It was essential that a method be found to measure the scattering and attenuation of the water as a function of wavelength. It is highly desirable to measure these parameters in situ, as water samples may change en route to the lab and while awaiting analysis. A transmissometer-nephelometer was purchased for this purpose. The instrument can measure the extinction of the light by water over a changeable path of 1m, 1/3m or 1/10m. It was equipped with interference filters designed to select the same wavelengths as the camera filters. It was possible to change the filters easily while on the boat. The instrument was also equipped with a sensor to detect light scattered at 90° from the incident beam. It was not possible to mount the spectral filters over the scattered light detector, however. As a check on the transmissometer measurements, it was decided to also use a spectrometer to measure extinction coefficients for water samples brought back to the laboratory for other analysis.

The scattering properties of sediment-laden water are important parameters in the radiative transfer model. In particular, it is desired to know the total scattering coefficient and the scattering phase function, which is a measure of the angular scattering of light. The spectral dependence must also be known in order for these to be useful in analyzing the multi-bank imagery.

The measurement of scattering phase functions is usually accomplished with a nephelometer. A nephelometer is an instrument equipped with a collimated light source and a movable photodetector which can detect light scattered at various angles. It is highly desirable to measure the scattering phase function in situ. However, the cost of these instruments is prohibitively high. In fact, to our knowledge, none are manufactured commercially.

Therefore, we had to settle for a laboratory-based nephelometer, also a very expensive apparatus. Several months were spent in an effort to build our own nephelometer, but stray light and sensitivity problems were overwhelming. This effort was abandoned when Dr. Phillip Cohen (Physiology Dept., UW-MSN) graciously offered us the use of his Brice Phoenix Light Scattering Photometer.

The Brice Phoenix Photometer can measure scattering from 30° to 135° . The light source is a mercury vapor lamp. To obtain spectral information the yellow (578 nm), green (546 nm), and blue (436 nm) lines can be isolated using special filters. The photometer has been used extensively with great success to measure scattering phase functions of various solutions. In particular, Dr. Hasong Pak (Oceanography Dept., Oregon State University, Corvallis, Oregon) has used a ship-based Brice Phoenix Photometer to measure the scattering of ocean water [3,4]. The main problem in using the scattering photometer is to obtain an absolute calibration for the scattered intensity. Pak *et al.* use a standard reference opal to accomplish this. Several researchers in physical chemistry suggested the use of Ludox (duPont), a colloidal silica, for which the absolute scattering can be calculated using Rayleigh theory. The photometer is calibrated by comparing the calculated to the measured scattering.

The calibration with Ludox is nearly finished. The data necessary to obtain a calibration by the method of Pak *et al.* is routinely taken with every set of measurements. A further check on the calibration will be obtained by measuring the scattering off Latex spheres. The size distribution of the spheres has been measured by Kirk Morgan (Geology Res. Asst., UW-MSN) using a Coulter Counter. With this information, Mie Scattering calculations can be run using programs developed in the Meteorology Department. These can be compared to the scattering calculated from the measured values and the Ludox calibration data to validate the calibration.

The photometer was to be used to measure the scattering of water samples brought back for analysis. The samples would be diluted successively with distilled water to obtain data on the dependence of scattering on concentration. Scattering would also be measured at the three wavelengths selected by the filters on the photometer.

3. Data Acquisition and Preliminary Discussion of Results

On 16 and 17 July 1977, a heavy rain sufficient to cause extensive runoff occurred. The following week was devoted to acquiring the necessary data as proposed. Overflights of the plume were made every day through 22 July. Color and color IR photographs were acquired in addition to the black-and-white narrow band photography. On 19 and 21 July, intensive water sampling was conducted simultaneously with the photography. On 18 and 20 July a few water samples were gathered and some water transmission readings obtained with the transmissometer.

a. Imagery

Most imagery was acquired at altitudes between 4000' and 6000' AMT (above mean terrain). The purpose of flying this high was to get a substantial portion of the plume and some shoreline in every frame. On several days heavy haze and slight to moderate overcast forced the aircraft to fly at lower altitudes. Test rolls were exposed on 23 July. These were to be cut up and subjected to various processing speeds. The results indicated a processing of 8 ft/min (2 tanks) was suitable. The event imagery was then processed at Precision Photo Lab as indicated. Stepwedges were placed on each roll of film. Problems had been encountered with placing stepwedges in portions of the film subject to light leaks, so stepwedges were also placed on separate pieces of unexposed film and run through the processor with the rolls themselves. Visual inspection of the film indicated that, as expected, the blue filter images exhibit less contrast and appear washed out due to atmospheric scattering by haze. The plume is well defined in the red images, and in some cases in the green images. Some rolls exhibit severe light leaks, probably a result of poorly closed film cassettes. However, there appears to be ample imagery for analysis with complete stepwedge calibration.

b. Meteorological Data

Complete atmospheric data was acquired on 19 July 1977. Pyroheliometer and incident flux measurements were made all morning every hour by David Lengyel (Meteorology student, UW-MSN). Lidar scans were obtained by Scott Shipley (Meteorology graduate student, UW-MSN) until late morning when the tape drive on the Lidar system broke down. The data set appears to be complete, but it has not been analyzed yet. An absolute calibration of the pyroheliometer response has been obtained and will be used to determine incident intensities. No atmospheric data were acquired on 21 July 1977 due to equipment failure.

The reflectance panels were deployed every day during the photography. The panels were designed to float on top of the water. However, it was evident from the dirt deposited on them that they were underwater at times. Because of this their reflectances and thus data extracted from them were not reliable. When the runoff events were over, the panels were cleaned and set on the ground while overflights were made of panels and rooftops. The panel reflectances were remeasured by photographing them on the ground with a standard grey card. These data have yet to be analyzed.

c. Water Measurements

In situ transmissometer measurements were acquired on all days. The transmissometer filters could not be used, however, because the turbid water attenuated the light too much. The nephelometer was also found to be useless due to the high intensity of multiply scattered light within the sediment itself. Transmissometer readings for both 1/3m and 1m path lengths were obtained wherever possible. To supplement the data, spectral absorbance measurements

were made in the laboratory water on several samples using a Beckman DU Spectrophotometer. The data have not been analyzed

Scattering measurements were made on successively more dilute solutions of several samples. The uncalibrated phase function appears similar to those found in the literature. These data will be analyzed when calibration of the photometer is completed.

4 Proposed Analysis

Selected frames of the imagery showing good contrast and detail will be digitized using the Optronics scanning densitometer. The densities will be converted to absolute exposures which will then be corrected for radiometric effects such as lens falloff. Computer programs for overlaying images have been developed and will be used to overlay images acquired simultaneously through the different filters.

One of the goals in developing the radiative transfer model is to find a functional relationship between light exiting from the water and sediment concentration. Most previous studies have assumed that there is a linear relationship between concentration and reflected light. No other investigations have attempted to find a functional relationship between reflected energy and the combination of concentration, viewing and solar zenith and atmospheric turbidity.

Two models will be studied. One will consist of assuming a linear relationship between sediment concentration and exposure in each waveband. Contour maps of sediment concentration will be prepared. The second, a radiative transfer model developed during this project, predicts the intensity of light coming from the lake water. Water sampling data and atmospheric data will be fed into this model, and the expected exposures on the film calculated for several points in the plume. If possible, a functional relationship between concentrations of sediment and intensity will be developed. The relationship determined by the model will then be used to predict sediment concentrations at various other points in the plume.

Finally, the relative value and success of the two models in predicting sediment concentrations will be compared.

E. Mixing and Water Chemistry

1. Vertical Mixing of Sediments

a. Background

A vertical transport mechanism which has received some attention in the past decade has been that of "salt fingering." This mechanism can best be pictured by considering a situation whereby warm salty water overlies fresh cold water. Since the warm salty water is buoyant, the system is gravitationally stable; there is a mean density increase downward.

If a parcel of warm salty water is displaced downward, it will lose heat much faster (~100 times) than it will lose salt. This parcel is then heavier than its neighbors, but remains quasi-suspended due to the relatively slow diffusivity of salt. This will result in a "salt finger" extending through the interface into the cold water [5]. In an analogous manner, "mud fingers" may be formed by having warm sediment-laden water overlie cold fresh water. In this case, sediment is transported downward through the interface faster than may initially be expected.

b. Field Studies

The attempt to observe the "mud fingering" phenomenon in the field has been somewhat disappointing. Due to the exceptionally dry spring and gradually warmer weather, it was generally felt that conditions in the field were not commensurate with those found necessary in the lab to invoke this type of convection. Nevertheless, during the sediment runoff experiment an attempt was made with the use of two scuba divers and an underwater camera to photograph possible fingering in the plume. It seems the small temperature difference between the sediment plume and the lake, the fact that small fishing boats had traversed the plume, and changes in wind and, therefore, plume direction all may have contributed to the reason why fingering was not observed in this attempt. It was still felt that this phenomenon can be observed in the field under the proper conditions, i.e. when the lake water is still cold as in the early spring or in the harbor of a cold lake such as Lake Superior. Later this fall, towards the end of October or beginning of November, when Wisconsin usually has its "Indian Summer," another attempt will be made to observe "mud fingering" in the field. This time, however, a quiet, secluded site will be chosen with pictures to be taken by one person wading into a shallow portion of the lake instead of with scuba divers. The first efforts provided good experience on how an attempt to photograph "mud fingering" in the lake should proceed. It is hoped this past experience will help in the coming mission to photograph and eventually quantify the "mud fingering" instability in the field.

c. Laboratory Studies

In the laboratory, a tank study is being undertaken to parameterize the occurrence of "mud fingering." A tank which simulates a two-dimensional warm water sediment-laden surface discharge or runoff onto a body of cold water is being used. A time sequence of photographs taken through the side of the tank with thermistor and thermocouple probes to measure temperature changes and gradients help quantify what is occurring. With various sediment sizes and concentrations, the mass fluxes as a function of temperature, time and location in the plume are being determined. Although some instrumentation problems have hindered progress, it appears that the initial problems, particularly those of lighting for the photography and probe time response, have been overcome. Some particularly interesting facets of this study have been observing the onset of fingering, its effect on the plume front, and the effect of the surface shear flow on the fingering. It is hoped that results in

addition to those strictly relating to the vertical sediment transfer as pertaining to the remote sensing of water resources, e.g., the shape of the plume front under different conditions, will be realized.

2. Water Chemistry

a. Introduction

In surface runoff waters, phosphorous that had previously been bound to soil particles by sorption or electrostatic interaction may be released into solution. The primary objective of the water chemistry group is to estimate the amount of phosphorous released from suspended sediment prior to sedimentation. Secondly, the phosphorous release rate and chemical factors affecting this rate will be examined. Finally, remote sensing will be used to augment the in situ data and evaluate sampling techniques.

b. Methods

The portion of Lake Mendota involved in the sampling program is illustrated in Figure 13. Sampling sites located along transects 1 and 3 and the creek site were sampled on 19 and 21 July during an exceptionally heavy runoff event. Vertical profiles consisting of a near surface (wrist deep), a deep (1 m above the bottom), and an intermediate sample (half the depth of the corresponding deep sample) were collected from all sampling sites with the exception of transect 2. Only near surface samples were collected from transect 2 on 19 July and none at all on 21 July. The deep site was sampled only on 21 July

Three motorboats were used to collect water samples. The approximate locations of sampling sites were determined by means of marker buoys. On-shore surveyors recorded the exact position of boats during a sampling interval. Boat crews and surveyors were coordinated such that a new site was sampled every 15 minutes.

Prior to laboratory analysis, samples collected on 19 July were stored in 10% HNO_3 -washed polyethylene bottles while samples collected on 21 July were stored in new, untreated polyethylene bottles. All samples were stored at 8°C. Filtered and unfiltered samples were stored under identical conditions.

Analyses have been completed for eight parameters, including turbidity, suspended solids, conductivity, chloride, dissolved reactive phosphorous (DRP), total dissolved phosphorous (TDP), 1N acid extractable phosphorous (AEP), and total phosphorous (TP). With the exception of suspended solids and AEP, all parameters were measured using techniques from Standard Methods [6]. Suspended solids were determined by filtration of 50 ml of sample through an oven-dried pre-weighed 0.4 μm polycarbonate filter. The filter is air-dried, oven-dried overnight at 55°C, and weighed on a micro-balance. The filtrate was stored at 8°C for 20 days and then

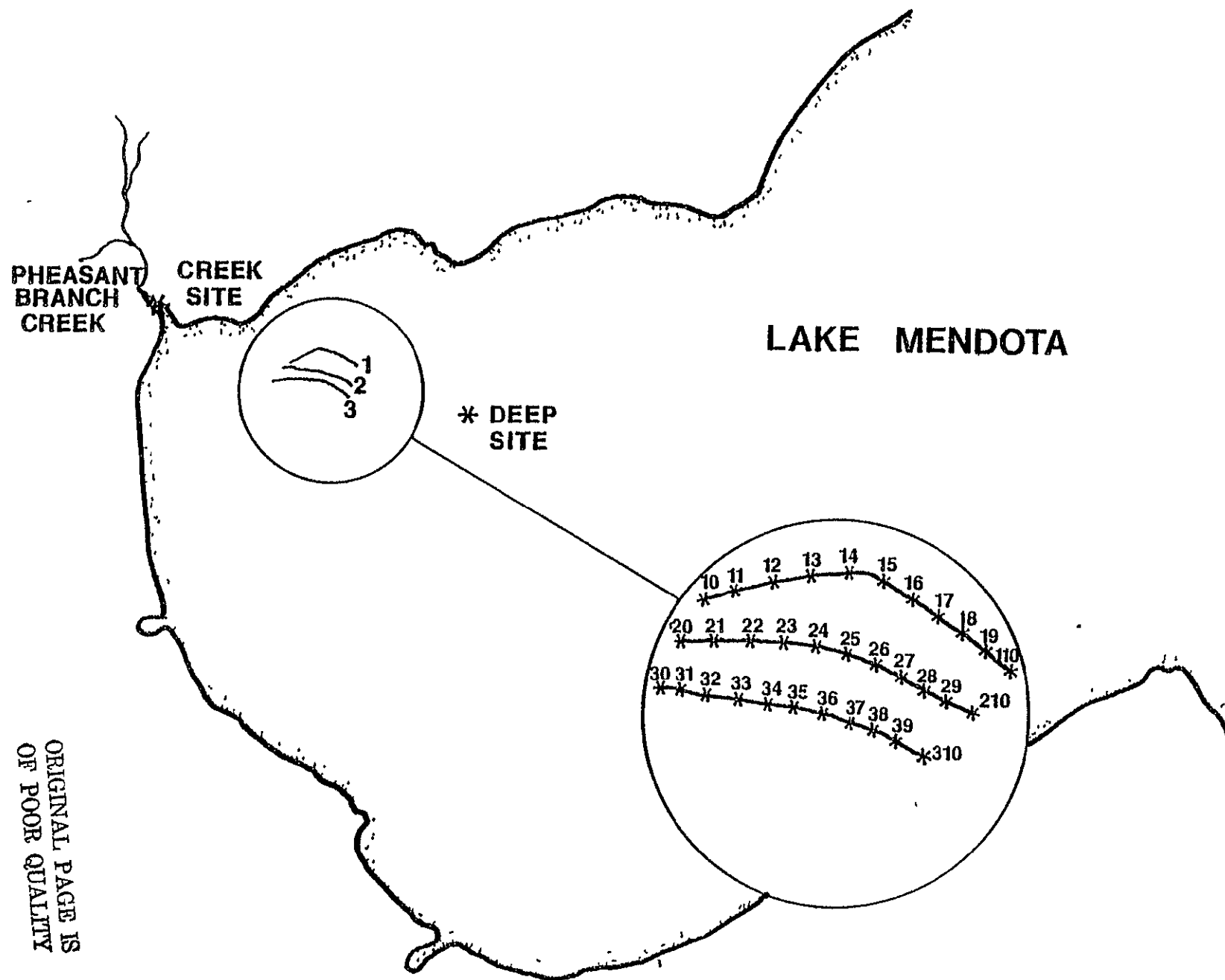


FIGURE 13. Sampling strategy.

ORIGINAL PAGE IS
OF POOR QUALITY

analyzed for DRP and TDP. AEP was measured using the technique described by Shah et al. [7]. The acidity of the sample was raised to 1N with H_2SO_4 . After four hours, the treated sample was centrifuged to remove particulates. After four days, the sample was analyzed for dissolved phosphorous. This procedure yielded an estimate of non-occluded inorganic phosphorous.

During the past year, a technique was developed to obtain particle size for a given water sample. In its present form, the technique involves the addition of a Calgon dispersing solution to 2 ml of sample. Next, the treated sample is filtered through a $0.4\mu m$ polycarbonate filter. After air drying the filter, it is mounted on an aluminum plug, carbon coated, and scanned using a scanning electron microscope (SEM). A transparency with an inscribed coordinate system is superimposed on the SEM video display. Using the coordinate system and a random number table, a random sample of 100 particles can be chosen and measured directly off the video display. Particle sizes can be calculated using the measurements and magnification. The sample preparation technique used is a modification of the Rukavira and Duncan procedure [8]. The counting and measuring system was developed by John Thresher (graduate student, Soils Dept., UW-MSN).

c. Results

Inspection of the data resulting from the analysis of the water samples reveals a decrease in suspended solids as the distance from the creek increases. A second trend is also revealed, the deep samples, in general, have higher concentrations than intermediate or near surface samples. Replicate samples always have lower suspended solid concentrations than the original samples if the boat remained anchored at that site between samples.

Total phosphorous appears to follow trends similar to suspended solids. All phosphorous forms decrease, like suspended solids, as one goes from creek to lake water. The total and dissolved forms measured were stored in acid-washed containers, hence some adsorption of phosphate by the walls of the containers probably occurred. The values listed have not been corrected to account for this effect.

Conductivity and chloride follow similar trends of increasing values as one goes from creek to lake for samples collected on 19 July. On 21 July, conductivity and chloride values appear to be less related to each other and to distance from the creek.

d. Discussion

Based on the suspended solids data, it would appear that the levels observed are actually much higher than would occur in an undisturbed mixing zone. The replicate samples indicate that a great deal of suspension, followed by rapid sedimentation is occurring. Current and wave action may resuspend some bottom sediment. However, visual sightings of boat trails indicate that the sampling procedure itself is the source of the high values. Turbulence created by

the boat engines appears to have created a highly localized area of high sediment concentration. In future work, boat motors will not be used.

Conductivity and chloride are closely related, based on the 19 July data, and probably can be used to trace river water in the mixing zone. On 21 July, the relationship between the two is much more diffuse, possibly due to the decay of the sediment plume. Future analyses for sodium, potassium, calcium and magnesium are planned to identify other more useful tracers.

Within the phosphorous forms measured, there appears to be little relative change with respect to each other. Due to the preservation techniques used, DRP values probably do not reflect environmental conditions since bacterial decomposition may have occurred during storage. This possibility is being evaluated at the present time. Six samples from 19 July were analyzed for DRP the same day the samples were collected. The six samples indicate that the dissolved phosphorous changes from mainly inorganic phosphorous in the runoff to mainly organic phosphorous in the lake. The TP and AEP values reflect the trends in the suspended solids data. This, too, may be an artifact of the sampling procedure that reflects bottom sediment chemistry rather than runoff sediment chemistry.

e. Future Plans

The analysis of samples collected in July 1977 will be completed after the Na, K, Ca, Mg and particulate organic carbon parameters have been measured. Plans are being made to monitor future runoff events on a somewhat smaller scale and after correcting past errors in sample collection and preservation. To obtain information on release rates, we will attempt to follow a well defined portion of the runoff waters as they leave the creek and mix with the lake water.

F. Data Acquisition and Storage for Field Operations

This proposal was an idea to develop a microprocessor-based magnetic cassette system for rapid and largely automatic acquisition of data telemetered from boats or fixed sampling stations, and to augment this with directly recorded bearings from a digital transit and ranges from a distance measuring equipment (DME) for boat location.

It was quickly found that the proposed budget was inadequate to obtain the needed capital items, the transit and the DME. Also, Dr. Fisher had inadequate time to do the necessary engineering. Accordingly, this proposal was shelved in favor of boat location by means of redundant transit sightings with conventional manual data logging in notebooks, and conventional sampling and recording procedures for water samples and boat-based measurements.

When put to the test, the manual and conventional methods were quite adequate. No immediate plans are being made to continue with the proposed development.

References

1. Davies, R. and J.A. Weinman, 1977. "Results from Two Models of the Three-Dimensional Transfer of Solar Radiation in Finite Clouds," Proceedings, Symposium on Radiation in the Atmosphere, Garmisch-Partenkirchen, 19-28 August 1976. Science Press, p. 630.
2. Joseph, J.H., W.J. Wiscombe and J.A. Weinman, 1976. "The Delta-Eddington Approximation for Radiative Flux Transfer," J. Atm. Sci., 33: 2452-2459.
3. Beardsley, G.F., Jr., H. Pak and K. Carder, 1970. "Light Scattering and Suspended Particles in the Eastern Equatorial Pacific Ocean," J. Geophys. Res., 75 2837.
4. Pak, H., G.F. Beardsley Jr., and P.K. Park, 1970. "The Columbia River as a Source of Marine Light-Scattering Particles," J. Geophys. Res., 75: 4570.
5. Turner, J. S., 1973. Buoyancy Effects in Fluids. Cambridge University Press.
6. American Public Health Association, American Water Works Association, and Water Pollution Control Federation. Standard Methods for the Examination of Water and Wastewater, 14th ed., 1975.
7. Shah, R., J. K. Syers, J.D.H. Williams and T.W. Walker, 1968. "The Forms of Inorganic Phosphorous Extracted from Soils by N Sulphuric Acid," New Zealand J. Agr. Res., 11 184-92.
8. Rukavira, N.A. and G.A. Duncan, 1970. "FAST - Fast Analysis of Sediment Texture," Proc., 13th Conf. Great Lakes Res., pp. 274-281.

IV. THE SEDIMENT RUNOFF EXPERIMENT

Coordinator

Lawrence T. Fisher, Remote Sensing Project Coordinator, Environmental Monitoring and Data Acquisition Group

Principal Investigators

See list of Principal Investigators in Section III.

ABSTRACT

During the spring and early summer of 1977, plans were laid to conduct a large-scale experiment in Lake Mendota following a runoff-producing rainstorm. The experiment included obtaining sediment and water samples, measuring spectral characteristics of sediments, taking black-and-white narrow band photographs, and obtaining photographs and field data in the nearby watershed.

The week of 16 to 22 July provided a splendid opportunity to conduct this experiment, with a 75-year rainstorm and heavy runoff on the night of 17 July. After a trouble-plagued failure on 18 July, the experiment was conducted successfully on 19 July and repeated after a second heavy rain and more sediment runoff on 21 July.

Black-and-white, color, and color infrared photographs were acquired daily until Saturday, 23 July, when the sediment plume had essentially dispersed.

A. Operational Planning for the Sediment Runoff Experiment

1. Test Site

Lake Mendota lies directly off the University of Wisconsin-Madison campus and is a well-studied lake. Its proximity and its general limnological characteristics made its choice as the experiment area highly desirable. Boats were readily available, as were lakeside laboratories. The Pheasant Branch watershed, covering some 6,000 acres and emerging into Middleton Bay at the western end of the lake, had long been a study area for several of the researchers involved in

on-land aspects of the experiment. Gauging stations along Pheasant Branch Creek are maintained by the USGS, an important adjunct. For these reasons, this watershed and its associated portion of the lake were chosen as the experiment area. (See Figure 14.)

2. Boats and Instrumentation

Early planning for experimental operations led us to the conclusion that several boats would be needed to acquire water samples and to make spectral measurements. We envisaged a set of three fixed lines, moored to buoys, each about 300M long. A boat would work along each line, moving from point to point at 15 minute intervals and taking water samples at each location at the surface and at various depths. Buoy lines would be set at approximate right angles to the plume, one near the stream outfall and two others at suitable distances, probably 200 to 300M apart, depending on plume characteristics.

A fourth boat would be free to maneuver throughout the plume, taking measurements with a transmissometer/nephelometer, and attending to grey reflectance panels, placed to provide calibration film densities.

3. Location Control

Boat locations were clearly needed. Rather than the concept of a combination transit/distance measurement equipment (DME) unit as originally proposed, it was decided to use conventional surveying and hand recording methods. Five stations around Middleton Bay were chosen, all had good fields of view of the bay and were positioned to allow redundant triangulation measurements to pinpoint boat locations; only three sites were actually used due to crew limitations.. Permission to use privately-owned locations was obtained and precise locations of the survey points was done.

A carefully designed measurement sequence was devised such that each boat and the ends of the three buoy lines would be sampled at fixed time points after each quarter hour. Styrofoam markers, coded by color and arrangement, were designed to mark each end of each line and each boat.

4. Communications

Communications were clearly needed. Arrangements were made to borrow seven 51 MHz radios from the Department of Military Sciences at the UW-MSN. Another portable radio was obtained from the Department of Natural Resources to be used for ground-to-air communications.

5. Flight Planning

Watershed researchers prepared flight lines over the watershed, and preliminary color and color infrared photography was acquired. Over the lake exact lines could not be established until plume characteristics were known. So generalized flight plans were prepared calling for 10 flight lines at altitudes of 6000 feet above terrain, along with beginning and ending lines at 2000 feet. Several experiments, both ground-based and aerial, were conducted to check exposures, filters,

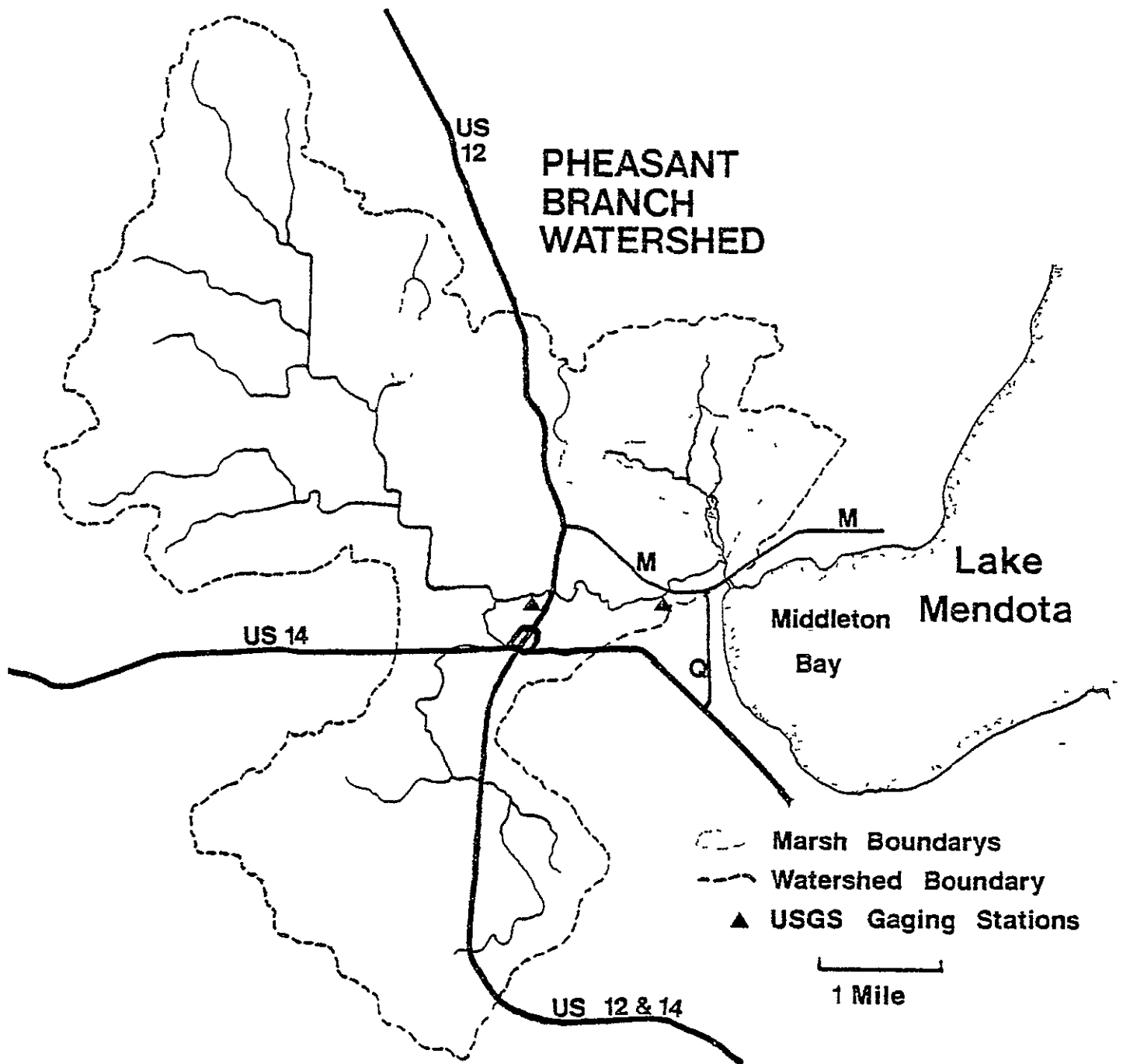


FIGURE 14. Sediment Runoff Experiment Site.

ORIGINAL PAGE IS
OF POOR QUALITY

and cameras, leading to the conclusion that filter wavelengths up to 6000 Å could be used if Tri-X film was exposed at 1/250 second and at maximum aperture settings (f2.8), provided it was "push processed."

A special camera mount was designed to carry four Hasselblads, all oriented the same way, with sufficient space to operate them and change film magazines, yet small enough to drop into a standard Fairchild mapping camera mount.

B. Preliminary Attempts

And then we waited. The ice melted on the lakes, and day by day temperatures rose until we were sure that cold water would not present lethal hazards in case of a boat tipover. Final exams came, and researchers's schedules changed. Several times it rained, often fairly hard. Three times runoff from Pheasant Branch Creek was sufficient to raise stream flow at the Highway 12 gauge to at least five cubic feet per second, and to introduce tantalizing amounts of sediment. Each time, the marsh just above proved its worth as a filter; not once was any change in inflow to the lake noticed, nor was there any noticeable sediment entering the lake. Conditions seemed ripe for a repeat of the drought summer of 1976, when only one storm caused any sediment runoff at all, and that minor. Summer arrived, and vacation schedules took various investigators to various places.

C. 16-17 July 1977

Plans had been made during the week of 11-15 July for another experimental flight on Monday, 18 July, to evaluate films, filters and exposures. On Saturday night, 16 July, about one inch of rain fell at the Dane County Airport; perhaps somewhat more in the Pheasant Branch watershed. Early in the afternoon of Sunday, 17 July, the Remote Sensing Project Coordinator stopped by the USGS gauge at Highway 12 and found higher water than at any time during the season. Further checks at the entrance to the lake revealed that mud was clearly washing into the lake! After many telephone calls, plans were settled. The experiment would begin on Monday morning, with aircraft support by the Department of Natural Resources (DNR) DC-3. Then, Sunday night, it rained. And rained...

D. 18 July 1977

By Monday morning, 18 July, the rain stopped after dropping about 3.5 inches at the Dane County Airport. Obviously, aircraft operations were out of the question due to low cloud cover that morning. A predicted "second front" of squall lines reinforced that decision (it never materialized). Plans were postponed until Monday afternoon when flying and photography conditions were expected to improve quickly.

At the experiment site, conditions were changed almost beyond recognition! The normally placid flow from the marsh into the lake was now a turbid,

roiling torrent. At Highway 12, the gauging station's weir was completely submerged. The previous day's runoff had been sufficient (marginally) for execution of the Sediment Runoff Experiment, but now a spectacular event was obviously happening.

Subsequent analysis by USGS concluded that the rainfall was a 75-year storm. Because the previous year's drought had left soils so dry, runoff was about a 4 to 5 year flood. There could be no question that this was the event we had hoped for, and more. Plans, therefore, proceeded as rapidly as possible. Final arrangements were made with the air crew. Radios were obtained. Boats were started from their anchorages. Ground crews went out into the watershed.

The rest of that day, frankly, was a disaster. The DC-3 showed up, rather sooner than expected, but the ground/air radio wouldn't work (its batteries were dead). The airplane photographed watershed flight lines and conducted two passes over the lake. Then it left (to pick up the Secretary of the DNR in a distant city, and to try to obtain storm event photography in Milwaukee). In fact, its loss didn't especially matter, for:

- (1) One of the four boats never got started due to electrical problems.
- (2) One of the buoy lines began to drift badly, dragging its anchor.
- (3) Another boat sheared a propellor pin, and for a long time seemed destined to drift, carrying a frustrated research assistant, until it made sufficient windage to fetch the far shore of the lake, five miles away (it was eventually rescued by a passing fisherman).
- (4) A third boat suffered electrical failure, and had to be towed back to shore by the only surviving boat.

It was, collectively, not one of our better days.

E. 19 July 1977

During Monday evening, coordination was done to resume operations the next morning, and to correct some of the faults which had become apparent. Early morning reconnaissance from a small aircraft showed that the sediment plume had survived the night well, and was a compact, approximately triangular body of extremely silty water filling all of the vicinity of the mouth of Pheasant Branch Creek (Figure 15). Some silt-laden water was continuing to emerge from the marsh into the lake, but stream flows were obviously diminishing quickly. Weather conditions, generally calm the previous day and night, continued, so that wind seemed unlikely to destroy the plume quickly. The day promised to be clear and very hot.

One of the boats disabled the day before was still out of service, and the non-operating air/ground radio could not be recharged or replaced. Otherwise, all equipment was operational. Boat crews were ready for operations by 9:00 A.M., with fixed lines deployed, and three surveying stations were operating. Each site was equipped with a radio, an instrument

ORIGINAL PAGE IS
OF POOR QUALITY

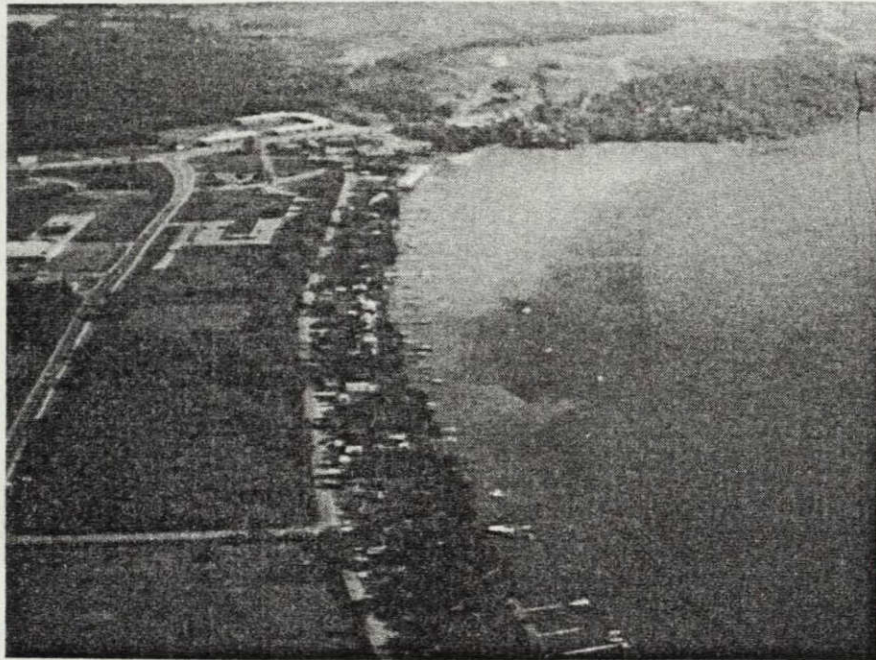


FIGURE 15. The sediment plume at 9 A.M., 19 July 1977 (Middleton Bay, Lake Mendota, Wisconsin).

TABLE X. Chronology of Aircraft Passes on 19 July 1977.

Pass	Altitude	Direction	Time Overhead	Remarks
1	2000'	N to S	not recorded	No boats operating but lines and reflectance panels deployed.
2	6000'	S to N	9 50 40	Boats were being deployed.
3	"	N to S	10 09 25	All boats operating as planned for remainder of operation.
4	"	S to N	10.25 10	
5	"	N to S	10 40 49	
6	"	S to N	10:54.08	
7	"	N to S	11 09 13	Camera magazine jammed on BLUE system (4800 Å filter). That system was not used for remainder of day.
8	"	S to N	11 34 02	
9	"	N to S	11.46 03	
10	"	S to N	11 59:46	
11	"	N to S	12:16:13	

ORIGINAL PAGE IS
OF POOR QUALITY

to obtain 35mm color and color infrared coverage were abandoned because atmospheric haze had become too dense for photography.

Late Wednesday night, a heavy storm began, with strong rain, lightning, and strong, gusty winds from the northwest. Before it ended, this storm had deposited another two inches of rain.

G. 21 July 1977

By Thursday morning, the previous night's storm had run its course, and clouds were beginning to dissipate. A hasty reconnaissance flight revealed several changes:

- (1) The old sediment plume, although still present, was much less turbid. Apparently it was beginning to sink.
- (2) Stream flow into the marsh was high again and very turbid. Its level and turbidity was perhaps comparable to conditions late Monday afternoon, when the previous flood was beginning to diminish. From the air we could see relatively little outflow from the marsh, which was apparently still charging. No very large amount of new muddy water had yet entered the lake from Pheasant Branch, although this situation changed somewhat during the morning.
- (3) A significant new plume had developed at Lake Mendota County Park, about 1 kilometer northeast of Pheasant Branch. This apparently came from flooded storm sewers draining an area heavily developed with apartment buildings, severe local rain must have occurred in that area. This muddy water looked as though it might gradually mix with Pheasant Branch inflow, confusing the hydrology even more than the mixture of old and new mud from Pheasant Branch itself.

Cloud cover remained heavy early in the morning, so flight operations and data gathering were postponed, beginning at about 10 00 A.M. instead of 9 00. About the same procedures were used as on Tuesday, with three boats collecting water and sediment samples and taking measurements, and three surveying stations recording positions. One change was that the fixed lines between buoys had been abandoned in favor of simple buoys marking ends of sampling transects. The lines themselves had proved useless for location because of bowing, and they interfered with boat operations.

Two of the investigators, qualified SCUBA divers, carried an underwater camera and a diver's flood light into the plume. They found diving conditions extremely poor due to heavy weed growth. They obtained no photography. They reported that the most sudden gradient of sediment concentration appeared to be in the midst of emergent macrophytes which form a thick bed about 150M off shore. It was conjectured that the weeds were inhibiting water circulation and were "trapping" the sediment plume.

Data gathering continued until about 13 08, interrupted from 10:55 to 12:11 to load more film. During the late morning, weather conditions improved for a while, but then began to deteriorate, with low scattered clouds developing. Haze also began to increase. Finally, sun glitter became

progressively more severe as sun angle increased. Therefore, the day's data gathering was halted after 7 of the planned 10 flight lines were flown.

More troubles developed with the BLUE camera system which failed early in the day. So most of the flight lines used only three cameras.

In spite of camera and lighting troubles and early termination, it was felt that sufficient data was acquired, both in the air and on the water, to make the day a success.

Late Thursday afternoon, the air crew repeated black-and-white photography with the narrow band filters (by this time, the defective camera had been placed back in service after replacing a fuse, so all four filters were again used). Color and color infrared 35mm images were also acquired, although haze had become so heavy that photography conditions were very marginal. (Some aircraft were filing instrument flight plans that afternoon!)

H. 22 and 23 July 1977

Friday was a clear, bright and cool day after a night with strong northeast winds. Flying conditions were superb, so we re-photographed the area, again with narrow band black-and-white film and with 35mm color and color infrared film. By this time, most of the runoff had ended, and stream flow into the marsh was dropping rapidly. Very little current was apparent as the marsh outflow entered the lake, although the water there remained extremely turbid. From the air, it was clear that considerable new sediment had entered from Pheasant Branch overnight; this mud was mixing with the old plume and several distinct fronts. The mud from Lake Mendota County Park had decayed into a thin stream hugging the north shore where it was evidently most protected from the wind, and to a small extent this mud was beginning to merge with that from Pheasant Branch.

By this time, crews and supplies were largely exhausted and more data had been acquired than had been planned. So no attempt was made to repeat the experiment. It was decided instead to continue twice daily photography as long as good conditions persisted. In fact, by Friday evening, it was apparent that the plume was rapidly sinking, so photographs were taken on Friday evening and repeated one last time on Saturday morning, again with splendid flying and photography conditions. On Saturday morning, the experiment was terminated.

V. OTHER APPLICATIONS

Principal Investigators

James L. Clapp, Director, Environmental Monitoring and Data Acquisition Group, and Professor, Department of Civil and Environmental Engineering

Lawrence T. Fisher, Remote Sensing Project Coordinator, Environmental Monitoring and Data Acquisition Group

Robert P. Madding, Outreach Coordinator, Environmental Monitoring and Data Acquisition Group

Frank L. Scarpace, Assistant Professor, Department of Civil and Environmental Engineering, and Institute for Environmental Studies

Graduate Assistants

Charles Dancak, Department of Electrical and Computer Engineering

Harland E. Hogan, Department of Landscape Architecture, and Botany

Barbara McKellar, Environmental Monitoring Degree Program

ABSTRACT

Several projects have been undertaken to expand the use of techniques developed through our main research funded by NASA. These projects would not have been possible without the fundamental research conducted over the past few years.

Projects and the sponsoring agencies reported here include airborne thermal scanning of rooftops (Wisconsin Power and Light), remote sensing and the energy extension service (U.S. Dept. of Energy), spruce budworm defoliation mapping using LANDSAT (U.S. Forest Service), thermal monitoring of heated discharges from electric power plants and paper mills (Wisconsin Dept. of Natural Resources), remote sensing data center (UW-MSN), LANDSAT land cover classification of watersheds (USGS), corn yield project (J.F. Mellor and Associates), and land cover determination from digital interpretation of high altitude aerial imagery (International Joint Commission).

A. Introduction

NASA core support has provided a technological base which can be used for projects unrelated to our main research. Application of our remote sensing techniques to other areas expands the utility of our approach and promotes remote sensing technology outside the realm of water quality. To incorporate

remote sensing or any new technology as an operational tool within a state (or states) requires a broad base of support. This support can come if many of the state agencies have had some (good) experience with remote sensing through projects they have helped accomplish. The following are brief descriptions of projects we have begun and our progress in them.

B. Airborne Thermal Scanning of Rooftops

This project began on a small scale in 1975-76 with airborne thermal scanning of rooftops to monitor energy loss. The Wisconsin Power and Light Company provided funds in 1976-77 for a pilot study of the Beloit, Wisconsin, metropolitan area.

The project goal was to encourage energy conservation in the home using thermal scanner imagery as a stimulus. This was our first effort to take thermal scanner imagery to an entire community. The data were processed with the limited expertise of the user in mind. Namely, the problems of navigation in the image ("where's my house?") and the identification of relative amounts of radiated energy from a rooftop were addressed. The first was solved by locating and labeling the streets on the image. The second was solved by color slicing the data; an individual can distinguish yellow from green much better than light grey from a shade darker. To perform these tasks a new approach (for us) to thermal scanner data processing was needed. The Man-Computer Interactive Data Analysis System (MCIDAS) at the UW-MSN Space Science and Engineering Center (SSEC) lent itself nicely to this approach. The digitally formatted scanner data, preprocessed to remove inherent tangential distortion, was segmented into "frames" of 672 columns by 500 rows and loaded onto a video disk. The segmenting was programmed to provide 10% overlap between adjacent frames to insure full coverage. The frames were displayed on a television monitor. Text strings were written over the TV image; software was developed to allow cursor control of the TV coordinates of the first character in the string and the orientation angle of the text string about the first character. Thus labelling non-horizontal streets became an easy task rather than a time-consuming letter-by-letter chore. The cursor controls were also used to generate the color enhancements interactively. The color enhanced frames with streets labelled were photographed. WPL was provided with slides and color negatives of the 61 frames required to cover the Beloit area.

Early news coverage of this project was excellent. In part this success was due to the exciting visual display offered by the real time color enhancing and text labelling of the MCIDAS system. Last winter, television stations from Madison, Rockford, Illinois, and Green Bay covered the project using the MCIDAS visuals as a vehicle. The Madison station sold the story to NBC who aired it on their network. WPL used their organization to promote press coverage in local newspapers and other media. The Department of Natural Resources (DNR), with whom we cooperate for data acquisition, began to use its public relations organization to encourage press coverage of this project.

A crucial aspect of this type of study is the contact made with the public. For the WPL funded study, WPL employees were to make the contact. Training in interpretation of the scanner imagery and long discussions on energy

conservation measures were provided to these people by the UW-MSN. The thrust of our approach was to use the scanner imagery as a lead-in to a total awareness of energy conservation in the home. Radiated energy loss through a rooftop is just one way a roof loses heat; roof heat loss is just one way a dwelling loses heat. A report by Smith et al. to the State Planning and Energy Office on Energy Conservation Techniques in Residential Space Heating was to be used as a guide.

Initial meetings with the public by WPL employees were received positively. The imagery scale required full screen slide projection or large prints (11"x14") to view individual homes. (The scale was smaller than we desired due to air turbulence during data acquisition which forced the pilot to fly 35% higher than planned. Another flight was scheduled but inclement weather kept us from accomplishing it.) The meetings were generally attended by 15 or 20 people and were run by one person. Individual attention was difficult with this approach.

One of the questions which frequently arose was, "How much insulation do the various colors represent?" We cautioned WPL that there were at least three factors which made direct correlation difficult. These factors are:

- (1) rooftop emissivity
- (2) roof pitch and surroundings (view factor)
- (3) attic ventilation

During the summer of 1977 WPL hired a limited term employee (LTE) to conduct a survey of 200 homes in the Beloit, Wisconsin area. We viewed this as a data gathering survey to give UW-MSN enough information to perform a correlation of attic insulation levels to thermal imagery. In addition, WPL desired to poll public opinion on its newest inducement to public energy conservation, The Energy Efficient Home Reduced Utility Rate proposal. (The state Public Service Commission in spring of 1977 ordered utilities to propose ways to induce the public to make their homes more energy efficient. WPL at that time shifted direction from thermal scanning to this new approach. As a result, our comparative study of the effectiveness of rooftop thermal scanning to stimulate energy conservation was not funded. We opted for reduced funds to perform the correlation analysis.) The LTE performed his own correlations. His report indicated almost no correlation between colors in the thermal images and a parameter defined in the report called "heat loss value." This parameter was calculated by multiplying the estimated attic area by the R-value of the attic insulation. His report estimates the uncertainty of the "heat loss value" parameter to be 50%. Considering the uncertainty in this parameter and the omission of rooftop emissivity, roof pitch, and attic ventilation factors, we were not surprised at the lack of correlation. We were very surprised and dismayed to read an Associated Press release that thermal scanning was a "flop." This news article was based on an interview with the LTE. Neither UW-MSN nor WPL knew of this interview prior to its release in the press. Appendix IV is the WPL response to the editor of the newspaper responsible for the article. We are currently working with WPL to ameliorate this problem.

Appendix V is a letter indicating positive use of thermal imagery for heat loss monitoring. The UW system Bureau of Facilities Management used

a scan of UW-Parkside buildings to zero in on two areas of water damaged insulation. These buildings have built-up flat roofs which do not have the ventilation and view factor problems of pitched roofs.

C. Remote Sensing and the Energy Extension Service

The Department of Energy (formerly ERDA) has funded 10 states to perform a 19-month pilot study on methods to promote energy conservation with the accent on personal contact with the public. Wisconsin received \$1.1 million from DOE to implement a statewide Energy Extension Service (EES). This project takes advantage of existing agencies and is, in part, patterned after the state's Agriculture Extension Service. Realizing the need for a better understanding of remote sensing applied to energy conservation, EMDAG will provide educational expertise through the EES energy audit training program. This program is designed to educate representatives from utilities, municipal agencies, and UW Extension in current audit methods and cost-effective energy conserving retrofit and construction recommendations.

The EMDAG part of the audit training program has received about \$25,000. This includes a scientist for 6 months, and a research assistant for one year. Spot radiometers, ground-based thermal imaging systems and airborne thermal scanning will be explained with emphasis on understanding the operational principles and basic concepts behind these devices. Strong emphasis will be placed on image interpretation and the inherent caveats with imagery and demonstrations (e.g., emissivity effects) providing graphic examples. The objective is to get auditors aware of the utility and limitations of remote sensing tools in performing home energy audits. Hopefully, the recent experience discussed above will be alleviated by this approach.

In addition, EMDAG will document research tests of various remote sensing tools now in use in energy audits. Should adequate tests be lacking, EES may fund EMDAG to perform them.

Research is currently underway to make in situ measurements of rooftop emissivities. A portable emissometer has been constructed and is being tested. EMDAG scientists have been cooperating with a local firm, Vanlen Views, to improve the emissometer design. They have been providing their AGA thermovision system at no cost to EMDAG. In addition to design improvements, the AGA system allows measurement of emissivity in the 2 to 5 micron waveband. Together with our measurements in the 8 to 14 micron waveband, we have been able to document the selective emissivity of plastic-coated metal films used originally as solar reflecting sheets applied to windows. Their utility as thermal infrared reflectors has been both questioned [1] and praised [2]. The study indicating these metalized plastic sheets were good infrared reflectors measured the reflectance in the 2 to 5 micron waveband. Our preliminary results indicate a (good) reflectance of about 0.7 in the 2 to 5 micron region. However, in the 8 to 14 micron region the reflectance drops to about 0.2. A blackbody at 300°K radiates less than 1.2% of its energy in the 2 to 5 micron region. It radiates 35% in the 8 to 14 micron region. Clearly the 8 to 14 micron waveband is significantly more important as an indicator of reflectance of thermal infrared energy for home energy conservation.

D. Spruce Budworm Defoliation Mapping Using LANDSAT

The use of LANDSAT MSS digital data and computer-assisted analysis techniques was investigated in a study funded by the U.S. Forest Service to detect and map areas of spruce budworm infestation in forest stands of balsam fir and white spruce. A LANDSAT computer-compatible tape was obtained from 11 July 1976 when peak foliage browning of fir and spruce was visible. Computer analysis was accomplished by the use of the Remote Sensing Applications Programs of the Environmental Monitoring and Data Acquisition Group. Color and color infrared, 70mm aerial photography at scales of 1:78,900 and 1:46,800 provided a record of ground conditions.

Training sets for computer classification were identified from a forest cover type map that was produced by photo-interpretation. Local vegetation patterns made the selection of small-sized training sets necessary. However, the training sets could be well located on a computer printout map with respect to prominent geographic features (e.g. lakes). Training set performance was based on the results from the intermediate program analysis and from a comparison of preliminary computer classifications with the cover type map. Spectral differences between many of the training sets representing different levels of defoliation could not be readily distinguished. The final training sets are those with distinct spectral differences and which best qualified to represent appropriate resource classes.

Nine resource classes were identified including 2 levels of coniferous infestation. Extensive and moderate infestation categories were used as classification levels to distinguish between the interpretations made by ground and remote sensing survey methods. An unsupervised, maximum likelihood classification (MAXLIK) program was used.

The classification printout maps from MAXLIK gave generally favorable results. The location and spatial coverage of all resource classes was fairly accurate when the computer classification map was compared with the cover type map and checked with the color infrared aerial imagery. Moderate infestation represents an intermediate class such that its cover type boundaries were not always clearly defined. Its distribution by computer classification, however, is consistent with the photo-interpretation results. The class is mostly associated with a Mixed Swamp Conifer cover type, as well as other heterogeneous composition types that do not qualify as Extensive Infestation.

The overall results of Extensive Infestation were good also, but there were classification errors. The spatial coverage of large, homogenous stands of fir and spruce with spruce budworm infestation compared well with the cover type map. Numerous small patches of coniferous infestation were also located by the computer classification. However, the class was unable to distinguish between different species types that were exhibiting defoliation properties similar to the fir and spruce.

More adequate training sets of these conditions would permit better analysis. The results indicate that the LANDSAT system can be used to identify and map areas of coniferous infestation, but that supplementary methods are required to determine the type and severity of defoliation that is present. Further analysis techniques such as multirate imagery are recommended to remedy some of the problems. Appendix VI is the final report of this study.

E. Thermal Monitoring of Heated Discharges from Electric Power Plants and Paper Mills

The pressure on the use of Wisconsin rivers as a heat sink for various industries continues to increase; DNR is keenly aware of this pressure. To begin to evaluate the effect of heated discharges on several major rivers in Wisconsin, a cooperative project was undertaken to map the area of influence of thermal plumes in these rivers. Thermal scanning has proven to be an effective tool for this type of effort. Funding (\$15,000) was made available to monitor fifteen power plants and five paper mills throughout the state on three different occasions. The overflights were planned to observe the annual maximum surficial extent of the thermal plumes.

A final report was delivered to DNR early in 1977. This report was patterned after a previous study of thermal plumes along the Wisconsin shore of Lake Michigan. A summary of that report is in press [3]. A thermal image of the plume from a given power plant on a given date was mounted on a page together with associated environmental data, areas enclosed within isotherms, water temperatures, plant data, and comments. A compendium of these pages together with a written report comprises the final report. The following are the major recommendations.

1. Ground Truth

A marked improvement over our previous thermal plume study was the measurement of surface water temperatures for ground calibration. DNR district personnel provided excellent ground truth. The major problem was the coordination of up to four separate field crews with the aircraft operation. Each crew had its own work and boat scheduling to contend with. Together with the intensive scheduling of the aircraft and the vagaries of the weather, these factors combined to frequently frustrate the most ardent attempts at a successful mission. By reducing the number of field crews required to be at different sites for a mission, the probability of a successful mission would be enhanced. Performing a primary calibration at the Blount Street discharge at the beginning and end of a mission is a possibility. These ground truth measurements combined with a technique for reducing atmospheric effects could result in an operationally less expensive calibration program. Changing the scanner wavelength sensitivity from a range of 8 to 14 microns to one of 10 to 11.5 microns considerably reduces atmospheric effects. Thus ground truth in Madison could be valid throughout the entire state provided the scanner level and gain settings were not changed.

2. Routine Monitoring

Routine thermal monitoring of thermal plumes is recommended. Public interest in all aspects of power generation has understandably increased with the dramatic increase in the number of power plants. Aerial remote sensing of thermal discharges is an inexpensive way to insure compliance with regulations, and keep the public informed of the extent of thermal discharges. New power plants should be monitored frequently initially to extend what has been reported herein. Routine monitoring would also be useful as a guide and a complement to other thermal plume sampling programs. Routine monitoring of every power plant in the state is not recommended. This study shows that many of

the discharges result in quite small thermal plumes. However, the small number of flights made over each power plant during drought conditions limits the utility of the data set as an indicator of typical conditions for some of the plants. To gain insight to size variations of significant river plumes routine monitoring is recommended.

3. River Monitoring

Analysis of thermal scanner data of river discharges is much more difficult than that of lake plumes. River plumes in general are much smaller than lake plumes. Larger plumes are forced by the river boundaries and flow patterns into long thin shapes. Most efficient analysis occurs when the relevant data (i.e., the plume) is contained within a square or nearly square two-dimensional data array. The larger the ratio between the relevant dimensions the less efficient the analysis. Basically, what happens is that all the data must be read into the computer but only a small percentage is useful. The percent of useful data points per scan line for lake plumes is about 30%, for river plumes this drops to about 10% or less. One possible method of circumventing this problem is to scan on a flight path perpendicular to the river instead of parallel to it. In many cases the plumes would be short enough to encompass their length in the width of one scan line. This would increase the useful data points per scanline to as high as 60% or 70%. The plumes small size and the river banks (cluttered with barges, boats, overhanging trees and other structures) make river plume discharges much more difficult to discern than lake discharges.

4. Thermal Standards

The thermal standards for power plant thermal plumes should be written operationally as a compromise between end-of-pipe standards and biological-effect standards. That is, standards should be based on information that can be obtained with a reasonable effort. Standard remote sensing monitoring procedures should be developed by EPA or ERDA. Such procedures should include standardized, routine, ground truth measuring techniques. The control of raw data through the entire processing procedure should also be standardized to insure that legal integrity is maintained. Every attempt should be made to avoid arbitrariness by continuing intensive biological effect programs at a few representative plants, rather than studying all plants on relatively limited bases.

F. Remote Sensing Data Center

All collections which were moved in November 1976 were reorganized into the new spatial setting, all visitors were assisted with information and imagery needs.

Through November and December 1976, 2600 frames of RB-57 high altitude color and color IR transparencies were cut from film rolls, labelled according to mission number, date of flight, frame number, and scale, and placed into protective plastic casings. The numerous flight lines of each

of the missions were then delineated on 1 500,000 scale Wisconsin maps to act as the collection's reference system.

In February 1977, work began on organizing and labelling a portion of the LANDSAT transparency collection. The 35mm slide collection was organized according to county. Other various collections were organized and integrated. This work was pursued until the end of the semester.

G. LANDSAT Land Cover Classification of Watersheds - with USGS

Local representatives of the U.S. Geological Survey are engaged in a project to model surface runoff characteristics of Wisconsin watersheds. One aspect of their work involves land cover classification of watersheds into the categories of (1) open water; (2) bare soils, including agricultural land; (3) agricultural crops; (4) wetlands, and (5) woodlands and forests. Since the University of Wisconsin Remote Sensing Project has invested considerable time and effort in the development of computer programs for general purpose analysis of remotely sensed data, including LANDSAT, we engaged in a small-scale project to try our procedures to provide classifications for some experimental watersheds.

LANDSAT data of southern Wisconsin from 12 September 1975 was available from our library, so it was chosen for analysis. There was a general dearth of ground verification information about ground cover in most of the scene, so representative areas which were generally well understood by our investigators were chosen. One area selected was the Portage, Wisconsin region where EMDAG is involved in a large-scale project sponsored by the Environmental Protection Agency, studying the environmental impact of coal-fired power plants. Another test area focused on the Yahara River watershed, familiar because it includes Madison and its lakes.

At the moment, our analysts are handicapped by the absence of any means to interact quickly with our computer. Our supervised classification procedures must use line printer output produced in batch computer runs, and we must pay substantial fees to the Madison Academic Computing Center (MACC). Classification costs of our maximum likelihood classifier were high (although its code is efficient, patterned after Eppler [4]), and the need to mosaic many pages of output made the classification inefficient. To lower computation costs, a "table lookup" classifier program, TABCLASS, was constructed after the basic design of Eppler [5]. This lowered processing charges substantially. Turn-around time, though, was still slow due to the cumbersome output procedures, although the resulting classifications were judged good by persons knowledgeable with the area.

Several years ago, our studies of thermal effects of heated water discharges from power plants into Lake Michigan required development of computer algorithms to locate points interior to an arbitrary closed polygon. The resulting algorithm [6] has proved useful several times since, and it has proven beneficial in this project. We were able to define watersheds in terms of a given LANDSAT scene's rows and columns, and classify only points inside that area.

After reviewing our results and assessing other options (including the General Electric Co. IMAGE 100 system at the EROS Data Center and Bendix Corporation's EMDAS system), the USGS has elected to procure their basic land cover classification through Bendix, sending their LANDSAT tapes to Ann Arbor, Michigan, and using a Madison-based video display, telephone linked to Ann Arbor, for the necessary interactivity. EMDAG still plays a role, however, and this is made possible both by our polygon handling routines and our LANDSAT lake classification procedures. As envisaged, we will be supplied with (latitude/longitude) coordinates of points bounding watersheds. Our navigation programs CONTRL and SATNAV, developed for lake classification, will be used to relate these coordinates to LANDSAT (row/column) coordinates. These in turn will be used by our "inside the polygon" programs to take pre-classified data to the Bendix system and find just that data inside specified watersheds. Color film classification results will be provided, but more directly, tabulations of surface areas classified in each of the various cover categories will be tabulated for use by the USGS modeling programs.

This effort is underway, and is expected to be completed during the next year.

H. Corn Yield From Digitized Low Altitude Airphotos

This project is funded by J. F. Mellor and Associates and is directed by F. L. Scarpace. Its intent is to investigate the feasibility of using low altitude digitized aerial imagery to monitor crop extent and yield. The project started in June of 1977. Thirteen missions have been flown over 30 fields. Only a few of the aerial images have been digitized, thus no significant results have been found.

I. Land Cover Determined from Digital Interpretation of High Altitude Aerial Imagery

This project is funded by the International Joint Commission on Water Quality in the Great Lakes and is directed by F.L. Scarpace. It is concerned with the investigation of the feasibility of digital interpretation of land cover information for input into hydrological models from high altitude aerial imagery. Thus far the results of the investigation have not been used directly in a model developed by the project. The results have been compared with traditional methods of acquiring the needed data for the model.

Two subwatersheds (Schoonemaker and Noyes creeks) in the Menomonee watershed were chosen to test these techniques. High altitude imagery (scale 1:120,000) flown by NASA was digitized with a ground resolution of 6 meters square. Land cover was classified within each watershed and compared with human photo-interpretation and data supplied by the Southeastern Wisconsin Regional Planning Commission (SEWRPC) which was used as input to the hydrological model. The computer classification included five land cover classes: impervious surfaces, tree cover, crop land, other vegetation, and water.

Three other urban watersheds were investigated using this technique. Imagery (scale of 1:130,000) of Detroit-Windsor, Toledo, and Rochester were acquired

from EROS Data Center, Sioux Falls, S.D. In these cases, NASA had not properly calibrated the imagery and the classification accuracy dropped to 80-85% from 95% for the digital classification within the Menomonee watershed. These results have indicated that it is possible to use high altitude imagery to obtain land cover information for input into a hydrological model within other urban watersheds. All the urban watersheds within the Great Lakes Basin could be accomplished in a similar manner.

References

1. Berman, S.M. and S.D. Silverstein, 1975. Energy Conservation and Window Systems, NTIS Report Number PB-243117.
2. Raugland, R., 1976. Infrared Survey of Solar Glaze Window Film. Test performed by Energy Conservation Consultants, Inc., for Kool View Company, October 1976. Unpublished.
3. Madding, R.P., F.L. Scarpace and T. Green III, 1977. "Thermal Plumes Along the Wisconsin Shore of Lake Michigan," Trans., Wisconsin Acad. of Sci., Arts and Lett.
4. Eppler, W. et al., 1975. "Canonical Analysis for Increased Classification Speed and Channel Selection. Proc., Mach. Proc. Remotely Sensed Data.
5. Eppler, W., 1974. "An Improved Version Ath Table Look-Up Algorithm for Pattern Recognition," Proc., 9th Intl. Symp on Rem. Sens. Envir.
6. Madding, R.P. and L.T. Fisher, 1975. "Interactive Analysis of Thermal Imagery," Proc., ASP/ACSM Spring Meeting.

APPENDIX I

A DNR EVALUATION OF THE LANDSAT
LAKE CLASSIFICATION PROGRAM

By

Ron Martin

and

Lee Liebenstein

Water Quality Evaluation Section

Wisconsin Department of Natural Resources

A DNR Evaluation of the LANDSAT Lake Classification Program

The LANDSAT lake monitoring program is a mechanism which can be employed to classify inland lakes greater than 20 acres in size to their trophic status. The current program is a cooperative effort between Wisconsin DNR and the University of Wisconsin. Goals of this program as viewed by DNR are twofold:

- (1) To establish guideline priorities for lake management practices (e.g. preservation and rehabilitation techniques)
- (2) To document long term lake eutrophication changes over time.

Through a computerized system, LANDSAT data can be used to classify all lakes over 20 acres in size at a minimal cost of 5-10 dollars per lake.

To adequately monitor lakes, sampling at least 2-3 times per year is required. Algae populations vary throughout the growing season so that no one time LANDSAT sampling technique would be adequate to classify a water body.

Several computer programs are needed to adequately classify lakes by remote sensing techniques. Data acquisition and handling is accomplished through programs entitled CONTROL, SATNAV, and EXTRACT. These programs cannot be executed without baseline data. This information is contained in a computer file called ACCESS. Before data can be entered into ACCESS, polygons are drawn around every lake greater than 20 acres in size on U.S.G.S. topographic maps. Apexes of these polygons together with control points (points that are easily identified on the satellite data) are numbered and placed into the file. Latitude and longitude were also established for these control points and stored in ACCESS. In addition to latitude, longitude and polygon apexes, file ACCESS contains county number and lake number and name.

The initial step for data gathering is the acquisition of computer tapes from the EROS Data Center in Sioux Falls, South Dakota. Approximately 40 tapes at a cost of \$200/tape would be needed to classify all the lakes in Wisconsin. Each tape contains a scene 115 x 115 miles which is subdivided into quarter strips called files. Each file covers a full length scene from a north to south direction. It is most systematic to work on the scenes from a file to file basis.

The first computer program, CONTROL, predicts the approximate ground area covered by the file of data. The program then selects the control points from the file entitled CONTROL-POINT, which are likely to be found in that particular file area. The Milwaukee scene contained three scenes; July 16, August 3, and September 26, 1975. Each scene contained three files with approximately 15 control points per file. These control points represent readily identifiable ground locations on various lakes. A minimum of ten control points are needed to determine the location of the lakes in each file. Row and column coordinates for each control point are recorded following an interpretation of typed printouts of the lakes in the various files (see figure 1). The time element involved in locating the control points for the Milwaukee scene was about 7 minutes per lake; nearly 700 man hours would be required to perform the manual operations in CONTROL for a statewide classification.

One of the problems encountered with the CONTROL program was the effect of cloud cover when trying to locate control points. For example, in the July 16, 1975, Milwaukee scene, the control point for Lake Sinissippi could not be properly located because it was obscured by cloud cover. Another problem experienced with CONTROL was that some of the smaller lakes could not be located on the U.S.G.S. quad maps. (i.e. July 16, 1975 scene, Crystal and Wyona were not found). It is possible that reflection from the land surface or cloud cover may have interfered with locating these lakes.

Once the rows and columns are recorded for each control point they are used in the next phase--program SATNAV. Program SATNAV performs a least squares adjustment to compute the coefficients of a third order polynomial which best predicts locations given the control point data set. These parameters are stored on a file at the conclusion of SATNAV, to be used in the next stage of the process--program EXTRACT.

SATNAV is a relatively inexpensive computer program to run provided it does not have to be run very often. The cost to run SATNAV for the Milwaukee scene was about \$4. Some of the problems encountered in the Milwaukee scene in SATNAV were due to programming errors which have since been resolved. Difficulty was also experienced in matching the predicted rows and columns with those that were measured. For example, in file 3 of the July scene, Muskego Lake was found to have a significant error in the measured latitude and longitude when compared to that predicted. The acceptable error for latitude and longitude is within 5-6 seconds; for Muskego Lake the latitude was off by 16 and the longitude by 11 seconds. In cases like Muskego Lake where there is a large error in latitude and longitude, the measured rows and columns are rechecked. If no error is detected, the control point for that particular lake should be thrown out. For the Milwaukee scene there were sufficient control points (10 per file) which were within the margin of error (within 2-3 rows or columns), that there was no problem in predicting the location of the rest of the lakes in the scene. However, in scenes such as in the southwest portion of the state where there are few lakes and fewer control points than the Milwaukee scene, larger errors in rows and columns may result in less than 10 control points in a given file that are within the acceptable range of error. Consequently, it may be difficult without sufficient navigation points to accurately predict the location of the lakes in the scene.

Program EXTRACT uses the information stored by SATNAV in the data collection process. This computer program checks each quarter scene (file) successively, to see if there is any intersection between the U.S.G.S. quads and the data. Upon location of a quad that intersects the data set, EXTRACT begins checking lake polygons within the quad for data. All data points within the lake polygons are checked for LANDSAT Band 7 values. Land masses and water bodies are delineated through Band 7. All data which the computer interprets in Band 7 as water bodies is stored for classification. The entire lake polygon is analyzed and the mean values for bands 4, 5, and 6, as well as the variances for these bands, are computed and stored in DATAFILE. A character representation of the data area of a given lake is printed out. These representations are then checked with maps to ascertain if the right lake was found. This process is done for all the lakes over 20 acres in the scene for each of the three dates. The next step in the process then is the classification program.

EXTRACT is a difficult program to understand and quite expensive to run. The cost for the Milwaukee scene for three dates was about \$20 to \$30 each time the program was run. Unfortunately EXTRACT was run unsuccessfully quite a number of times which involved a large expenditure of money. Many problems were encountered in the syntax of the program itself. Hopefully most of the bugs in the system have been worked out as a result of a trial and error type system used on the Milwaukee scene. If the persons who wrote the program would establish a command sequence that would be assured of working for EXTRACT it would greatly help those that will run the program in the future.

After program EXTRACT has extracted data for each lake for three dates, the next step of the process is the actual classification of lakes. A computer program entitled CLASSIFY goes through DATAFILE and corrects for atmospheric scatterings and absorption. An airport runway and a clear lake are used as a steady state index to determine the amount of atmospheric absorption. Once the data is corrected for atmospheric effects, the output is put into a file for classification.

Corrected data is then used to classify lakes as to lake type and trophic condition. The categorization system that is presently being used was developed by Dick Lillie of the DNR Bureau of Research. They are delineated into class numbers as shown below:

LAKE CLASSIFICATION SCHEME		
<u>Class</u>		<u>Class#</u>
Oligotrophic	O	1
	Om	2
	Mo	3
Mesotrophic	M	4
	Me	5
	Em	6
Eutrophic	E	7

Secchi disc and organic nitrogen data along with personal experience was used by DNR limnologists to classify 29 lakes using the above system.

A linear regression model for predicted trophic class status was developed for utilization with LANDSAT data. The parameters used in the model are the individual sums of the data, corrected for atmospheric affects, for bands 4, 5, and 6 as well as the variances for each of those bands over the three dates for each lake. The best fit equation is:

$$\text{Trophic class} = TC = 1.362 + 0.8147(B5) - 0.389(B4) - 0.0967(B6) + 0.1509(VB4) - 0.2053(VB5)$$

B4, B5, and B6 indicate the sum of the corrected data for Bands 4, 5, and 6 respectively over the three dates for each lake. VB4 and VB5 are the sums of the variances of the corrected data within the lake on each day for Bands 4 and 5 respectively. The sum of the variances for Band 6

was insignificant and therefore was not included in the equation. The R^2 value of the regression is 93.8% after adjustment for degrees of freedom. This means that 93.8% of the data variability is explained by the regression analysis.

The other aspect of classifying lakes is an attempt to "type" classify the lakes. Lake types are either silt, clear, algae, or tannin depending upon the lakes spectral signature. A box classifier was used to determine the data values for the spectral signature. Additional data is needed in the form of ground truth to verify the "type" classification.

The output generated from program CLASSIFY is listed by county with the lake number, name, trophic class, type class, and number of dates used for the classification (See figure 2). To adequately classify the lakes, it is necessary to have tapes from three dates during the summer.

To check the validity of the linear regression model, the authors of this report field inspected 18 lakes in the Milwaukee scene. A subjective classification was agreed upon based on secchi disc readings, organic nitrogen, total phosphorous, and visual observations of the littoral zone (see table 1). These subjective classification numbers were then put into the linear regression model for comparison with those classification numbers predicted by LANDSAT. The R^2 value of the regression was 72.1% following the adjustment for degrees of freedom. This model again showed that LANDSAT has a good reliability in the prediction of trophic status classes.

- Based on the linear regression model developed from our data, a prediction of trophic class status was compiled for all the lakes in the Milwaukee scene. Results of our predictive run for this scene is contained in Appendix A. In comparison with the results obtained by the classification system used by the university (with ground truth correlation done by the Bureau of Research, DNR) our program varied on twenty lakes (by 2 trophic class numbers or more).

Reasons why these trophic class numbers disagree can be explained as follows:

- 1) Our data was collected on a "one-shot" basis during the summer. LANDSAT averages the data collected on lakes over three different dates.
- 2) Ground truth data as collected by the Bureau of Research was a result of samples obtained over 4 separate dates during the year.

Our results probably are not as accurate as earlier runs done by the university because of lack of ample ground truth data. Based on our one time sampling for ground truth verification, our correlation with the linear regression model was quite acceptable. The type classification for the program needs additional ground truth data for correlation. For example, algae type lakes show up as tannin or silt lakes. In some cases the reverse can also be true. Additional ground truth data will be required to establish a spectral signature for each water type class.

In conclusion, we feel that the LANDSAT Program for classification of lakes compares favorably with the ground truth data collected on lakes to date. All the significant lakes in the state (greater than 20 acres) could be classified economically by using this technique. Utilization of one full time employee plus assistance from an LTE could accomplish a statewide lake classification in about a year. Any effort to manually classify lakes rather than using the LANDSAT approach would be prohibitively expensive and time consuming. The flexibility of LANDSAT is a strong advantage over the manual classification of lakes. The six districts within DNR could establish their own trophic status schemes for their respective regions.

It is extremely beneficial for personnel working on LANDSAT to have a good background in statistics and computer science. Due to our initial lack of knowledge in these areas, we encountered difficulties in understanding program technology and computer terminology. For example, the EDIT program gave us considerable problems in executing the programs. In addition, a standardized format should be written listing the proper run sequence for each of the programs, and stored in files that are inaccessible to meddlers. With such a format, any changes in personnel would have a minimum impact on the classification process.

Several frustrating problems occurred with our first attempt at using the computer programs, because of changes in the computer programs themselves. Prompt notification to DNR personnel using the classification system of any alterations in the programs would have alleviated many of the problems.

LANDSAT holds promise for depicting changes in trophic status of lakes over time as well as developing strategies for water resource management programs. Should the LANDSAT effort prove successful on a statewide basis, the Wisconsin DNR would again show itself a national leader in water resource and pollution control programs.

Figure 1 shows the typed printout for Beaver Dam Lake. The control point is marked by a red X with row and column coordinates of 932 and 459 respectively.

NO: 154 10: 14-001 NAME: BEAVER DAM

QUADRANGLE: FOX LAKE

SEQ: 2

LANDSAT SCENE 2193-15575 FILE 1 OF 4 03AUG75 RUN AT 22:26:10 04/06/77

405 410 415 420 425 430 435 440 445 450 455 460 465 470 475 480 485 490 495 500 505 510 515 520

910
915
920
925
930
935
940
945
950
955
960

910
915
920
925
930
935
940
945
950
955
960

405 410 415 420 425 430 435 440 445 450 455 460 465 470 475 480 485 490 495 500 505 510 515 520

ORIGINAL PAGE IS
OF POOR QUALITY

Figure 2 depicts the output generated from program CLASSIFY for Waukesha County.
 The output includes lake number and name, trophic class, type class, and number
 of dates used for classification.

LAKES CLASSIFIED FOR WAUKESHA COUNTY

LAKE NO	LAKE NAME	CLASS	TYPE	DATES
1	ASHIPPUN	3	ALGAE	3
2	BEAVER	1	ALGAE	3
3	BIG MUSKEGO	7	ALGAE	3
4	CORNELL	3	ALGAE	3
5	CROOKED	3	ALGAE	3
6	DENOON	4	CLEAR	3
7	DUTCHMAN	2	ALGAE	3
8	EAGLE SPRING	4	ALGAE	3
9	FOREST	2	ALGAE	3
10	FOWLER	3	ALGAE	3
12	HUNTERS	3	ALGAE	3
13	KEESUS	3	ALGAE	3
14	LAC LA BELLE	5	HUMIC	3
16	LOWER GENESEE	3	ALGAE	3
17	LOWER NASHOTAH	1	CLEAR	3
18	LOWER NEMAHBIN	4	HUMIC	3
19	LOWER PHANTOM	3	CLEAR	3
20	HERTON MILLPOND	5	ALGAE	3
21	MID GENESEE	2	ALGAE	3
22	MONTERI MILLPOND	1	ALGAE	1
23	MOOSE	2	ALGAE	3
24	NAGAWICKA	4	CLEAR	3
25	NORTH	4	CLEAR	3
26	OCONOMOWOC	2	CLEAR	3
28	OTTAWA	6	ALGAE	3
29	PEWAUKEE	5	HUMIC	3
30	PINE	1	CLEAR	3
31	PRETTY	3	ALGAE	3
32	RAINBOW SPRINGS	4	ALGAE	3
33	SCHOOL SECTION	5	ALGAE	3
34	SILVER	3	HUMIC	3
35	SPRING	6	ALGAE	3
36	UN. S23, 14T8R17	4	ALGAE	3
37	UPPER GENESEE	2	ALGAE	3
38	UPPER NASHOTAH	1	ALGAE	3
39	UPPER NEMAHBIN	3	CLEAR	3
40	UPPER OCONOMOWOC	4	ALGAE	3
41	UPPER PHANTOM	3	ALGAE	3
42	WATERVILLE MILLPOND	4	ALGAE	3
43	WOOD	2	ALGAE	3

Table 1

<u>Lake Name</u>	<u>Total P (mg/l)</u>	<u>Org-N (mg/l)</u>	<u>Secchi Disc (ft)</u>	<u>Ranking Based on Total P, Org-N and Secchi Disc</u>	<u>Objective Rating Based on Observations</u>	<u>Composite Rating (Objective plus Ranking)</u>	<u>Little- Ratios</u>
Big Green	.02	0.8	10	2	1	1	1
Little Green	.36	3.2	1.0	12	6	5	6
Puckaway	.36	4.5	0.8	13	6	6	7
Fox	.18	2.6	2.2	10	5	6	5
Nagawicka	.04	1.8	3.8	7	5	4	4
Pine	.08	0.7	12	3	2	1	2
Lac LaBelle	.04	0.9	7.5	4	3	4	3
Nemahblin	.04	1.3	6.0	6	3	3	3
Oconomowoc	.02	0.9	5.8	5	3	3	3
Lake Wisconsin	.17	1.8	2.0	9	7	7	6
Swan	.08	1.1	2.2	8	3	5	4
Mason	.24	3.3	1.2	11	4	6	6
Jordan	.02	0.6	10	1	2	2	1
Beaver	-	-	-	-	2	-	2
Devil's Lake	-	-	-	-	1	-	1
Mendota	-	-	-	-	5	-	5
Monona	-	-	-	-	5	-	5
Wingra	-	-	-	-	7	-	7

Appendix A is the output generated from the classification of the lakes in the southeastern section of Wisconsin (the Milwaukee scene). It is based on the linear regression model developed from our data.

LAKES CLASSIFIED FOR COLUMBIA		COUNTY		
LAKE NO	LAKE NAME	CLASS	TYPE	DATES
1	BECKER	2	ALGAE	2
2	CRYSTAL	4	ALGAE	3
3	GEORGE	3	ALGAE	2
5	LAZY	5	ALGAE	3
6	LONG	2	ALGAE	2
7	PARK	5	ALGAE	3
8	SILVER	1	ALGAE	2
9	SPRING	4	ALGAE	3
10	SWAN	2	ALGAE	2
11	WYONA	6	ALGAE	1

LAKES CLASSIFIED FOR DANE		COUNTY		
LAKE NO	LAKE NAME	CLASS	TYPE	DATES
1	BASS	7	ALGAE	3
2	BELLEVILLE MILLPOND	7	ALGAE	2
3	BRANDENBURG	3	ALGAE	2
4	CRYSTAL	1	ALGAE	2
5	FISH	3	CLEAR	1
6	HARRIET	4	ALGAE	2
7	KEGONSA	4	ALGAE	3
8	MENDOTA	3	CLEAR	3
9	MONONA	3	HUMIC	3
10	MUD T6R10	6	ALGAE	3
11	MUD T7R10	3	ALGAE	3
12	MUD T7R12	3	ALGAE	3
13	WAUBESA	4	HUMIC	3
14	WINGRA	5	ALGAE	3

LAKES CLASSIFIED FOR DODGE		COUNTY		
LAKE NO	LAKE NAME	CLASS	TYPE	DATES
1	BEAVER DAM	6	ALGAE	3
2	COLLINS	3	ALGAE	3
3	EMILY	4	ALGAE	3
4	FOX	7	ALGAE	3
5	LOST	4	ALGAE	3
6	SINISSIPPI	3	ALGAE	3
7	UN S15T9R14 ?	5	ALGAL	3

LAKES CLASSIFIED FOR FOND DU LAC COUNTY

LAKE NO	LAKE NAME	CLASS	TYPE	DATES
1	AUBURN	4	ALGAE	3
2	BERNICE	4	ALGAE	3
4	FOREST	2	ALGAE	3
5	KETTLE MORaine	4	ALGAE	3
6	LONG	3	ALGAE	3
7	MAUTHE	3	ALGAE	3
8	MUD	5	ALGAE	3
9	RIPON POND ?	7	ALGAE	3
10	WOLF	4	ALGAE	3

ORIGINAL PAGE IS
OF POOR QUALITY

LAKES CLASSIFIED FOR GREEN COUNTY

LAKE NO	LAKE NAME	CLASS	TYPE	DATES
1	ALBANY MILLPOND	6	ALGAE	2
2	DECATUR	7	ALGAE	2
3	ZANDER	3	ALGAE	1

LAKES CLASSIFIED FOR GREEN LAKE COUNTY

LAKE NO	LAKE NAME	CLASS	TYPE	DATES
1	BIG TWIN	4	ALGAE	3
2	GREEN LAKE	1	CLEAR	3
4	LITTLE TWIN	4	ALGAE	3
5	SPRING T14R11	5	HUMIC	3
6	SPRING T15R13	4	ALGAE	3

LAKES CLASSIFIED FOR JEFFERSON COUNTY

LAKE NO	LAKE NAME	CLASS	TYPE	DATES
1	BLUE SPRING	6	SILT	3
2	GREEN ISLE	6	ALGAE	3
3	HAHN	5	ALGAE	2
4	HOPE	6	ALGAE	3
11	LAKE KOSHKONONG	7	ALGAE	3
5	LOWER SPRING	4	ALGAE	3
6	MUD	6	ALGAE	3
7	RIPLEY	4	CLEAR	3
8	ROCK	3	CLEAR	3
9	ROME MILLPOND	3	ALGAE	3
10	UPPER SPRING	4	ALGAE	3

LAKES CLASSIFIED FOR KIMOSHA

COUNTY

LAKE NO	LAKE NAME	CLASS	TYPE	DATES
3	CAMP	5	ALGAE	2
4	CLINTER	4	ALGAE	2
8	GEORGE ?	7	ALGAE	2
9	HOOKEE	7	ALGAE	2
11	MONTGOMERY	4	ALGAE	1
12	MUD	7	ALGAE	2
13	PADDOCK	6	ALGAE	2
15	ROCK	3	ALGAE	3
16	SHANGRILA	6	ALGAE	3
17	SILVER	7	ALGAE	3
18	VOLTZ	6	ALGAE	1

LAKES CLASSIFIED FOR MANITOWOC

COUNTY

LAKE NO	LAKE NAME	CLASS	TYPE	DATES
2	CARSTENS	7	ALGAE	1
3	CEDAR	1	CLEAR	2
8	PIGEON	2	ALGAE	2
11	WILKE	4	HUMIC	2

LAKES CLASSIFIED FOR MARATHON

COUNTY

LAKE NO	LAKE NAME	CLASS	TYPE	DATES
31	ZZZZZZ 31	3	HUMIC	3
33	ZZZZZZ 33	5	ALGAE	3

LAKES CLASSIFIED FOR MARQUETTE

COUNTY

LAKE NO	LAKE NAME	CLASS	TYPE	DATES
1	BIRCH	1	ALGAE	2
3	COMSTOCK	2	ALGAE	2
4	CRYSTAL	1	ALGAE	2
5	EMERY	7	ALGAE	1
7	ENNIS (MUIR)	4	ALGAE	1
8	HARRISVILLE POND	2	ALGAE	2
9	KILBY	3	CLEAR	1
10	KNIGHTS	4	ALGAE	1
12	NETCALF	3	ALGAE	1
14	NESHKORO MPD.	2	ALGAE	2
17	PETERS	3	ALGAE	1
20	SHARON	2	ALGAE	2
21	SILVER	2	ALGAE	2
22	SPRING	1	ALGAE	2
23	TUTTLE	2	ALGAE	2
26	WHITE	1	ALGAE	3

LAKES CLASSIFIED FOR OZAWAKE

COUNTY

LAKE NO	LAKE NAME	CLASS	TYPE	DATE
1	GRAFTON MILLPOND ?	5	ALGAE	3
2	HARRINGTON BCH. ST. PK. QU	2	ALGAE	3
3	LAC DU COURS	7	SILT	3
4	PIT LAKE DOESN'T SHOW	4	ALGAE	3
5	SPRING	4	ALGAE	3
6	THIENSVILLE MILLPOND	5	ALGAE	3

LAKES CLASSIFIED FOR RACINE

COUNTY

LAKE NO	LAKE NAME	CLASS	TYPE	DATES
2	BROWNS	3	CLEAR	3
3	BUENA	6	ALGAE	3
4	EAGLE	6	ALGAE	3
6	KEE NONG GO MONG	5	ALGAE	3
8	TICHIGAN	5	ALGAE	3
9	WAUKEESEE	4	ALGAE	3
10	WIND	6	HUMIC	3

LAKES CLASSIFIED FOR ROCK

COUNTY

LAKE NO	LAKE NAME	CLASS	TYPE	DATES
1	CLEAR	2	ALGAE	3
2	FULTON POND	7	ALGAE	1
3	GIBBS	4	ALGAE	3
4	LEOTA	5	ALGAE	2
5	SPAULDINGS POND	4	ALGAE	2
6	STORRS	7	ALGAE	3

LAKES CLASSIFIED FOR SHEBOYGAN

COUNTY

LAKE NO	LAKE NAME	CLASS	TYPE	DATES
1	CROOKED	3	ALGAE	3
2	CRYSTAL	2	ALGAE	3
3	ELKHART	1	ALGAE	3
4	ELLEN	4	ALGAE	3
5	FRANKLIN MILLPOND	6	ALGAE	3
6	KOHLER MILLPOND	3	ALGAE	2
7	LITTLE ELKHART	4	ALGAE	3
8	RANDOM	5	ALGAE	3
9	SEVEN	3	ALGAE	3

LAKES CLASSIFIED FOR WALWORTH COUNTY

LAKEL NO	LAKEL NAME	CLASS	TYPE	DATES
1	ARMY	4	ALGAE	3
2	BEULAH	2	CLEAR	3
3	BOOTH	2	CLEAR	3
5	COMUS	7	ALGAE	3
6	CRAVATH	7	ALGAE	3
7	DELAVER	4	ALGAE	3
9	GREEN	2	CLEAR	3
8	LAKE GENEVA	2	CLEAR	3
12	LORAIN	2	ALGAE	2
14	LULU	3	ALGAE	3
15	MIDDLE	3	ALGAE	3
16	MILL	3	ALGAE	3
17	NORTH	3	ALGAE	3
19	PETERS	5	ALGAE	3
21	PLEASANT	2	CLEAR	3
22	POTTERS	5	ALGAE	3
23	RICK	5	ALGAE	3
24	SWAN	4	ALGAE	3
25	TURTLE	4	ALGAE	3
26	WANDAWEGA	3	ALGAE	3
27	WHITEWATER	5	ALGAE	3

LAKES CLASSIFIED FOR WASHINGTON COUNTY

LAKE NO	LAKE NAME	CLASS	TYPE	DATES
1	AMY BELL	3	ALGAE	3
2	BARK	5	ALGAE	3
3	BIG CEDAR	3	CLEAR	3
4	DRUID	3	CLEAR	3
5	ERLER	3	ALGAE	3
6	FIVE	2	ALGAE	3
7	FRIESS	4	ALGAE	3
8	GREEN	4	ALGAE	3
10	LOWE	4	ALGAE	3
11	LUCAS	3	ALGAE	3
12	PIKE	4	HUMIC	3
13	SILVER	2	ALGAE	3
14	TWELVE	7	SILT	3
15	WALLACE	4	ALGAE	3
16	WEST BEND MILL POND NOT	6	ALGAE	3

LAKE'S CLASSIFIED FOR WAUKESHA

COUNTY

LAKE NO	LAKE NAME	CLASS	TYPE	DATE
1	ASHIPPUN	3	ALGAE	3
2	BEAVER	2	ALGAE	3
3	BIG MUSKEGO	7	ALGAE	3
4	CORNELL	4	ALGAE	3
5	CROOKED	3	ALGAE	3
6	DENON	4	HUMIC	3
7	DUTCHMAN	3	ALGAE	3
8	EAGLE SPRING	4	ALGAE	3
9	FOREST	2	ALGAE	3
10	FOWLER	3	ALGAE	3
11	GOLDEN	4	HUMIC	3
12	HUNTERS	3	ALGAE	3
13	KEESUS	3	ALGAE	3
14	LAC LA BELLE	4	ALGAE	3
15	LITTLE MUSKEGO	4	HUMIC	3
16	LOWER GENESEE	4	SILT	3
17	LOWER NASHOTAH	2	ALGAE	3
18	LOWER NEMAHBIN	4	ALGAE	3
19	LOWER PHANTOM	3	ALGAE	3
20	MERTON MILLPOND	5	ALGAE	3
21	MID GENESEE	2	ALGAE	3
22	MONTERY MILLPOND	4	ALGAE	3
23	MOOSE	2	ALGAE	3
24	NAGAWICKA	3	CLEAR	3
25	NORTH	3	CLEAR	3
26	OCONOMOWOC	2	CLEAR	3
28	OTTAWA	6	ALGAE	3
29	PEWAUKEE	4	CLEAR	3
30	PINE	2	CLEAR	3
31	PRETTY	3	HUMIC	3
32	RAINBOW SPRINGS	4	ALGAE	3
33	SCHOOL SECTION	5	ALGAE	3
34	SILVER	2	ALGAE	3
35	SPRING	6	ALGAE	3
36	UN S23,14TER17	5	ALGAE	3
37	UPPER GENESEE	3	ALGAE	3
38	UPPER NASHOTAH	2	ALGAE	3
39	UPPER NEMAHBIN	2	CLEAR	3
40	UPPER OCONOMOWOC	4	ALGAE	3
41	UPPER PHANTOM	4	ALGAE	3
42	WATERVILLE MILLPOND	4	ALGAE	3
43	WOOD	3	ALGAE	3

ORIGINAL PAGE IS
OF POOR QUALITY

LAKE CLASSIFIED FOR WAUSHARA

COUNTY

LAKE NO	LAKE NAME	CLASS	TYPE	DATES
2	BIG HILLS	1	CLEAR	1
11	JOHN'S	1	ALGAE	2
13	KUSEL	1	CLEAR	1
14	LITTLE HILLS	1	ALGAE	2
15	LONG	1	ALGAE	1
17	LUCERNE	1	ALGAE	2
20	MIDDLE	3	ALGAE	3
21	MOUNT MORRIS	1	ALGAE	1
22	NAPOWAN	1	CLEAR	1
23	NORWEGIAN	6	ALGAE	1
24	PEARL	2	ALGAE	3
29	PORTERS	1	ALGAE	2
31	ROUND S35T20R11	1	CLEAR	1
32	SILVER S32T20R11	1	CLEAR	1
34	SPRING	4	ALGAE	3
35	UPPER WHITE R. MPD.	1	ALGAE	2
37	WILSON	1	CLEAR	1

ASSESSMENT OF AQUATIC ENVIRONMENTS BY REMOTE SENSING

Michael S. Adams
Frank L. Scarpace
James P. Scherz
William J. Woelkerling

Edited by James P. Scherz

IES REPORT 84

September 1977

Environmental Monitoring and
Data Acquisition Group
Institute for Environmental Studies
University of Wisconsin-Madison



C-2
This research was supported in part by NASA Office of University Affairs Grant No. GL 50-002-127; NSF-IBP Interagency Agreement AG-199,40-193-69; with the U.S. Atomic Energy Commission and the Oak Ridge National Laboratory, and NSF Grant BMS-75-1977.

ABSTRACT

Over the past decade there has been considerable interest in the possible use of remote sensing as a tool for monitoring water quality. From 1968 to 1976, interdisciplinary work at the University of Wisconsin-Madison, in cooperation with state agencies, was devoted to investigating this topic. The effort involved theoretical studies in the physics of remote sensing and the modeling of energy/water interactions, as well as the application of remote sensing and ground truth data collection to lake classification. Data from laboratory, field, aircraft, and satellite indicate that remote sensing can be used successfully and practically in water quality investigations of turbidity, suspended solids, and biomass production in lakes. Biomass production relates to lake trophic conditions, so the techniques described can also be used for trophic classification. Specific examples are given in which remote sensing has been used in mapping algae and macrophytes and in classifying Wisconsin lakes by their trophic state.

###

The contents of this report do not necessarily reflect the views and policies of the supporting agencies, nor does the mention of trade names or commercial products constitute endorsement or recommendations for use

###

For information about publications, write to

Communications Office
Institute for Environmental Studies
University of Wisconsin-Madison
610 Walnut Street, 120 WARF Bldg
Madison, WI 53706

TABLE OF CONTENTS

I.	INTRODUCTION by James P. Scherz	11
II.	THE NATURE OF AQUATIC ENVIRONMENTS by Michael S. Adams	13
A.	PRIMARY PRODUCTION AND EUTROPHICATION	13
B.	WATER QUALITY	14
C.	IMPORTANT WATER QUALITY PARAMETERS	15
1.	Phosphorus (P)	15
2.	Nitrogen (N)	16
3.	Chlorophyll <u>a</u>	16
4.	Water Clarity	16
5.	Organic Carbon	16
D.	LAKE CLASSIFICATION	17
1.	Oligotrophic Lakes	18
2.	Hardwater Marl Lakes	18
3.	Bog-dystrophic Lakes	19
4.	Eutrophic Lakes	19
5.	Interrelationships and Common Ontogeny of the Four Main Lake Types	19
III.	WATER QUALITY PARAMETERS ASSOCIATED WITH REMOTE SENSING by James P. Scherz	21
A.	TURBIDITY, PARTICULATES, AND THE REMOTE SENSING OF WATER QUALITY . .	21
1.	Field Methodology for Ground Truth Measurements of Particulates	23
2.	Laboratory Methodology for Ground Truth Measurements of Particulates	24
B.	MACROPHYTES AND THE REMOTE SENSING OF WATER QUALITY	27
1.	Field Sampling of Aquatic Macrophytes	27
2.	Laboratory Methodology for Ground Truth Measurements of Macrophytes	29
C.	TIMING OF REMOTE SENSING SAMPLING	29
IV.	REMOTE SENSING: BASIC CONSIDERATIONS by James P. Scherz and Alan R. Stevens	32
A.	BACKGROUND	32
B.	THE ELECTROMAGNETIC SPECTRUM AND BASIC RELATIONSHIPS	33
C.	ATMOSPHERIC EFFECTS	36

D.	REFLECTION CHARACTERISTICS	36
E	ENERGY BALANCE	37
F.	PHOTOGRAPHY	38
1.	Black and White Film	38
2.	Normal Color Film	40
3	Color Infrared Film	41
4	Filters	42
5.	Cameras	44
6.	Multiband Cameras	46
G	RADIOMETERS	48
H.	SCANNERS	49
1.	Thermal Scanners	49
2	Multispectral Scanners	49
I	ANALYSIS OF MULTISPECTRAL DATA	52
V.	REMOTE SENSING AND WATER - MODELING AND ANALYZING ENERGY RELATIONSHIPS by James P. Scherz	54
A.	GENERAL	54
B	ALGAE IN MADISON AREA LAKES	57
C	RED CLAY IN LAKE SUPERIOR	59
D	SURFACE EFFECTS	62
E	LABORATORY APPARENT REFLECTANCE VS. TURBIDITY AND SUSPENDED SOLIDS .	64
F	OBTAINING THE VOLUME REFLECTANCE VALUE, ρ_v , IN THE LABORATORY	69
G	LABORATORY DIFFERENCE (D_1)	70
H.	LABORATORY FINGERPRINTS FOR MATERIAL ADDED TO WATER	71
I	BOAT LEVEL ANALYSIS AND MODELING	75
1	General	75
2	Obtaining ρ_{v_1} In The Field	77
3.	Laboratory Data Compared to Boat Level Data	78
J	AIRBORNE AND SATELLITE MODELING	80
1.	Airborne or Satellite Residual, R_1''	81
2	Solving For Volume Reflectance, ρ_v	82
3.	Modeling and Solving For Atmospheric Parameters	83

K	SATELLITE DATA ANALYSIS	88
L.	BOTTOM EFFECTS IN SATELLITE IMAGERY	90
M.	MODELING LIGHT PENETRATION AND RETURN IN A LAKE	92
	1. Magnitude of Energy That Returns From Below the Secchi Disc Reading and From Various Layers of Water	97
	2 Penetration of Different Wavelengths of Light	99
N	PRACTICAL ANALYSIS OF SATELLITE REMOTE SENSING DATA AND LAKE CLASSIFICATION	99
	1. General	99
	2. Ground Truth For Remote Sensing Lake Classification	102
	3. Lake Classification Using LANDSAT	103
	TECHNICAL NOMENCLATURE USED IN CHAPTER V	113
VI.	THE ANALYSIS OF REMOTE SENSING DATA by James P. Scherz and Frank L. Scarpace	117
A.	GENERAL	117
B	MULTISPECTRAL SCANNER DATA	117
C	PHOTOGRAPHIC ANALYSIS	118
	1 The D-Log E Curve	119
	2. Obtaining Relative Exposure of Objects Photographed by Using the D-Log E Curve	121
D	BLACK AND WHITE REVERSAL FILM - LANDSAT SCENE ANALYSIS	121
E	COLOR FILM ANALYSIS	123
	1 Color Negative Film	123
	2. Color Reversal Film	124
	3 Color Infrared Film	126
F	COMPUTER ANALYSIS EQUIPMENT	126
G	OPERATIONAL LAKE ASSESSMENT PROGRAMS USING LANDSAT DATA	130
VII.	APPLICATION	134
A	EXAMPLE 1 TURBID WATER LOCATED BY AERIAL IMAGES by James P Scherz	134
B	EXAMPLE 2 MACROPHYTE MAPPING by Michael S Adams and Todd Gustafson	135
	1 Macrophyte Community Mapping by Photo Interpretation	135
	a Preliminary community delineation	136
	b Obtaining ground truth	136
	c Example of macrophyte community mapping by photo interpretation	137

2. Macrophyte Community Mapping by Photoanalysis	141
a. Macrophyte community differentiation	142
b. Macrophyte quantity estimation by microdensitometer analysis of aerial images	147
C. EXAMPLE 3: REFLECTANCE FINGERPRINTS FROM DIFFERENT ALGAL TYPES AND THEIR LABORATORY-TO-SATELLITE TRANSLATION by James F. Thorne, William J. Woelkerling, and James P. Scherz	149
1. Laboratory Fingerprints for Different Algal Types	150
2. Phytoplankton Quantity and Low Altitude Photography	155
3. Translating From Laboratory to Satellite Fingerprints	156
D. EXAMPLE 4: THE CASE OF PRAIRIE LAKE FROM SATELLITE TO GROUND by James P. Scherz	156
1. Locating Problem Lakes From Color Coded Satellite Maps	156
2. Low Altitude Photography and Observations	160
3. Collecting Ground Truth at Prairie Lake and Rice Creek	168
4. Prairie Lake Later	172
a. Sample site #1	173
b. Sample site #2	175
c. Sample site #3	177
d. Flow Calculations	177
ACKNOWLEDGMENTS	180
APPENDIX A — SOURCES FOR METHODS OF WATER QUALITY ANALYSIS USED AT THE UNIVERSITY OF WISCONSIN-MADISON ON WORK DESCRIBED IN THIS REPORT	182
APPENDIX B — GENERALIZATIONS OF DEVELOPMENT PROCESS FOR COLOR FILMS	183
APPENDIX C — CURVES FOR C_2 TO RELATE SATELLITE TO LABORATORY DATA	186
APPENDIX D — CONSTRUCTING A D-LOG E CURVE FOR COLOR REVERSAL FILM	195
APPENDIX E — REFLECTANCE FINGERPRINTS FOR MARL LAKES AND LAKES CONTAINING SUSPENDED GLACIAL ROCK FLOUR	199
APPENDIX F — CORRELATION OF STANDARD WATER QUALITY DATA WITH LANDSAT COLOR CODED MAPS	204
REFERENCES	222
GLOSSARY	228

FIGURES

1.	Classical trophic lake types	17
2.	Outline of common ontogeny of four main lake types	20
3.	Correlation of suspended solids to turbidity for three lake types	22
4.	Relationships between turbidity (T) and Secchi disc readings (S) for Wisconsin lakes sampled during 1974/1975	24
5.	Schematic showing relationships among turbidity, suspended solids, dissolved solids, and color	25
6.	Schematic showing relationships among total, volatile, and nonvolatile solids	26
7.	Plot of light penetration versus time (Madison area lakes)	30
8.	Effect of seasons of year on the total suspended solids at Duluth Harbor, Lake Superior	31
9.	The electromagnetic energy spectrum	34
10.	White light broken down into the individual colors of the visible and near visible spectrum	35
11.	Solar radiation curves	35
12.	Energy reflected from a blue object	36
13.	Typical reflection curves for live green vegetation and green netting material	37
14.	Cross section of black and white film	38
15.	Sensitivities of various black and white emulsions	39
16.	Cross section of normal color film	40
17.	Sensitivity of typical normal color film	40
18.	Sensitivity of color infrared film	41
19.	Typical transmission curve for short band blocking type Wratten filters	43
20.	Narrow band pass filter	43
21.	Itek nine lens camera	47
22.	Portable 4-camera bank being used from the open window of a small fixed-wing aircraft	47
23.	Schematic of thermal scanner	50
24.	Schematic of multispectral scanner	51
25.	Multispectral imagery	51
26.	Crop identification and mapping by computer processing of multispectral data	53
27.	Components of light showing on an aerial image caused by various interactions of light in, on, and through the water	55
28.	LANDSAT images of lakes near Madison, Wisconsin	57
29.	Strength of backscatter signal received by band 5 of LANDSAT, Madison area lakes	58
30.	LANDSAT image of southwestern Lake Superior	60
31.	Volume reflectance from laboratory analysis and apparent reflectance from LANDSAT imagery for the water in Lake Superior near Duluth, Minnesota	61
32.	Suspended solids map for southwest end of Lake Superior made from LANDSAT image and a curve as shown in Figure 31	62

33.	Approximate surface reflection component from clear water	64
34.	Direct energy relationships in the laboratory	64
35.	Laboratory backscatter expressed as % lab apparent reflectance (AP) versus suspended solids	67
36.	Laboratory backscatter expressed as laboratory apparent reflectance (AP) plotted against turbidity for 127 different lake samples collected over three years	68
37.	Characteristic laboratory fingerprints of two types of material in water	72
38.	Laboratory reflectance difference curves (D_1) or fingerprints for clear water type lakes with various amounts and types of algae present	73
39.	Laboratory reflectance difference curves (D_1) for humic lakes	74
40.	Direct and indirect energy relationships in the field	76
41.	Characteristic fingerprints from satellite residual signal, R_1 , for three water types	90
42.	Effect of sand bottom and macrophytes on satellite fingerprint of a clear lake containing some humic material	91
43.	Effect of heavy weeds and mud bottom on signal expected from humic lake	92
44.	Modeling of light that penetrates to and returns from the Secchi disc at the Secchi disc reading	94
45.	Transmittance analysis of different lake waters	95
46.	Hypothetical Secchi disc readings, $2.3/\alpha$, for different waters at different wavelengths	96
47.	Determining percentage of upwelling energy from suspended particles at different depths	98
48.	Interaction of different wavelengths of energy with water	100
49.	Effect of time of year on reflectance fingerprints in an algal lake	101
50.	Water temperature, dissolved oxygen, and nitrates plotted against time	102
51.	Effect of red clay on clear Lake Superior water	105
52.	Scheme used to classify lakes from LANDSAT data based upon Wetzel data in Figure 1 and the clear water, humic, and algal lake types estimated by aerial observations	106
53.	Satellite residual fingerprints for clear, moderate, and intensely humic lakes (Profile I in Figure 52)	107
54.	Satellite residual fingerprints of moderately humic lakes containing various amounts of algae (Profile II in Figure 52)	108
55.	Satellite residual fingerprints of nonhumic type lakes (clear water type) containing various amounts of algae (Profile III in Figure 52)	109
56.	Example lake classification color coded map from multispectral analysis of LANDSAT data by the Bendix MDAS system	111
57.	Obtain radiance values from satellite tape count using calibration curves for the LANDSAT satellite multispectral scanners	118
58.	D-Log E curve for a black and white negative film	119
59.	Schematic of equipment used to analyze film and water samples	120
60.	D-Log E curve for a black and white positive film	122
61.	D-Log E curve for three layers of normal color film processed to a color negative	123

62.	Sketch of dye development and transmittance for normal color film	124
63.	D-Log E curves for a normal color reversal transparency (slide film) . . .	125
64.	PEP terminal for analyzing LANDSAT tapes	127
65.	Bendix MDAS terminal for multispectral analysis of LANDSAT tapes	128
66.	Satellite spectral signatures for three types of lakes from Bendix MDAS analysis	129
67.	Image scene as viewed on the PEP terminal	133
68.	LANDSAT satellite image taken 12 August 1972 showing the southwest end of Lake Superior near Duluth	135
69.	Color infrared photographs of Lake Wingra, Madison, Wisconsin	139
70.	Spectral signatures of some of the Lake Wingra image types of macrophytes	143
71.	Lake Wingra vegetation map of 14 July 1971	144
72.	Mean values and 95% confidence intervals for film transmittance ratios used for differentiation of the Lake Wingra image types of macrophytes	146
73.	Regression analysis of <i>Myriophyllum</i> harvest data and film densities that were standardized by using readings from open water areas	148
74.	Regression analysis of <i>Oedogonium</i> harvest data and film densities	148
75.	Laboratory reflectance differences and energy absorption data for a green alga (<i>Scenedesmus quadricauda</i>)	150
76.	Laboratory reflectance differences and energy absorption data for a diatom (<i>Navicula</i>)	151
77.	Laboratory reflectance difference and energy absorption data for a blue-green alga (<i>Anabaena variabilis</i>)	152
78.	Suspended solids versus reflectance in the absorption bands of three types of algae	153
79.	Suspended solids versus turbidity for 71 water samples collected in 1974	154
80.	Plot of green reflected energy as measured by aerial photography versus chlorophyll <u>a</u> concentration for blue-green algae in nonhumic waters	155
81.	Laboratory reflectance differences for three types of cultured algae . . .	157
82.	Laboratory reflectance differences, D_1 , for two types of cultured algal mixtures	158
83.	Integrated laboratory reflectance differences for algal types compared to LANDSAT signal for different algal lakes	159
84.	LANDSAT scene of northern Wisconsin taken in August 1972	161
85.	Bendix MDAS computer color categorized printout from multispectral analysis of LANDSAT data for a portion of northern Wisconsin	163
86.	Cattle yard encompassing the springs of Rice Creek that runs into the north end of Prairie Lake	166
87.	Use of green energy in May to penetrate water and show cow paths in Rice Creek	167
88.	Some effects of cows near and in Rice Creek	169
89.	Cows on west bank of Rice Creek near sample site #1	170
90.	A view of Rice Creek from sample site #1 looking south toward Prairie Lake	170
91.	Map and lab data relating to water samples collected from Prairie Lake on 17 August 1976	171

92	Looking east to sample site #1 on Rice Creek	174
93.	Looking south on Rice Creek from sample site #1	176
94	Comparison of 1976 and 1977 water quality data and approximate flow calculations	178
95.	Color additive process (mixing light)	185
96.	Color subtractive process (mixing pigments)	185
97.	C ₂ for band 4	187
98.	C ₂ for band 5	188
99.	C ₂ for band 6	189
100.	C ₂ for band 7	190
101.	Constructing a D-Log E curve for color reversal film	198
102.	Reflectance curves for marl lake and water containing glacial rock flour — laboratory fingerprints and expected satellite fingerprints	200
103.	Satellite residual fingerprints for marl lakes and lakes containing glacial rock flour	201
104	Particle size distribution for two waters containing glacial rock flour	203
105	Trophic classification scheme for LANDSAT water categories as a function of dissolved tannin and suspended algae material	211
106	Color versus Secchi disc readings — Minnesota water depth	212
107	Chlorophyll <u>a</u> versus Secchi disc readings — Minnesota water data	212
108	Plot of Secchi disc readings versus Chlorophyll <u>a</u> for lakes lying along Profiles I and II in Figure 105 — Minnesota water quality data	213
109	Secchi disc readings versus Chlorophyll <u>a</u> — along Profile III, Figure 105	214
110.	Secchi disc readings versus estimated algae content — along Profile III, Figure 105	214
111.	Secchi disc readings versus estimated tannin content — along a profile between I and II in Figure 105	215
112	Secchi disc readings versus the sum of green and brown colors in lakes as observed on MDAS color coded output	216
113	Color versus estimated tannin content — along a profile between I and II in Figure 105	217
114	Chlorophyll <u>a</u> versus estimated algal content, Profile III, Figure 105	218
115	Chlorophyll <u>a</u> versus total phosphorus	219
116	Amount of green color observed on MDAS color coded printout in 1/10's	220
117	Data pertaining to marl lakes when they were printed out as turquoise by MDAS on the color coded output maps	221

TABLES

1	Typical output for one county relating to lake turbidity derived from bands 5 and 7 of LANDSAT analysis	132
2.	Identification key for Lake Wingra image types	2
3	Water quality parameters associated with different MDAS lake categories shown in Figure 105	206

I. INTRODUCTION

This report summarizes seven years of work at the University of Wisconsin-Madison on the application of remote sensing to water quality monitoring. The investigations began in 1968 as a joint effort between personnel at the UW-Madison and several Wisconsin state agencies. In 1969, support was obtained from the National Aeronautics and Space Administration (NASA) Office of University Affairs through Grant No. NGL 50-002-127. The joint investigation grew to include experts from botany, physics, civil engineering, and environmental studies. At the UW-Madison, this multidisciplinary project was administered by the Environmental Monitoring and Data Acquisition Group (EMDAG) of the Institute for Environmental Studies (IES). Research on littoral zone aquatic macrophytes also received support from the National Science Foundation (NSF) through the Eastern Deciduous Forest Biome, United States-International Biological Program, under Interagency Agreement AG-199, 40-193-69 with the Atomic Energy Commission-Oak Ridge National Laboratory, and through NSF grant BMS-75-1977 to the UW-Madison (principal investigator for both NSF grants was M. S. Adams).

Initial remote sensing work on water quality concentrated on photometric laboratory studies, and boat level and low altitude aerial photography. The culmination of the project was an analysis of imagery from the ERTS (LANDSAT)* satellite. This imagery was used to develop a trophic classification of about 800 lakes in Wisconsin. A portion of this effort was supported by the Wisconsin Department of Natural Resources (DNR). The Princeton Electronic Products (PEP) computer terminal at the UW-Madison was used for preliminary data manipulation and reduction. More advanced work on the LANDSAT data then was done on the Bendix Multispectral Data Analysis System (MDAS) under another NASA grant (NAS 5-20942). Although the MDAS analysis was not part of the NASA grant to the UW-Madison, the success of the MDAS work depended on the previous work done under this grant. Therefore, some of the MDAS results are also mentioned in this report. This combination of university theory and MDAS equipment has created an effective, operational system for classifying lakes over large geographical areas.

One of the original purposes of this multidisciplinary investigation was to determine to what extent remote sensing could be used to measure and monitor water quality. By 1975 the staff concluded they had learned enough to produce a report that would consolidate the new knowledge gained. The anticipated departure of key personnel further stimulated the writing of this report, in order to preserve the knowledge gained by all parties on the project.

In Chapter II the nature of aquatic environments is discussed. Chapter III covers water quality parameters associated with remote sensing. The basic science of remote sensing and the correlation of conventional water quality indicators with remote sensing signals are discussed in Chapters IV and V.

* In 1974, two years after it had begun functioning, the Earth Resources Technology Satellite (ERTS) was renamed LANDSAT. This report discusses satellite data before and after the name change, but for simplicity only LANDSAT will be used.

In Chapter V theoretical models are used to explain how light signals are modified by water volume, the bottom, the surface, and atmospheric effects. An understanding of these interactions is crucial when using remote sensing for water quality work. For analyzing oil slicks, only the surface effects are important, for bottom weed analysis, the bottom signals are necessary. For analyzing material mixed with the water itself the only important signal is the energy backscattered from the water volume — all other signals are troublesome noise. This report shows workable techniques for obtaining this signal by removing noise from surface and atmospheric effects. Once these effects are removed the signals from the bottom lake weeds are also free from such noise and can be better analyzed.

Chapter VI touches on the mechanical aspects of analyzing film and satellite data, and explains how conventional satellite data analysis systems designed for land cover mapping were modified to determine water quality.

Chapter VII includes four examples where remote sensing has been used in mapping, or in investigating water quality problems.

II. THE NATURE OF AQUATIC ENVIRONMENTS

Before one can talk about using remote sensing for water quality monitoring it is first necessary to define what is meant by water quality. The quality of inland lakes is often expressed in terms of the lake's trophic state. A lake with extreme nuisance algal blooms or a lake that is choked with aquatic weeds is often said to be eutrophic. A very clear lake is called an oligotrophic lake. A lake that is intermediate between an oligotrophic and a eutrophic lake may be called a mesotrophic lake. Bog-dystrophic (or humic lakes*) and marl** lakes are two other types of lakes that are important for a complete lake classification scheme. This chapter discusses traditional methods of lake classification.

A. PRIMARY PRODUCTION AND EUTROPHICATION

Likens (1972) defined eutrophication, from an ecosystem point of view, as "nutrient or organic matter enrichment, or both, that results in high biological productivity and a decreased volume within an ecosystem." In this case, volume refers to the volume of a lake filling up with accumulating organic matter. Rodhe (1969) reviewed the classical use of phytoplankton production of organic matter (Naumann 1919), nutrient concentrations in lakes (Weber 1907), and hypolimnetic oxygen concentrations with the corresponding presence of certain bottom-dwelling animals (Thienemann 1918), as indices of oligotrophic or eutrophic lakes. On the basis of these considerations, eutrophic lakes would be expected to have high phytoplankton production of organic matter, oxygen depletion near the lake bottom, and certain kinds of organisms (specifically, certain kinds of Chironomid larvae) on the bottom. Conversely, oligotrophic lakes would be expected to have low nutrient levels, low phytoplanktonic production of organic matter, high oxygen levels, and other species of Chironomid larvae on the bottom.

Likens discussed a measure of eutrophication that considers the importance of allochthonous organic matter. Allochthonous organic matter is imported to the lake from its drainage basin, as contrasted with autochthonous organic matter that is formed by photosynthetic activities of plants in the lake. The difference between autochthonous and allochthonous organic matter supply to lakes was recognized early in this century by Birge and Juday (1927).

* In the northern latitudes, especially where spruce and tamarack swamps are prevalent and the soil is acid, many lakes have a brown, tea-like color. This color is associated with undecomposed organic matter and materials such as tannic acid, iron and manganese. In the literature such water has been described as "Gelbstoff," yellow substance, brown water, humic material, or tannin water, etc. In this report such material will be called humic material and lakes where it is present will be called humic lakes.

** Marl is an earthy, unconsolidated deposit in freshwater lakes, consisting chiefly of calcium carbonate mixed with clay or other impurities. Fine precipitating calcium carbonate particles in suspension can cause a distinct blue-green color in marl lakes.

Classically, eutrophication was considered part of the natural process of aging in some undisturbed lakes (Likens). Rapid acceleration of the process by effects of man has been given the name "cultural eutrophication" (Hasler 1947). The metabolism of oligotrophic lakes, having low productivity, is regulated significantly by low transport levels of inorganic nutrients from areas outside the lake but within the drainage basin.

Eutrophication rate is most often controlled by the amount of phosphorus received by a lake. An outstanding example of the importance of phosphorus was demonstrated by a large-scale lake fertilization experiment in a lake in northwestern Ontario, located on Precambrian Shield bedrock (Schindler 1974). The biology and chemistry of the lake was representative of about half the waters that drain to the Laurentian Great Lakes. The lake is constricted in the middle, which allowed the two parts of the lake to be physically separated by a plastic curtain. One basin was fertilized with phosphorus, nitrogen, and carbon. The other basin received only nitrogen and carbon. The basin receiving phosphorus quickly developed a dense growth of phytoplankton.

Lake succession, or development, can proceed from eutrophic to oligotrophic states (Margalef 1968), in contrast to the usual direction of change. Successional changes toward oligotrophy can be natural if nutrients from runoff waters are not continuously transported to lakes (Hutchinson 1967, Likens). Also, man can control inputs of nutrients to lakes by management procedures. This can force lake succession toward oligotrophy (Edmundson 1970, Oglesby 1969), as in the case of sewage diversion from Lake Washington in Seattle (Edmundson). The diversion quickly resulted in a reversal in the trophic status of the lake.

Historically, the term eutrophication has been generally misused. Excellent detailed discussions on the historical development of the term and its misuse can be found elsewhere in the literature (National Academy of Sciences 1969, Likens 1972, Hutchinson 1973, Vallentyne 1974, Wetzel 1975). A basic problem with early consideration of eutrophication was that only phytoplankton were considered to be important among the primary producers in lakes. Recently the importance of the littoral zone macroflora has been recognized as a source of organic matter production in lakes (Westlake 1965, Adams and McCracken 1974, Wetzel 1975).

B WATER QUALITY

The subject of water quality is indeed complex. The public has the right to expect drinking water that is odor-free, tastes good, has a pleasant appearance (i.e., is clear), and is free from toxic inorganic chemical substances, organic poisons, and harmful bacteria. People generally desire recreational lakes that are relatively clear, not smelly and not choked with algae. The swimmer, boating enthusiast, and water skier prefer their lakes to be relatively free of submersed aquatic macrophytes (large aquatic plants), some of which can be called weeds. On the other hand, the bass fisherman prefers to have some weeds in the lake in which he fishes. Most people probably consider large quantities of submersed macrophytes undesirable.

Algae can be divided taxonomically into a number of divisions or phylla. One major division, the green algae (Chlorophyta), has many genera represented in lakes, but these algae do not annoy people unless the algae are present in large quantities. The diatoms (Class Bacillariophyceae of the Chromophyta), like the green algae, are well represented in lakes but generally are not considered offensive. Another division, the blue-green algae (Cyanophyta), tends to smell and so is more offensive to people, particularly during periods of active growth. The blue-greens are characteristic of lakes that have considerable inputs of inorganic nutrients. Representative examples from this group of algae are *Anabaena* and *Aphanizomenon*.

Another way to divide the algae is to separate them with respect to the specific ecological habit they exhibit. Algae suspended in the water column due to their own buoyancy are the phytoplankton. Algae attached to macrophytes are called epiphyton. Algae that occur in the upper levels of mud sediments are called epipelagic algae. Algae of most concern to the public are the phytoplankton and the epiphyton. Both kinds may develop nuisance growth levels. Some epiphytic algae develop mat-like growth habits and occur almost as a lid over macrophyte communities. An example is the dense mat of *Oedogonium* (a green alga) that occurs over the water milfoil macrophyte community in Lake Wingra, in Madison, Wisconsin (Figure 68).

C IMPORTANT WATER QUALITY PARAMETERS

Brief mention of the more important measurable water quality parameters is made here. Methods of measuring certain parameters needed for use as ground truth data in remote sensing are discussed in Chapter III.

For methods of measuring inorganic and organic water chemistry parameters, refer to Golterman and Clymo (1969) and to Standard Methods for the Examination of Water and Waste Water, American Public Health Association (1971).

1 Phosphorus (P)

Phosphorus is the least abundant of the major plant nutrients and most commonly limits growth of plants in lakes (Vollenweider 1971). Measurements of only the dissolved inorganic phosphate in water are meaningless since this inorganic phosphate is only about 5% of total phosphorus (Wetzel 1975). Most of the phosphorus in lakes is in the organic phase (Wetzel 1975). About 70% of the organic P is particulate (sestonic), the rest is dissolved or colloidal.

Total phosphorus in lakes ranges from less than $5 \mu\text{g l}^{-1}$ * for the most oligotrophic lakes, to more than $100 \mu\text{g l}^{-1}$ in hypereutrophic bodies of water (Vollenweider). Most eutrophic lakes range from 30 - $100 \mu\text{g l}^{-1}$. The measurement of phosphorus loading to lakes requires analysis of P concentrations in both drainage waters and hydrologic inputs. There is little correlation between sediment phosphorus and lake productivity (Wetzel 1975). More important are conditions related to phosphorus exchange between sediment and the water column. Productivity of lakes can generally be reduced by limiting phosphorus input.

* $\mu\text{g l}^{-1}$ = microgram per liter = 1/1,000 milligram per liter

2 Nitrogen (N)

Since plant growth in oligotrophic lakes is often limited by phosphorus, many of these lakes can actually have a large surplus of nitrogen. The nitrogen cycle in lakes is regulated primarily by bacteria. In very eutrophic lakes, nitrogen available for growth may be low. Fixation of atmospheric nitrogen by microorganisms (conversion of nitrogen gas to ammonium) requires an energy output by plants in the lake. Large quantities of usable nitrogen may enter in the groundwater routes rather than in surface flow (surface entries to lakes are more common for phosphorus). Total N may range from less than 400 to more than 3700 mg/m³ (milligrams per cubic meter) (Wetzel 1975).

3 Chlorophyll a

Chlorophyll a can be used as an index of eutrophication, since chlorophyll is a component of suspended algae (phytoplankton). Chlorophyll a is used this way in Michigan's inland lake Self Help Program.*

4 Water Clarity

Secchi disc measurements of water clarity are commonly used, the Michigan Department of Natural Resources is using such measures along with chlorophyll a in their survey of Michigan lakes. A Secchi disc disappears from sight at a depth at which 5% to 10% of the transmitted light occurs. From the Secchi disc readings, approximate extinction coefficients for light in the lake can be calculated (Ruttner 1963).

5 Organic Carbon *

Organic carbon is central to the metabolic dynamics of lakes and streams, and its importance cannot be overemphasized. Most of the organic carbon of natural waters is either dissolved organic carbon (DOC) or particulate organic carbon (POC). The ratio DOC:POC is from 6:1 to 10:1 in most lakes and streams. As eutrophication increases, total organic matter increases, and the ratio of DOC to POC increases disproportionately. Living POC is a small percentage of total POC. Lakes can receive organic carbon from the watershed, from the littoral macroflora, and from photosynthate excretion by algae. Macrophytes excrete about 5% of their photosynthate to the lake during growth, and provide large amounts of organic carbon to the lake upon their death and decay. Extensive allochthonous inputs of refractory (relatively less degradable than labile) organic carbon produce the brown water of dystrophic lakes.

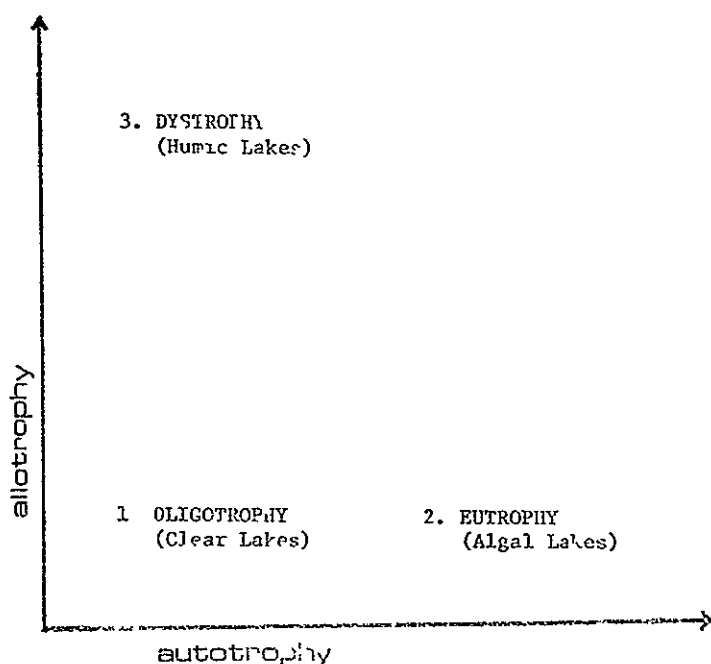
References to methods of analyses for the different fractions of organic carbon may be found in Golterman and Clymo (1969). See Wetzel (1975) for an excellent review of the subject and Melchiorri-Santolini and Hopton (1972) for detailed reports and discussion.

* D. P. Tierney and A. Massey, Inland Lake Management Unit, Water Quality Appraisal Section, Bureau of Water Management, Michigan Department of Natural Resources. personal communication.

D LAKE CLASSIFICATION

Lakes are classified on the basis of their trophic state. This classification considers both rates of supply of organic matter from autotrophic and allotrophic sources (Figure 1). However, primarily only the phytoplanktonic photosynthetic contribution of autochthonous formation of organic matter has been considered. The contribution of littoral zone macrophytes has been ignored.

FIGURE 1. Classical Trophic Lake Types (from Wetzel 1975, as modified from Rodhe 1969)



Notes for Classification

ALLOTROPHY= refers to biological productivity influenced by an outside source

AUTOTROPHY= refers to biological productivity influenced by a source in the lake

1 Oligotrophy= refers to low biological productivity resulting in clear water

2 Eutrophy = refers to high biological productivity causing eutrophic lakes

3 Dystrophy = refers to large amounts of resistant humic substance causing brown water or humic lakes

A more current view of lake classification has been established by Wetzel; the reader is referred to his recent text (Wetzel 1975) in which the modern view is extensively described. The following paragraphs briefly summarize points that are relevant to this report. The discussion of the evolution of different lake types emphasizes the role played by organic matter inputs. The discussion also considers that the productivity of lakes incorporates the plants of the littoral zone. As pointed out by Wetzel, the tendency persists among North American limnologists to exclude littoral zone production dynamics when considering whole-lake metabolism. The role of the littoral zone has even been ignored in several recent modeling simulations.

1 Oligotrophic Lakes

Oligotrophic lakes have low primary productivity (low production of organic matter within the lake), mainly due to low input of inorganic nutrients from outside the lake. Such lakes are often relatively large and deep. Low production results in low decomposition. The hypolimnion (lower zone of water, beneath the thermocline or region of rapid temperature decrease with increase in depth) is high in oxygen. The high oxygen levels result in rather low nutrient release from the sediments, reinforcing the low primary productivity. In oligotrophic lakes phytoplankton and littoral vegetation are much less important (in terms of numbers and productivity) than in more nutrient-rich lakes. The low levels of organic matter mean also that chemical complexing of organic materials with inorganic nutrients is reduced. This chemical complexing is important for phytoplankton growth. Such oligotrophic lakes are considered clean by the public. Devil's Lake in Wisconsin, Lake Superior in North America, and quite a number of alpine lakes in the world are examples of classical oligotrophic lakes. However, it is important to remember that a continuum or gradient exists among the various lake types described here.

2 Hardwater Marl Lakes

Wetzel has suggested that the development of a eutrophic lake from an oligotrophic lake can be affected by the input of carbonates and associated cations. Lakes can be sustained in a state of reduced productivity by the lowered nutrient availability that exists in hardwater marl lakes. Such lakes are important to identify in any classification scheme used in the vicinity of the Laurentian Great Lakes; about 11% of lakes in Michigan are estimated to be marl lakes.

Under the extremely buffered conditions of such lake water, a large number of inorganic-organic interactions occur. For example, phosphorus, iron, and manganese form insoluble compounds. The primary production that does occur is dominated by certain macrophytes such as *Scirpus subterminalis*. Low production of organic matter leads to low levels of dissolved organic compounds, which in turn support only low numbers of bacteria. The paucity of bacteria implies poor production of organic micronutrients, which in turn limits algal growth. Low available inorganic carbon (due to very high pH) also reduces the photosynthesis of algae. Thus, a complex feedback loop exists to limit production in lakes which, on the basis of large inputs of phosphorus, would otherwise become eutrophic.

3 Bog-dystrophic Lakes

The most common materials in allochthonous imports to lakes are the decay-resistant humic substances from terrestrial plant remains. Dystrophic or humic lakes are those that receive large inputs of such resistant substances. Christman and Ghassemi (1966) point out that natural waters with a yellow to brown color are common in many parts of the world. The coloring compounds are thought to be complex polymers of phenolic compounds which Christman and Ghassemi have further shown to be chemically similar to bark and soil extracts.

Dystrophic lakes may develop a dense littoral community of bog plants, dominated by *Sphagnum* moss. In typical bog lakes the littoral vegetation completely dominates that lake and is the supply of organic matter, both dissolved and particulate. At the same time, phytoplankton production in the open water is low. Dystrophic aquatic systems include both lakes which receive extensive inputs of humic substances from terrestrial sources, and closed bog lakes with extensive littoral vegetation. The large allochthonous loading of humic materials and the low pH that occurs from the cation exchange processes in the littoral bog vegetation result in decreased microbial metabolism. This produces an accumulation of organic matter and a reduction in nutrient availability. Such factors preclude high photosynthesis by the phytoplankton populations, even though adequate free carbon dioxide is available.

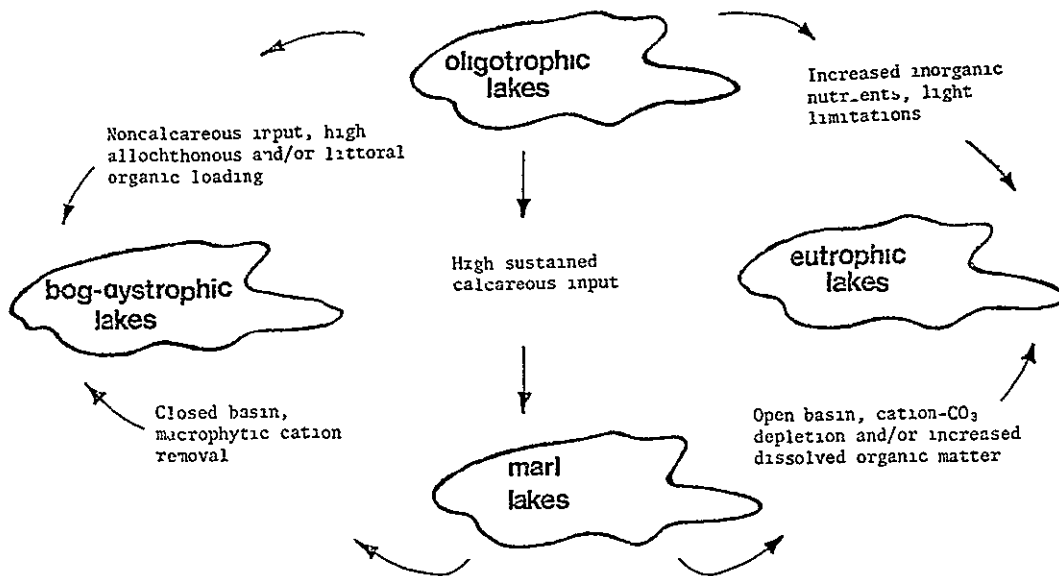
4 Eutrophic Lakes

Eutrophic lakes contain positive feedback loops which act to maintain the highly productive, eutrophic state, within certain limits. High levels of inorganic nutrients from the watershed lead to high algal and macrophytic photosynthesis. The high productivity of these plants produces a high level of organic matter in the lake, which increases bacterial numbers and activity. Extensive bacterial use of oxygen below the photic zone (zone of sufficient light for photosynthesis) produces an anaerobic (oxygen deficient) hypolimnion. Low oxygen at the lake bottom encourages high nutrient release from sediments. High levels of bacterial activity provide for the complexing of inorganic nutrients with organics, making the inorganic nutrients more available to algae for growth. In this report eutrophic lakes will be those with biomass caused either by algae, macrophytes, or a combination of these types. Both algae and macrophytes can be detected by remote sensing systems.

5. Interrelationships and Common Ontogeny of the Four Main Lake Types

Figure 2 indicates the factors that lead to the three main lake types that can develop from oligotrophic lakes. Note that marl lakes can develop into either eutrophic or bog-dystrophic lakes.

FIGURE 2 Outline of Common Ontogeny of Four Main Lake Types
(from complex diagram of Wetzel 1975)



As will be detailed in Chapter V, proper analysis of satellite data yields different reflectance signals from oligotrophic and marl, humic, and eutrophic lakes. It is also possible to ascertain various degrees within each class and to determine lakes that fall between one class and another. Signals originating from sand bottoms are also unique and can be classified and mapped by computer analysis of satellite data.

ORIGINAL PAGE IS
OF POOR QUALITY

III. WATER QUALITY PARAMETERS ASSOCIATED WITH REMOTE SENSING

The quality of fresh water depends on a large number of factors. Many have no correlation to parameters recorded by remote sensing (Scherz, Graff, and Boyle 1969). The water quality parameters that can be measured by remote sensing are associated with characteristic modifications of backscattered sunlight (energy). The water quality parameters that relate most directly to the energy signal backscattered from the volume of a lake are turbidity, various measures of solids, and water color (Scherz, Klooster, and Van Domelen 1973, and Scherz and Van Domelen 1975)

A TURBIDITY, PARTICULATES, AND THE REMOTE SENSING OF WATER QUALITY

If light impinges downward on very clear water of infinite depth, the signal that returns upward to a sensor will be that backscattered from the surface and from water molecules. Light in distilled water will penetrate to more than 100 feet and the small amount of energy that is backscattered from the pure water molecules will be primarily blue in color. Figure 30 shows a picture of Lake Superior where the water at site a is of a quality approaching that of distilled water. The water at site a also has a depth of about 1,000 feet. This site is an approximation of pure water of infinite depth.

As very fine rock particles are added to clear water, the backscattered signal shifts to the color green. Examples are Lake Louise in Alberta, Canada, where the material is glacial rock flour and the Silver Bay, Minnesota area where fine taconite particles have added a green halo to the waters of Lake Superior. The transmittance through such green halo water can still be quite high — up to 10 feet or more.* As larger particles are added to water the color of the backscattered signal shifts to the color of the material itself.

The total amount of visible light energy backscattered from a column of water can be measured as the turbidity of the water. Any airborne sensor operating in the visible region measures backscattered light from a column of water. One would expect instruments sensitive to all light to give results that correlate to turbidity. Scherz, Crane, and Rogers (1975) demonstrated good correlation between turbidity and remote sensing imagery from a variety of natural water types. Therefore, there is a primary correlation between remote sensing imagery and turbidity. Instruments that measure turbidity, such as the Hach turbidity meter do not differentiate light of different colors. Turbidity is therefore a color-blind measurement and falls short of multicolor needs. However, because turbidity is the only traditional water quality parameter that by definition and by proven observations can be universally correlated to remote sensing imagery, it is the most important parameter in the remote sensing of water quality.

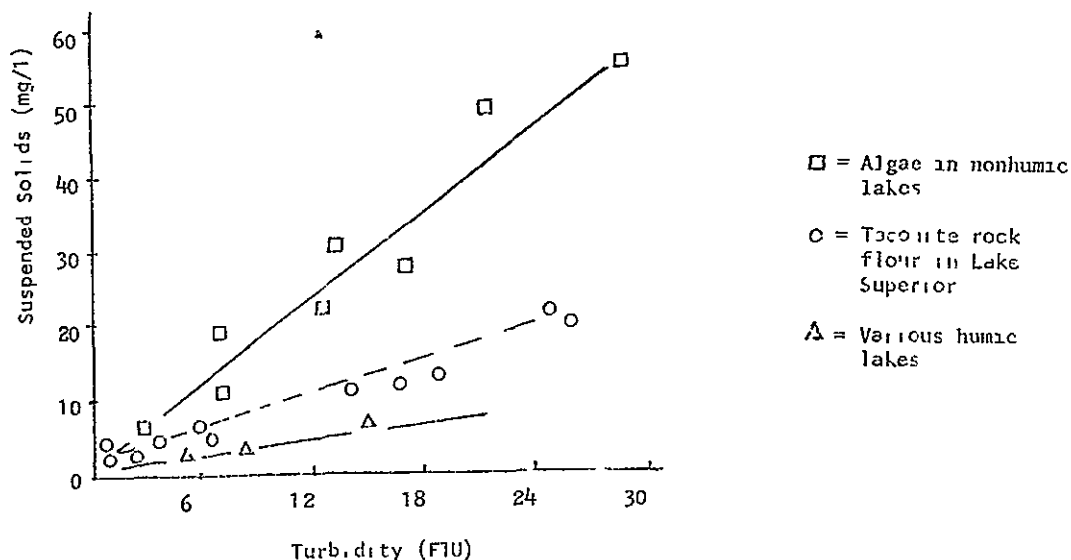
Figure 36 illustrates that the strength of the backscattered signal correlates with turbidity. Primary correlations depend only on the optical properties of the medium, and thus only to turbidity which is by definition an optical parameter.

* Fine precipitating particles of calcium carbonate in marl lakes can also cause a blue-green backscatter. See Appendix E.

The particles that cause light to be backscattered can be inorganic or organic material. The amount and size of particles in the water as well as their composition determine the amount and type of light backscattered. The correlation of secondary water quality parameters to backscattered light depends on the composition of the solid materials and how these materials correlate with turbidity. For example, if an inorganic waste from a steel mill discharges into a clear body of water, the weight of ferric iron may correlate with the amount of particulate material in the water. This particulate material causes the backscatter and correlates with the turbidity and the turbidity correlates with the signal on the remote sensing image (Scherz 1972). So in this case, the remote sensing imagery correlates not only with turbidity and weight of solids, but with iron as well.

However, if the material in the water is green algae and not iron, the correlation will be different. With the algal case, the correlation can be extended to chlorophyll *a* concentration (a property of all algae). In both cases the specific correlations (with iron or with chlorophyll *a*) are secondary correlations. Figure 3 illustrates that there is a different correlation between turbidity and the weight of three different types of suspended solids in water. These materials are algae, rock flour from a taconite rock crushing operation, and humic material.

FIGURE 3. Correlation of Suspended Solids to Turbidity for Three Lake Types (Scherz and Van Domelen 1975).



ORIGINAL PAGE IS
OF POOR QUALITY

If the correlation between a particular suspended solid and turbidity is known, it is possible to measure turbidity from remote sensing data (a primary correlation) and then use a solid-turbidity curve such as that in Figure 3 to find out what the suspended solid concentration is from the secondary correlation.

In summary, the strength of a single band of backscattered energy correlates primarily only to turbidity. Therefore, theoretically turbidity can be mapped by a single remote sensing signal providing one type of material enters a uniform water. Other parameters can also be mapped if their correlation to turbidity is known for that particular situation.

1 Field Methodology for Ground Truth Measurements of Particulates

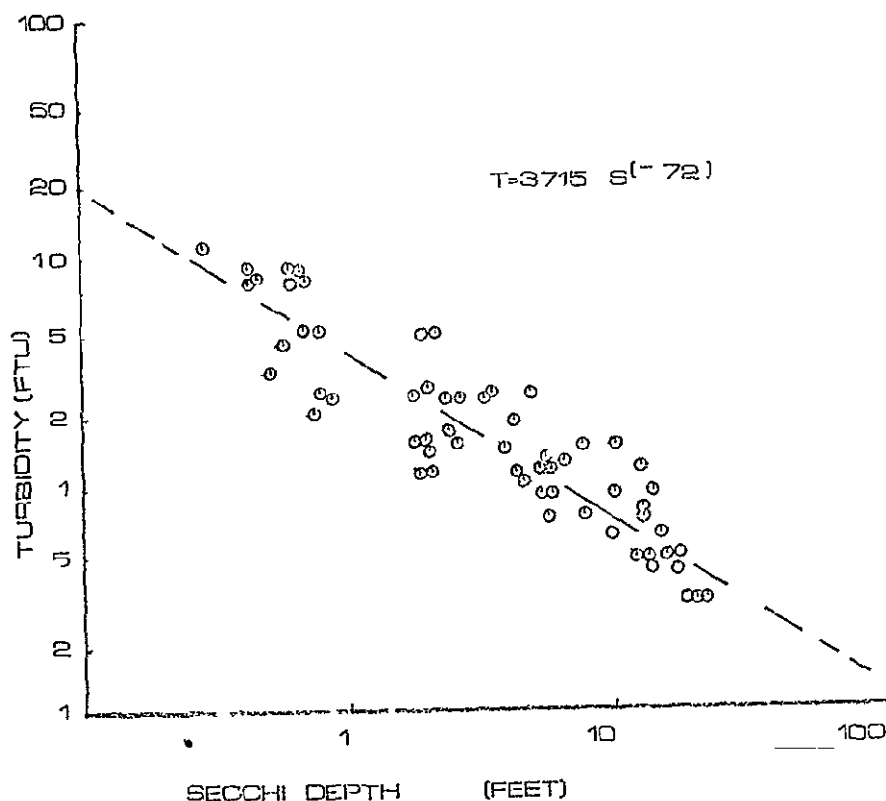
Sampling methods for open water ground truth measurements depend heavily on the accuracy and type of information required as well as the amount of time available for sampling. Because many open water solid concentrations change so rapidly, samples should be taken as close to the time of overflight as possible. Since materials can be heterogeneously distributed in a lake (Hutchinson 1967), a method must first be derived for referencing the sample location. Marker panels on the lake may be used for small-scale investigations, whereas large-scale investigations (i.e., in a satellite) must rely upon simple navigation skills for proper locations in the lake in question.

Water samples may be taken at the surface by dipping, or at various depths with bottle samplers (Schwoerbel 1970), or by using a hose and pump. As will be described in Chapter V, the water sample should be integrated from the surface to the depth to which light no longer penetrates in order to correlate the actual water quality with what the remote sensor records. Samples taken by water bottles are often mixed in representative proportions for assessing the amount of material present throughout the water column. Water samples should be iced in polyethylene bottles and immediately taken to the laboratory for analysis.

A quick method for determining turbidity of a water sample in the field uses the Secchi disc (Hutchinson 1957). The Secchi disc is a white or black and white disc that is lowered into the water until the disc is no longer visible. The depth of disappearance is called the Secchi disc depth. There is a correlation between turbidity and the Secchi disc depth because both are measures of the amount of light backscattered by materials in the water.

Figure 4 shows a correlation between Secchi disc depth and turbidity for numerous water samples from many different lake types in Wisconsin. It must be pointed out that the Secchi disc reading depends upon many factors such as the type of day, cloud cover, and the sharpness of the observer's eye. The Secchi disc reading is a simple, nonprecise field method for measuring turbidity, whereas the turbidity meter is a much more precise, laboratory method.

FIGURE 4 Relationships Between Turbidity (T) and Secchi Disc Readings (S) for Wisconsin Lakes Sampled During 1974/1975.



2. Laboratory Methodology for Ground Truth Measurements of Particulates

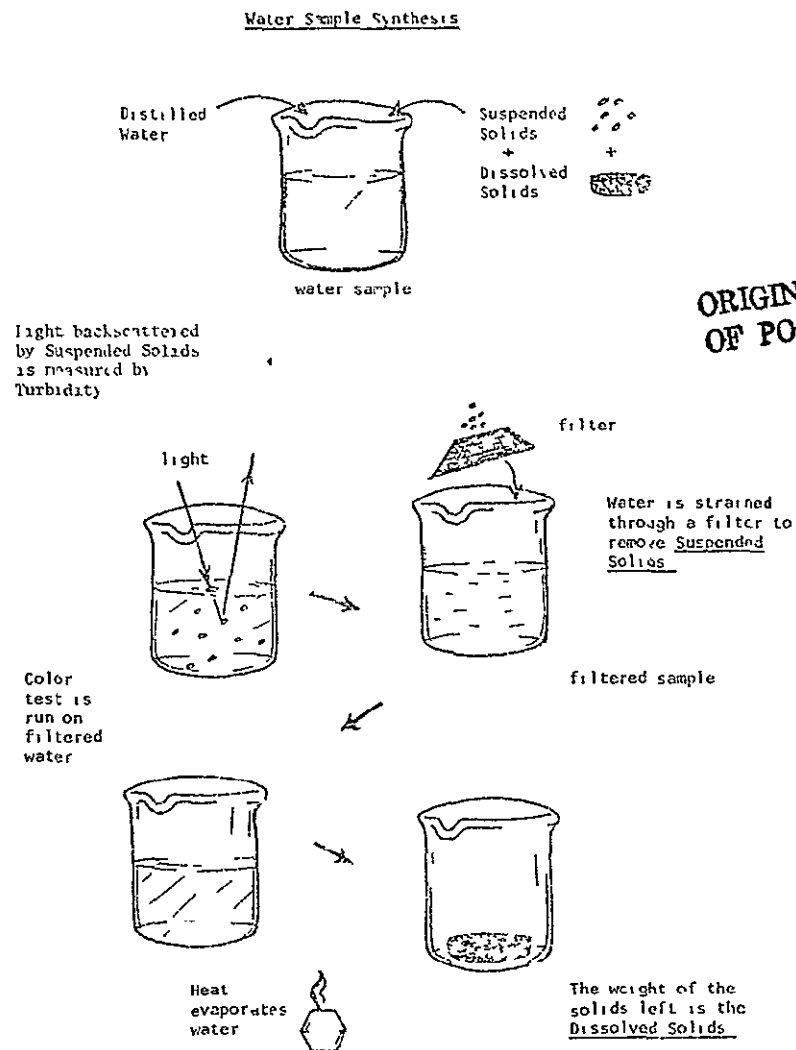
The following methods represent the ones used by UW-Madison remote sensing researchers in their water quality investigations. For convenience, sources for the description of these methods are listed in Appendix A

The standard method for determining turbidity is the candle method. Turbidity measurements are based on the light path distance through a standard water suspension which just causes the image of a standard candle flame to disappear. The longer the path length, the lower the turbidity. For example, a path length of one inch implies a turbidity of about 1,000 Jackson Turbidity Units (JTU); one foot, 200 JTU, and two feet about 100 JTU

Recently, electronic turbidity meters have come into use. Their results are expressed relative to the turbidity of standard formazin polymer suspensions (hence the units — Formazin Turbidity Units or FTU's). Turbidities of natural lake waters range from about 0.4 FTU's for very clear water up to about 200-300 FTU's for very turbid water.

Suspended solids in water cause turbidity (backscattering of light). However, dissolved substances may influence turbidity by absorbing light which might otherwise have been reflected. Figure 5 illustrates the relationships among turbidity, suspended solids,* dissolved solids, and water color.

FIGURE 5. Schematic Showing Relationships Among Turbidity, Suspended Solids, Dissolved Solids, and Color.

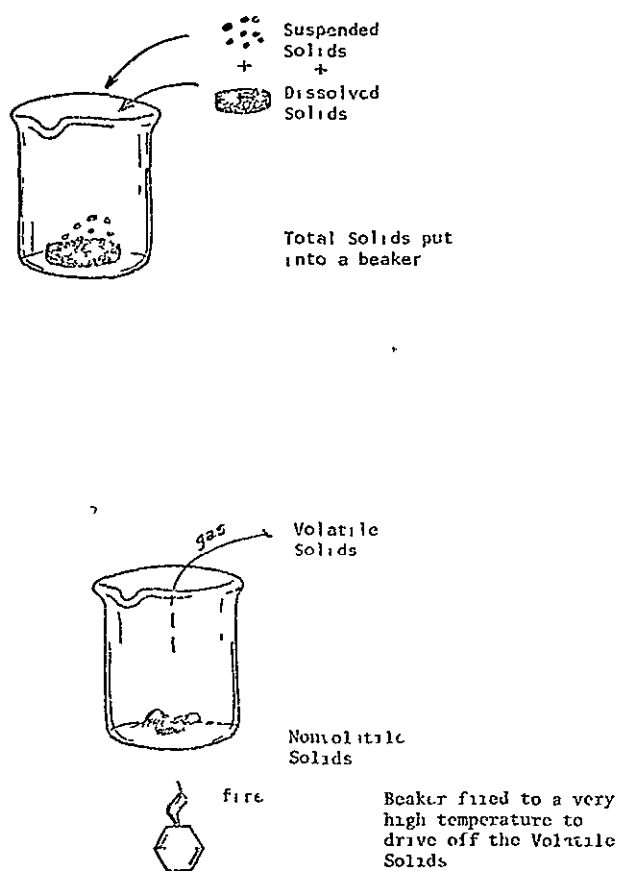


ORIGINAL PAGE IS
OF POOR QUALITY

* Suspended solids can be measured directly by filtering, drying, and weighing the filtered material

Suspended solids are commonly broken into two categories, volatile and nonvolatile. The primary basis for this separation is to distinguish organic solid material from inorganic solid material. All the organic material can be volatilized by exposure to a temperature of 600° C for twenty minutes. Figure 6 illustrates the relationships among total suspended solids, volatile suspended solids, and nonvolatile suspended solids.

FIGURE 6 Schematic Showing Relationships Among Total, Volatile, and Nonvolatile Solids.



ORIGINAL PAGE IS
OF POOR QUALITY

The effect of dissolved solids on absorption of light can best be assessed by using the standard test for color. Remote sensing investigators of lake water quality must be particularly careful to heed the influence of humic substances. The substantial modifications of the total reflectance signal caused by these dissolved solids can be a major error in water quality determination.

In the open water zone of lakes the suspended solids are most often organic matter. The abundance of total organic carbon (TOC), especially particulate organic carbon (POC) correlates positively with tendencies toward eutrophication. In such cases the POC is a measure similar to total suspended solids. The measurement of POC has the advantage of lower levels of detection accuracy than the measurement of total suspended solids.

The positive growth response of free floating algae to lake enrichment makes these organisms a well-known indicator of water quality. In the open water zone of lakes, chlorophyll a is found only in algae and represents a discriminative test for their presence as well as their quantity. Chlorophyll a concentration provides the best secondary correlation between remote sensing imagery and algal quantity (Thorne 1977).

B MACROPHYTES AND THE REMOTE SENSING OF WATER QUALITY

Aquatic macrophytes can play an important and sometimes even dominant role in the production dynamics of freshwater lakes. Although these plants are generally limited to the shallow water zone at a lake's edge, they may be very patchy in their distribution. The spatial orientation of macrophytes (horizontal and vertical) with respect to the lake surface may change with wind patterns. This phenomenon can cause differences in image appearances. Encrustations of calcium and magnesium carbonates or diatoms can also affect the appearance of these plants on imagery. Therefore, sampling and remote sensing of aquatic macrophytes must be done under carefully controlled conditions.

1 Field Sampling of Aquatic Macrophytes

Methods for sampling aquatic macrophytes are almost as numerous as the number of different types of macrophytes. Most methods have some features in common, and the most common methods are included here.

Because macrophytes are so patchy in their distribution, a number of samples should be taken to assess the average density of plant material. For most macrophytes a sampling area of 0.1 meter² is sufficient for each sample taken (this area, although not necessarily square, is known as a quadrat). To encourage complete objectivity, statistical sampling designs are desirable. Samples can be taken at regular intervals along a line to cover all portions of the plant community (called regular sampling design), but such sampling is not statistically testable. To subject sampling data to statistical analysis, a random sampling design may be employed. In the random sampling design, the

community is placed on a hypothetical grid system. Sample coordinates are then derived from a random numbers table. Although this design assures randomness of sample location, it invites the possibility of missing important areas of the plant community. To overcome this difficulty, the investigator can employ a stratified random sampling design. This design assures random location of sampling points as well as a sampling of all sections of the plant community. Samples are located in smaller grids along a line through the community. A number of sampling point coordinates are randomly chosen in each of the smaller grids along the line established through the plant community.

Statistical analyses of sampling data should include average biomass per unit area (\bar{x}), the variance (S^2), the standard error $S_{\bar{x}}$, the 95% confidence interval and the minimum number of quadrats that can be sampled and still assume statistical validity. Calculations for these values are presented as follows.

$$(1) \quad \bar{x} = \frac{\text{Total of the observation}}{N} \quad \text{where } N = \text{the total number of observations}$$

$$(2) \quad S^2 = \frac{\sum x_1^2 - (\sum x_1)^2 / N}{N - 1} \quad \begin{array}{l} \text{where } x_1 = \text{the } i\text{th observation} \\ S^2 = \text{the variance} \end{array}$$

$$(3) \quad S_{\bar{x}} = \frac{S}{\sqrt{N}} \quad \text{where } S = \text{the standard deviation of the sample}$$

$$(4) \quad 95\% \text{ CI} = \bar{x} \pm t_{0.05} S_{\bar{x}} \quad \begin{array}{l} \text{where CI = Confidence interval} \\ t_{0.05} = t \text{ value from Student's } t \text{ distribution} \\ \text{with } N-1 \text{ degrees of freedom at } 0.95 \\ \text{probability level} \\ \text{df} = \text{degrees of freedom} = N-1 \end{array}$$

$$(5) \quad N_{\min} = \frac{S^2}{0.01 \bar{x}^2} \quad \text{where } N_{\min} = \text{minimum number of quadrats which can be sampled to give a standard error of 10\% or less of the mean, considered an adequate sample for most purposes}$$

As will be noted in Chapter VII, these sampling designs and statistical calculations also can be used for analysis of imagery from aerial photography.

In the field, macrophyte stem density (instead of biomass) is often determined as the number of stems counted within the quadrat. The data are then converted to numbers of stems per standard unit area (usually per meter²). Plants may also be physically removed from the community and transported in polyethylene bags (iced) to the laboratory for analysis. Previous attempts to estimate biomass of submergent aquatic macrophytes have involved difficult harvesting of known lake surface areas using SCUBA. This method has proved difficult in turbid water with canopy-forming species because the diver must operate by touch, not sight. In response to the need for defining a quadrat of known surface area and harvesting the macrophytes in the entire water column defined by that area, numerous mechanical samplers have been tried. However, none are as efficient as diving at this point.

Aerial photography also can be used in conjunction with field sampling to make seasonal measurements of filamentous algae that often overgrow aquatic macrophytes. Sampling points again are located by use of a statistical sampling design. All plant material (algal and macrophytic) to a depth of 32 centimeters should be harvested. Separation of filamentous algae from macrophyte stems is facilitated by soaking them in a 20% formaldehyde solution for 30 minutes. This sample material should also be iced in polyethylene bags for transport to the laboratory for analysis.

2. Laboratory Methodology for Ground Truth Measurement of Macrophytes

Macrophyte density can be measured in terms of dry weight or ash-free dry weight per meter² (biomass) as well as numbers of stems per meter² (plant stem density). To assess the dry weight of a stand per unit area, the field sample should be subsampled, weighed, and dried at 70°C for three days. By heating the sample at a high temperature all the organic material in the plant sample can be volatilized. The amount of ash (assumed to be inorganic material associated with the plant) can be assessed. Subtraction of the weight of the ash from the total dry weight yields a number proportional to the organic matter content of the plants. This quantity is the ash-free dry weight.

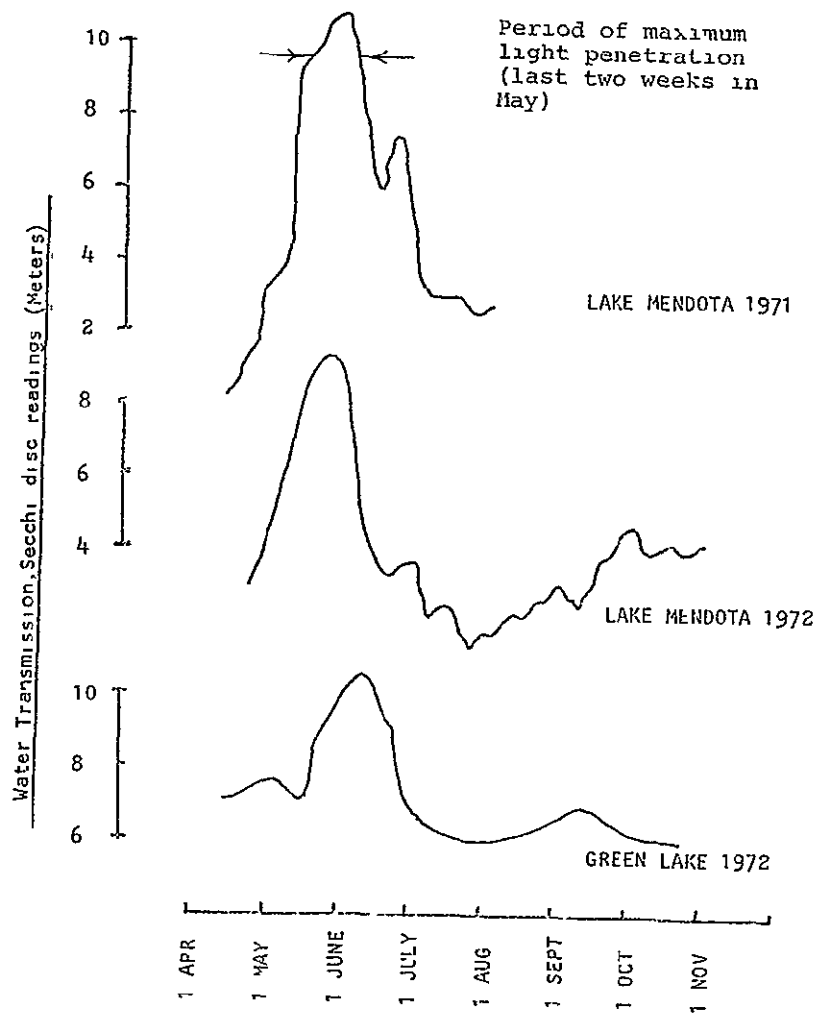
C TIMING OF REMOTE SENSING SAMPLING

If the discharge from a continuous industrial operation such as a paper mill is being monitored, it is easy to sample and compare data from one day to the next. Also, data taken in one month can reliably be compared to that taken in another month and a consistent indication of the status of the industrial operation can be obtained. The only variable here is the addition of the essentially unchanging pollutant to the water used by the industrial operation.

In classifying lakes, however, sampling is not such a simple matter. Lake water properties are dynamic and change with the seasons. There is little basis for comparing a Secchi disc reading taken in May to another in August. The changes of the Secchi disc readings in one lake taken in May and August may be much greater than the changes from one lake to another. Figure 7 shows the monthly

fluctuation in water turbidity as measured by the Secchi disc. Note the period of minimal turbidity (maximum light penetration) late in May. Note also that turbidity seems greatest in the months of July and August.

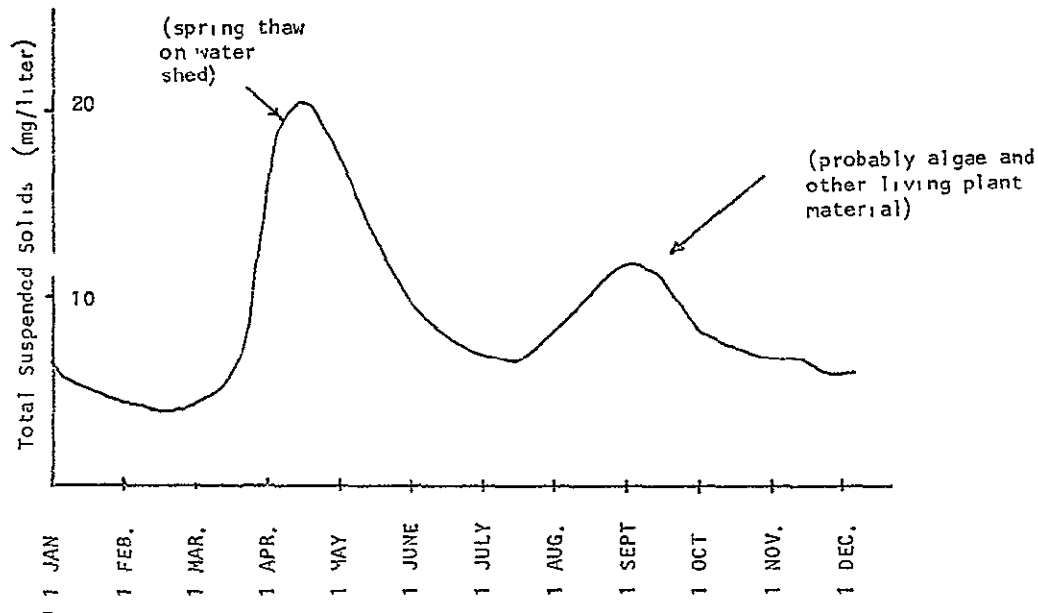
FIGURE 7 Plot of Light Penetration Verses Time (Madison Area Lakes)
(from Stauffer 1974).



ORIGINAL PAGE IS
OF POOR QUALITY

Figure 8 shows the seasonal fluctuation of suspended solids in Duluth Harbor, Lake Superior. The heavy concentration of solids in early spring is apparently due to silt and other material carried into the lake during and after the spring thaw. The high concentrations of nutrients from this runoff also are available for some early green algae and diatom production. The type and duration of runoff and the rate at which the water warms in early spring to support early algal growth can vary greatly from lake to lake. Note also in Figure 8 that there is another peak in suspended solids in late August. As will be shown in Chapter V, other indicators show that maximum algal growth usually is in late August. Limnologists have long known that open water phytoplankton biomass is high in spring and again in late summer. The summer peak in biomass production is generally more reliable than the spring maximum and more indicative of the lake's trophic state (Hutchinson 1967). Many aquatic macrophytes also reach a peak biomass in late summer (Adams and McCracken 1974). Considering all these data, the ideal time for remote sensing for detecting biomass or for lake classification seems to be the latter part of August to the first part of September.

FIGURE 8. Effect of Seasons of Year on the Total Suspended Solids at Duluth Harbor, Lake Superior (from Sydor 1973)



IV. REMOTE SENSING BASIC CONSIDERATIONS

To understand how remote sensing can be applied as a tool for monitoring water quality, it is first necessary to understand how remote sensing works. This chapter gives an overview of the electromagnetic energy spectrum. It also describes remote sensing instruments that have the greatest potential for monitoring water quality from either aircraft or satellites.

A BACKGROUND

Remote sensing is detecting the nature of an object without actually touching it. The term is new, but man has used rudimentary forms of remote sensing for centuries. By using his sense of sight, for example, he knows that white flakes falling to earth in winter is snow.

The camera was probably the first mechanical remote sensing device and is still the most important today. It was invented about 1839 and was used in 1849 to make maps for the U.S. Army Corps of Engineers. During the Civil War, cameras were mounted on balloons and used for aerial reconnaissance. In World War II, infrared film added another facet to aerial photography. Camouflage netting reflects infrared energy in an entirely different way than vegetation. Infrared photography could easily differentiate between the two, although they appear similar to the human eye. Recent developments in aerial photography such as color film, color infrared film, and multiband photographic systems, have greatly increased the amount of useful information that can be obtained from aerial photographs.

The human eye has a spectral range of 0.4 to 0.7 microns*. The spectral response of photography is about 3 times as wide, ranging from 0.3 to 1.2 microns. Except for special films used in astronomy etc., most films used for remote sensing work are designed to sense from 0.38 to 0.9 microns. Other remote sensing instruments operate in parts of the electromagnetic spectrum well beyond the range of the human eye or even of special photography (Figure 9). For example, it is possible to use infrared thermal scanners in an open field at night to count deer by sensing their body heat. It is also possible to sense differences in water temperature down to $\pm 1/2^\circ\text{C}$ by using airborne thermal radiometry or a thermal scanner.

Since World War II, radar instruments have been developed that can penetrate dense clouds and obtain images of almost photo-like quality day or night. With airborne magnetometers, submerged submarines and magnetic iron ore can be detected. Instruments that "look at" the ultraviolet scatter from the atmosphere have been able to detect mercury vapor given off by underground ore deposits.

* 1 micron (μ) = 10^{-6} meters = 1/1000 millimeter

For water quality investigations the photographic region of the electromagnetic spectrum from 0.38 to 0.9 microns and the thermal regions of 3.5-5.5 and 8-14 microns are most useful. This report deals primarily with the 0.38 to 0.9 micron region of the electromagnetic spectrum and with aerial cameras and multispectral scanners that operate in this region.

B. THE ELECTROMAGNETIC SPECTRUM AND BASIC RELATIONSHIPS

Electromagnetic energy operates as a wave function. The length of any wave (λ) is equal to the velocity of propagation of the wave (c), divided by the wave's frequency (f), or $\lambda = c/f$

Energy can be defined by either its frequency, which is usually the case when discussing radio energy, or by its wavelength. In this report energy will be defined by its wavelength. For example, visible light is composed of energy from 0.4 to 0.7 microns in wavelength. Visible light is either caused by energy emitted from a hot object such as the sun, light bulbs, or flares, or by reflection of such energy from these sources.

Any object which has a temperature above 0°Kelvin (K) emits energy according to the Stefan-Boltzmann Equation:

$$W = \alpha \epsilon T^4$$

where, W = Radiant Emittance
(watts/cm²)

α = Stefan-Boltzmann Constant
(f. 67×10^{-12} watt/cm²-deg⁴)

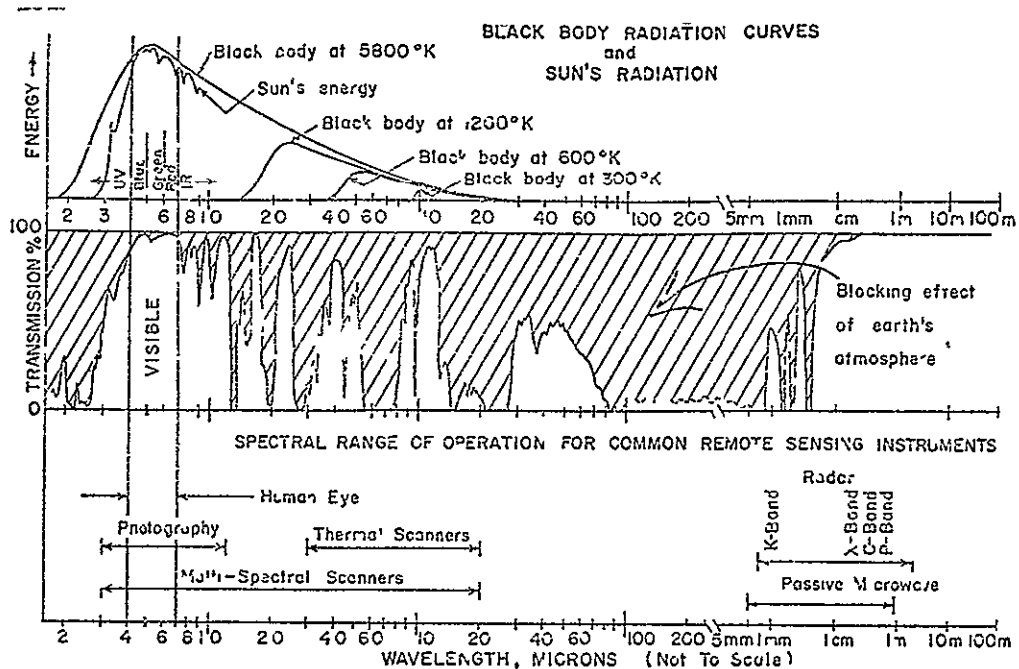
ϵ = Emissivity Factor

T = Degrees Kelvin

This equation defines a theoretical blackbody curve and points out that emittance energy is dependent on temperature.

The theoretical blackbody (or object) is the standard against which emitted energy from a real object is compared. If a blackbody was at a temperature of about 300°K the radiation distribution curve would peak at about 10 microns (Figure 9). As the black object, say a piece of black iron, becomes hotter it radiates more energy because the molecular interactions become more rapid. The frequency of wave propagation increases, and the energy distribution curve shifts to shorter wavelengths (to the left in Figure 9). As the temperature of the black object continues to increase, the radiation curve first intercepts the long wavelengths of the visible spectrum and the object glows with a dull red color. With higher temperatures the spectral shift continues and the color changes to orange, yellow, and white, respectively. If an object is hot enough, it might appear the same color as the sun, which corresponds to a blackbody curve at a temperature of about 5800°K. Exceedingly hot stars, hotter than our sun, actually have a blue color because of further shift in these curves toward the shorter wavelengths with greater temperatures.

FIGURE 9. The Electromagnetic Energy Spectrum



White light can also be broken down into its component colors or wavelengths by passing it through a prism or grating. Wavelengths from approximately 0.4 to 0.5 microns appear blue to the human eye, those from about 0.5 to 0.6 microns appear green, and wavelengths from about 0.6 to 0.7 microns, red. Energy with wavelengths shorter than 0.4 microns is called ultraviolet (UV) energy, and energy with wavelengths longer than 0.7 microns is called infrared (IR) energy (Figure 10).

Cameras are limited to the 0.3 to 1.2 micron range because photographic emulsions are not sensitive to wavelengths longer than 1.2 microns and the atmosphere scatters energy with wavelengths shorter than about 0.3 microns, effectively blocking it from the camera's lens. Another factor is the wavelengths that can pass unhindered through the particular type of glass in the lens. Also, very little of the sun's total energy occurs in wavelengths longer than 1.2 microns. Atmospheric absorption also occurs in the longer wavelengths (Figure 9 and Figure 11).

FIGURE 10 White Light Broken Down Into The Individual Colors Of The Visible And Near Visible Spectrum

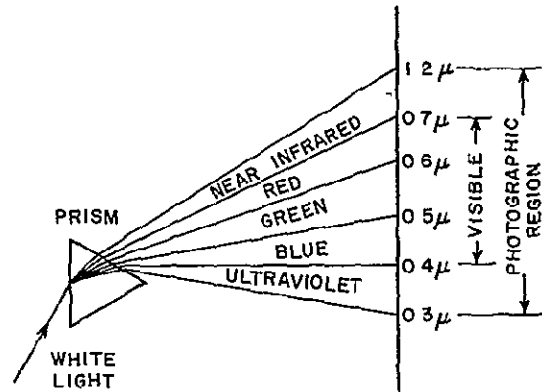
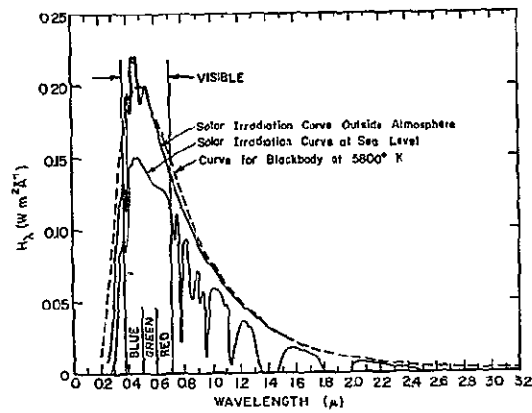


FIGURE 11 Solar Radiation Curves



ORIGINAL PAGE IS
OF POOR QUALITY

C ATMOSPHERIC EFFECTS

Certain materials existing in the atmosphere, such as moisture, carbon dioxide, and ozone cause some of the energy passing through it to be absorbed or blocked (Figure 9). Also shown in Figure 9 are clear bands or "windows" in the atmosphere through which energy can pass with considerably less interference.

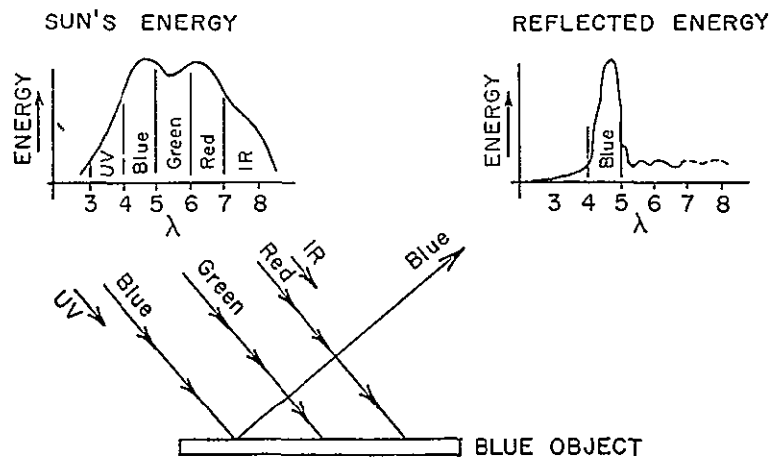
Because the blackbody radiation curves for objects of average earth surface temperatures peak at about 10 microns, the far infrared window (8-14 microns) is the most efficient for thermal sensing. The middle infrared (3.5 to 5.5 microns) window is also commonly used for thermal scanning because it is less costly to construct and use instruments that operate in this region.

D REFLECTION CHARACTERISTICS

Since solar radiation contains all wavelengths that comprise the colors blue, green, and red (as well as ultraviolet and near infrared), it appears white because the combination of these three basic colors makes up white light. On a hazy day, sunlight may appear yellow because the shorter wavelengths of blue light are scattered by the haze and dust suspended in the atmosphere. Yellow light, composed of green and red, can pass through the haze.

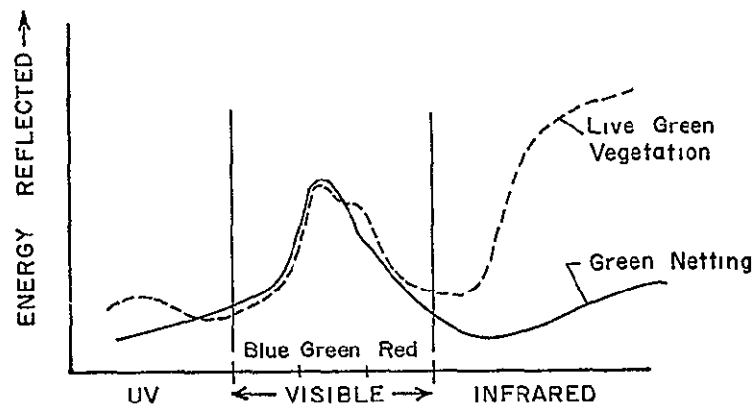
Every object in the world appears to have its own characteristic color because of the selective absorption and reflection characteristics of the object. A blue material for example, might have a reflection curve as shown in Figure 12, while a purple object would reflect red as well as blue light.

FIGURE 12 Energy Reflected From a Blue Object



Objects can be separated on the basis of their characteristic reflection curves in parts of the ultraviolet and infrared as well as in the visible region of the spectrum. By sensing in the ultraviolet and infrared bands, two objects sometimes can be distinguished which appear to have the same color in the visible spectrum. Living vegetation has a much greater infrared reflection than green (camouflage) netting (Figure 13). When these two objects are photographed in the visible portion of the spectrum, they appear the same, but when photographed with infrared-sensitive film, the difference is obvious.

FIGURE 13 Typical Reflection Curves for Live Green Vegetation and Green Netting Material



E ENERGY BALANCE

When sunlight strikes an object some energy is reflected depending on the reflection characteristics of the material. That energy not reflected may be absorbed. Energy absorbed raises the object's temperature and is reradiated at longer wavelengths according to the blackbody curves.

In the case of a translucent or semi-transparent medium such as the earth's atmosphere, some energy is scattered, such as blue light on a hazy day. The sunlight which is not scattered, the yellow light, passes through. Some of the energy is absorbed and heats the atmosphere. In general, then

Total Energy = Energy reflected + Energy scattered + Energy absorbed

ORIGINAL PAGE IS
OF POOR QUALITY

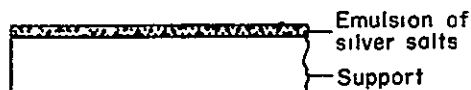
This is the general energy balance equation which applies not only to the atmosphere but also to all objects which receive radiation such as water and objects within water. For example, the sun's energy striking a water body is either reflected from the water surface, or scattered from particles within the water volume, or absorbed and converted to heat.

F PHOTOGRAPHY

1. Black and White Film

Ordinary film is made of a light-sensitive emulsion of silver salts (silver halides) painted onto an appropriate plastic backing or support (Figure 14). An emulsion can be made sensitive only to ultraviolet and blue light as is the case with the emulsion on most photographic printing paper. Because of this feature, a red or yellow safelight does not expose printing paper. The emulsion on black and white film can be made sensitive to ultraviolet, blue, and green light, such a film is called orthochromatic film. With this type of film only a deep red safelight can be used. Yet another emulsion can be produced which is sensitive to ultraviolet and all of the visible colors including red. Such a black and white film is called panchromatic film and no safelights can be used with it. Because its sensitivity range is the same as the human eye, black and white panchromatic film is the optimum film for most conventional uses.

FIGURE 14. Cross Section of Black and White Film.

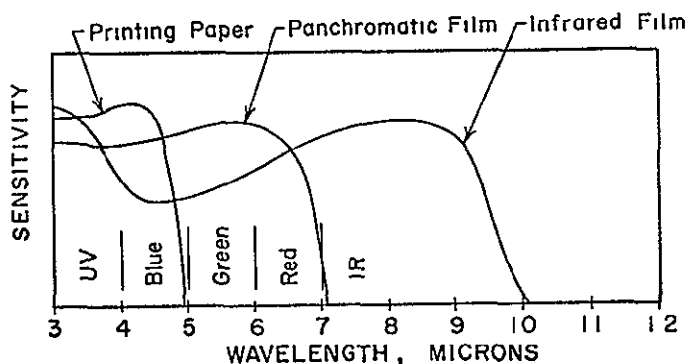


When panchromatic film is exposed by light focused through the camera lens, all of the visible light sensitizes the grains in the emulsion. The captured image is not visible, however, until the film is put into a developer solution where the sensitized grains of silver salts are changed into particles of pure black silver. Next, the film is washed in an acidic stop bath to stop the action of the developer. It is then put into a hypo (fixer) solution which washes out the unused silver salts, and finally it is rinsed with water and dried.

The resulting image is black and clear with intermediate tones of grey which correspond to the light reflected or emitted by the object photographed. Where the light reflected from the object was bright, the film turns black. Conversely, where no light was reflected from the object to the film, the image will be clear. The film tones are opposite to the tones as they exist in reality and the film is called a negative. To get a positive print, light is passed through the negative to expose the printing paper emulsion. The print is then processed in much the same manner as the film.

Most untreated silver salt emulsions are sensitive to only the ultraviolet and shorter wavelengths of the visible spectrum, i.e., blue light. By treating these silver salts with special dyes it is possible to make the film sensitive to longer wavelengths. By further treating the emulsion during its manufacture it is possible to extend the emulsion's sensitivity into the near infrared region (0.7 to 1.2 microns) (Figure 15). The result is called black and white infrared film.

FIGURE 15 Sensitivities of Various Black and White Emulsions



With black and white infrared film, as with panchromatic film, the image is black and white with intermediate tones of grey. Contact prints and enlargements can also be made in exactly the same manner as with panchromatic film. The only difference is that man's use of the spectrum is slightly more effective because he can photograph images caused by energy wavelengths longer than those he can see.

2. Normal Color Film

An advancement that made photography more useful was the manufacture of normal color film. Although color film emulsion consists of silver salts, it differs from black and white film because it has three layers (Figure 16). Each layer performs much the same job as the single layer on the black and white film except that by means of special treatments during manufacture, individual layers are made sensitive to separate colors of the visible and near visible spectrum. The top layer in most color films is sensitive to blue light, the second is responsive to green and blue light, and the bottom layer reacts to red and blue light. A blue-blocking filter is built into the emulsion between the top two layers which prevents blue light from exposing the bottom two. This results in three emulsions, each sensitive to blue, green, and red light, respectively (Figure 17).

FIGURE 16. Cross Section of Normal Color Film

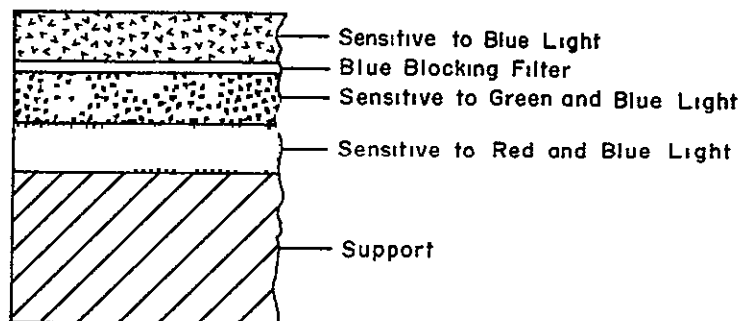
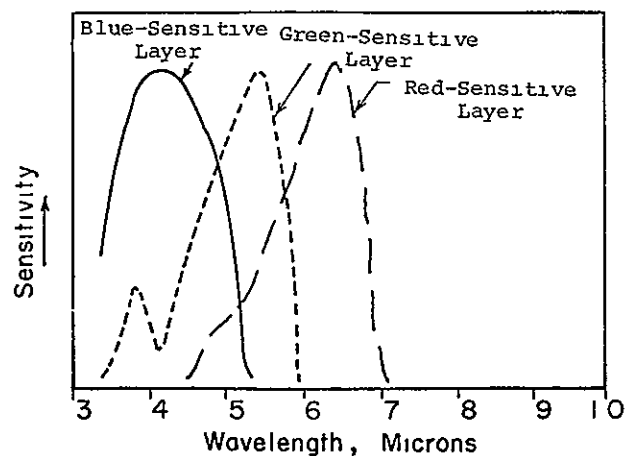


FIGURE 17 Sensitivity of Typical Normal Color Film



Color film is exposed in the same manner as black and white film. Light entering the camera is captured on the layer or layers of the emulsion corresponding to the color or combinations of colors of the original scene. The first steps of the color developing process accomplish much the same thing as the development of black and white film — exposed halides in each layer are turned into black crystals of silver salts. The remainder of the processing depends on whether the film is color negative or color reversal film. A color negative film produces a negative prior to the print. Color reversal film results in a correct tone color transparency directly from the film, e.g., a color slide.

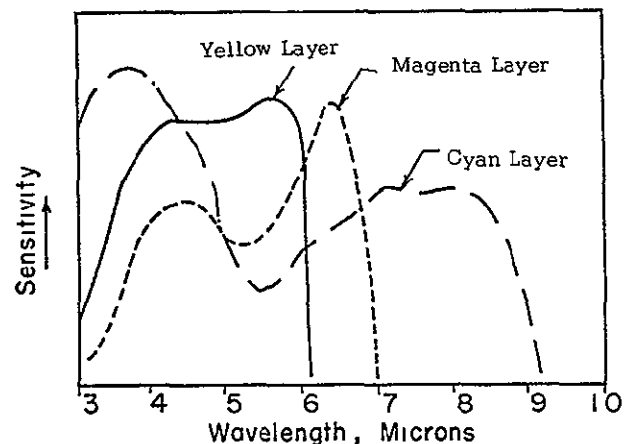
The exact development process for a color film depends on the film manufacturer and the chemistry for that particular film. However, in the interests of simplicity, some generalizations can be made in describing the development process for both color negative and color reversal films (see Appendix B). In any color photographic process, the resulting picture is actually three individual images. With normal color film, be it color negative or color reversal type, the final color tone is matched as closely as possible to the original color of the object.

3. Color Infrared Film

The color infrared film used today also has three emulsion layers — each sensitive to a different part of the spectrum. As with black and white emulsions, the silver salts of the color film can be treated chemically during manufacture to alter the spectral sensitivity of each layer. Figure 18 illustrates the shift in peaks of the sensitivity curves for the three layers. The sensitivity of the yellow-forming layer (originally sensitive to blue light) now is sensitive to ultraviolet, blue, and green light. The magenta-forming layer (originally sensitive to green light) has its sensitivity peak shifted to the red portion of the spectrum while it remains sensitive to ultraviolet light. The third layer (originally sensitive to red light) has its sensitivity extended so it will react to both ultraviolet and infrared light.

FIGURE 18 Sensitivity of Color Infrared Film
Kodak Type 8443.

In color reversal development the yellow layer changes to its complement blue, magenta to green, and cyan to red.



ORIGINAL PAGE IS
OF POOR QUALITY

As a result of this sensitivity shift, any item that reflects ultraviolet, long-wave red, and infrared light will appear red on the final processed picture. Items reflecting green light will show blue, and reflected red light will appear green. For this reason the film is commonly known as false color film. For operational use a yellow filter is used that absorbs blue energy, converts it to heat, and does not allow it to reach the film. With such a "minus-blue" filter a blue object appears black, a green object appears blue, a red object green, and an object reflecting infrared energy appears red. In other words, when color infrared film is used with a yellow filter the colors are shifted one color toward the longer wavelengths.

4 Filters

Another variable that must be considered when using photography for remote sensing — the wavelengths of energy that reach the emulsion — can be governed by placing filters between the object and the emulsion. Filters are used to keep the unwanted part of available light from falling on the emulsion. Often two items may appear to reflect the same color when viewed in the visible portion of the spectrum but may have different reflection characteristics in the near infrared region (Figure 13). In addition to using the red forming layer of color infrared film to show this difference, black and white film could be used with a filter to block all the visible light and allowing only infrared energy to pass to the infrared sensitive film.

Filters are available in either glass or dried gelatin film form, the latter being less expensive and easy to cut to a desired size. Since there is a large selection of filters to choose from, a choice is made much easier by consulting a publication on filters available through photo dealers. The proper selection of a filter is a function of the spectral response of the item to be sensed.

In the above example where it was desired to photograph only in the infrared region of the spectrum, it is necessary to cut out energy of wavelengths below 0.7 microns. To do this one of the #87 series of Kodak Wratten filters could be used. Because this filter blocks out the shorter wavelengths, it is referred to as a short wave blocking filter. Various other short wave blocking filters are available to screen out different wavelengths across the photographic spectrum (Figure 19).

Occasionally only a narrow band of the spectrum is of interest. Many filters are available which allow the transmission of only a specific band, depending on the spectral location of the band and its width (Figure 20). If the exact area of interest can not be isolated by using an existing filter, two or more filters can be used together to obtain the desired results. However, best results are normally obtained by using the least number of filters as possible because extra filters cause light loss and image distortion.

FIGURE 19. Typical Transmission Curve for Short Band Blocking Type Wratten Filters.

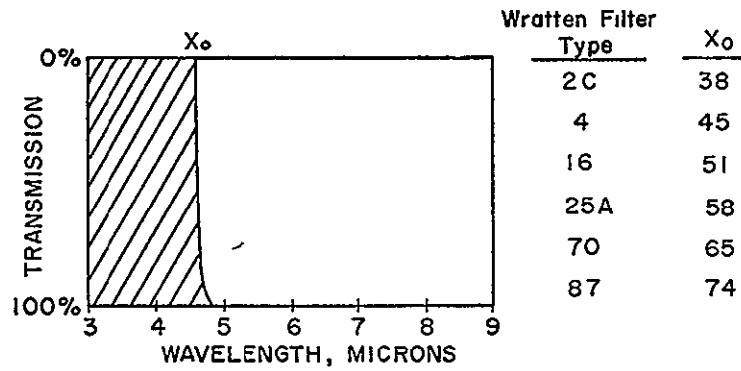
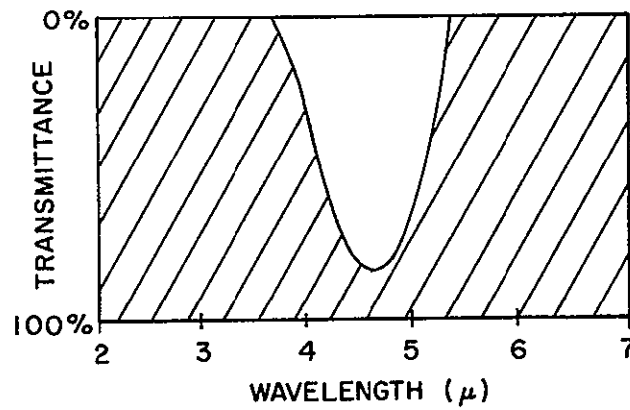


FIGURE 20. Narrow Band Pass Filter (Kodak Wratten Filter #48)



ORIGINAL PAGE IS
OF POOR QUALITY

A haze filter is one of the short wavelength blocking types that filters out short waves in the blue and ultraviolet region. Since very short waves are more easily scattered by the atmosphere than longer wavelengths, the short waves cause haze and give the sky its characteristic blue color. Haze is obviously undesirable in aerial photography so some form of haze filter is almost always used.

Although the longer wavelengths give better haze penetration, filtering out shorter scattered visible light causes loss of detail in the shadows. Details in shadows are illuminated by blue skylight. In some cases, it may be necessary to pick up these details, then the shorter blue light should not be filtered out. The proper choice of filter depends on the particular application.

5 Cameras

One of the variables in photography — the amount of energy reaching the film — is controlled by proper use of the camera. The camera is perhaps the most important instrument in remote sensing because it is relatively inexpensive and is capable of projecting an extremely high quality image onto the film.

The camera, in its simplest form, is nothing more than a black box with a pinhole that allows light to pass into it and expose the film. Many improvements have been made. Some of these include the addition of a lens system to replace the pinhole, an adjustable aperture to control the size of the lens opening, a shutter control to regulate the time the shutter remains open, a film advance mechanism, light meters, and many other devices to control variables and increase the ease and speed of operation.

The shutter opens for a prescribed period of time to allow light to enter and expose the film. Numerous types of shutters have been tried and are in use today. The common types are between-the-lens shutters, used extensively in aerial photography, and focal plane shutters.

For precise photometric analysis the between-the-lens shutter is preferable because the opening and closing of the lens uniformly changes light intensity across the film. There is a falloff of light near the edges of the photo due to the lens. But this falloff is predictable with the between-the-lens shutter, and such falloff can be corrected for. With the focal plane shutter, however, the shutter is like a slit in a window shade that passes over the film. Not only is there lens falloff, but the shutter itself causes an additional differential in exposure as the shutter speeds up and slows down. This variable shutter exposure changes from camera to camera, and with temperature and shutter speeds. It is extremely difficult to remove focal plane shutter effects in photo analysis work. However, cameras with focal plane shutters are more versatile, cheaper, and more commonly used. Therefore, focal plane shutters are often the most economical means of obtaining images for photo interpretation and for photometry work where shutter effect may not be significant or where standard field reflectance panels are used to eliminate such effects.

The camera pinhole has been replaced by a lens but the geometry is still much the same as with the pinhole camera. The fact that the opening is made larger by the lens diameter means that more light can enter the camera and exposure time can be decreased. However, as the diameter of the lens opening increases, image distortion increases and there is a decrease in depth (or field) of focus.

The pinhole camera is in focus for all objects no matter what their distance from the camera. When a lens is used instead of the simple pinhole, the lens maker's equation for relating the object distance, image distance and focal lengths must be considered.

$$\frac{1}{f} = \frac{1}{i} + \frac{1}{o}$$

f = focal length of the lens
i = image distance
o = object distance

For a given "i" distance, "o" can be changed by a certain amount and not cause the image to go out of focus. This leeway in the "o" distance is called the depth of field. The larger the lens diameter, the shorter becomes the depth of field.

The focal length of any lens divided by the diameter of its opening gives a number known as the aperture or "F" of the lens. This F is an expression of the brightness of the image striking the film. Modern cameras have a diaphragm which controls the size of the opening from the full diameter of the lens down to an opening approaching a pinhole. At times it is necessary to have a lens camera function somewhat like a pinhole camera, especially when it is desirable to have objects at various distances from the camera all in sharp focus at the same time.

The adjustable aperture also makes it possible to adjust the image brightness to correspond with desired shutter speeds and yet keep the total film exposure great enough to obtain quality photographs. For example, from moving aircraft it is usually necessary to use a fast shutter speed of about 1/500 or 1/1000 second to prevent image blurring. The aperture in this case is open (F number decreased) until the image is bright enough to account for the desired shutter speed and the sensitivity of the film.

The single lens aerial camera, along with all other cameras, has been improved because of refinements in lens making techniques. One of the primary objectives of lens making for aerial mapping work is to cut down on geometric lens distortion. With the color and color infrared films presently being used in metric mapping cameras,* the lenses must also eliminate color distortion. Other important developments in advanced aerial photography include very long focal lengths and wide angle lenses for telephoto and large area applications, respectively.

* Cameras used to obtain highest metric or position accuracy for topographic mapping purposes are called metric cameras.

The typical aerial mapping camera today is equipped with an extremely high quality lens so that the resolution is high enough and distortion low enough to allow reasonably precise metric measurements from resulting photographs. These cameras also are capable of shutter speeds to 1/500 or 1/1000 of a second or faster. The camera is generally equipped with an intervalometer that regulates the time between exposures. The better intervalometer system cameras can cycle as rapidly as a few seconds between exposures or in special cases even faster.

Modern aerial cameras are also often equipped with controls by which the operator can regulate the orientation of the optical axis, and in most cases, compensate for the crab angle of the aircraft (a sideways shift in direction due to a cross wind). The magazines of most modern aerial mapping cameras are built to handle a 9½ inch by 200 foot roll of aerial film that is automatically advanced and then during exposure is held in the focal plane by an air pressure system.

Although aerial mapping cameras are made to produce a picture on which man can make relatively precise measurements, such measurements are not always required. Often an investigator is simply interested in monitoring changes in spectral reflection that would be involved in identifying certain types of crops or trees, possibly mapping an algae bloom, or monitoring water pollution. In such cases the spectral responses are more important than the ultimate in metric accuracy.

6. Multiband Cameras

The multilens camera was developed to better observe different parts of the spectrum. This camera has two or more lenses, each normally has a different filter combination such that each image represents different parts of the spectrum. This allows the interpreter to compare imagery of the same area at the same time but in different spectral regions. Typical examples of the multilens camera are the four lens and nine lens models (Figure 21).

Multilens cameras exist where different types of films are used as well as different filter combinations. For example, it is possible to photograph the same area simultaneously with normal color and color infrared film.

Also it is possible to simultaneously use several small format cameras (70 millimeter [mm] and 35 mm) for multiband work. For metric accuracy and higher resolution, over a specific area photographed, the 70 mm format is preferable. For cost consideration and ease of use, the 35 mm format is preferable (Clegg and Scherz 1975).

For a two camera system, studies have shown that the cost of 70 mm photography is about 1/6 that of the 9 inch mapping camera and the cost of 35 mm photography is about 1/25 that of the 9 inch camera.

FIGURE 21. Itek Nine Lens Camera. All 9 lenses point downward at the same area. Each lens has a different filter in front of it and photographs a different part of the photographic spectrum. The resulting 9 photographs shown to the left contain many spectral tone reversals from one lens system to the other.

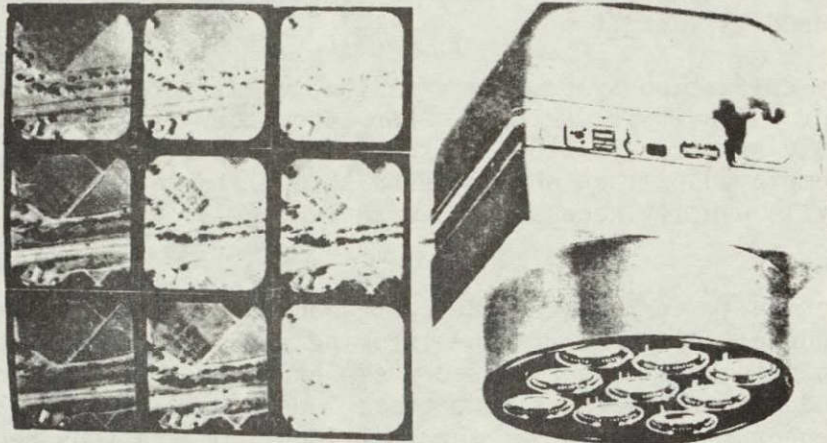
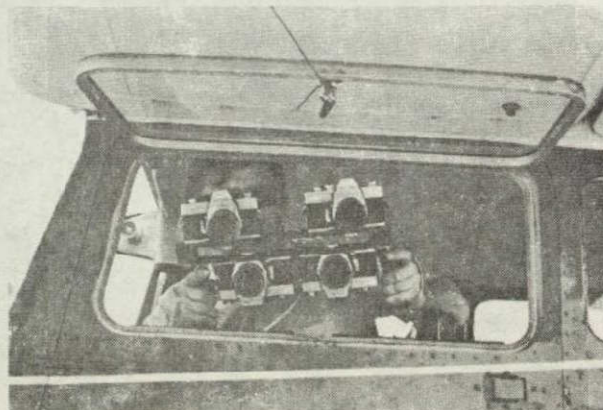


Figure 22 shows a bank of four 35 mm cameras used from the window of a small airplane. It was found that for most environmental mapping two cameras were adequate; one using color film and the other using color infrared film. With such a system the 4 bands of blue, green, red, and photographic IR are recorded with each simultaneous exposure. These four bands can be separated later by projecting the resulting slides through red, blue, and green filters or by copying the slides with black and white film using blue, green, and red filters.

FIGURE 22. A portable 4-camera bank being used from the open window of a small fixed-wing aircraft. These cameras are 35 mm and each contains a different film-filter combination. Courtesy of the UW-Madison Civil & Environmental Engineering Department.



G. RADIOMETERS

A radiometer is a nonimaging device that measures an absolute value of energy emitted from an object directly, or the solar energy reflected from it. A radiometer may be sensitive to energy from ultraviolet to the far infrared region, depending upon the type of sensing element being used. The readings from a radiometer operating in the blackbody or thermal emission range of the spectrum can be converted directly to temperature if the emissivity of the object sensed is known.*

The energy collection system for a radiometer differs according to the type of work for which it is designed. For laboratory or close field work in the photographic spectrum, a fiber optic probe, with or without a light collecting head, is employed. If an object is at some distance from the probe, a pointing capability is usually necessary, and the energy is gathered by a telescopic device.

The collection system directs the energy onto an energy-sensitive detector which is a transducer that converts the incoming radiation into electrical current. Two common detectors that are used are photo resistors and photo diodes. Different detectors are sensitive to various spectral ranges, and a particular type of sensor is often chosen for individual applications because of its spectral range of sensitivity. Detectors operating in the thermal area must be cooled during operation to make them function properly. Liquid nitrogen is often used for such cooling.

Usually it is desirable to detect energy within a specified spectral band. To do this a filter to block undesired energy or a diffraction grating to fan out the incoming energy can be used. By placing the detector in the proper geometric position within the fan it will sense only the energy range of interest. Other times it is desirable to record the total incoming energy across a broad region of the spectrum and no filter or grating systems are necessary.

Radiometers can operate either in the visible, photographic, or thermal part of the energy spectrum. A radiometer sensitive to thermal energy and mounted to point vertically down from an aircraft would produce a chart indicative of the temperature of the terrain directly below the aircraft's flight line. These thermal sensors have been used very effectively in determining surface thermal patterns in water down to $\pm \frac{1}{2}^{\circ}$ Centigrade.

*The energy emitted from an object according to the blackbody radiation curves is expressed by the Stefan-Boltzmann Equation that states the total emitted energy is a function of both temperature and an emissivity constant. Since this emissivity is constant over a body of water, thermal radiometers and thermal scanners will show temperature patterns in the water.

H. SCANNERS

Mechanical scanners are actually very sensitive scanning radiometers which scan a scene and produce an image in much the same manner that a picture is recorded by television cameras. These images are made up of a series of scan lines, each similar in nature to the chart or graph output from a radiometer, except that the signal strength across the scan is turned into light intensity on a cathode ray tube. The scan lines are made up of cells of instantaneous fields of view which become the resolution of the system and are defined by the size of the collection optics. The output from scanners, like the output from television cameras, can also be stored on magnetic tapes and manipulated by computers for specific applications.

1. Thermal Scanners

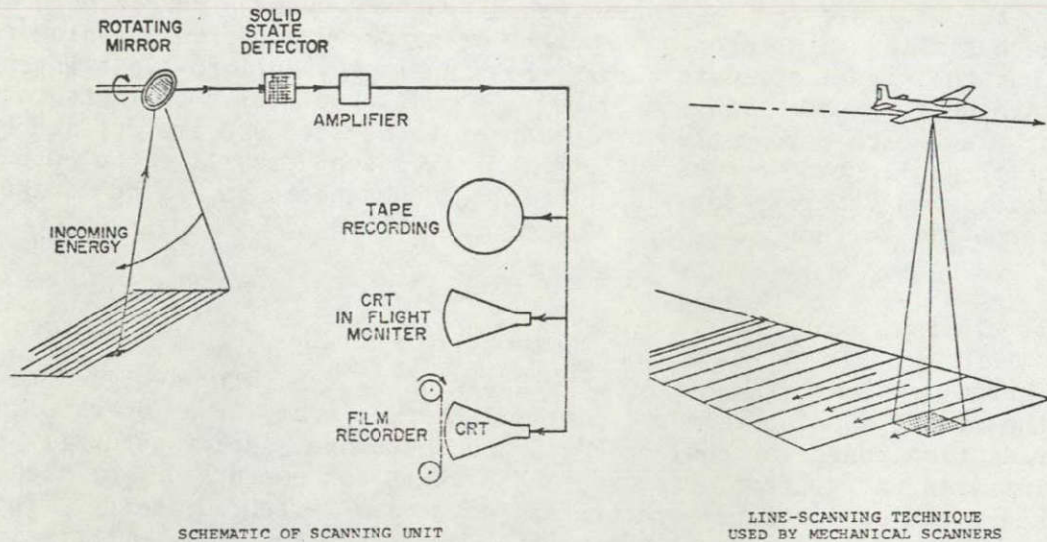
Thermal radiometers or thermal scanners are especially designed to operate in the middle and far infrared parts of the spectrum. They operate in the blackbody radiation range for cool objects, and therefore detect naturally emitted thermal infrared energy from objects. These units can operate day or night because they sense the object's temperature and not solar reflected energy. They can also be used when there is a light haze because the longer wave thermal energy is less apt to be scattered by particles suspended in the atmosphere.

Scanner mechanics can be broken down into three basic systems: 1) energy collection, 2) detection, and 3) data recording systems. The collection system is a mirror mounted on a shaft parallel to the flight line. The mirror is set at an angle so that the image of the ground below the flight line is reflected back into the scanner housing and to the detector (Figure 23). The shaft on which the mirror is mounted spins, causing the mirror to sweep a swath across the ground perpendicular to the flight line. As the plane advances, the mirror scans another swath which is adjacent to the first. This results in the spinning mirror scanning a continuous series of adjacent sweep lines laterally across the flight path.

2. Multispectral Scanners

A multispectral scanner is similar to the thermal scanner, except that it can operate in the ultraviolet, visible, and near infrared regions and sometimes in the middle and far infrared areas as well. The main reason for using the multispectral unit is that it allows an investigator to view imagery individually in a number of different narrow bands. This property allows one to locate certain wavelengths that are more important than others for the particular application at hand. Modification of image intensity by lens falloff and shutter effects (a problem in precise analysis of multiband photography) is of no concern with the multispectral scanners because there is usually no lens nor shutter.

FIGURE 23. Schematic of Thermal Scanner.



The systems of a multispectral scanner are: 1) energy collection, 2) energy separation assembly, 3) detection, and 4) data recording systems. The energy collector is a mirror mounted on a spinning shaft that scans the terrain laterally across the flight line just as with the thermal unit (Figure 24). The separating assembly is a prism or diffraction grating that splits incoming energy into smaller bands while passing them on to the detector system. The shorter the wavelength, the greater the angle between the incoming light and light passed through to the detectors (Figure 10).

By placing a number of individual detectors at proper geometric positions in the path of the light passed through the prism or grating, each detector will sense the energy for its particular wavelength band. A multispectral unit is usually referred to as an "n" channel unit, "n" being equal to the number of detectors. Some multispectral scanners operate with as many as 18 channels, but that much information may become redundant. Most research limits channels to four, six, or nine throughout the entire photographic spectrum.

The recording apparatus of the multispectral unit performs almost exactly the same function as it does in the thermal unit except there are more channels. Information can be played through a cathode ray tube for immediate visual monitoring and for film making. Tapes are almost always made. From the tapes an image can be made for each channel so that an analyst can make meaningful comparisons (Figure 25). More importantly the data from each channel can be fed into a computer where automatic and precise analysis of tremendous amounts of data can be accomplished.

ORIGINAL PAGE IS
OF POOR QUALITY

FIGURE 24. Schematic of Multispectral Scanner.

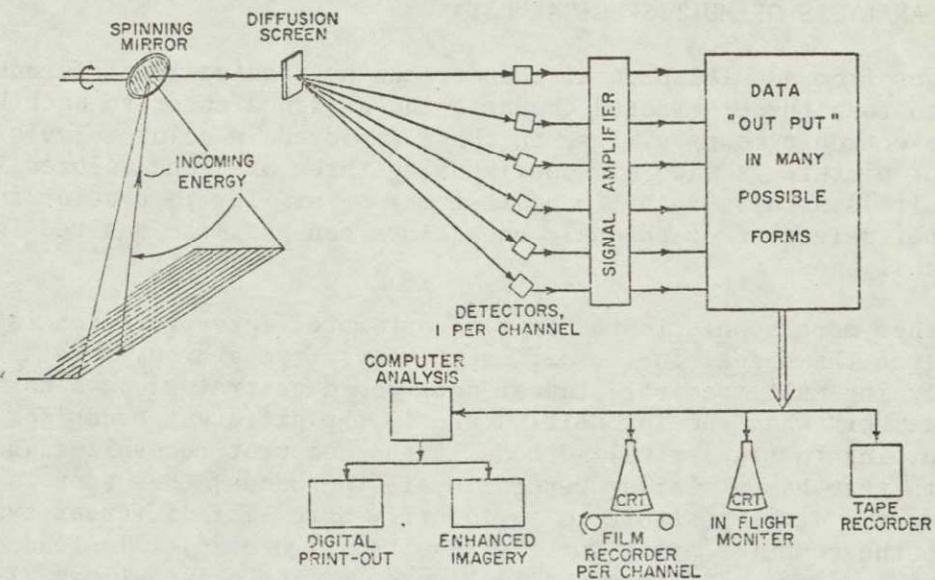
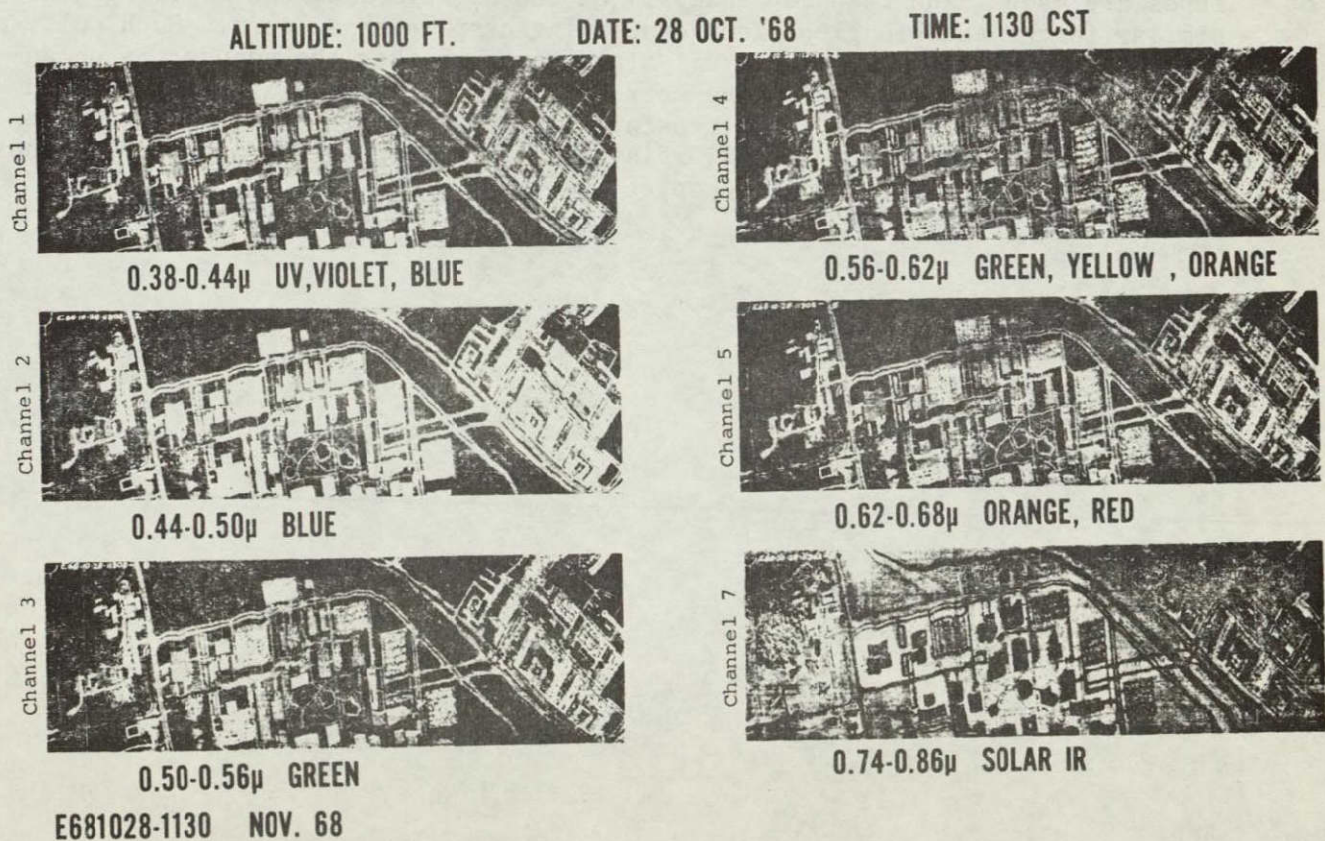


FIGURE 25. Multispectral Imagery. Courtesy of Bendix Aerospace Systems Division, Ann Arbor, Michigan.

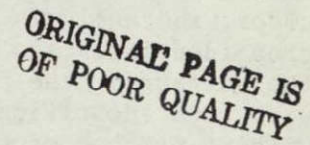


I. ANALYSIS OF MULTISPECTRAL DATA

Images from a multispectral scanner can be treated in different ways. One way is to take three selected channels and assign a color to each by using filters or electronic means similar to those employed in color television. A composite color picture is made by superimposing three of these colored images. The result is a false color image that may be similar to a color infrared photo. Proper selection of channels and colors can maximize desired interpretation capabilities.

Another more sophisticated type of automated interpretation is to computer analyze the signal in the different bands from a crop, such as corn. A computer analyzing multispectral scanner data could be trained on a corn field to "remember" what the intensities are in the different bands for the corn. According to statistical methods if the computer recognizes another part of the earth that has a similar return in all the bands, this spot is also identified as corn. It is possible to so identify dozens of different types of crops and have the computer print out the results (Figure 26). Instead of the printout being a series of letters as in Figure 26, the printout can also be different colors displayed on a color TV set (i.e., red for corn, brown for soybeans, green for alfalfa, etc.).

Multispectral scanners aboard satellites are by necessity somewhat more complex, but the analogy to the aircraft scanner will suffice for this report. Signals from the satellite scanners are transmitted to earth before the images and tapes are made. The computer analysis of the signals from the tapes is quite similar to the example given for identifying crops such as corn. Such multispectral scanner data can be used to classify land cover whether the scanner is on an aircraft or a satellite. If done correctly, the system can also be modified to classify water types. To successfully accomplish this task, however, the user must understand the physical relationships between light and water. These relationships are discussed in Chapter V.



This computer printout, which identifies and shows the distribution of corn (C), wheat (W), soy bean stubble (S), and bare soil (B), attests to the practicality and usefulness of multispectral data gathering and processing techniques for agricultural applications.

V. REMOTE SENSING AND WATER - MODELING AND ANALYZING ENERGY RELATIONSHIPS

A. GENERAL

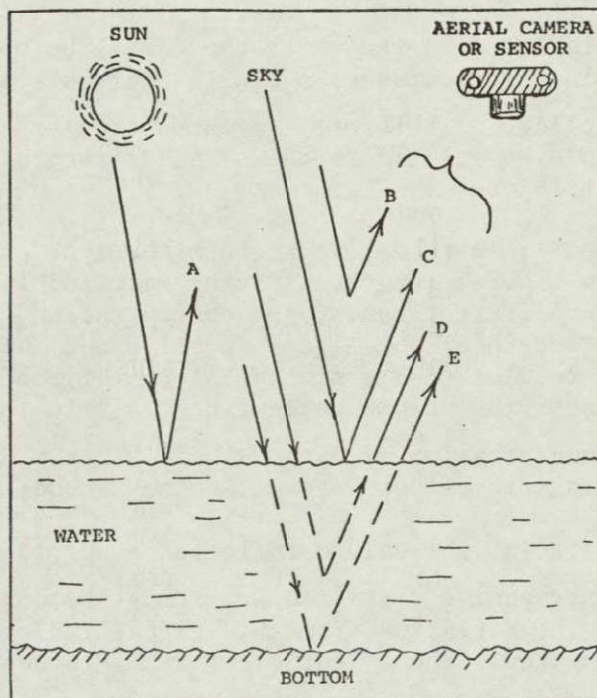
When remote sensing is applied to nonwater targets such as different types of crops, the analysis is considerably less complicated than with water. For crop identification and mapping only the reflected energy that returns from the surface of the plants is considered. Atmospheric effects are a factor with crop identification and mapping, but if there is a uniform atmosphere without patches of puffy clouds or ground fog, the atmospheric effects can be considered uniform for all points on a particular image frame and accounted for in analysis. The remote sensing imagery must, of course, be taken at the right season of the year and at the correct time of day for optimum identification. This time factor is prevalent in all remote sensing operations.

When remote sensing is used for mapping or monitoring water quality the process becomes considerably more complex. The primary signal that indicates water quality is the volume reflectance or backscattered energy caused by materials in the water. However, in addition to this desired signal there may be a signal caused by the reflection of skylight from the water surface. This signal acts like a mirror reflecting back the image of the sky. Even if there are waves, this reflection (although chopped up) is still there. To make matters more complex, the surface reflection is specular reflection and follows Snell's Law. All other materials on the surface, within, or on the bottom of the water body behave as diffuse reflectors which must be analyzed using Lambert's Law.

Therefore, when airborne photos or LANDSAT images are used for water quality work, the sunlight and skylight interact with the water surface, the particles in the water volume, and in some cases with the bottom. All of these signals combine to form the total signal from the water body. This total signal is modified by the atmosphere prior to its reaching the satellite sensor (Figure 27).

There is a different volume reflectance (ρ_v) or backscatter for each color (wavelength) of light. The volume reflectance for a water is primarily caused by light being diffusely reflected from suspended particles in the water between the water surface and the depth where the energy is extinguished. Pure or distilled water is assumed to contain no suspended material; therefore its volume reflectance is essentially zero. However, even in the laboratory there will be some diffuse backscatter from distilled water caused by water molecules, dust, foam, or other impurities on the water surface. Let the laboratory diffused reflectance from impurities on the water surface be indicated by ρ_{SL} . There is a different ρ_{SL} for each color or wavelength of energy (Van Domelen 1974).

FIGURE 27. Components of Light Showing on an Aerial Image Caused by Various Interactions of Light In, On, and Through the Water.



- A = Surface Reflection of the Sun
- B = Atmospheric Scatter
- C = Surface Reflection of Skylight
- D = Volume Reflectance of Water
- E = Bottom Effects

Note: Both Atmospheric Scatter, B, and Surface Reflection of the Sky, C, cause the apparent reflectance of an aerial photo to be higher than the laboratory analysis, which measures only volume reflectance, D. It must be assured that bottom effects, E, are insignificant and that there is no sun reflection, A, in the area of the photo being analyzed.

As material is added to the volume of a pure water sample the only factor that will be significantly altered will be the volume reflectance ρ_v . The dust, foam, and other impurities (ρ_{SL}) are likely to remain unchanged. In some cases oil slicks can alter this ρ_{SL} but in all other cases it is considered unchanging (Scherz and Van Domelen 1975). Each material added to water, such as red clay,

white paper mill waste, green taconite rock flour, blue-green algae, etc., has a unique spectral reflectance signature which is indicated by the ρ_v at different wavelengths. The LANDSAT satellite has four different sensor bands* so the type of material in water should be detectable.

As more material is added to the water there will be more particles to backscatter the light; the volume reflectance, ρ_v , will increase, as will the total signal sensed by the satellite. Therefore, for a particular type of material, its concentration should be related to the signal strength sensed by the four bands of the LANDSAT satellite.

So, it should be possible to determine both the type of material and its general concentration from LANDSAT images. Type of material is related to the relative signal strength in different bands, and concentration of material is related to the absolute strength of the signal in all bands. To adequately accomplish such analysis the total signal from LANDSAT must first be manipulated so that only some function of the volume reflectance, ρ_v , is left, for only ρ_v relates to the type and concentration of materials in water. Surface effects, bottom effects, and atmospheric effects are all noise sources which must be removed.

To remove these effects, the volume reflectance, ρ_v , of distilled water or a very clear lake approaching distilled water must be determined in the laboratory or in the field. The deviation from this signal indicates what impurities have been added to the water. The ρ_v for clear water is best determined in the lab because indirect skylight and wave action effects can be eliminated. On the LANDSAT image a clear lake that approaches distilled water must be used for calibration. Using the LANDSAT signal from this lake and the known volume reflectance for its clear water it is possible to eliminate the surface and atmospheric effects and have residual signals that are indicative only of the type and concentration of material added to the pure water of other lakes.

Important nomenclature used in this chapter is listed at the end of this report to help the reader follow the theoretical modeling used to arrive at volume reflectance from airborne and satellite imagery.

In developing the relationship between the amount of material in water and the strength of the backscattered signal in any one band, two example sites are given. One site is in Lake Superior where very heavy amounts of red clay are mixed with the clear water of the lake. The second site covers the Madison area lakes where various amounts of algae occur in late summer in the otherwise relatively clear waters.

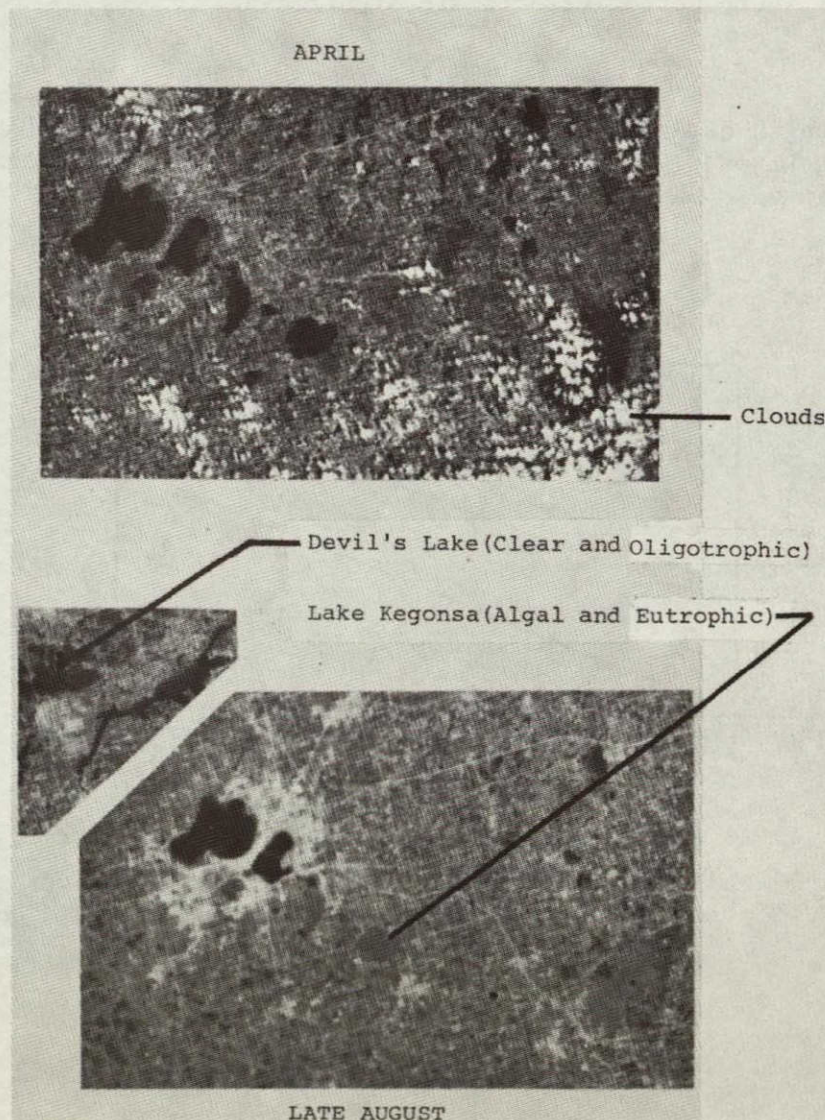
* The multispectral scanner aboard ERTS 1 (LANDSAT) has four bands which are called band 4 (sensitive to green), band 5 (sensitive to red), band 6 (sensitive to short IR), and band 7 (sensitive to somewhat longer IR). A blue sensitive band was not used because of the high scatter of blue light by the atmosphere.

In developing the ability to differentiate between types of material such as red clay and green algae, again the Lake Superior and Madison area sites are used. Where it has been determined that the material in the lakes is algae, then the amount of material in the water correlates to nutrient enrichment of the lakes or to their trophic classification.

B. ALGAE IN MADISON AREA LAKES

Figure 28 shows two LANDSAT images of lakes near Madison, Wisconsin. The upper image was taken in early spring shortly after the ice had thawed; there was essentially no algal growth in any of the lakes. All lakes appear essentially the same brightness on the LANDSAT image.

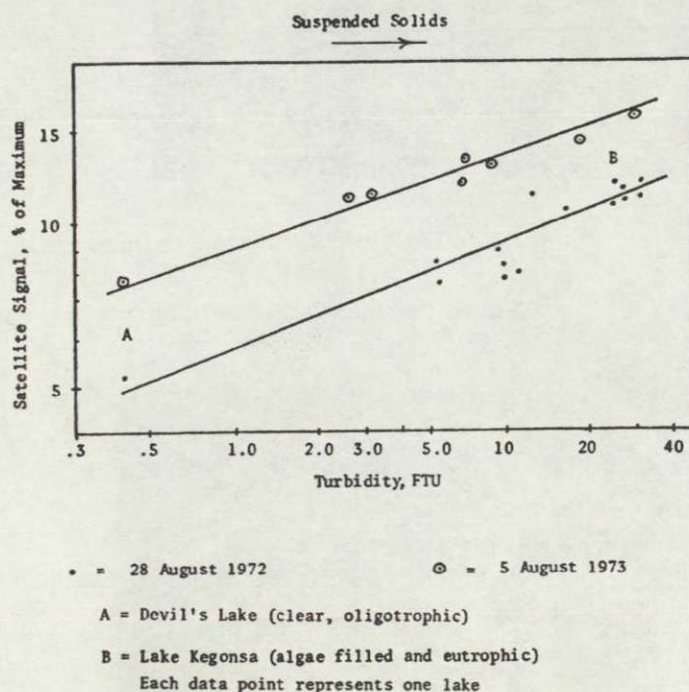
FIGURE 28. LANDSAT Images of Lakes Near Madison, Wisconsin in Early Spring When Algae and Lake Weed Growth is a Minimum and in Late August When it is Maximum. Band 5 (red) (Scherz, Crane, and Rogers 1975).



The lower image shows the same area in late August when algae and macrophyte growth are at a maximum. Those lakes which have an abundance of nutrients (the most eutrophic) have heavy algal growths. The energy from the skylight and sunlight interacts with this suspended algae and is backscattered to the satellite. The denser the algal growth, the more the backscatter and the brighter it appears on the LANDSAT image. A clear (oligotrophic) lake such as Devil's Lake in Wisconsin does not have enough nutrients present to sustain significant growth of algae, so it has approximately the same strength of backscattered signal in August as in early spring. Highly eutrophic lakes such as Lake Kegonsa have backscattered signals so high in August that they are virtually indistinguishable from the green fields in Figure 28.

Figure 29 shows the strength of the backscatter signal from Madison area lakes as sensed from the LANDSAT satellite on two different days in late summer. These signals are plotted against turbidity. It is obvious from Figure 29 that for a particular day there is a good correlation between the LANDSAT signal, turbidity, and trophic classification. However, for a different day the height of this correlation curve shifts. This shift is caused by different atmospheric effects from day to day. If the exact location of the curve for a particular day is determined, it can be used to map turbidity if there are no humic lakes present or lakes where bottom effects are significant.

FIGURE 29. Strength of Backscatter Signal Received by Band 5 of LANDSAT. Madison Area Lakes. Note Shift in Height of Curve for Different Days Due to Atmospheric Change (Scherz, Crane, and Rogers 1975).



For humic lakes, the tannic acid or other materials in the water creates a dark brown color which absorbs energy. On the curve of Figure 29 such a lake would probably lie below the curve for the other lakes. A lake with a sand bottom would create a point which lies far above the curves for the other lakes. In order to handle humic and sandbottom lakes the spectral signatures must be analyzed first so the lakes can be separated. Once the bottom lakes have been removed from the analysis and the other lakes have been put into classes of humic and nonhumic lakes, curves such as those in Figure 29 can be used to categorize the lakes as to turbidity and possible trophic classification. The lakes in Figure 29 are essentially nonhumic lakes with various amounts of algae present and no bottom effects.

From the analysis of Madison area lakes, it might be concluded that there is a simple relationship between satellite signal strength and eutrophication. If the material in the water causing the backscattered signal is only algae, then indeed there is this relationship. But there is other material besides algae that causes turbidity and the backscattered signal.

C. RED CLAY IN LAKE SUPERIOR

Figure 30 shows a LANDSAT scene of Lake Superior near Duluth. Lake Superior is a very deep lake approaching distilled water in clarity. However, near the city of Superior, Wisconsin, there is a heavy discharge of red clay material that causes an increased backscattered signal from the water (Scherz and Van Domelen 1973). As more of this red clay is added to the water the amount of backscattered energy increases. Figure 31 shows the relationship between the percentage of maximum possible signal from this water as sensed in the laboratory and by the satellite for different amounts of solids and turbidity.

In the laboratory, the water samples all have the same surface reflection situation and atmospheric effects, and the correlation of laboratory reflectance to turbidity and suspended solids is constant for all days. However, the satellite signals have different surface and atmospheric effects for each day. If two simultaneous water samples are taken at the time of a satellite overflight then for that day it is possible to establish the exact position of the curve relating satellite signal to turbidity (and for that particular material also the correlation of satellite signal to suspended solids). Once the position of the curve is established for that day then the exact values of turbidity and solids can be mapped.

Figure 32 shows such a map. The satellite signal-to-solids relationship (Figure 31) used to make the map holds only for red clay on that day and would not work for algae, as in the Madison area lakes. To determine from satellite data whether material is red clay, algae, humic material, or some other substance, multispectral signals must be analyzed to find a unique fingerprint from each water type. Such an analysis necessitates first removing atmospheric and surface effects from the signals.

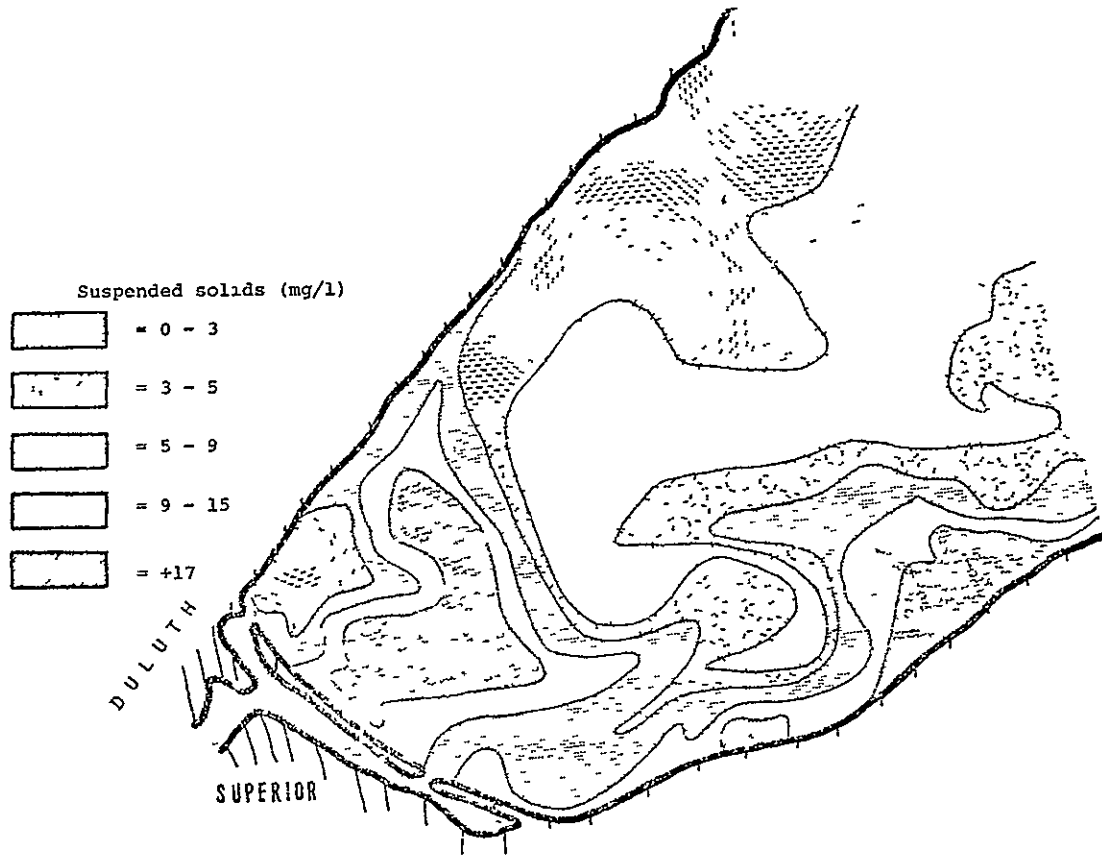
To do this, a detailed laboratory approach is first used and the results from this work are then extrapolated to a boat level situation and then to an airborne sensor.

FIGURE 30. LANDSAT Image of Southwestern Lake Superior. 12 August 1972.
 Band 5. Red Energy. Pure Water of Essentially Infinite Depth at "a."
 Water With Turbidity as High as 100 FTU at "b." Note the Step Wedge at
 the Bottom of the Frame Which is Used for Radiation Calibration (Scherz,
 Crane, and Rogers 1975).

ORIGINAL PAGE IS
 OF POOR QUALITY



FIGURE 32. Suspended Solids Map for Southwest End of Lake Superior Made From LANDSAT Image and a Curve as Shown in Figure 31 (from work by Prof. Michael Sydor, University of Minnesota at Duluth)



Western Lake Superior water quality, August 12 1972, from densitometry of LANDSAT image E-1020-16252-5

D. SURFACE EFFECTS

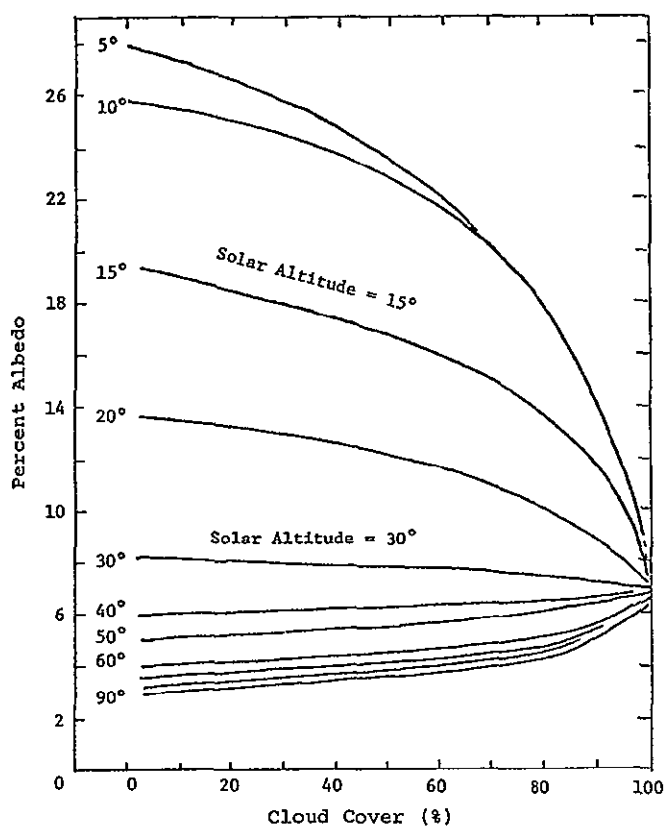
The atmospheric signal (signal B in Figure 27) changes from day to day as meteorological conditions change. The surface signal (signal C in Figure 27) is also dependent upon meteorological conditions and changes drastically due to changes in altitude of the sun, cloud height, and wave conditions.

Piech and Walker (1971) have shown that the ratio of solar irradiance (total energy coming from the sun) to sky irradiance (total energy coming from the skylight) is 7:1 on a clear day, 3:1 on a hazy day, and 1:1 on a day with thin clouds. This means that the skylight contributes 12% of the total irradiance on a clear day, 25% on a hazy day, 50% on a day with thin clouds, and 100% on an overcast day. This also means that the relative strength of the skylight signal from a clear day to an overcast day varies by 8.3 times ($100\% \div 12\%$), or 830%.

ORIGINAL PAGE IS
OF POOR QUALITY

Another indicator of the magnitude of factors effecting the surface signal is shown by some Russian work reported by Kondrat'yev. Figure 33 shows curves for his work as modified by Van Domelen (1974). The Russian study was on a very clear lake where the volume signal was a known unchanging factor and essentially negligible. The total energy coming up from this clear lake was compared to the energy coming down. The ratio of the two is called albedo. The albedo on this clear lake is essentially caused only by the surface signal component. Therefore, Figure 33 shows the change in surface reflection component or surface albedo under different conditions. The magnitude of the changes are impressively large.

FIGURE 33. Approximate Surface Reflection Component From Clear Water. Data by Ter-Markaryants, USSR, Reported by Kondrat'yev in 1965. To Obtain Spectral Values for 0.45, 0.55, 0.65, and 0.75 Microns, Multiply Curve Values by 0.7, 1.0, 0.75 and 0.58, Respectively. These Modifications From Ph.D. Thesis by John F. Van Domelen (1974).

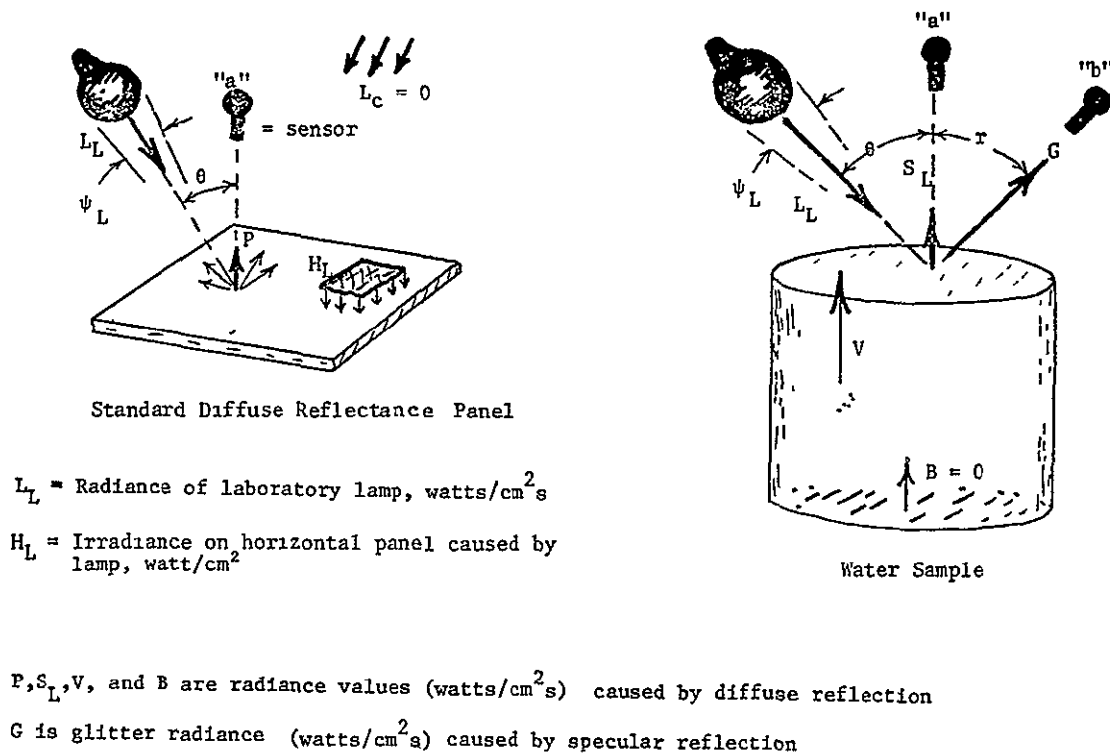


E. LABORATORY APPARENT REFLECTANCE VS. TURBIDITY AND SUSPENDED SOLIDS

The volume reflectance, ρ_v , can be obtained by the scheme shown in Figure 34.

In a darkened laboratory, a lamp shines light onto a standard Barium Sulfate (BaSO_4) diffuse reflectance panel and onto the water sample. The water sample is in a tube 62 meters long which has a black bottom. Shorter tubes will cause overriding bottom signals that make the results confusing or meaningless, as will a bottom that is too reflective. The sides of the tube are lined with diffusely reflective white chronoflex that returns side-scattered energy simulating adjacent water volumes in the field.

FIGURE 34 Direct Energy Relationships in the Laboratory (Scherz, Crane, and Rogers 1975)



ORIGINAL PAGE IS
OF POOR QUALITY

The radiance of the lamp is L_L in watts/cm²s.* As viewed from the level of the panel or water sample the solid angle of the lamp is ψ_L steradians. The total irradiance that reaches the level of the panel at right angles to the rays is $L_L \psi_L$. The total irradiance available on the panel per unit area, H_L , is.

$$H_L = L_L \psi_L \cos \theta \text{ (watts/cm}^2\text{)}$$

where θ is the angle between the lamp and the vertical as shown in Figure 34. The indirect illumination from the ceiling L_c (watts/cm²) is zero in the perfect laboratory setup.

Lambert's Law states that P , the diffuse radiance returning into space from the panel, is.

$$P = \frac{H_L}{\pi} \rho_{PL} \quad (1)$$

where ρ_{PL} is the diffuse reflectance of the panel

Since the dust, foam, and other impurities on the water surface also behave as diffuse reflectors, their signal, S_L , also follows Lambert's Law.

$$S_L = \frac{H_L \rho_{SL}}{\pi}$$

where ρ_{SL} is the diffuse reflectance of the impurities on the water surface in the laboratory. The suspended particles in the water volume are also diffuse reflectors and cause V , the radiance from the water volume

$$V = \frac{\rho_V H_L}{\pi}$$

where ρ_V = the diffuse reflectance of the particles in the water volume

The signal G is the specular reflection of the lamp from the water surface and does not follow the laws of diffuse reflection. Where $\theta = r$, as in Figure 34, the signal G is specular reflection of the lamp's radiance from the surface,

$$G = \phi L_L \text{ (watts/cm}^2\text{s)}$$

* Watts/cm²s means watts per square centimeter per steradian. This is the energy available at the point of interest per unit of solid angle (steradian)

and where ϕ = the specular reflection of the surface,

$$\phi = \frac{(n_w - n_a)^2}{(n_w + n_a)^2} \quad \text{in which}$$

n_w = index of refraction of water = 1.333, and

n_a = index of refraction of air = 1.000 -- so that

$$\phi = \frac{(1.333 - 1.000)^2}{(1.333 + 1.000)^2} = 0.020$$

This value holds fairly well out to angles of θ and r of about 40 degrees off the vertical. Most remote sensing operations fall within this range.

The total signal from the water as seen by the sensor is W

$$W = V + S_L$$

$$W = \frac{\rho_v H_L}{\pi} + \frac{\rho_{SL} H_L}{\pi}$$

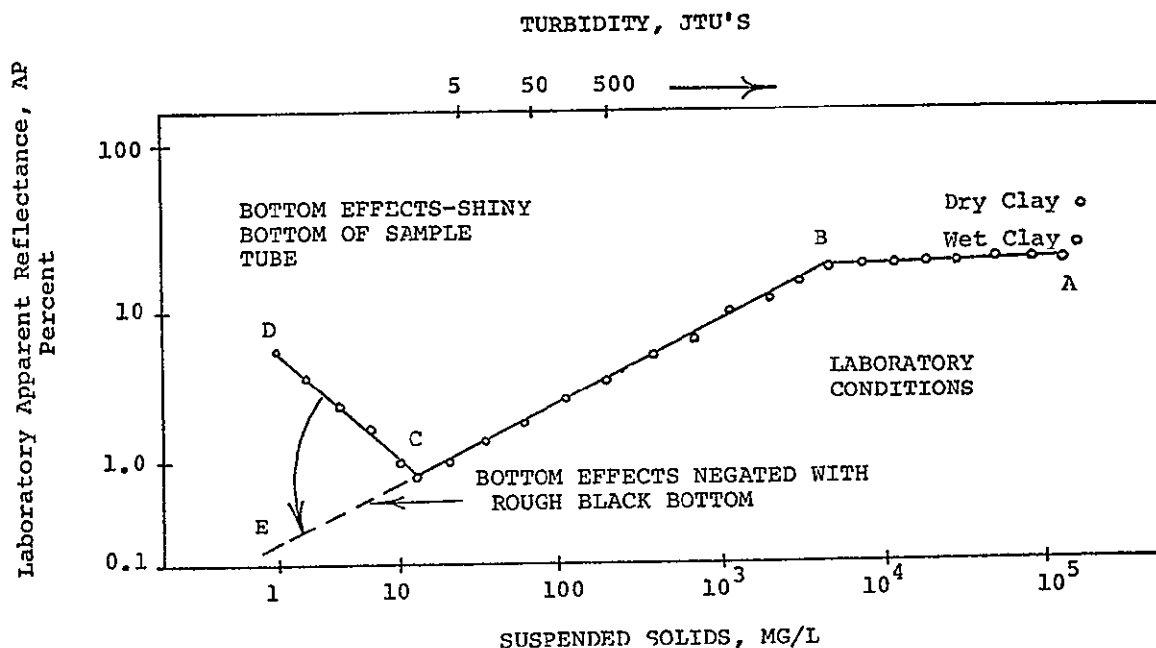
$$W = (\rho_v + \rho_{SL}) \frac{H_L}{\pi} \quad (2)$$

The ratio of this signal W to the signal from the panel is called laboratory apparent reflectance, AP . From equations 1 and 2:

$$AP = \frac{W}{P} = \frac{\frac{H_L}{\pi} (\rho_v + \rho_{SL})}{\frac{H_L}{\pi} (\rho_{PL})} = \frac{\rho_v + \rho_{SL}}{\rho_{PL}} \quad (3)$$

Figure 35 shows the relationship of apparent laboratory reflectance (AP) with different amounts of red clay mixed in distilled water. Figure 35 also shows that at exceedingly high concentrations of clay the mixture behaves as a mud, and there is very little change in reflectance with changes in moisture content (between points A & B). At a concentration of less than about 8000 mg/l of suspended solids the apparent reflectance begins to decrease in an almost perfectly linear manner (between points B & C). Once the solution becomes clear enough so the shiny white bottom of the sample tube becomes visible (point C on curve) the apparent reflectance, AP , increases linearly as the water becomes clearer (between points C & D). However, when a very black and rough bottom is substituted for the shiny bottom of the sample tube, the curve continues downward on the linear relationship (C to E on the curve) toward a minimum value which corresponds to zero suspended solids.

FIGURE 35. Laboratory Backscatter Expressed as % Lab Apparent Reflectance (AP) Versus Suspended Solids. Synthesized Water Samples Made Up By Mixing Red Clay From Near Duluth, Minnesota, With Distilled Water. This Curve Shows the Relationship For the Red Part of the Energy Spectrum (modified from Scherz and Van Domelen 1973).



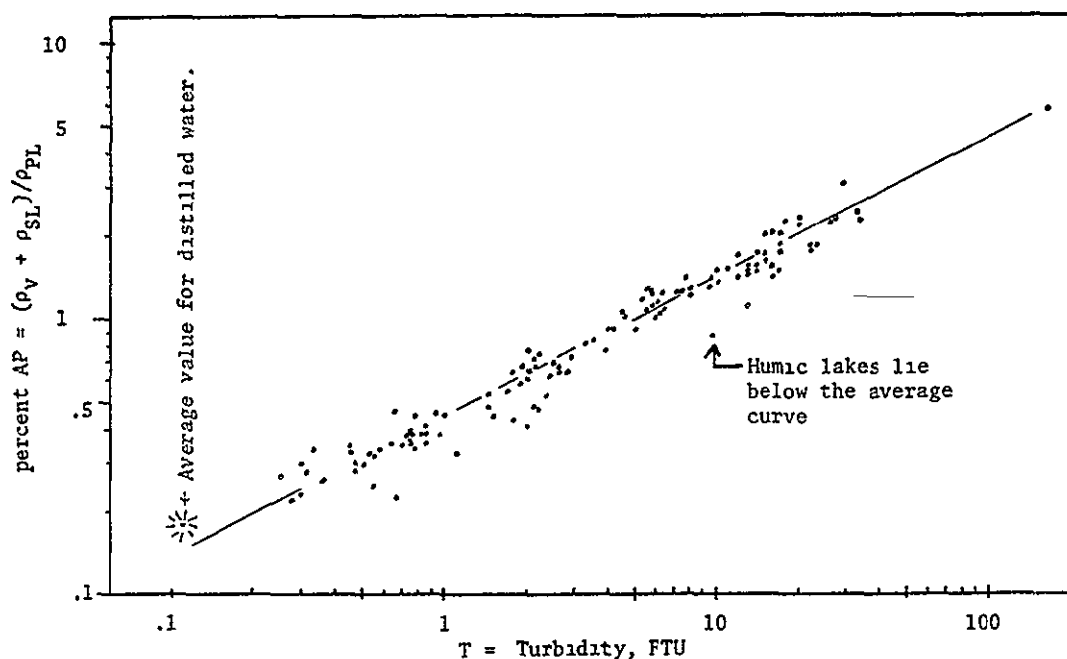
From the curve in Figure 35 it can be clearly seen that in the normal range for lake waters (suspended solids and turbidities between about 200 and zero) there is a good linear relationship between the amount of material added to distilled water and the energy backscattered from that material. The curve in Figure 35 also shows the possible troublesome problem of bottom noise that can be caused by energy reflecting from the bottom of the water sample. The bottom noise problems can occur both in laboratory and field conditions. The bottom noise effects depend somewhat on the wavelength of energy being considered. Generally, blue-green energy penetrates the furthest into the water. This penetration matter will be discussed later in this chapter.

Curves similar to Figure 35 have been made for red clay, white clay, paper mill waste, and various industrial pollution materials including black inklike material. This work has shown that, generally speaking, the curve of backscatter-to-turbidity is universal, but the precise curve of backscatter (expressed as turbidity) and suspended solids varies for different materials.

ORIGINAL PAGE IS
OF POOR QUALITY

Figure 36 shows lab apparent reflectance values (AP) as they relate to turbidity for 127 different natural lake waters in Wisconsin. Such lakes varied from very clear lakes to those with high turbidities caused by silt and clay and various types of algae. All such suspended materials increased the backscatter signal. Some lakes had high concentrations of dark humic material in them. Such dissolved humic material absorbed rather than scattered light. Such lakes caused data points that lie below the average curve. Had the humic lakes been removed from the data the curves in Figure 36 would have had less scatter. Nevertheless it is felt that Figure 36 illustrates very well the universal relationship between backscatter (AP) and turbidity caused by suspended particles.

FIGURE 36 Laboratory Backscatter Expressed as Laboratory Apparent Reflectance, (AP), Plotted Against Turbidity for 127 Different Lake Samples Collected Over Three Years. This Curve is for Red Light (0.65 Microns). The Average Turbidity and AP Value of 50 Laboratory Distilled Water Samples is also Shown (modified from Scherz, Crane, and Rogers 1975)



The least squares curve relating turbidity (T) to lab apparent reflectance (AP) for all those different water samples in Figure 36 is

$$T = 5.21 (AP)^{2.00}$$

Figure 36 also shows the average turbidity and apparent reflectance values associated with 50 laboratory distilled water samples

F. OBTAINING THE VOLUME REFLECTANCE VALUE (ρ_v) IN THE LABORATORY

Let subscript "1" indicate values for distilled water and subscript "1" indicate values from any water sample #1 (more turbid water).

Therefore, from Equation 3, the lab apparent reflectance for a sample of distilled water is

$$AP_1 = \frac{\rho_{v1} + \rho_{SL1}}{\rho_{PL}}$$

and the lab apparent reflectance for water sample #1 is

$$AP_1 = \frac{\rho_{v1} + \rho_{SL1}}{\rho_{PL}}$$

Assume the dust, foam, and other elements of surface reflectance for both samples to be identical, then:

$$\rho_{SL1} = \rho_{SL1} = \rho_{SL}$$

Figure 36 shows that the average apparent reflectance for distilled water is about 0.18% (Note that this is for the color red only) So for the color red

$$AP_1 = \frac{\rho_{v1} + \rho_{SL}}{\rho_{PL}} = 0.18\%$$

and ρ_{PL} for the $BaSO_4$ reflectance panel was determined to be $39\% \pm 2\%$ across the photographic spectrum, so

$$AP_1 = \frac{\rho_{v1} + \rho_{SL}}{39} = 0.18\%$$

ORIGINAL PAGE IS
OF POOR QUALITY

From various tests in the lab and the field a rough estimated value for ρ_{SL} is 0.02%.

This leaves a value for the volume reflectance for distilled water (ρ_{v_1}) to be:

$$\rho_{v_1} = 0.18\% (.39) - 0.02\% = 0.05\%$$

$$\rho_{v_1} = 0.05\%$$

This example is for the color red only but it shows how the process could be repeated for any color or wavelength energy

To obtain the volume reflectance of water sample #1 (ρ_{v_1}), compare the radiance of the water sample #1 to the radiance of the standard reflectance panel and use the following equation:

$$AP_1 = \frac{W_1}{P} = \frac{\rho_{v_1} + \rho_{SL}}{\rho_{PL}}$$

Which for a $BaSO_4$ panel becomes

$$AP_1 = \frac{\rho_{v_1} + \rho_{SL}}{39}$$

Since ρ_{SL} is assumed to be 0.02% for the color red, and AP_1 is measured experimentally, it is not difficult to solve for ρ_{v_1}

G LABORATORY DIFFERENCE (D_i)

However, there is an easier and more accurate method for solving for ρ_{v_1} . This second method also will work for any value of ρ_{SL} and does not require its solution. For a particular lab setup (no bottom signals present) an apparent reflectance is first run on distilled water

$$AP_1 = \frac{W_1}{P}$$

and then the apparent reflectance is obtained for water sample #1.

$$AP_1 = \frac{W_1}{P}$$

By subtracting the apparent reflectance for distilled water from the apparent reflectance for any water sample, a difference results that is caused mainly by the difference in the reflectance of the material added to the pure water of sample #1. D_1 indicates the laboratory difference for any water sample

$$D_1 = AP_1 - AP_1 = \frac{W_1}{P} - \frac{W_1}{P} \quad \text{or}$$

$$D_1 = \frac{(\rho_{V_1} + \rho_{SL})}{\rho_{PL}} - \frac{(\rho_{V_1} + \rho_{SL})}{\rho_{PL}}$$

$$D_1 = \frac{\rho_{V_1} - \rho_{V_1}}{\rho_{PL}}$$

The laboratory difference for sample #1, D_1 , is easily obtained in the lab for any desired color or wavelength. Because the reflectance of the BaSO_4 panel is constant across the photographic spectrum at 0.39% then $\rho_{PL} = 0.39$ for any wavelength. And

$$D_1 = (\rho_{V_1} - \rho_{V_1}) / .39$$

The difference in volume reflectance between sample #1 and distilled water indicates that some suspended materials have been added to the pure water to make up water sample #1

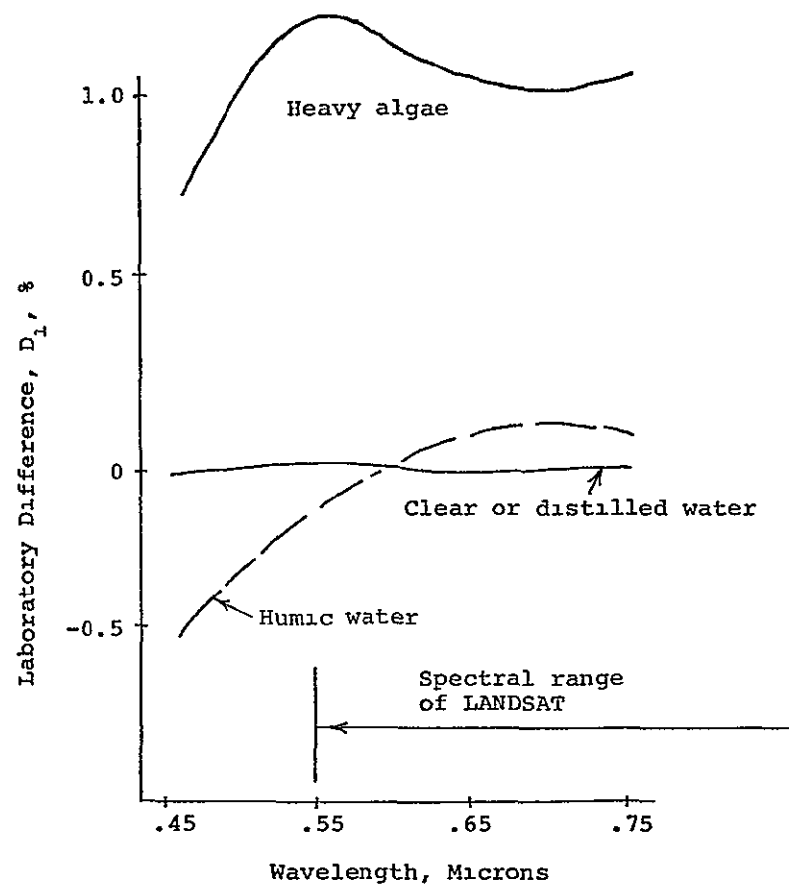
The Laboratory Difference, D_1 , plotted against wavelength, provides the laboratory fingerprints for different materials added to pure water.

H LABORATORY FINGERPRINTS FOR MATERIAL ADDED TO WATER

Laboratory difference spectra for lake samples depend upon the amount and types of material added to the lake water. The more material added, the greater will be the deviation of the fingerprint from that of distilled water. Figure 37 shows these fingerprints for a lake with dense algal development and a humic lake. The difference curve (or fingerprint) for distilled water is flat at approximately zero. The more algae that is added to clear water the greater will be the height of its curve above zero. Fingerprints for lesser concentrations of algae will be closer to the zero line. Different types of algae will have slightly different shaped fingerprints. Figure 38 shows lab difference curves for clear water type lakes with different amounts and types of algae present.

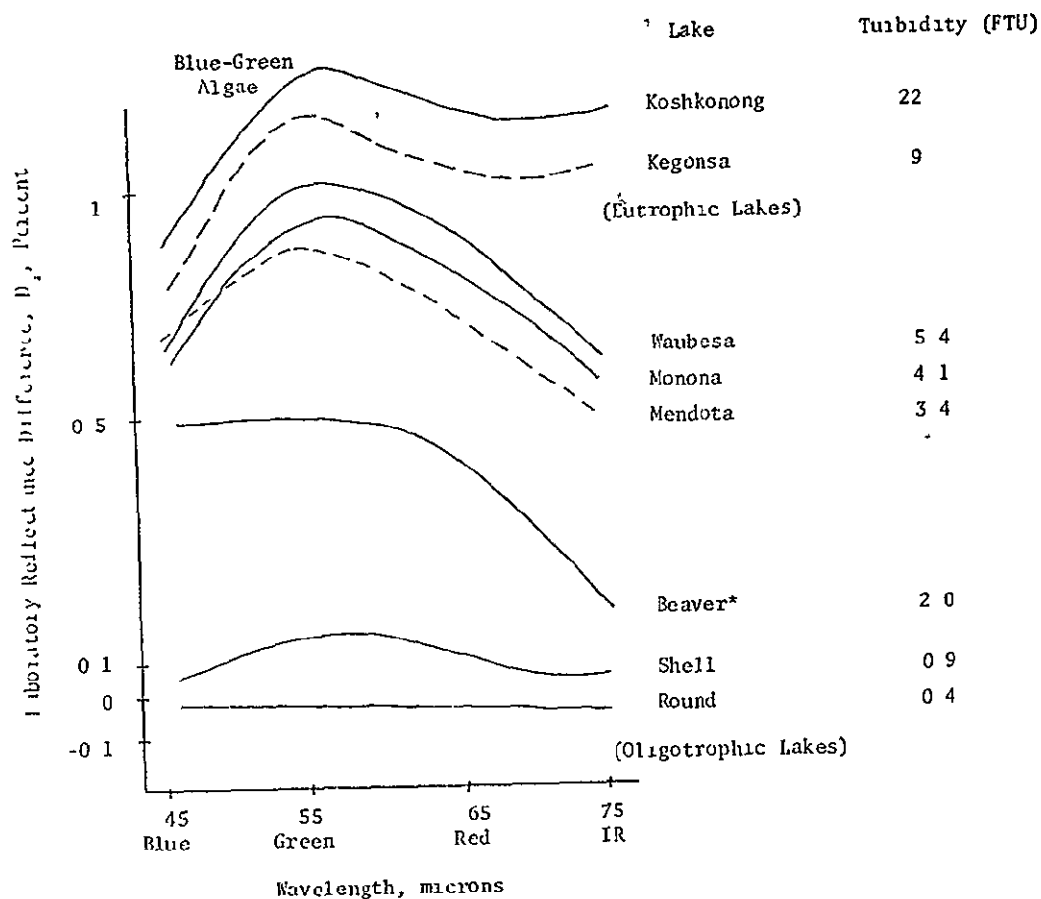
ORIGINAL PAGE IS
OF POOR QUALITY

FIGURE 37 Characteristic Laboratory Fingerprints of Two Types of Material in Water.



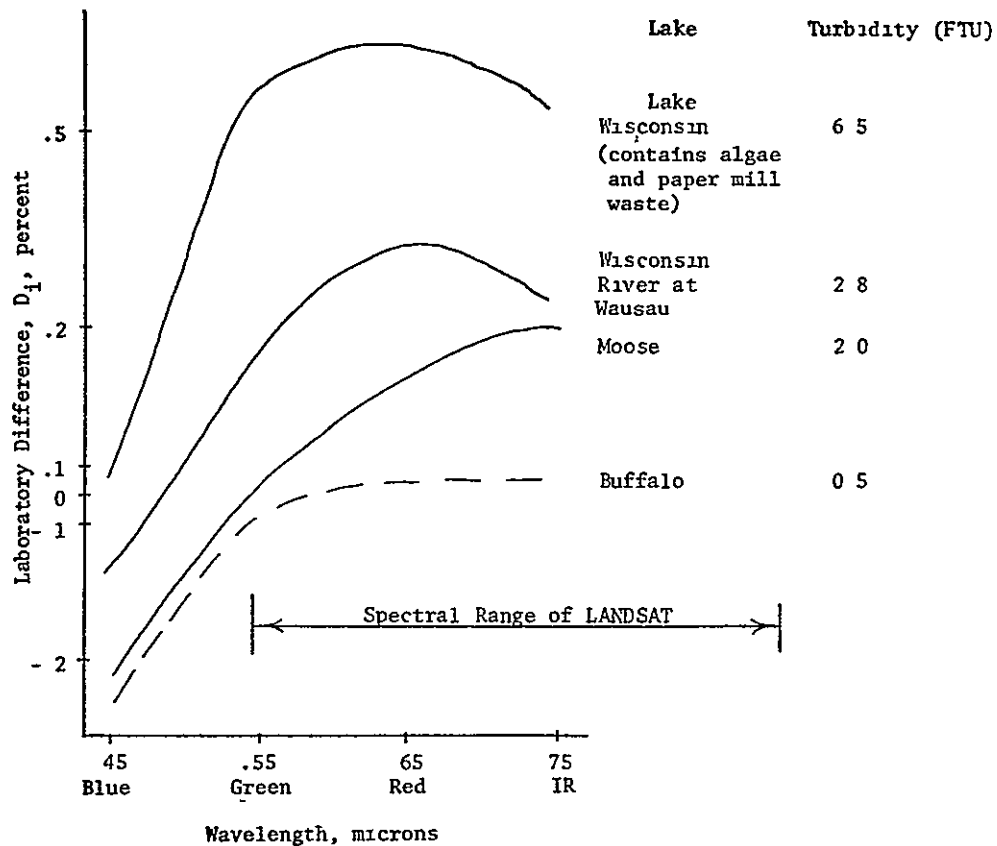
21 1945, 12, 19, 1946, 1947
5, 11, 16, 19, 21, 27, 28

FIGURE 38 Laboratory Reflectance Difference Curves (D_1) or Fingerprints for Clear Water Type Lakes With Various Amounts and Types of Algae Present (Scherz, Crane, and Rogers 1975)



Because humic materials in humic lakes absorb the short blue and blue-green wavelengths, the fingerprints for these lakes dip below the zero line for distilled water. Lesser amounts of humic substances will cause less depression in the blue part of the curve. A mixture of humic water and algae can occur. However a lake with both algae and humic material has a more depressed curve in the blue region than a lake with just algae present. Figure 39 shows laboratory difference curves for humic lakes.

FIGURE 39. Laboratory Reflectance Difference Curves (D_1) for Humic Lakes
Lake Wisconsin Contains Algae Also (Scherz, Crane, and Rogers 1975)



Other materials added to pure water such as red clay have their own unique fingerprints. It is possible to obtain these fingerprints by proper analysis of satellite data as well as laboratory data. The only real difference between the lab fingerprints and the satellite fingerprints is the slightly longer wavelengths that the satellite fingerprint senses compared to the laboratory fingerprint. Figure 39 shows that the satellite multispectral scanner does not contain data from the blue portion of the spectrum, while the lab data do. The satellite fingerprint extends further into the infrared region than does the laboratory fingerprint. Also, there is a different scale for the y axis between the lab and satellite fingerprint. The scale factor is a function of the lab reflectance panel and the meteorological conditions only (discussed later in this chapter). Essentially, the scale factor does not change the shape of the real fingerprint curve - just the numbers on the vertical scale used in its plotting.

The models and equations needed to analyze satellite data must first be developed for the situation where the sensor is outside under skylight and near the water surface, e.g., mounted on a boat.

I BOAT LEVEL ANALYSIS AND MODELING

1. General

Let the superscript ' denote signals sensed outside at boat level that contain skylight reflection components. For example, let W' be the total signal coming upward from a lake to a sensor mounted in a boat. The signal W is the signal from water to a sensor in the lab.

When the water being analyzed is out-of-doors as in Figure 40, the direct radiance of the sun is L'_s , and the average indirect radiance from the skylight is L'_c . According to Lambert's Law the total irradiance effecting a horizontal surface due to this skylight is

$$H'_c = L'_c \pi$$

The sun's direct contribution to the irradiance at water level is $H'_s = L'_s \psi \cos \theta$. The symbol ψ represents the solid angle of the sun as viewed at ground level and θ is the angle between the sun and the vertical (Figure 40). Let the total irradiance from both the sun and skylight be H'_o

$$H'_o = H'_s + H'_c$$

$$H'_o = L'_s \psi \cos \theta + L'_c \pi$$

The diffuse signal from a field reflectance panel, P' , would be

$$P' = \frac{H'_o \rho_p}{\pi}$$

where ρ_p = the reflectance of this field panel

Also following Lambert's Law for diffuse reflectance, S'_s , the diffuse reflectance caused by leaves, dirt, foam, and other impurities on the water surface is

$$S'_s = \frac{H'_o \rho_s}{\pi}$$

where ρ_s = the field diffuse reflectance from foam, leaves, and other dirt on the water surface Also V' , the radiance from the water volume is

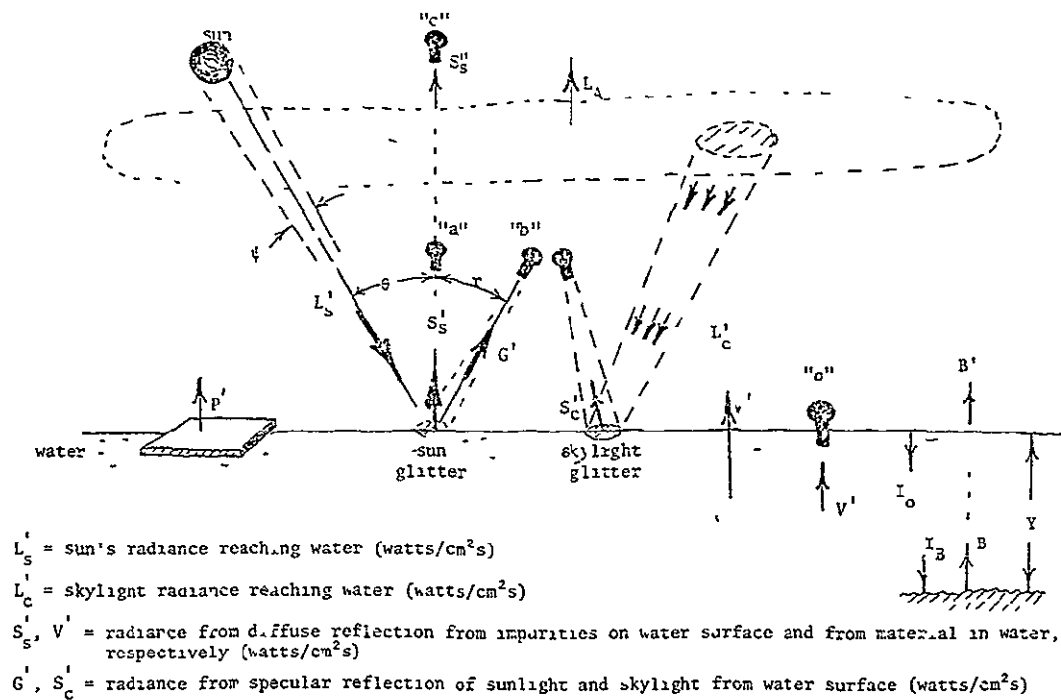
$$V' = \frac{H_o \rho_v}{\pi}$$

The specular reflection of the sun from the water surface (sun glitter) is

$$G' = L'_s \phi = .020 L'_s$$

where ϕ is the specular reflection from the surface.

FIGURE 40 Direct and Indirect Energy Relationships in the Field (from Scherz, Crane, and Rogers 1975).



ORIGINAL PAGE IS
OF POOR QUALITY

In a similar manner the specular reflection of the skylight from the water surface is S'_c

$$S'_c = \phi L'_c = .020 L'_c$$

The total signal from the water is W'

$$W' = V' + S'_s + S'_c$$

$$W' = \frac{\rho_v H'_o}{\pi} + \frac{\rho_s H'_o}{\pi} + .020 L'_c$$

$$W' = (\rho_v + \rho_s) \frac{H'_o}{\pi} + .020 L'_c \quad (4)$$

2. Obtaining ρ_{v_1} In The Field

Volume reflectance (ρ_v) of a particular lake can be determined in the field with a ground truth instrument such as the Bendix RPMI Ground Truth Instrument.* This can be done most easily by pointing the sensor telescope down through the surface of the water as in Position "d" in Figure 40. Assuming no significant bottom signal, the sensor at "d" only reads the radiance from the water volume V' .

$$V' = \frac{\rho_v H'_o}{\pi}$$

H'_o can be obtained directly by using the Bendix RPMI instrument or a reading can be taken on the field reflectance panel and the $\frac{H'_o}{\pi}$ value determined as follows

$$P' = \rho_p \frac{H'_o}{\pi}$$

* RPMI = Radiant Power Measuring Instrument developed by Aero Space Systems Division of Bendix Corporation (Rogers, Peacock, and Shah 1973)

$$\frac{H'_O}{\pi} = \frac{P'}{\rho_P} \quad \text{and}$$

$$\rho_V = V' \frac{\rho_P}{P'}$$

The V' and P' are readings from the boat mounted sensor and the ρ_P can be determined in the laboratory by comparing the reflectance of the field panel to the reflectance from the BaSO_4 standard. Thus, the ρ_V can also be obtained in the field for any water sample with a boat mounted sensor. However, due to variations in skylight and wave action in the field, the laboratory determination of ρ_V is a magnitude more precise than field determinations.

3. Laboratory Data Compared to Boat Level Data

It is necessary to understand how to translate laboratory values to values obtained by a boat level sensor. The difference between the two is due to possible difference in standard reflectance panels, difference in illumination energy, and specular reflection of skylight from the water surface.

The radiance from the panel in the laboratory is

$$P = \frac{H_L}{\pi} \rho_{PL}$$

The radiance from very clear or distilled water in the lab is

$$W_1 = (\rho_{V_1} + \rho_{SL}) \frac{H_L}{\pi}$$

The radiance from water sample #1, (more turbid) in the lab is

$$W_1 = (\rho_{V_1} + \rho_{SL}) \frac{H_L}{\pi}$$

If W_1 is subtracted from W_1 , the result is called Laboratory Residual for water sample #1, R_1

$$R_1 = W_1 - W_1 = (\rho_{V_1} - \rho_{V_1}) \frac{H_L}{\pi}$$

The lab apparent reflectance AP_1 for sample #1 is

$$AP_1 = \frac{W_1}{P} = \frac{\rho_{V_1} + \rho_{SL}}{\rho_{PL}}$$

The lab difference is D_1

$$D_1 = AP_1 - AP_1 = (\rho_{V_1} - \rho_{V_1}) \frac{1}{\rho_{PL}}$$

From Equation 4, for the boat level sensor the total signal from the water is

$$W'_1 = (\rho_V + \rho_S) \frac{H'_O}{\pi} + 0.020 L'_C$$

The signal from the panel is

$$P'_1 = \rho_P \frac{H'_O}{\pi}$$

The boat level residual signal obtained by subtracting the clear water signal from the lake #1 signal is.

$$R'_1 = W'_1 - W'_1 = (\rho_{V_1} - \rho_{V_1}) \frac{H'_O}{\pi}$$

The boat level apparent reflectance (relative to the field panel) is

$$AP'_1 = \frac{W'_1}{P'_1} = \frac{\rho_{V_1} + \rho_S}{\rho_P} + \frac{0.020 L'_C \pi}{\rho_P H'_O}$$

If a white styrofoam reflectance panel* is used in the field, then $\rho_P = \rho_{PL}$. Also if the lake surface is relatively clean and free from undue foam, leaves, and dust so that surface contaminants are assumed to be the same as in the laboratory (i.e., $\rho_S = \rho_{SL}$) then

* White styrofoam makes a good field reflectance panel. Its reflectance across the photographic spectrum is essentially constant at 39% which is the same as that for $BaSO_4$. For some field studies, especially with dark water, a grey reflectance or black reflectance panel is also useful.

$$AP_1' = AP_1 + \frac{0.020 L_c' \pi}{\rho_p H_o'}, \text{ and the boat level difference is}$$

$$D_1' = AP_1' - AP_1 = \frac{\rho_{v_1} - \rho_{v_1}}{\rho_p}$$

$$\text{Therefore } D_1' = D_1$$

J. AIRBORNE AND SATELLITE MODELING

Let the superscript " denote signals received by a sensor on an aircraft or a satellite. This superscript means these signals have been modified by the atmosphere between the earth's surface and the airborne sensor. So W'' , W_1' , and W denote the total signals from a water sample as detected by airborne mounted, boat mounted, and laboratory sensors, respectively.

When the signal from the water level such as S_s' in Figure 40 passes upward through the atmosphere it is attenuated by the atmospheric transmittance τ ; $S_s'' = S_s' \tau$. Also the atmospheric backscatter, LA, is added to the signal. Therefore, the total signal from the water as sensed at "c" in Figure 40 is:

$$W'' = (V' + S_s' + S_c') \tau + LA$$

$$W'' = \frac{\rho_v H_o' \tau}{\pi} + \frac{\rho_s H_o' \tau}{\pi} + .020 L_c' \tau + LA$$

$$W'' = (\rho_v + \rho_s) \frac{H_o'}{\pi} \tau + .020 L_c' \tau + LA \quad (5)$$

If the subscripts 1 and 1 represent distilled water and a turbid lake (#1), respectively, then

$$W_1'' = (\rho_{v_1} + \rho_s) \frac{H_o'}{\pi} \tau + .020 L_c' \tau + LA$$

$$W_1'' = (\rho_{v_1} + \rho_s) \frac{H_o'}{\pi} \tau + .020 L_c' \tau + LA$$

1. Airborne or Satellite Residual, R_1''

. Subtracting the airborne signal of the clear water lake from the signal from lake #i yields what is here defined as the airborne residual (R_1'') for lake #1. If the sensor is aboard a satellite this term is called the satellite residual.

$$R_1'' = W_1'' - W_1''$$

$$R_1'' = (\rho_{V_1} - \rho_{V_1}) \frac{H_O' \tau}{\pi} \quad (6)$$

Note that except for a different constant factor $\frac{H_O' \tau}{\pi}$ the above equation is the same as the equation for the laboratory difference that was used to obtain the fingerprints for materials added to pure water

Laboratory difference

$$D_1 = (\rho_{V_1} - \rho_{V_1}) C_1$$

Airborne or satellite residual.

$$R_1'' = (\rho_{V_1} - \rho_{V_1}) C_2$$

$$\text{where } C_1 = \frac{1}{\rho_{PL}} \text{ and } C_2 = \frac{H_O' \tau}{\pi}$$

Since ρ_{PL} for styrofoam is essentially constant at 0.39% for all wavelengths of interest, for a styrofoam panel

$$C_1 = \frac{1}{\rho_{PL}} = \frac{1}{0.39} = 2.6$$

$$C_1 = 2.6$$

The variables in C_2 are H'_O and τ . These are dependent on the elevation of the sun and the atmospheric clarity existing at the instant the image was taken. These are also very dependent on wavelength. Francis J. Ahern and his colleagues at the Canada Centre for Remote Sensing are involved in calculating atmospheric parameters such as τ by using the Turner model and radiances from clear lakes obtained from LANDSAT data (Ahern et al. 1977; Turner and Spencer 1972). Ahern has calculated and furnished values of $H'_O \tau$ determined from Lake Ottawa on clear and hazy days in 1976. These curves of $H'_O \tau$ for the four different LANDSAT bands are given in Appendix C. Although more work is needed on the area of these atmospheric effects the curves in Appendix C illustrate that it is theoretically possible to relate laboratory data to satellite data by:

$$\frac{R''_1}{D_1} = \frac{(\rho_{v_1} - \rho_{v_1})}{(\rho_{v_1} - \rho_{v_1})} \frac{C_2}{C_1} = \frac{C_2}{C_1}$$

$$R''_1 = \frac{C_2}{C_1} D_1 \text{ and}$$

$$D_1 = \frac{C_1}{C_2} R''_1$$

2 Solving For Volume Reflectance, ρ_v

Again assuming the volume reflectance of distilled water, ρ_{v_1} , to be known, from Equation 6:

$$\rho_{v_1} = R''_1 \frac{\pi}{H'_O \tau} + \rho_{v_1}$$

So if the atmospheric factors for that particular day ($\frac{\pi}{H'_O \tau}$) are solved for,

then the volume reflectance of lake #1 (ρ_{v_1}) can be calculated from airborne data

3 Modeling and Solving For Atmospheric Parameters

From Equation 5 the total signal from a lake as detected by an airborne sensor is

$$W'' = W' \tau + LA$$

$$W'' = (\rho_v + \rho_s) \frac{H_o'}{\pi} \tau + 0.020 L_c' \tau + LA$$

Similarly the signal from the panel (P' at boat level) becomes P'' when sensed by the airborne sensor

$$P'' = P' \tau + LA$$

$$P'' = \rho_p H_o' \frac{\tau}{\pi} + LA$$

As has already been stated, the airborne residual for lake #1, R_1'' is as follows:

$$R_1'' = W_1'' - W_1'$$

$$R_1'' = (\rho_{v_i} - \rho_{v_1}) H_o' \frac{\tau}{\pi}$$

but since R_1' (boat level residual) = $(\rho_{v_i} - \rho_{v_1}) \frac{H_o'}{\pi}$, then

$$R_1'' = R_1' \tau \text{ or } \tau = R_1''/R_1' \quad \longleftarrow \tau$$

In other words if there are two lakes, one a very clear lake and another with significant suspended matter present, and if the strength of their backscattered signals are recorded both from boat and airborne levels, then by simple subtraction and division the atmosphere τ can be calculated *

It is also possible to use the Ahern curves in Appendix C. first C_2 must be calculated from

$$C_2 = \frac{R_1''}{D_1} C_1 = \frac{H_o' \tau}{\pi}$$

* Some correction factors may be necessary however to account for such things as the fact that light backscattered from water behaves according to the laws of photometry in a logarithmic rather than a linear manner See Appendix C

then by entering the curves with the appropriate sun elevation angle it is possible to obtain a value for τ as with the example given in Appendix C.

LA can be solved for, using the backscattered signals from a lake, as follows:

$$W'' = W' \tau + LA$$

Therefore:

$$LA = W'' - W' \tau \longleftarrow LA$$

LA can also be determined using the energy backscattered from a uniform diffuse reflector such as a standard reflectance panel. The strength of the energy backscattered from this panel must be determined both at ground level (P') and from the airborne level (P'')

$$P'' = P' \tau + LA$$

and

$$LA = P'' - P' \tau \longleftarrow LA$$

The total irradiance from both the sun and skylight as sensed at ground level is H'_0 . Panel reflectance data can be used to solve for H'_0 as follows.

$$P'' = \rho_p H'_0 \frac{\tau}{\pi} + LA$$

or.

$$H'_0 = (P'' - LA) \frac{\pi}{\tau \rho_p} \longleftarrow H'_0$$

If the surface of a lake is relatively clean (free from foam, etc.) so that the specular reflectance in the field can be assumed to be the same as in the laboratory ($\rho_s = \rho_{SL}$) then it is also possible to calculate an effective value for skylight radiance L'_c .

$$AP'_1 = \frac{W'_1}{P'_1} = AP_1 + 0.020 \frac{L'_c}{\rho_p H'_0} \text{ and}$$

$$L'_c = \frac{\rho_p H'_0}{0.020\pi} (AP'_1 - AP_1) \longleftarrow L'_c$$

Of course a value for L'_c can be obtained by other methods such as pointing a field radiance measuring instrument at various portions of the sky and then by certain mathematical integrations determining an effective average value for L'_c .

Once L'_c is obtained, then it is possible to calculate a value for H'_c , the total irradiance from the skylight

$$H'_c = \pi L'_c \longleftarrow H'_c$$

Also the sun's irradiance H'_s can be obtained by

$$H'_s = H'_o - H'_c \longleftarrow H'_s$$

The airborne apparent reflectance for lake #1 (AP''_1) can be obtained by relating water signals to a diffuse reflectance standard and can be compared to boat level and laboratory data by using a factor K which combines several atmospheric terms (Scherz and Van Domelen 1975) Let:

$$K = 1 + \frac{LA\pi}{\rho_p H'_o}$$

Assuming that laboratory panel and water specular reflectance are equal to those in the field ($\rho_p = \rho_{PL}$ and $\rho_s = \rho_{SL}$) then it can be shown that

$$AP''_1 = \left(\frac{\rho_v + \rho_s}{\rho_p} \right) \left(\frac{1}{K} \right) + \frac{0.020 L'_c \pi}{\rho_p H'_o} \left(\frac{1}{K} \right) + (K - 1) \left(\frac{1}{K} \right)$$

The above is the universal equation for apparent reflectance The airborne and boat level data can also be related by

$$AP''_1 = (AP'_1) \frac{1}{K} + (K - 1) \left(\frac{1}{K} \right)$$

If measurements are made at boat level, the atmospheric backscatter LA drops to zero and K becomes 1.0

$$K = 1 + \frac{LA\pi}{\rho_p H'_o} = 1 + 0 = 1$$

and AP_1'' becomes AP_1' , so

$$AP_1' = \frac{\rho_{V_1} + \rho_S}{\rho_P} + \frac{0.020 L_C' \pi}{\rho_P H_O'}$$

This is also the same as:

$$AP_1' = AP_1 + \frac{0.020 L_C' \pi}{\rho_P H_O'}$$

If measurements are being made in the laboratory, L_C' drops to zero and AP_1' becomes AP_1

$$AP_1 = \frac{\rho_{V_1} + \rho_S}{\rho_P}$$

The factor K can also be used for relating airborne, boat level, and laboratory differences (D_1'' , D_1' , and D_1)

The airborne difference for lake #1 (D_1'') is

$$D_1'' = AP_1'' - AP_1'' = \frac{W_1''}{P''} - \frac{W_1''}{P''}$$

$$D_1'' = \left(\frac{\rho_{V_1} - \rho_{V_1}}{\rho_P} \right) \left(\frac{1}{K} \right) =$$

$$D_1'' = (D_1') \left(\frac{1}{K} \right) \text{ or } K = D_1' / D_1''$$

but the boat level difference D_1' equals the laboratory difference D_1 when the field and laboratory panels are of the same material ($\rho_P = \rho_{PL}$) so,

$$D_1' = D_1$$

and

$$D_1'' = D_1' \left(\frac{1}{K}\right) = D_1 \left(\frac{1}{K}\right)$$

or

$$K = D_1' / D_1''$$

The factor K is used when ratios are calculated for signals from lakes to those from a diffuse reflector of known reflectance. Many times from high altitudes, especially satellite altitudes, no diffuse reflectors of known reflectance are available. In such cases if a clear water lake occurs somewhere in the image the signal from it (W_1'') can be used as a standard. Then this clear water signal is subtracted from the signal from another lake (#1) and the airborne residual results.

$$R_1'' = W_1'' - W_1' = (\rho_{v_1} - \rho_{v_1}') \frac{H_0' \tau}{\pi}$$

The residual for this lake can also be calculated for the boat level situation. At boat level the atmospheric attenuation factor (τ) is 1.0 because there is essentially no atmospheric path for the signal to travel

$$R_1' = W_1' - W_1'' = (\rho_{v_1} - \rho_{v_1}') \frac{H_0'}{\pi}$$

or

$$R_1' = R_1'' / \tau$$

For obtaining boat level values such as W_1' , W_1'' , AP_1' , AP_1'' , R_1' , D_1' , etc., two simultaneous boat level readings must be taken on different lakes. This can be accomplished by two portable field radiance units such as the Bendix RPMI instruments (Rogers, Peacock, and Shah 1973)

If absolute values from airborne data are to be obtained, then some atmospheric factors must be known. If the values for airborne difference D_1'' and airborne residual R_1'' are used, most of the atmospheric factors drop out. The airborne residual value R_1'' is used in satellite analysis because it has the least number

of atmospheric components and requires no field panel. From it come the satellite fingerprint curves for different materials added to pure water that closely match the fingerprint curves obtained from analysis of laboratory data using the laboratory difference equation.

$$\text{Laboratory fingerprints: } D_1 = AP_1 - AP_1 = (\rho_{V_1} - \rho_{V_1}) \frac{1}{\rho_{PL}}$$

$$\text{Airborne fingerprints: } R_1'' = W_1'' - W_1'' = (\rho_{V_1} - \rho_{V_1}) \frac{H_0' \tau}{\pi}$$

From the above it can be seen that if the total irradiance on the earth's surface, H_0' , and the atmospheric transmittance, τ , do not change over a remote sensing scene, then R_1'' (from satellite analysis) can be compared to the D_1 from laboratory analysis and the only difference between the two will be a constant which is dependent on the lab panel (ρ_{PL}) and the atmospheric conditions at the time of the overflight ($H_0' \tau$) *

K. SATELLITE DATA ANALYSIS

For LANDSAT image analysis for water quality mapping a very clear lake must be located which can be used as a substitute for distilled water used in the laboratory analysis. A lake with a Secchi disc reading of at least 10 to 15 feet should be used. Also, aerial observations should be made or color photos taken to assure that there is no bottom showing in this test lake.

Let W_1'' equal the satellite raw reading in some band for this clear lake (Lake #1)

Let W_1'' equal the raw readings in the same band for Lake #1, the lake in question.

The raw readings for Band 4 (green) and Band 5 (red) are very high due to atmospheric effects, and some differential water signals are perhaps 1% of these raw readings. Therefore these raw readings do not appear very meaningful (Figure 66)

However, if W_1'' is subtracted from W_1'' the residual is due primarily to the material in the water of Lake #1. Raw readings are taken from the four bands of the LANDSAT scanner

* See Figure 31 and Appendix C. In Figure 31, the changes in slope of the satellite reflectance curves for different days is due to changes in $H_0' \tau$ and logarithmic correction factors given in Appendix C

The four bands of LANDSAT cover the electromagnetic energy spectrum as follows:

Band 4. 0.50 to 0.60 microns - green energy
 Band 5. 0.60 to 0.70 microns - red energy
 Band 6. 0.70 to 0.80 microns - infrared #1
 Band 7. 0.80 to 1.10 microns - infrared #2

Plot the total signal from Bands 4, 5, 6, and 7, as centering on wavelengths 0.55, 0.65, 0.75, and 0.95 μ , respectively. Figure 41 shows such a plot of the satellite residual, R_1'' , for these four LANDSAT bands. Three types of waters: clear, humic, and algal, are readily differentiated. Note the similarity of these fingerprints with those obtained from the lab data (Figure 37). However, while the laboratory differential fingerprints cover the .45 and .75 μ part of the spectrum, the satellite residual fingerprints cover the 0.55 to 0.95 μ part of the energy spectrum. Other than this shift of wavelength for the x axis and the change in scale factor in the y axis (C_1 for the laboratory data and C_2 for the satellite data) either the satellite data or the laboratory data can be used to plot the fingerprints of the material added to clear water of any lake sample. The shape of the fingerprint for a lake such as Lake #1 is really determined by the factor $(\rho_{V_1} - \rho_{V_1})$ plotted for different wavelengths. For the satellite data, R_1'' is plotted against wavelength (Figure 41)

$$R_1'' = (\rho_{V_1} - \rho_{V_1}) H_o' \frac{\tau}{\pi} = (\rho_{V_1} - \rho_{V_1}) C_2$$

For the laboratory data, D_1 is plotted against wavelength (Figure 37).

$$D_1 = (\rho_{V_1} - \rho_{V_1}) \frac{1}{\rho_{PL}} = (\rho_{V_1} - \rho_{V_1}) C_1$$

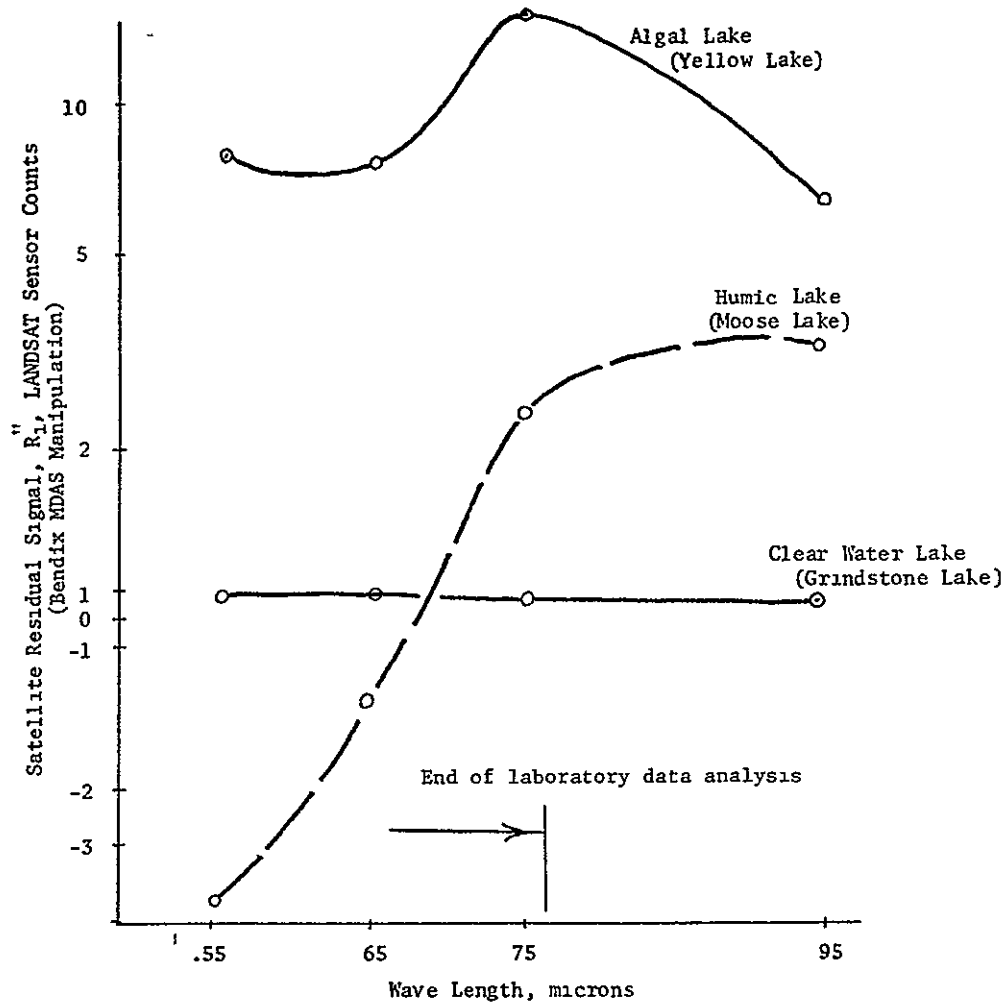
The values on the y axis for the two figures vary only by the factor

$$\frac{R_1''}{D_1} = H_o' \frac{\tau}{\pi} / \frac{1}{\rho_{PL}} = \rho_{PL} H_o' \frac{\tau}{\pi} = \frac{C_2}{C_1} *$$

Therefore, by use of R_1'' and the resulting satellite fingerprints it is possible to separate lakes into different classes by LANDSAT signals alone. Also, computers designed specifically to analyze multiband satellite data can readily perform the manipulations necessary to arrive at satellite fingerprints for different material of various concentrations in water.

* Also see Appendix C for refinements.

FIGURE 41. Characteristic Fingerprints From Satellite Residual Signal, R_1 , For Three Water Types (Scherz, Crane, and Rogers 1975)



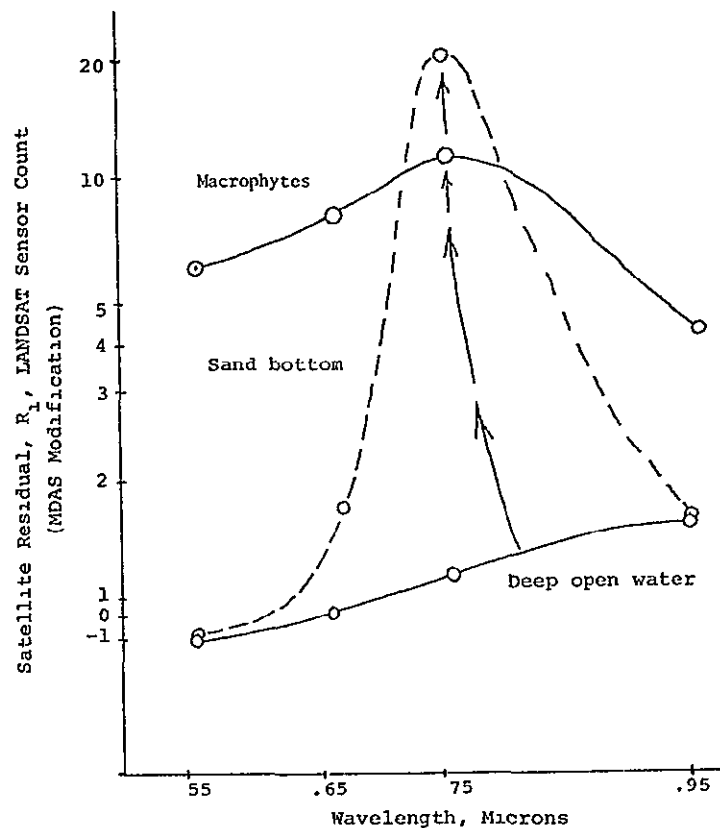
L BOTTOM EFFECTS IN SATELLITE IMAGERY

The bottom effect problem is a difficult noise factor in satellite classification of lakes. Bottom signals can show in any of the lake types. The type of bottom (dark mud, light sand, or green weeds), also will give a different characteristic modification to signals from each of the water types. The depth to bottom also affects the strength of the signal and its spectral distribution.

The bottom effect problem in lakes can best be studied by analyzing spring imagery when the lakes are clear and free of algae and the bottoms are the most apparent. Where bottom signals are strong they yield a characteristic fingerprint and can be separated from the various lake types.

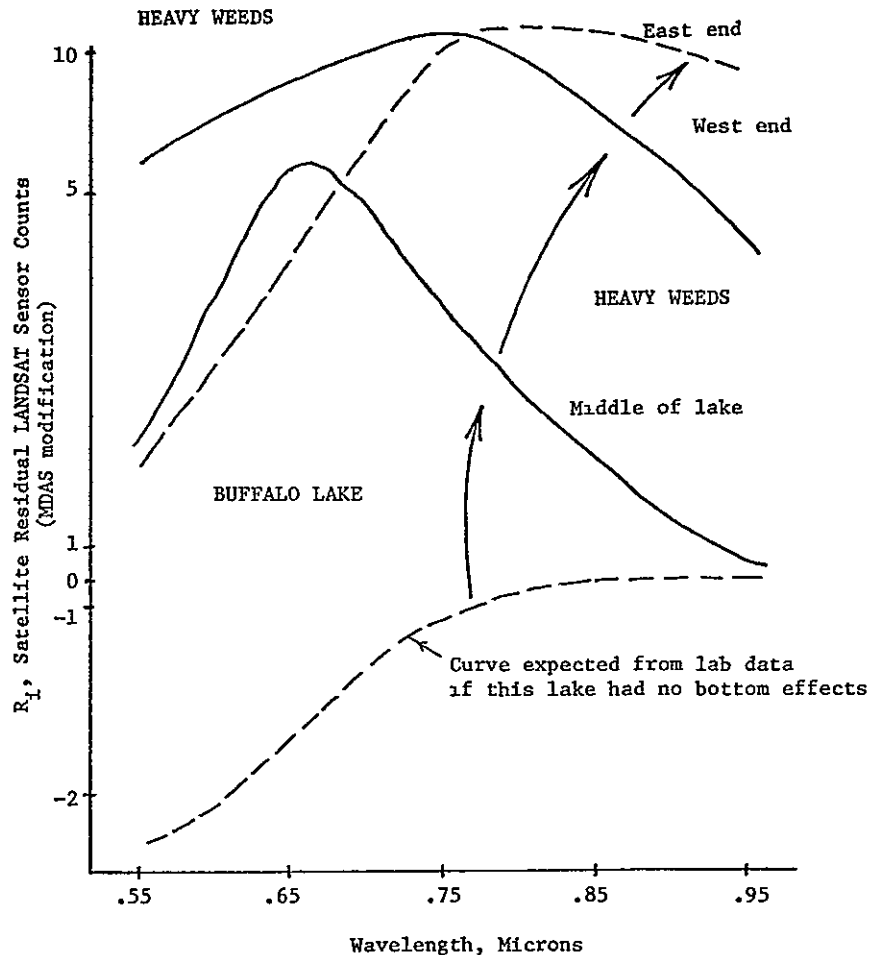
Figure 35 showed how significant the effect of the bottom of the sample tube is in the laboratory. For clear water the effect of the shiny white bottom could be several times larger than the signal from the water itself. Similar conditions can occur in field situations. Figure 42 shows the effect of a sand bottom and macrophytes on the total signal coming from a lake that has nearly clear water but with a small amount of humic material present. The total signal from the part of the lake with the visible sand bottom is several times greater than the magnitude of the signal coming from the deep water where no bottom effect is present. Fortunately the fingerprint from the sand bottom is different than those from algae, humic material, or red clay, etc. The computer analyzing satellite data can be trained to recognize sand bottom conditions. The signals from macrophytes are also unique and can be recognized by the computer. However, each kind of macrophyte has a different fingerprint. Even the same kind of macrophyte at different depths has different fingerprints. But generally speaking for macrophytes as well as sand bottoms, the fingerprints are unique enough so that the computer can recognize and map them as such (Figure 43)

FIGURE 42 Effect of Sand Bottom and Macrophytes On Satellite Fingerprint of a Clear Lake Containing Some Humic Material.



ORIGINAL PAGE IS
OF POOR QUALITY

FIGURE 43 Effect of Heavy Weeds and Mud Bottom on Signal Expected From Humic Lake. Although the Water is Low in Turbidity and Free of Algae (Figure 39) This is an Eutrophic Lake Because the Nutrients are Converted to Heavy Macrophyte Growth



M. MODELING LIGHT PENETRATION AND RETURN IN A LAKE

To effectively correlate lab, field, and satellite data, it is necessary to model the penetration of each color of energy in different waters. This depth of penetration is modeled as it relates to the easily obtained Secchi disc readings. Also it is sometimes important to collect water samples from a lake to get a composite sample in accordance with the percentage of energy that returns from the different water layers -- from the surface to the depth where the sun's energy is extinguished. This can be accomplished by using the Secchi disc reading, the model, and the curves shown in this section.

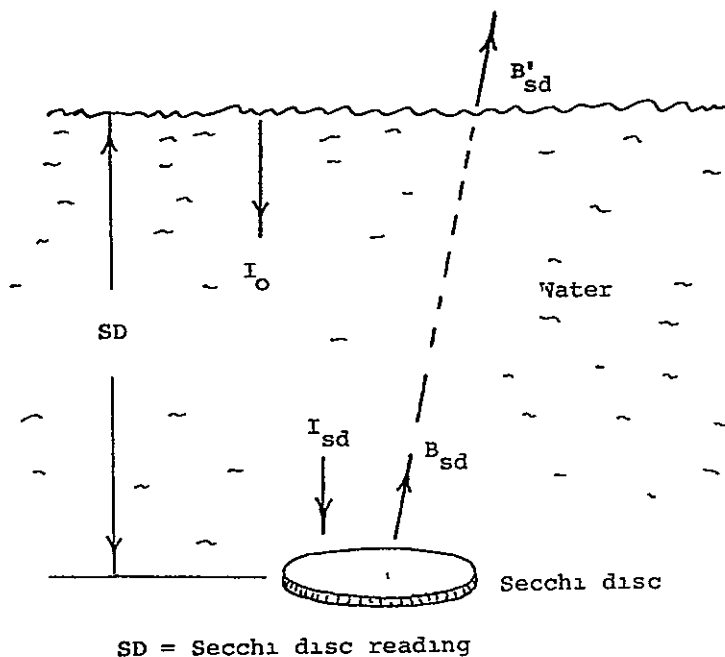
The importance of collecting water samples at the correct depth cannot be overemphasized. In one case at a steel mill near Chicago, Lake Michigan water on one side of a breakwater appeared dark brown to the airborne sensors and to observers due to the discharge from a nearby polluting steel mill. In contrast the water on the other side of the breakwater was very clear Lake Michigan water. When water samples were obtained to correlate the field data to the remote sensing images, the water samples from both sides of the breakwater were identical -- both being very clear water. This did not correlate at all with the different tones on the aerial image. Then it was discovered that the water samples had both been grab samples taken at the surface of the lake. On the side of the breakwater near the steel mill there was about six feet of very clear water overlying the polluted water from the steel mill. This polluted water was heavier and settled toward the bottom below where the surface sample was collected. Most of the sun's energy penetrated through the clear water surface layer and interacted with the lower polluted water. Certain wavelengths of energy were reflected back by the steel mill pollution and this energy again passed upward through the clear water layer and reached the airborne sensors. If the water samples had been collected in accordance with the amount of energy returning from the different layers in clear water then some of this steel mill pollution would also have been obtained in the water sample. It was from this study that the following depth penetration modeling and curves were developed (Scherz 1972)

In Figure 40 the energy that penetrates below the water surface is I_0 . The energy that reaches the bottom through depth "Y" is I_B . From Beer's Law: $I_B = I_0/e^{(\alpha Y)}$, where $e = 2.718$ and α is the extinction coefficient of the water

If a white Secchi disc is lowered into the water to the Secchi disc depth (SD) until it is no longer visible, then according to Holmes (1970) the energy I_{sd} that penetrates to this Secchi disc depth is approximately $1/10 I_0$. Therefore, as a working approximation $e^{(\alpha SD)} = I_0/I_{sd} = 1/0.1 = 10$, and $SD = \ln 10 = 2.3$, therefore $SD = 2.3\alpha$ (Figure 44, also Scherz and Van Domelen 1975).

The extinction coefficient is obtained by passing light through the water sample rather than recording the energy backscattered from it. The same sample tube is used as with the reflectance work except the tube has a glass bottom for transmittance analysis. (Figure 59 shows a sketch of the equipment used for water transmittance work.) The transmittance data seems exceedingly precise and there are transmittance fingerprints even more differentiable than those from the reflectance studies. Accurate and reliable transmittance fingerprints can be plotted for different materials in water from transmittances between 100% and 0001% (Figure 45). It seems that a very valuable water analysis potential exists for such a multispectral transmittance system. However, it is energy backscattered to remote sensors that is of primary interest here and especially energy coming from different layers of water between the surface down to the depth of the Secchi disc reading.

FIGURE 44. Modeling of Light That Penetrates to and Returns From the Secchi Disc at the Secchi Disc Reading.



I_0 = radiance available just below the water surface
(watts/cm²s)

I_{sd} = radiance available at Secchi disc approximately =
 $1/10 I_0$ (watts/cm²s)

H_{sd} = total irradiance available on Secchi disc (watts/cm²)

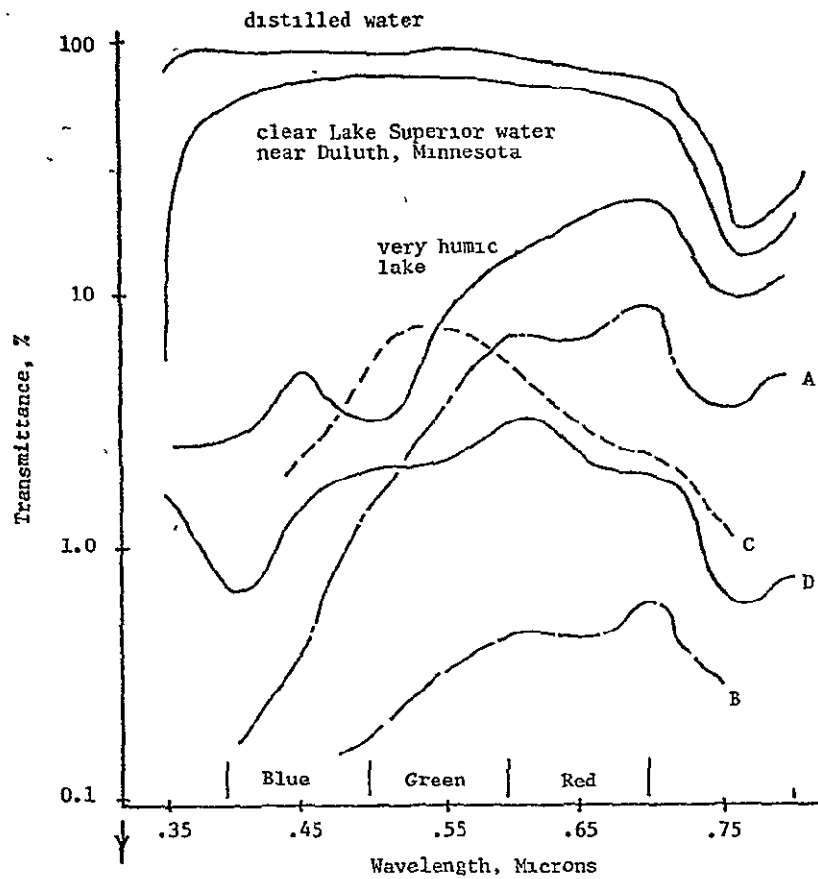
B_{sd} = radiance upward from Secchi disc = $\frac{H_{sd}}{\pi} \rho_{sd}$ (watts/cm²s)

ρ_{sd} = diffuse reflectance of Secchi disc

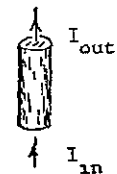
B'_{sd} = radiance from Secchi disc that upwells from water surface,
approximately $1/10 B_{sd}$ (watts/cm²s)

ORIGINAL PAGE IS
OF POOR QUALITY

FIGURE 45. Transmittance Analysis of Different Lake Waters. Accurate and Reliable Curves Can be Plotted to Transmittances of 0.0001%



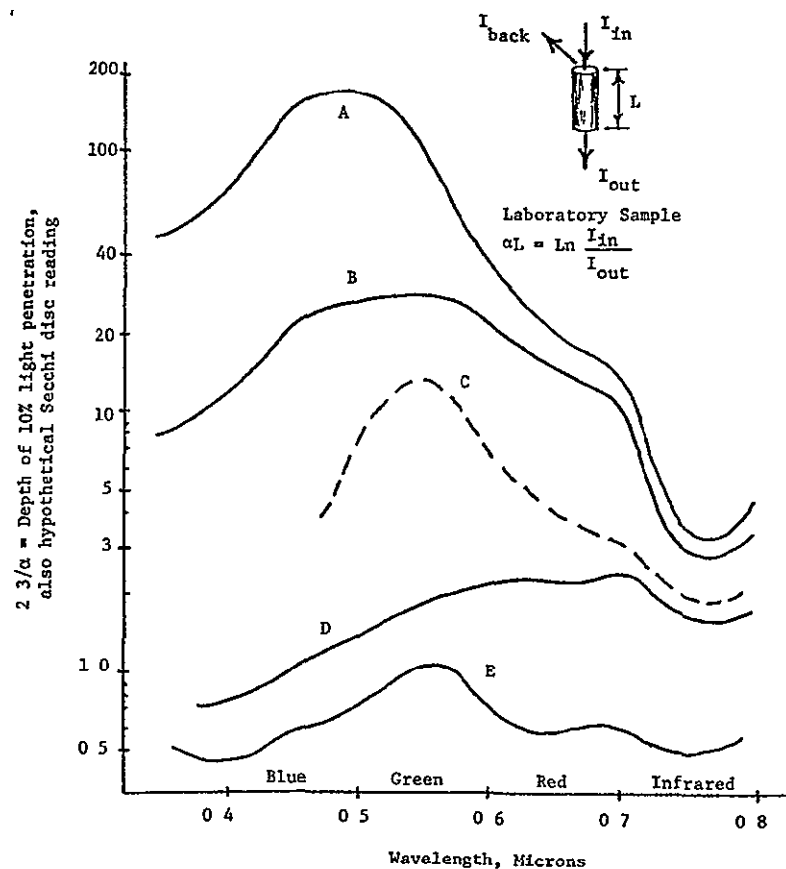
- A = Red clay in Lake Superior (low concentration)
- B = Red clay in Lake Superior (heavy concentration)
- C = Green "halo water" in Lake Superior from taconite rock flour
- D = Green algae in nonhumic lake (low concentration)



$$\text{Transmittance} = \frac{I_{\text{out}}}{I_{\text{in}}}$$

SD is the hypothetical Secchi disc reading for a particular wavelength. It is assumed that about 10% of the sun's energy reaches this depth. In actual practice the Secchi disc reading, like the turbidity reading, gives an average value across the entire visible spectrum while remote sensing investigations are mostly concerned with specific wavelengths. The extinction coefficient, α , like the hypothetical Secchi disc reading (SD), can be obtained for different wavelengths. Figure 46 shows such values of SD for various waters as well as actual Secchi disc readings. From these curves one can obtain an understanding of the penetration of different wavelengths of energy into various waters compared to the readily obtained Secchi disc reading. The reflectance of the white Secchi disc is almost always greater than the reflectance of bottom material, so if the bottom is deeper than the Secchi disc reading it will not be visible to the eye (however, it might be significant to more sensitive sensors).

FIGURE 46 Hypothetical Secchi Disc Readings, $2.3/\alpha$, for Different Waters at Different Wavelengths.



Sample	Water	Actual Secchi disc reading
A	Distilled water	NA
B	Lake Superior, clear	32 ft.
C	Taconite rock flour	9.5 ft.
D	Moderate red clay	6 ft.
E	Heavy algae	1.3 ft.

1. Magnitude of Energy That Returns From Below the Secchi Disc Reading and From Various Layers of Water

Figure 44 shows a sketch which can be used to model the energy that returns from a Secchi disc and from various layers above that depth. The radiance available just below the water surface is I_o . About 1/10 of this energy remains after passing through water with a thickness equal to the Secchi disc depth. The radiance reaching the Secchi disc depth is called I_{sd} , $I_{sd} = 1/10 I_o$.

According to Lambert's Law the total irradiance available on the Secchi disc is $H_{sd} = \pi I_{sd}$ (watts/cm²); let B_{sd} be the radiance returning upward from the Secchi

disc. Lambert's Law states that. $B_{sd} = \frac{H_{sd}}{\pi} \rho_{sd}$ (watts/cm²s) where ρ_{sd} is the diffuse reflectance of the Secchi disc.

The diffuse reflectance of a white styrofoam panel (ρ_p) was computed as 39%.

Assuming the reflectance of the Secchi disc to be the same, then B_{sd} , the energy returning upward from the Secchi disc is

$$B_{sd} = \frac{H_{sd}(\rho_{sd})}{\pi} = I_{sd}(0.39) = \frac{1}{10} I_o (.39) = .039 I_o$$

The portion of this energy that returns upward to the water surface, B'_{sd} , is approximately

$$B'_{sd} = 1/10 B_{sd} = 0.039 I_o = 0.39\% I_o$$

To calculate the amount of energy that returns from various layers in the water volume, 5 equal layers of thickness, "d" are created above and below the Secchi disc reading, $d = SD/5$ (Figure 47). Let I_{in} be the energy striking any layer and I_{out} be the energy transmitted through it (Figure 46). The energy backscattered by the particles in that layer is I_{back} . Let "b" be the unit backscatter, $b = I_{back}/I_{in}$, and let "t" be the unit transmittance through layers of thickness d, $t = I_{out}/I_{in}$ (Figure 47). From the extinction formula

$$\alpha d - \ln(I_{in}/I_{out}) = \ln(1/t)$$

but $\alpha = 2.3/SD$ and $d = SD/5$ so $\alpha d = \ln(\frac{1}{t}) = \frac{2.3}{SD} \times \frac{SD}{5} = \ln(\frac{1}{t})$ From this

$\ln(\frac{1}{t}) = .46$ and $t = 0.63$. From analyzing all possible water samples, the unit backscatter "b" will change depending on the type of material but will lie between 0.37 and 0. If in Figure 47 the light transmitted and backscattered from one unit volume is followed to the next until the energy is extinguished or reaches the surface, then the total energy coming from particles in each layer ($\Delta V'_1$) can be calculated. From layer 1, $\Delta V'_1 = b I_o$. From layer 2, $\Delta V'_2 = b I_o t^2 F$,

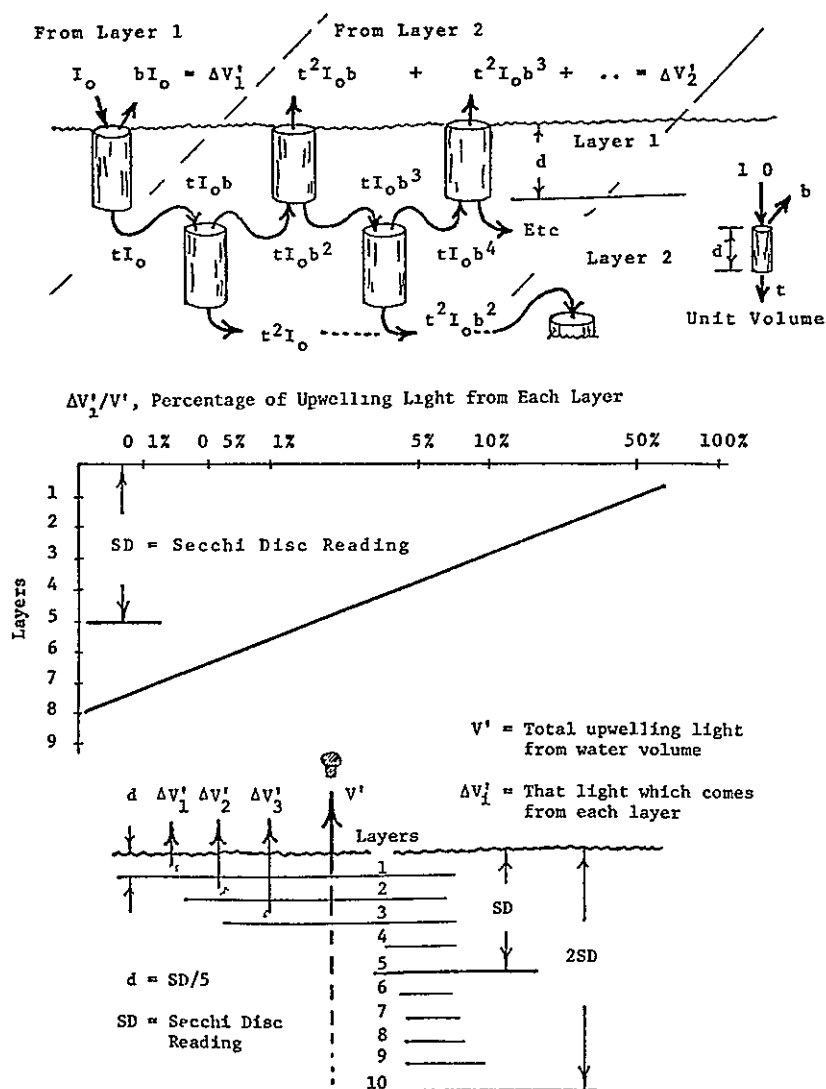
where $F = (1 + b^2 + b^4 + b^6 + \dots)$. For any layer (1):

$$\Delta V'_1 = b I_0 t^{(21-2)} F^{(21-3)}$$

The sum of all the $\Delta V'_1$ for all layers is V' ; $V' = \Delta V'_1 + \Delta V'_2 + \Delta V'_3 + \dots$

The percentage of V' that comes from the first level is $\Delta V'_1/V'$ which for a variety of natural waters is 59%, from the second and third layer it is 24% and 9.5%, respectively. Figure 47 shows a graph of the percentage of energy that comes from each of the layers.

FIGURE 47 Determining Percentage of Upwelling Energy From Suspended Particles at Different Depths Also Percentage of Composite Water Samples to be Collected at Different Depths (Scherz and Van Domelen 1975)



This graph is helpful when used with a Secchi disc reading. It shows how to integrate a water sample to get a representative collection of water particles which cause the backscatter returned to sensors from the total water volume. The composite water sample should be collected with an approximate 59% coming from the first layer, and 24% and 9.5% coming from layers 2 and 3, respectively, etc. Each layer is 1/5 of the Secchi disc reading. Also, the curve in Figure 47 can be used to ascertain what portion of the total signal V' still originates from below the Secchi disc reading. This knowledge can be useful for bottom studies.

2. Penetration of Different Wavelengths of Light

In clear water the maximum penetration of light occurs in the blue-green region (Figure 46). As different materials are added to clear water the penetration maximum may be any wavelength depending on the particular material in the water. Generally speaking, however, the penetration of infrared energy into water is low.

Ultraviolet energy seems to reflect off the surface of the water like a mirror. Because of this phenomena UV energy is especially useful for analyzing oil slicks*. Most of the infrared energy seems to be absorbed in a few inches of water. This makes the infrared wavelength especially good for detecting water/land boundaries and even wet soils. Figure 48 illustrates how different wavelengths of energy in the photographic portion of the energy spectrum interact with water.

N. PRACTICAL ANALYSIS OF SATELLITE REMOTE SENSING DATA AND LAKE CLASSIFICATION

1 General

The desirable remote sensing signal is the backscattered signal from the target. For lake classification the target is primarily the material in lake water. Some lakes have much material -- some have little. Those lakes with much material have more in some seasons than in others. In early spring after the ice melts lakes are often relatively free from green and blue-green algae. However, some diatoms may bloom then. Most of the nuisance algae from the previous summer dies during the winter**. By late summer those lakes that have a great deal of nutrients present (phosphates and nitrates), have heavy growth of green and blue-green algae and macrophytes.

In the autumn the sun sinks further to the South, the water begins to cool, and a net decrease in living algae often occurs. The amount of energy backscattered by particles in the water also decreases. Figure 49 shows the seasonal fluctuation of apparent reflectance, (i.e., the backscattered energy) from the algae in

* Polarized light is also useful for oil slick analysis

** Some observations indicate that this dead organic material seems to add to the humic or brown water concentrations in some northern waters which appear to be especially brown at spring "breakup"

Lake Mendota. Maximum reflectance from the algae occurs near the beginning of September. The maximum apparent reflectance also will correspond with the minimum amount of dissolved oxygen at the period of maximum temperature as shown in Figure 50 (Scherz 1977). The maximum differentiation in backscatter caused by nutrients in different lakes is a period during the last part of August to the first week in September. This is the time when lake classification by LANDSAT data should be accomplished.

FIGURE 48 Interaction of Different Wavelengths of Energy With Water (Scherz 1971).

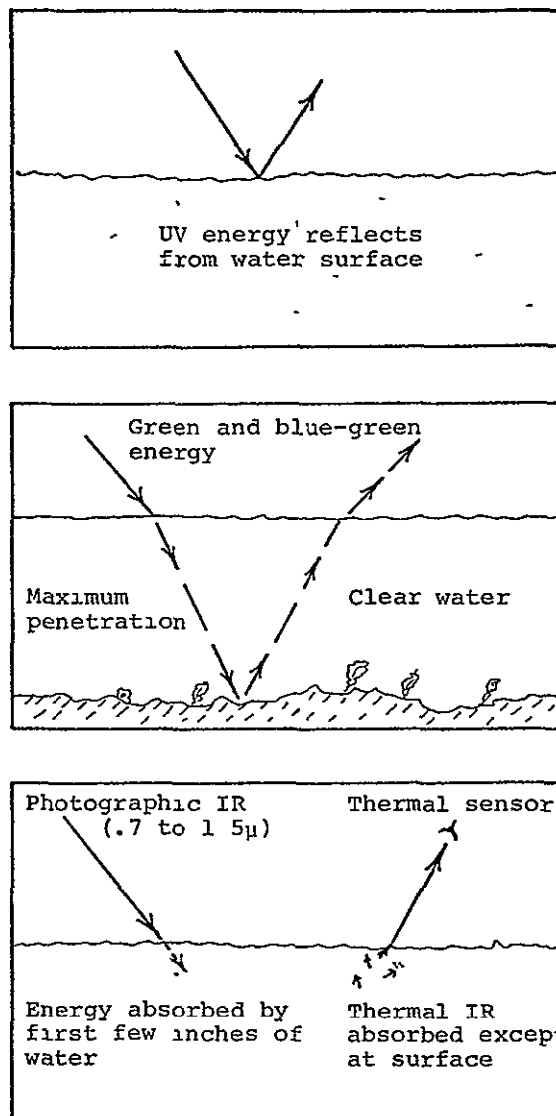


FIGURE 49. Effect of Time of Year on Reflectance Fingerprints in an Algal Lake.
Lake Mendota Laboratory Data (modified from Scherz, Crane, and Rogers 1975)

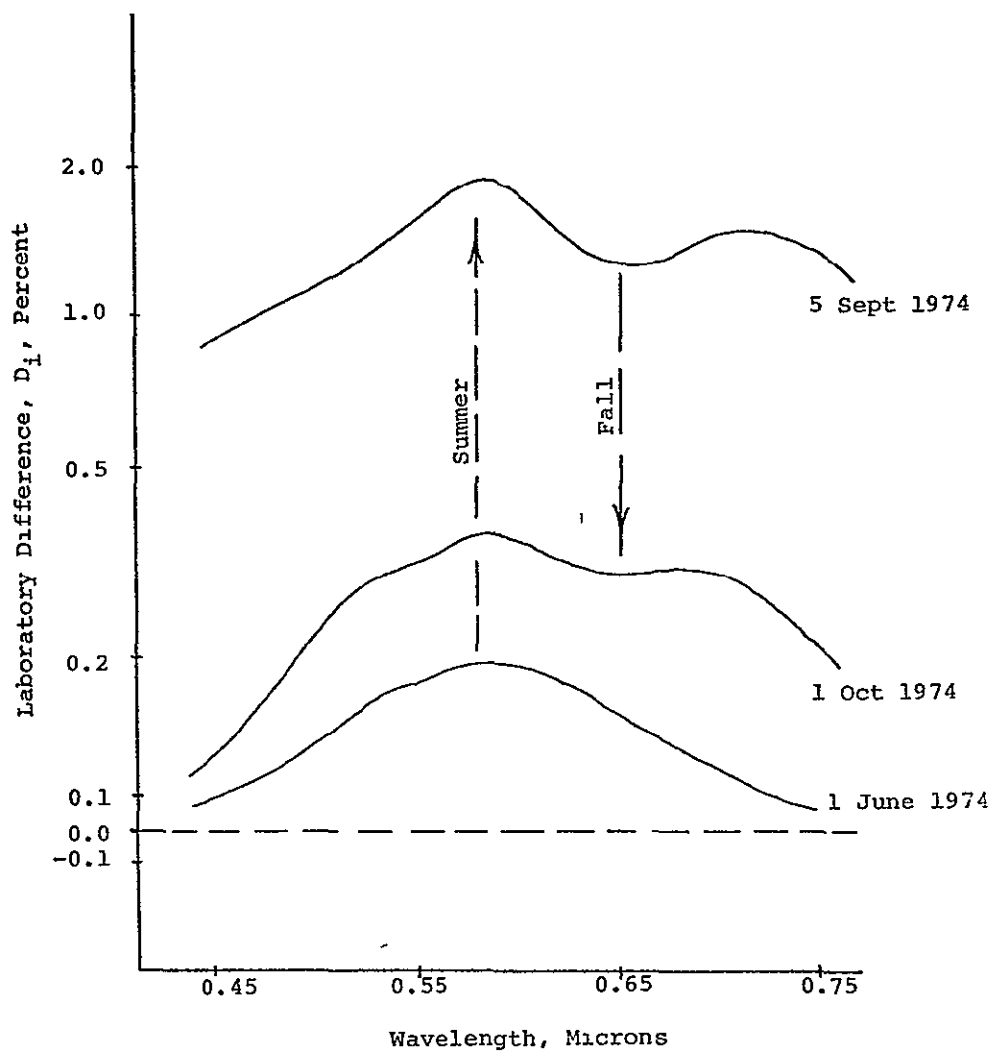
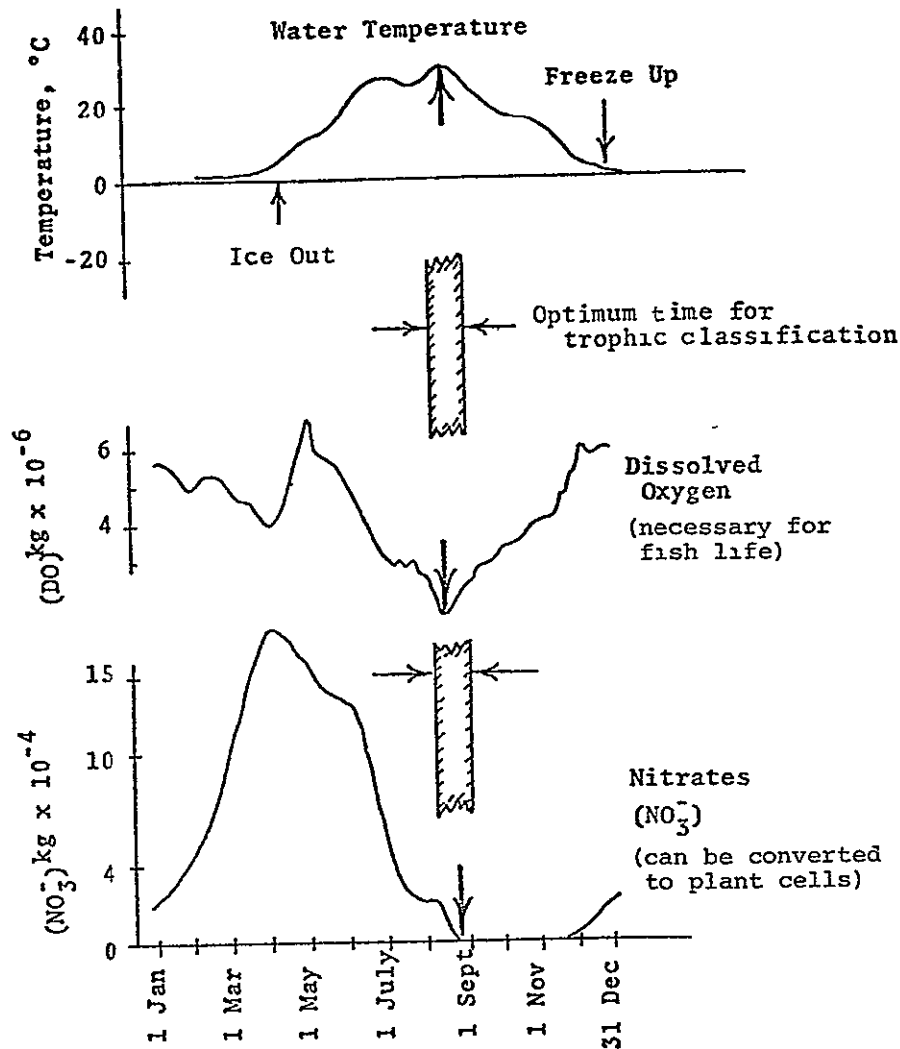


FIGURE 50. Water Temperature, Dissolved Oxygen, and Nitrates Plotted Against Time Lake Mendota, 1971 Data From Robert Elihu Stauffer, Ph.D Thesis, University of Wisconsin, 1974



2. Ground Truth For Remote Sensing Lake Classification

In the machine analysis of LANDSAT imagery and subsequent classification of lakes, the computer needs to be trained on at least one lake of each type (i.e., very clear lakes, humic lakes, lakes with algae, and lakes where bottom effects and weeds are present). Various means were tested for the best method of finding such lakes. New ground truth, existing data, aerial photos, and aerial observations were used. It was usually impossible from aerial photography to differentiate a clear lake from a humic lake because of differences in skylight conditions and altitude on various flights. The difference between a clear and humic lake was easily detected, however, by aerial observation from a small fixed wing aircraft.

For such differentiation purposes, the human eye is a better aerial sensor than an aerial camera and a photointerpreter. Also there may be months of delay in obtaining good aerial photos, but an aerial observation can be made instantly any time weather permits. Clear days are, of course, better for all aerial observations of lakes except when observing and photographing oil spills, then a completely overcast day is best (Van Domelen 1974 and Scherz and Van Domelen 1975).*

The aerial observation system for lake classification described here was developed to determine which lakes should be sampled by ground truth teams from the Wisconsin DNR and the UW-Madison simultaneous with LANDSAT overflights. Aerial observations were also useful throughout the development of a satellite classification system. Also, lake classification maps from the Bendix Multispectral Data Analysis System (MDAS) were field checked using aerial observations by experts from the UW-Madison and the Wisconsin DNR.

Basically, the aerial observer flying over a lake should look for five things: clear water (C), brown humic water (H), algal water (A), visible bottom (B), and lake weeds (W). A lake may be basically clear water (C), but have some humic material (H) and some algae (A). Such a lake might be described as C4, H2, A4, which would be the code classification for the water of that particular lake. The 4, 2 and 4 would be the estimated part in 1/10's that each material contributes to that lake. If about 30% of the lake (e.g., the west end) had sand bottom showing, the notation could be B = 30% W end. Also the strength of the light reflected from the bottom could be estimated. A sandy beach would have 100% of the signal coming from the sand, and a sand bottom (BS) deep in the lake and no longer visible would have a zero percent signal. A note such as (BS 2-5, 30%, W end) would mean that sand bottom shows over 30% of the west end of the lake with an estimated strength two-tenths to five-tenths of the possible signal from the sand itself. The total observation code for this lake including the sand bottom would be as follows: C4, H2, A4, (BS 2-5, 30%, W end). Other notations can be: G for green colored rock flour, BM for mud bottom, D for dirt and silt, WS for surface weeds, and WB for bottom weeds, etc. With such a system it was possible to rapidly and roughly classify any lake with an accuracy usually sufficient to locate the best test lakes for MDAS computer training and for water sampling.

3 Lake Classification Using LANDSAT

Although aerial observations proved to be good rough estimates of whether bottom and weeds were showing and whether there was algae present, the exact amount of algae in one lake compared to the algae in another lake could not be determined with any real precision. What is needed for such a comparison is an aerial image

* On an overcast day the total signal from an oil spill is much greater than from water with no oil. This is because of a greater reflection of the skylight from the oil than from the water. On an overcast day the total signal from the water and oil increases as the depth of the oil increases. On a clear day, however, the total signal can decrease with increased oil depth. This is explained by an interplay of energy transmitted through the oil (to and from the water) and the skylight component reflected from the oil surface. The relative change in skylight-to-total light on a clear and overcast day accounts for this phenomena.

from high altitude showing all lakes at the same time. LANDSAT images were analyzed on the interactive Princeton Electronic Products (PEP) Terminal at the UW-Madison to study the spectral signatures of different lakes. Then the Bendix MDAS analysis and mapping system was used to do the actual categorization and to produce color coded printout maps.

In testing the Bendix MDAS classification, it was necessary to first flag those lakes where bottom effects were present. It is not possible to simply take the total signal coming from a lake (bottom signal included) and run a blind classification for trophic status. Work by Boland (1975 and 1976) in Southeastern Wisconsin shows the potential for using LANDSAT for trophic classification. However, the classification system used in this study looked at the entire signal from many lakes in Wisconsin which have most of their signals caused by bottom effects. * Such a classification scheme could not work in another area where there were different types of bottoms present.

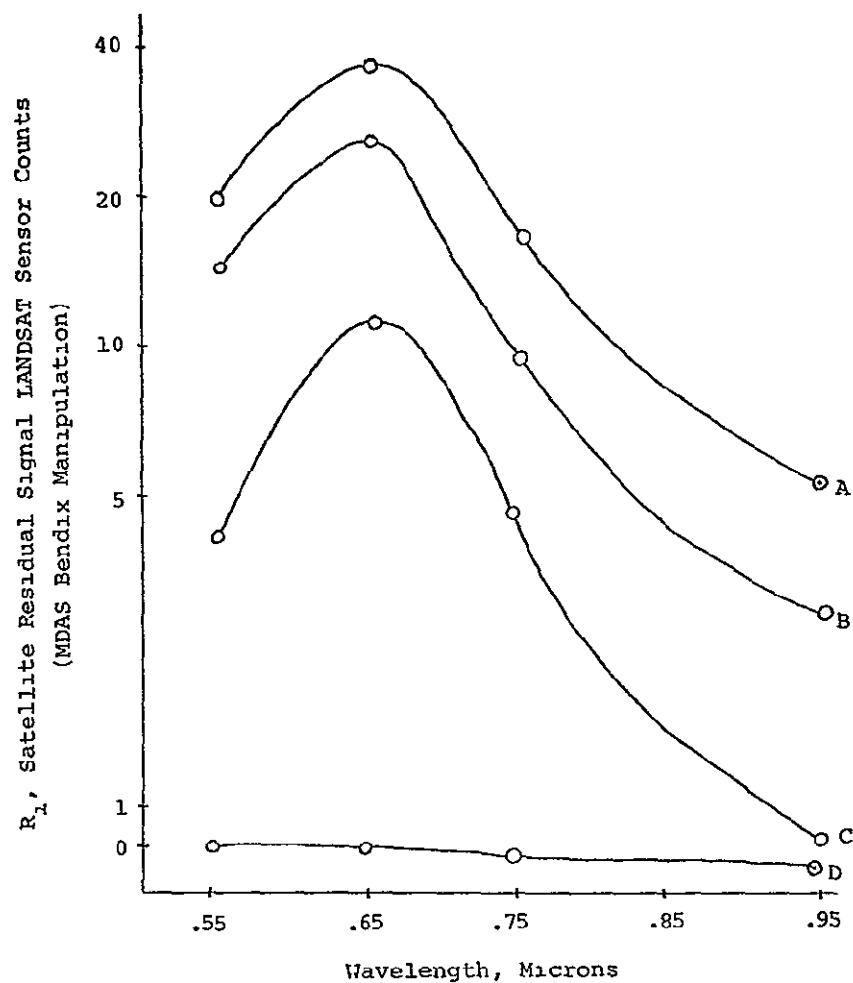
For a universal classification scheme that would include lakes where bottom noise is the predominant signal, such bottom lakes must be removed from further analysis. Then the computer can reliably classify those lakes where bottom noise does not exist. Lakes with bottom effects must be classified by other means, such as ground methods, aerial photography, or aerial observations. Overriding noise simply cannot be mixed with meaningful signals and achieve meaningful results, no matter how sophisticated the mathematical manipulations. The noise must be removed.

The computer can easily identify lakes where bottom problems exist from analysis of residual fingerprints as shown in Figure 42. Lakes where silt was present were also identified by the computer and had residual fingerprints not unlike those shown in Figure 51. Both bottom lakes and silt lakes were given a yellow color on the multicolor final printout. Lakes with dense macrophyte populations were also identified (Figure 43) and were assigned a red color on the color coded printout.

Thus the lakes that were left were (1) clear lakes, (2) humic lakes and (3) lakes with various amounts of algae. The graph by Wetzel (Figure 1) was modified and used to classify such lakes. On the y axis, estimated humic water content was plotted on a scale that varied between zero and 10, and estimated clear water content was plotted on a scale that varies from 10 to zero. Similarly on the x axis, algae was plotted between zero and 10 and clear water between 10 and zero (Figure 52).

* Two such lakes with overriding bottom signals in this study were Lake Como and Lac La Belle. Lake Como was classified from LANDSAT data as trophic class 7 (toward eutrophic). However, our studies estimate that 50% of the signal from this lake is bottom noise in July and 60% in late September. Lac La Belle was classified as trophic class 15 (toward oligotrophic). However, this is a clear lake where sand bottom is visible over the entire lake at all seasons. The estimated proportion of the total signal caused by bottom noise is about 20% in August and approaches 90% in late fall and early spring.

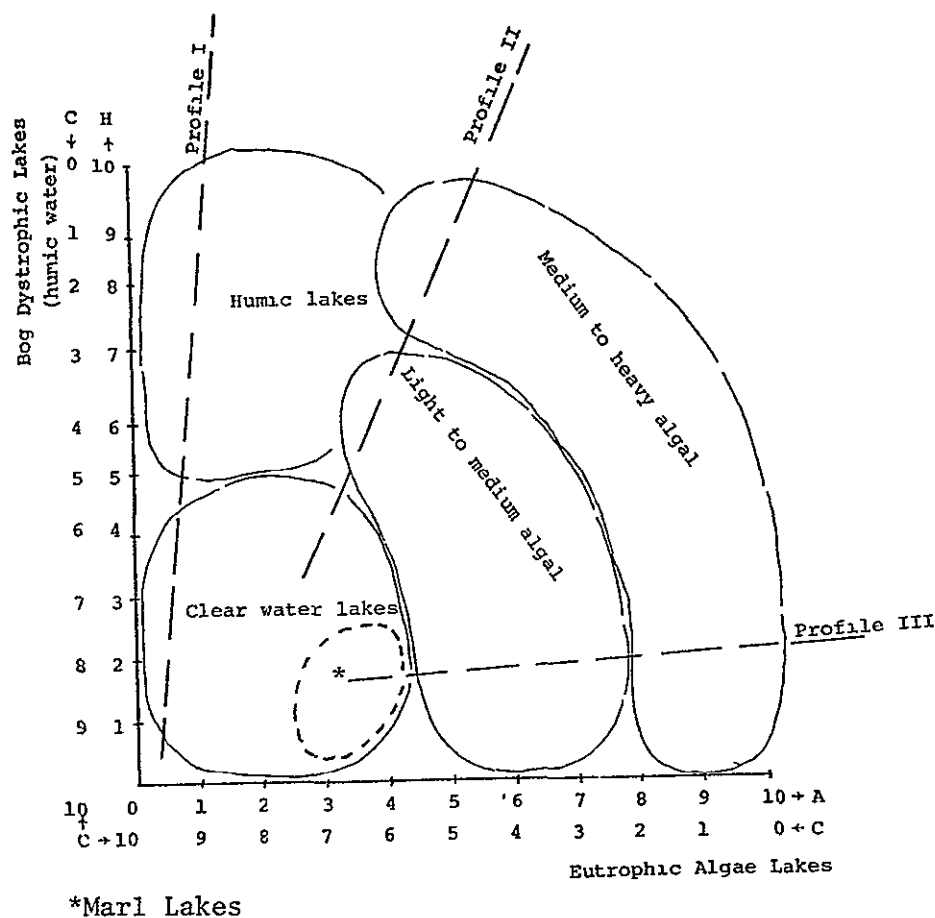
FIGURE 51. Effect of Red Clay on Clear Lake Superior Water (Scherz, Crane, and Rogers 1975).



Site	Approx. Turb. (FTU)	Approx. Solids (mg/l)
A	100	400
B	50	200
C	5	50
D	0.2	0

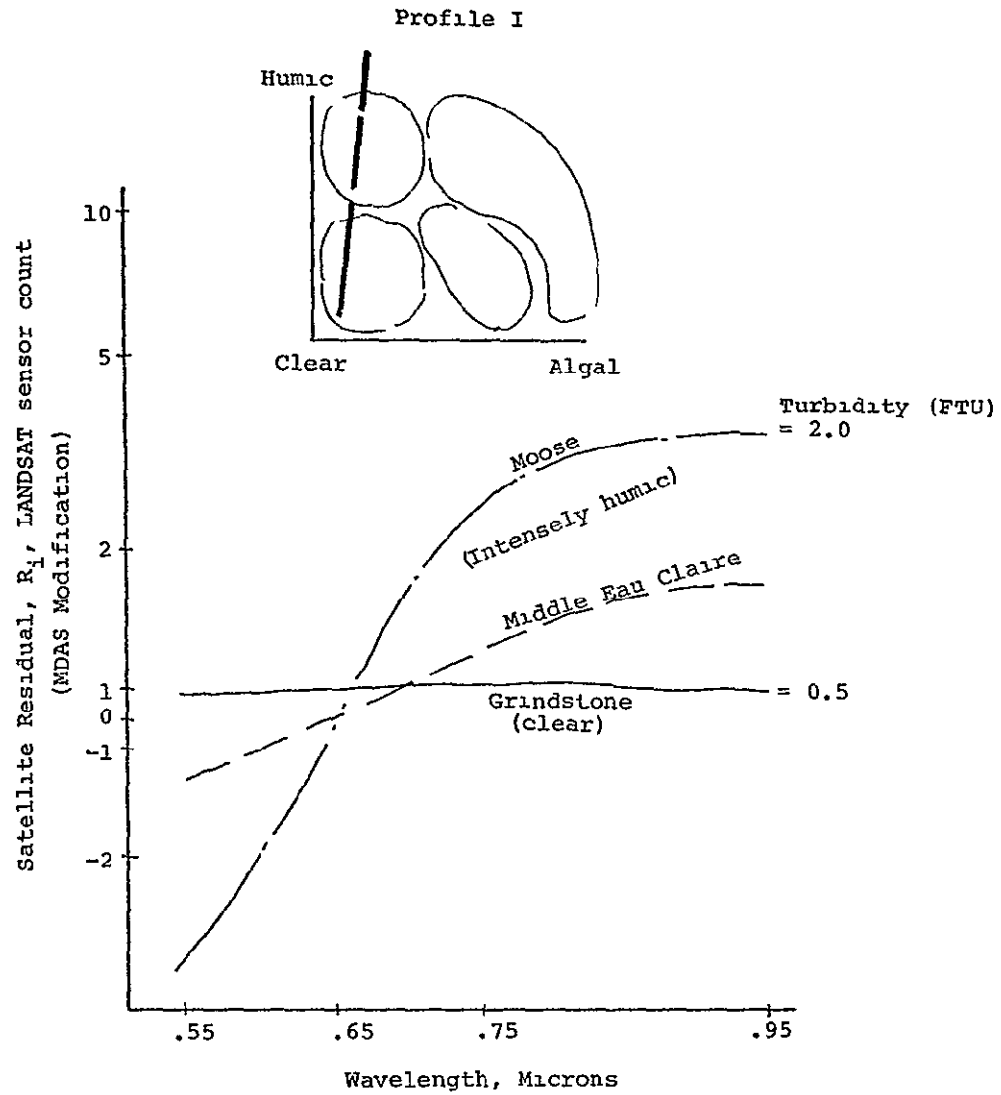
ORIGINAL PAGE IS
OF POOR QUALITY

FIGURE 52. Scheme Used to Classify Lakes From LANDSAT Data Based Upon Wetzel Data in Figure 1 and the Clear Water, Humic, and Algal Lake Types Estimated by Aerial Observations. Satellite Residual Fingerprints of Lakes Along Profiles I, II, and III are Shown in Figure 53, 54, and 55, Respectively



Therefore, on this x-y plot all lakes with various concentrations of algae and humic material in the water can be plotted from their unique spectral signatures or fingerprints. About 40 different categories of such mixed water lakes within this plot can be recognized by the computer but only four major classifications were chosen to be printed out because the human eye can only detect a limited number of different colors on the final MDAS color coded classification map. For the water types the four classifications used were humic lakes (printed as brown), clear waters (dark blue), light-to-moderate algae (blue-green), and moderate-to-heavy algae (dark green). Various profile lines running radially from the zero part of the curve in Figure 52 are therefore lines showing different amounts of algae in waters containing various amounts of humic material. Figures 53, 54, and 55 show various profiles of lakes with different mixtures of clear water, humic water, and algae. Marl lakes also lie along Profile III on Figure 52 and on this project were classified as clear water lakes. A separate category of marl lakes is also possible. See Appendix E.

FIGURE 53 Satellite Residual Fingerprints for Clear, Moderate, and Intensely Humic Lakes (Profile I in Figure 52)



ORIGINAL PAGE IS
OF POOR QUALITY

FIGURE 54. Satellite Residual Fingerprints of Moderately Humic Lakes Containing Various Amounts of Algae (Profile II in Figure 52). Three Lakes Near Ely, Minnesota. TSS = Total Suspended Solids.

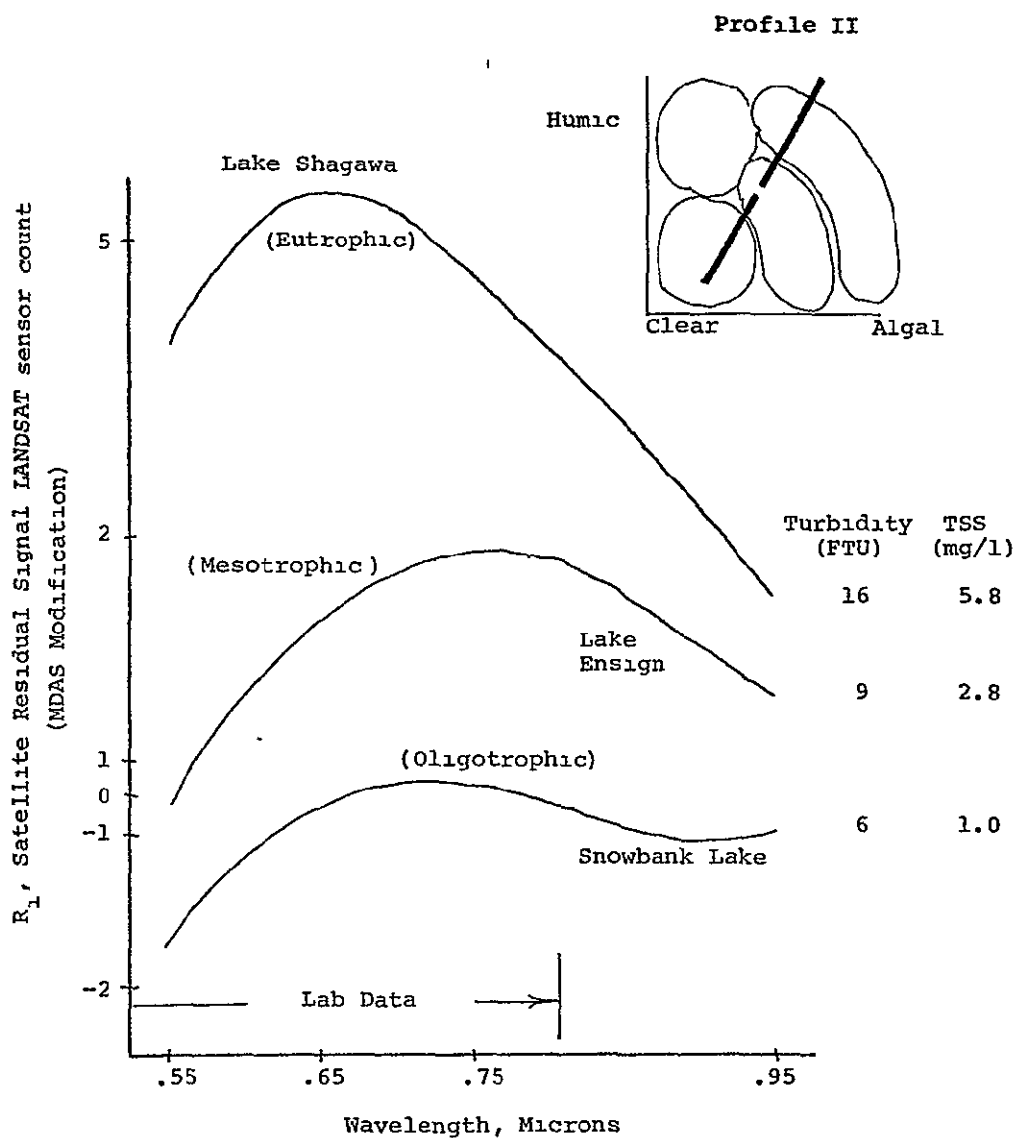
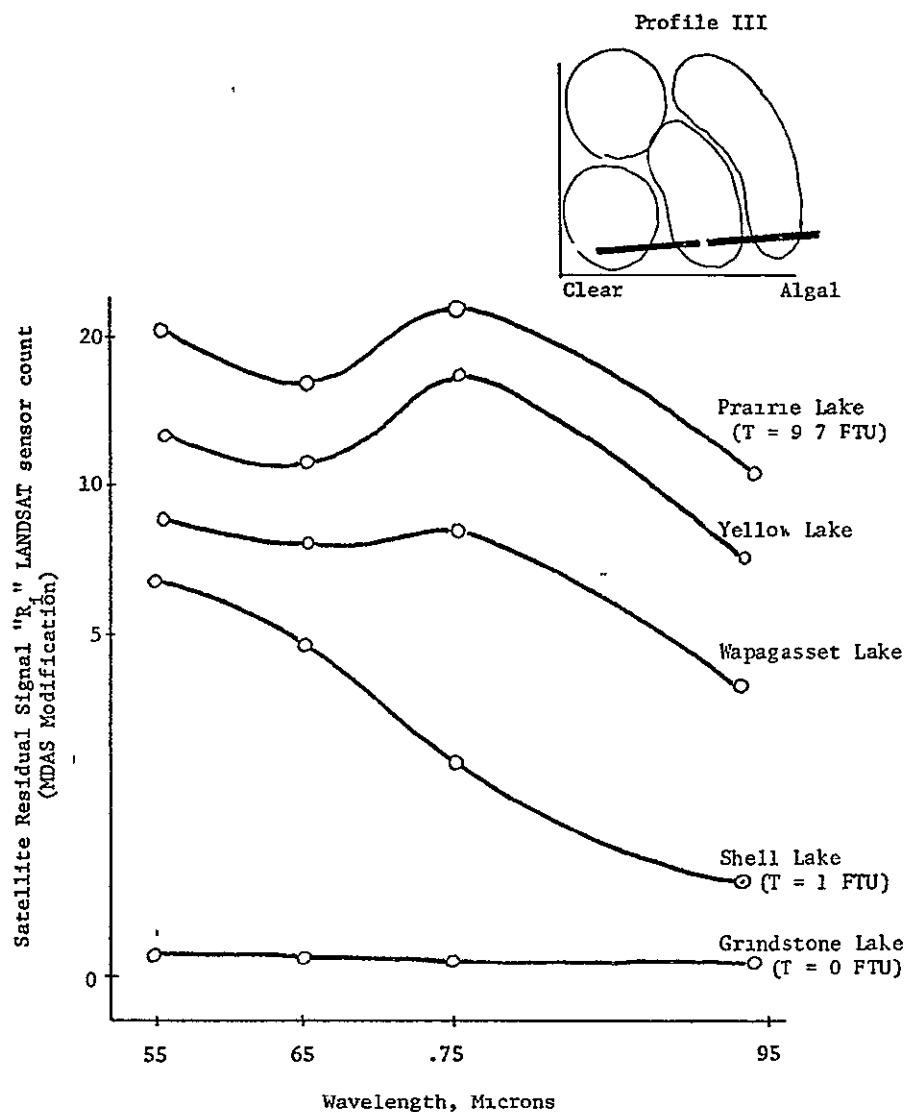


FIGURE 55 Satellite Residual Fingerprints of Nonhumic Type Lakes (Clear Water Type) Containing Various Amounts of Algae (Profile III in Figure 52).
T = Turbidity



About 800 lakes were classified by the MDAS system as having humic water, clear water, light-to-medium algae, medium-to-heavy algae, silt, or lakes where the bottoms were showing. Heavy surface lake weeds could also be identified and were printed as red. Three tones of grey were used for urban areas, clear fields, and forests. Black represented unclassified portions of the scene. Clouds showed as black and their shadows were sometimes red or brown.

It was found that when humic water lakes with mud bottoms (mud bottoms depress the curve for a humic lake) were combined with wild rice (which raises the curve) the sum was a signature which is identical to that of a deep humic lake. Therefore the humic water classification (brown code) also includes some rice lakes, but such rice lakes are usually important and their locations are known because the gathering of wild rice is a licensed activity. It was thought that the mixing of the rice beds with the humic lakes would cause no real trouble on the MDAS printout map. Further work combining spring and fall LANDSAT imagery into an eight-channel tape could probably isolate the wild rice beds.

Three separate field observers checked the output maps and found between 87% and 99% correct classification * This gave an average of 93% correct with a probable error of $\pm 6\%$. The estimated error between the different observers checking any one set of lakes was about $\pm 8\%$. The percent correct classification was concluded to be as good as any available method of checking the results. Figure 56 shows an example of the Bendix MDAS color categorized map for lake classification near Madison, Wisconsin

* An airplane flew over each lake to be field checked in late August. Aerial observers in the plane had the color coded lake classification map in hand (made from previous year's data) and made notes as to whether the MDAS categorization was excellent, good, satisfactory, poor, or unsatisfactory. Excellent, good, and satisfactory were considered a correct classification. There was some obvious change in lake categories from one year when the imagery was acquired to a year later when the map was field checked. However, such change was anticipated to be less than about 5%.

ORIGINAL PAGE IS
OF POOR QUALITY

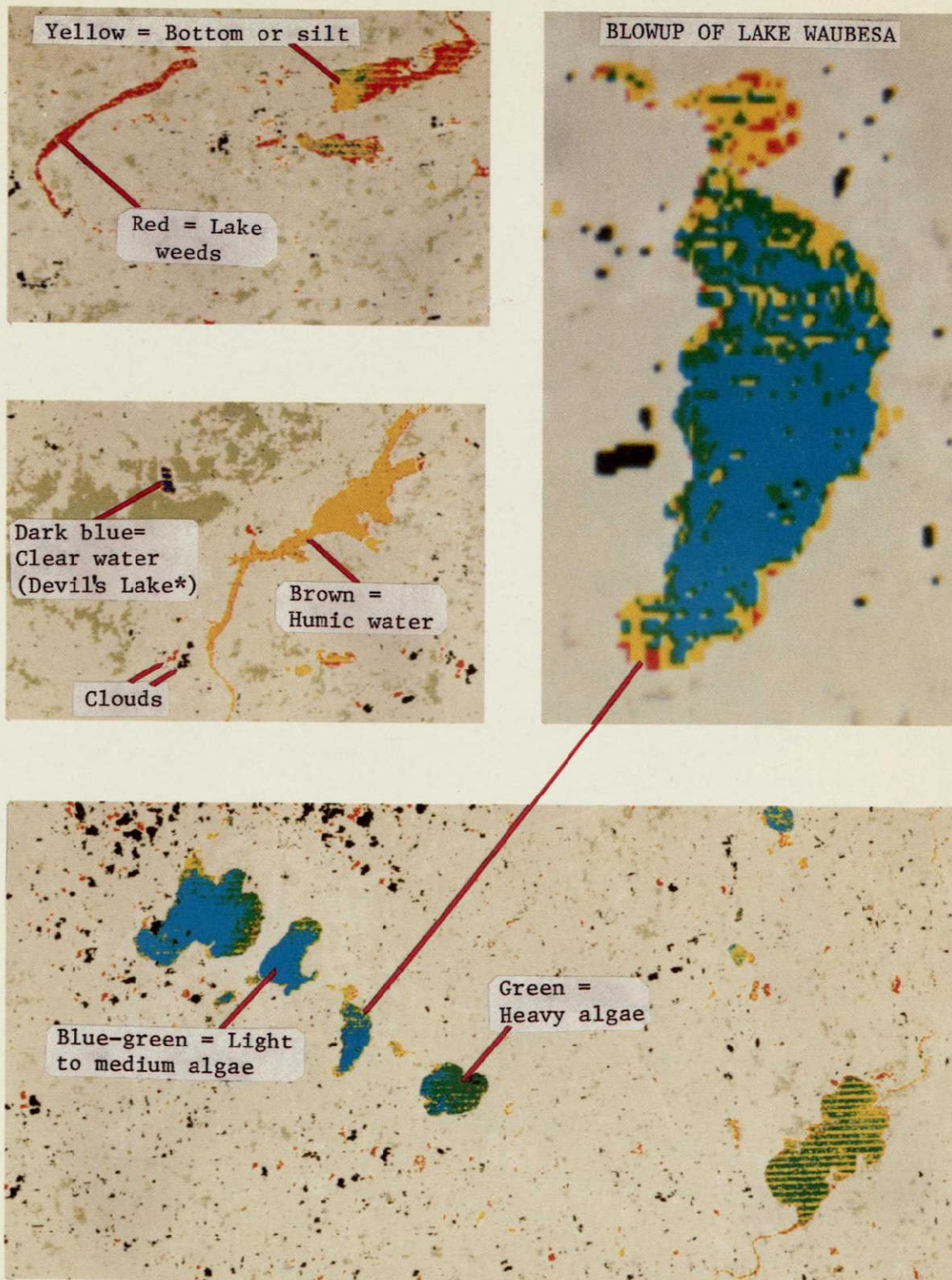


FIGURE 56. Example lake classification color-coded map from multispectral analysis of LANDSAT data by the Bendix MDAS system. Madison area lakes, August 1973.

* Devil's Lake used as deep clear water standard for the analysis of this scene.

D_1, D_1', D_1''	laboratory difference, and differences obtained from boat and airborne-mounted sensors, respectively. Difference between apparent reflectance from water #1 and a very clear, pure water (water #1).
e	2.718
F	factor used in modeling energy upwelling from various layers in water. $F = (1 + b^2 + b^4 + b^6 + \dots)$
G	specular reflection of laboratory lamp from water surface, watts/cm ² s.
G'	specular reflection of sunlight from water surface, watts/cm ² s, (boat level analysis).
H_C'	skylight irradiance on flat surface at ground level, watts/cm ² s, $H_C' = \pi L_C'$
H_L	total irradiance available in laboratory for sample being analyzed, watts/cm ² . The source is a laboratory lamp
H_O'	total irradiance at earth's surface ($H_O' = H_S' + H_C'$) caused by both the sun and skylight, watts/cm ² .
H_S'	irradiance on horizontal surface at the earth's surface caused by sunlight, watts/cm ²
H_{sd}	total irradiance available on the Secchi disc at the Secchi disc depth (watts/cm ²).
I_B	downwelling energy available at the bottom of a water body (watts/cm ² s).
I_{back}	energy backscattered from a unit water sample (watts/cm ² s)
I_{in}	energy striking a unit water sample (watts/cm ² s).
I_o	downwelling energy available just below the water surface (watts/cm ² s)
I_{out}	energy transmitted through a unit water sample (watts/cm ² s).
I_{sd}	downwelling energy that reaches the Secchi disc at the Secchi disc reading (watts/cm ² s)

LA	backscattered signal or radiance caused by the atmosphere between the earth's surface and an airborne sensor, watts/cm ² s
L _c	ceiling illumination in laboratory, watts/cm ² s.
L _c [']	skylight radiance reaching water, watts/cm ² s (boat level analysis).
L _s [']	sun's radiance reaching water, watts/cm ² s (boat level analysis).
L _L	radiance of laboratory illuminating lamp, watts/cm ² s.
P, P ['] , P ^{''}	radiance from reflectance panel to laboratory, boat and airborne sensors, respectively, watts/cm ² s.
R ₁ ^{''}	airborne residuals for lake #1. The residual is obtained by subtracting the signal from a very clear lake (W ₁ ^{''}) from the signal of the lake in question, e g , from lake #i. $R_1'' = W_1'' - W_1' = (\rho_{v_1} - \rho_{v_1}') H_o' \frac{\tau}{\pi}$
R ₁ , R ₁ ['] , R ₁ ^{''}	residuals obtained from laboratory, boat level, and airborne sensors, respectively Lake water #1
S _c [']	radiance caused by specular reflection of skylight from water surface, watts/cm ² s, (boat level analysis)
S _L	radiance from diffuse reflectance of impurities on the water surface, laboratory signal, watts/cm ² s.
S _s ['] , S _s ^{''}	radiance caused by diffuse reflection from impurities on the water surface (foam, dirt, leaves, etc), watts/cm ² s (boat level analysis and airborne analysis, respectively).
SD	Secchi disc reading In the depth analysis modeling it is assumed that 10% of the energy penetrates to the Secchi disc reading depth
t	transmittance through a unit water sample, $t = I_{out}/I_{in}$, watts/cm ² s.
V, V ['] , V ^{''}	radiance caused by diffuse reflection from material in water volume to laboratory, boat mounted and airborne sensors, respectively, watts/cm ² s

ORIGINAL PAGE IS
OF POOR QUALITY

$\Delta V'$	upwelling energy above the water surface which originates from a particular layer in the water (watts/cm ² s).
$\Delta V'_1, \Delta V'_2, \Delta V'_i$	upwelling energy above water surface that originates from layer 1, 2, and i in the water, respectively (watts/cm ² s).
W, W', W''	total radiance from water to: laboratory, boat and airborne sensors, respectively, watts/cm ² s.
watts/cm ²	watts per square centimeter, a measure of irradiance or total radiant energy available on a surface.
watts/cm ² s	watts per square centimeter per steradian, a measure of the nonpoint radiant energy impinging on a point per unit of solid angle measured from that point. Used with radiance.
Y	vertical distance between water surface and bottom.
α	extinction coefficient for energy passing through water.
ϕ	specular reflection of a water surface, considered to be 0.020 for angles near the vertical.
ρ_{PL}, ρ_p	diffuse reflectance of laboratory and field panels, respectively.
ρ_{SL}, ρ_s	diffuse reflectance of foam, dust, and other impurities on water surface in laboratory and field, respectively.
ρ_{sd}	diffuse reflectance of Secchi disc.
ρ_v	volume reflectance of a water column; diffuse reflectance
$\rho_{v_1}, \rho_{v_{\#1}}$	volume reflectance of material in water (sample 1 and distilled water, respectively).
ψ	solid angle of the sun as viewed on the earth's surface, steradians
ψ_L	solid angle of laboratory lamp as seen by the object being analyzed, steradians.
τ	atmospheric transmittance between ground level and airborne sensor or satellite.

Subscripts 1 and #1 denote waters 1 and #1 (distilled), respectively

Superscripts ' and '' denote data from boat and airborne sensors, respectively

Lack of superscript denotes laboratory data

VI. THE ANALYSIS OF REMOTE SENSING DATA

A GENERAL

The desirable remote sensing signal in all cases is backscattered energy from the target. However, the absolute value of this backscattered signal is of less importance than its value relative to total energy available. The absolute amount of energy backscattered from a particular object will be greater on a bright day than on a dark day when there is less energy available. It is the ratio of energy backscattered/energy available (percentage) that is unique for a particular material. This percent reflectance at different wavelengths accounts for the unique reflectance fingerprints of different materials.

In order to handle this relative reflectance problem (energy returned/energy available), a reflectance panel is often used as a standard in laboratory, boat level, and airplane data analysis. In the absence of a standard reflectance panel, another known reflection standard can be used such as a clear water lake. With this in mind, let us see how remote sensing data can be analyzed to obtain the absolute values of energy that reach the sensor.

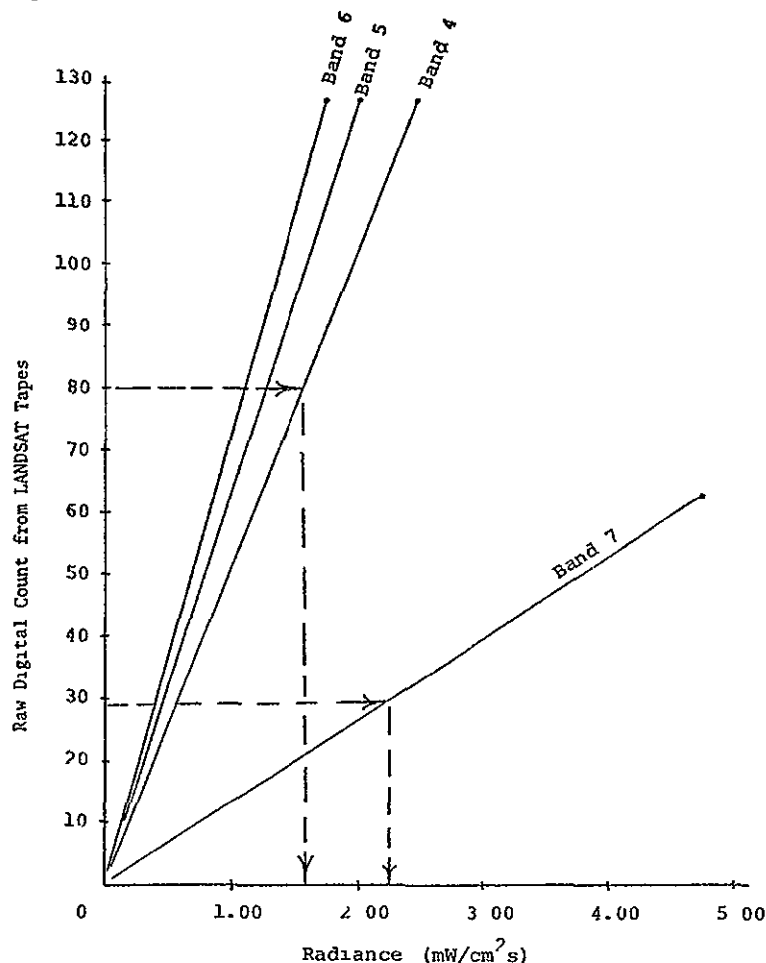
B. MULTISPECTRAL SCANNER DATA

A multispectral scanner senses a portion of the earth's surface in several different wavelengths. The energies that return from this spot are converted into electrical impulses which are read out from the scanner. For calibrated thermal scanners, a very cold and a very hot surface are sensed in each revolution of the scanner. For scanners operating in the photographic portion of the spectrum a very dark and a very bright surface are similarly used in calibrating each scan of the instrument. If the response of sensor readout is linear with the energy received then interpolation between the signals from the cold and the hot standard will determine the unknown energy from a spot in-between. Therefore, it is not a difficult matter to obtain a correlation curve between the count on a multispectral scanner detector and the radiance it receives (Figure 57). Once the raw count is known from the computer tape (which is obtained from the multispectral scanner), it is then possible to enter the curves and obtain the intensities of the energy striking the scanner from that portion of the earth.

Raw computer data may first be manipulated to improve statistical analysis and classification. For example, the scale can be multiplied by some factor to allow statistical use of whole numbers rather than fractions. With the Bendix MDAS computer analysis system the raw data from Bands 4, 5, and 6 are first multiplied by four, and the data from Band 7 are multiplied by two before classification analysis begins. Therefore, the calibration curves for the MDAS system are like the curves in Figure 57 except the y axis is increased by some factor.

ORIGINAL PAGE IS
OF POOR QUALITY

FIGURE 57. Obtain Radiance Values From Satellite Tape Count Using Calibration Curves For The LANDSAT Satellite Multispectral Scanners.



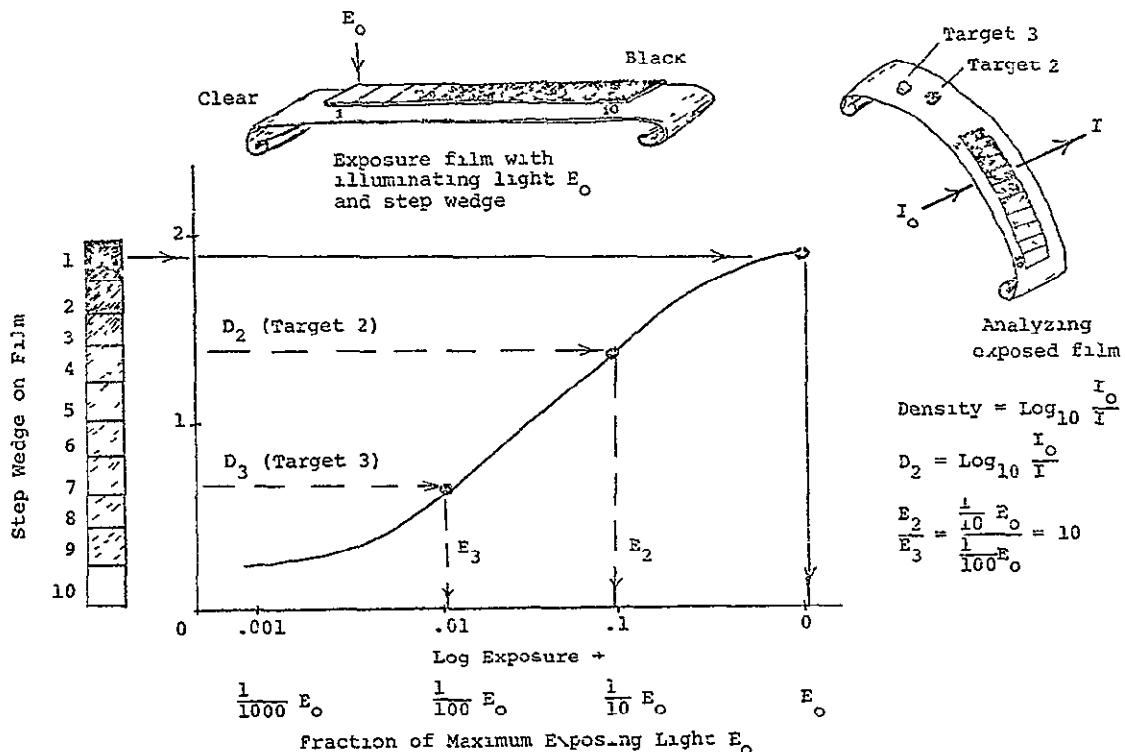
C PHOTOGRAPHIC ANALYSIS

When a signal passes through a lens and is captured on camera film, there are several more factors that must be considered than with the multispectral scanner data. First the lens and its properties must be considered. There is less energy available at the edge of a photograph than in the center. And with cameras with a focal plane shutter, the amount of energy across the frame may be a function of the movement of the shutter. The way to calibrate this sort of lens and shutter falloff is to photograph a uniformly illuminated source (such as a piece of opal glass lit from behind), and then analyze the brightness of the film that results. Calibrations like this can be made for cameras (Scherz 1972 and Van Domelen 1974) and should always be considered when doing microdensitometer work on a film. However, if a standard reflectance panel is immediately adjacent to where a reflectance sample is being analyzed the falloff patterns may not be so important (Klooster and Scherz 1974).

1. The D-Log E Curve

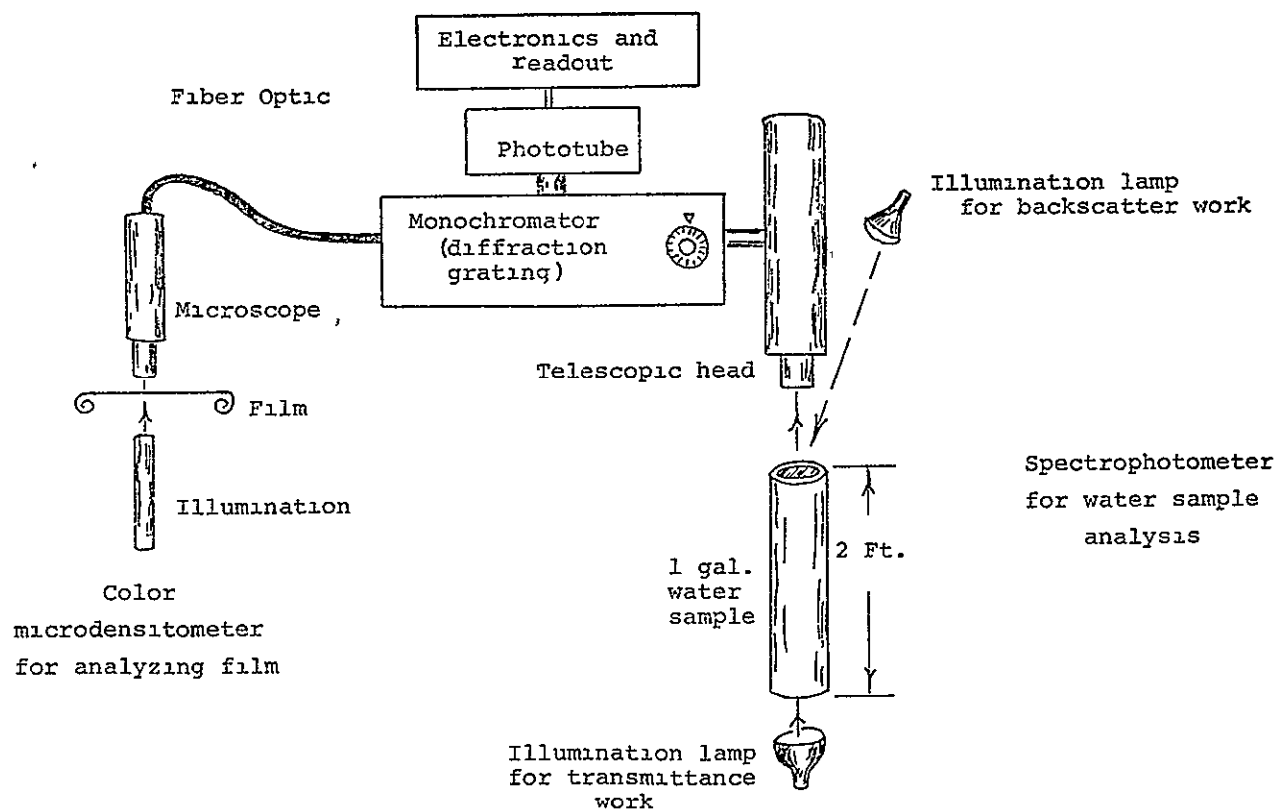
Another important factor in photography is the density-log exposure curve (D-Log E) of the film (Klooster and Scherz 1974). After light hits the film and the film is developed, part of the negative turns to black silver and becomes dense to light passage. The more light, the darker becomes the developed film. However, the film's darkness (or density) is also a function of the time in the developer, the temperature of the developer, and the age of the film. Therefore, to determine the relationship between density (which can be measured) and the amount of energy exposing the original film, a D-Log E curve must be made for that particular film. Such D-Log E curves are made by exposing different known amounts of energy onto the film and measuring the densities that are created (Eastman Kodak Company 1967, Smith 1968, and Baines 1970). This exposure variation can be accomplished by varying exposure time or light intensity. The most convenient way is to photograph a step wedge or to lay a step wedge across the film and expose it. A step wedge is a piece of transparent material that has different amounts of black silver deposited on each step. For example if step 1 is clear and the light that passes through it is E_0 , then light that passes through each of the other steps is some known percentage of E_0 (Figure 58). The variation of the amount of light passing through the step wedge and exposing the film is what creates the x axis of the D-Log E curve.

FIGURE 58. D-Log E Curve For A Black And White Negative Film. Obtain Relative Values Of Exposing Energy By Analyzing A Black And White Film That Also Has A Step Wedge Exposed Somewhere On The Film



The percentage of E_0 that passes through each of the steps is either given by the manufacturer or can be determined in the laboratory with a microdensitometer. Using a microdensitometer for analyzing transmittance of film is similar to analyzing transmittance of light passing through a water sample except that the film or step wedge replaces the water sample. The equipment for film analysis is smaller than what is used for water sample analysis (Figure 59). A microdensitometer that can be adjusted to analyze a particular color or wavelength of light is a spectral (or color) microdensitometer. On a spectral microdensitometer, light falls into a microscope and passes through a prism or diffraction grating on to a detector head which produces a readout signal. The prism or grating is rotated so that a particular color falls on the detector head (Figure 59). When analyzing black and white film there is no color data and the spectral microdensitometer can be set at any color, or wavelength.

FIGURE 59 Schematic Of Equipment Used To Analyze Film And Water Samples.



The developed film will show a negative image of the step wedge. This image is called a film wedge. The step 1 which was clear on the step wedge is darkest on the negative film wedge because the exposing light E_0 passing through this part of the step wedge was essentially unchanged in intensity (Figure 58). The density of each step on the film wedge can be analyzed by the microdensitometer. Let I_0 be the energy from the illuminating light for the microdensitometer

analysis. If the film is put in-between the illuminating light and the microdensitometer sensor, let the energy that passes through the film be called I . The transmittance (T) of the film is $\frac{I}{I_0}$. Density is defined as $\log_{10} \frac{1}{T}$ which is also

$\log_{10} \frac{I_0}{I}$. Therefore, if a film wedge has six different steps recorded on it, then the density of these particular steps can be analyzed and the density or y axis of the D-Log E curve obtained. This density for each step is plotted against the energy that originally passed through each step of the wedge and exposed the film.

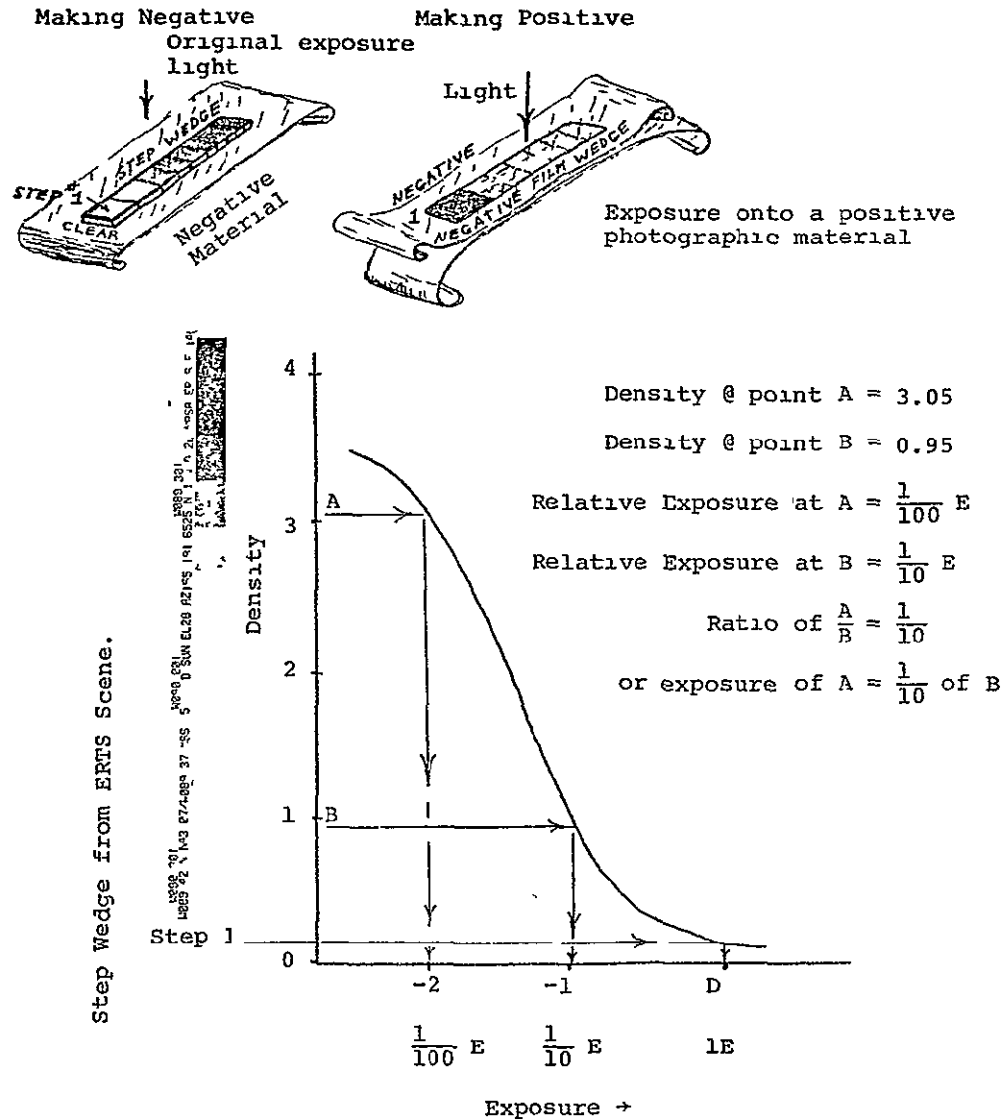
2 Obtaining Relative Exposure Of Objects Photographed By Using The D-Log E Curve

By such a process it is possible to shine the beam of the microdensitometer light through particular targets (such as targets 2 and 3 in Figure 58) and obtain the densities on that particular scene and then come back to the D-Log E curve and find the relative values of the exposing radiance. Notice that only relative intensity is obtained; no absolute intensity is possible. For absolute intensity there must be something in the photographed scene with an absolute intensity such as a calibrated light source. Obtaining absolute intensity is very difficult with a camera.

D. BLACK AND WHITE REVERSAL FILM - LANDSAT SCENE ANALYSIS

A calibrated sensor system is available for the LANDSAT multispectral scanner. LANDSAT tapes can be converted into black and white images and both negative and positive prints can be acquired. A film wedge is still shown on each scene of such LANDSAT imagery. On a positive transparency the film wedge has undergone a reversal and becomes a positive film wedge rather than a negative film wedge. The D-Log E curve therefore makes a mirror image of itself as is shown in Figure 60. From the densities obtained by analyzing LANDSAT images and the D-Log E curve, and the absolute calibration data published by NASA, it is possible to find the absolute radiance entering the scanner for each part of the scene.

FIGURE 60 D-Log E Curve For A Black And White Positive Film. The Photographic Reversal Step Wedge Printed On A LANDSAT Positive Transparency Is Used To Obtain The Relative Values Of Energy Exposing Different Parts Of The Scene.



E. COLOR FILM ANALYSIS

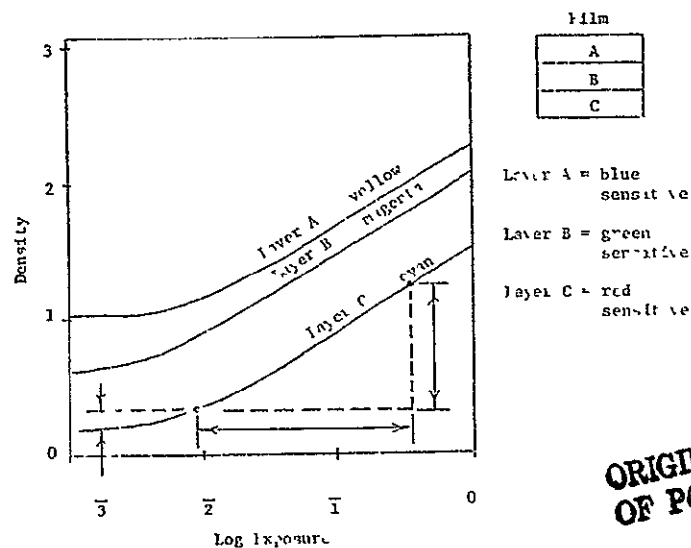
1. Color Negative Film

With normal color film processed to a color negative, the blue-sensitive layer turns to a yellow dye, the green-sensitive layer turns to a magenta dye, and the red-sensitive layer turns to a cyan dye. Therefore if a color film were used to photograph a grey scale step wedge each step would expose a certain amount of silver in each of the blue, green, and red-sensitive layers on the film in accordance with the amount of energy received by the three layers. (Colors of white and grey are made up of equal amounts of blue, green, and red light)

Assume a grey step wedge were exposed on a color film which was processed to a color negative. Then place a yellow filter over this color negative and analyze the strength of light passed through the film wedge (and the yellow filter), a yellow density could be obtained for each step of the film. The densities for each step could be plotted up on a y axis and a D-Log E curve could be constructed similar to a D-Log E curve for a black and white negative film. The resulting D-Log E curve for the blue-sensitive layer would look similar to the curve for the negative black and white step wedge shown in Figure 58.

By placing a magenta filter over the color negative film being analyzed, a similar D-Log E curve could be constructed for the second or green sensitive layer of the film. Likewise a cyan filter over the color negative would make it possible to obtain the D-Log E curve for the red sensitive layer of the film. For a color film all three of these D-Log E curves would be plotted up on the same piece of paper. Such a graph is then often used to determine the relative sensitivities of each layer (necessary for matching particular film types to particular types of light sources) (Figure 61).

FIGURE 61. D-Log E Curve For Three Layers Of Normal Color Film Processed To A Color Negative. The Layers A, B, And C Turn To Colors Yellow, Magenta, And Cyan, Respectively. Measurements Shown Can Be Used For ASA Speed Determinations And Color Balance (Modified From Manual Of Color Aerial Photography, American Society Of Photogrammetry, 1968).

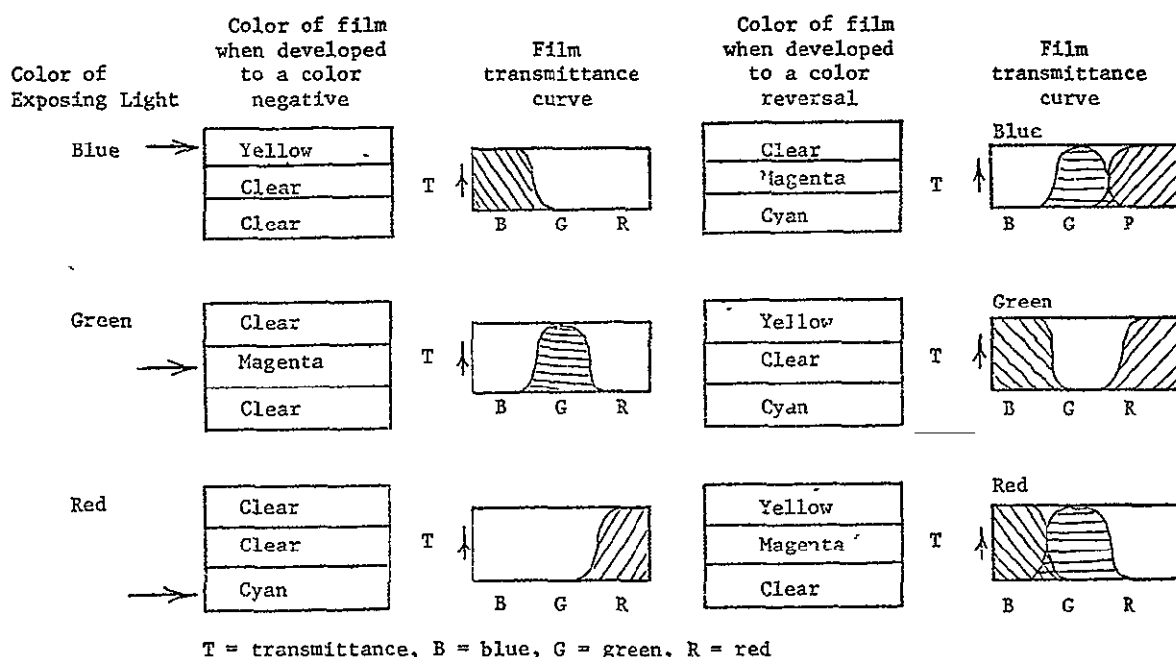


ORIGINAL PAGE IS
OF POOR QUALITY

2. Color Reversal Film

When color film is processed in a color reversal development then the dyes are formed in those layers where no light struck. The silver and dyes in the layers where light struck are washed away. In other words if light struck the blue-forming layer, dyes would be formed in the other two layers (magenta and cyan dyes). The combination of magenta and cyan dyes creates the color blue (Figure 62). Similar processes occur for the green sensitive and red sensitive layers.

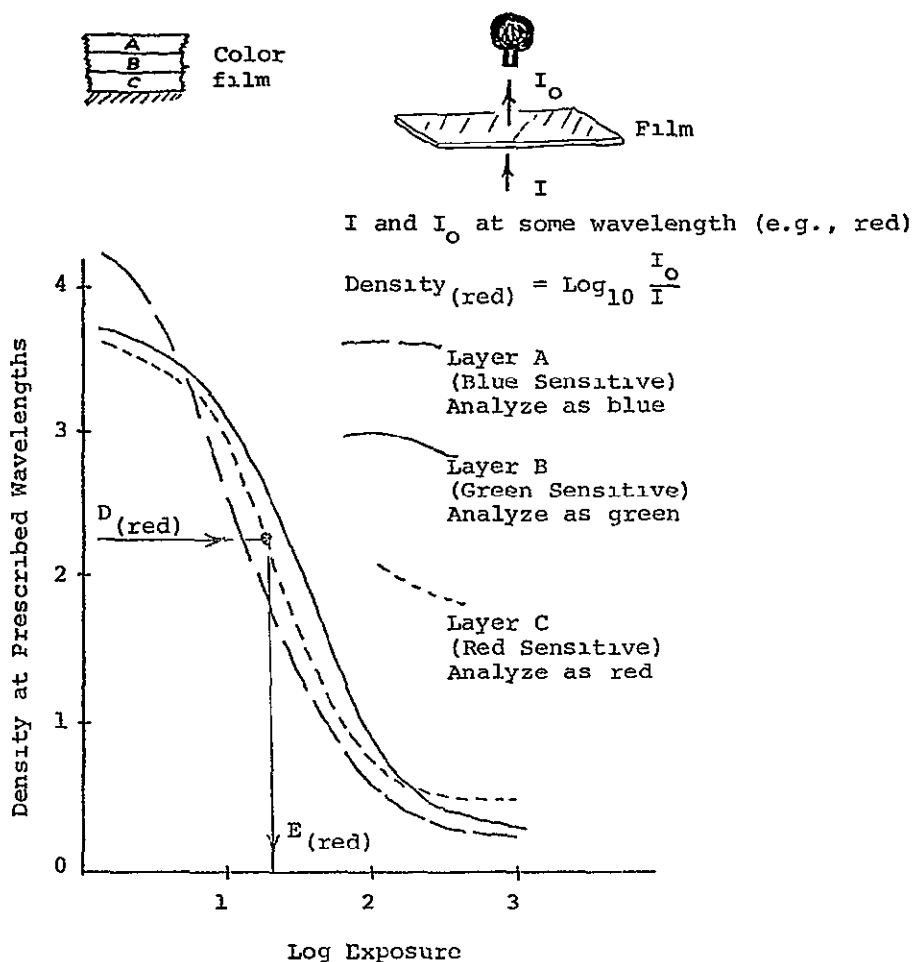
FIGURE 62. Sketch Of Dye Development And Transmittance For Normal Color Film For Color Infrared Film, Essentially The Same Process Takes Place Except Colors For The Exposing Light Change To Green, Red, And Infrared



Therefore where blue light exposed the normal color reversal film, the film when processed by a color reversal technique would allow the color blue to pass. The stronger the exposing blue light the more blue light would be transmitted through the processed film. A spectral microdensitometer can be tuned to the color blue to obtain the energies passed through different steps of a step wedge photographed by or contact printed on the color film. The resulting D-Log E curve would be for the blue-sensitive layer of the film. This only works for color reversal film, however. For color negative films, filters of magenta, cyan, and yellow must be used when analyzing the different layers on the film because a spectral microdensitometer cannot be tuned to a color like magenta (made up of blue and red light).

Because there is a tone and color reversal in the color reversal development process the resulting curves correspond in shape to film positive rather than film negative step wedges (Figure 63).

FIGURE 63. D-Log E Curves For A Normal Color Reversal Transparency (Slide Film). If The Film Were A Color Infrared Film, Layer "A" Would Be Sensitive To Green, But Would Shift To Green And Layers "B" And "C" Would Be Sensitive To Red And Infrared, Respectively The Color Microdensitometer Analysis, However, Would Be The Same As With Normal Color Film.



ORIGINAL PAGE IS
OF POOR QUALITY

If the D-Log E curves for the three layers of a normal color film lie essentially on top of each other, the film is a well-balanced color film. However, if one of the layers has a higher position on the D-Log E plot then this is a poor balance for this film to that particular light source. Such cases occur when color film designed for daylight use outdoors is used indoors under a sodium light which is deficient in blue light. Film designed to be used indoors under sodium light has a blue-sensitive layer which is much more sensitive than the other layers.

Appendix D explains the construction of a D-Log E curve for color reversal film.

3. Color Infrared Film

If the color reversal film were color infrared film rather than normal color film the processes described above and depicted in Figures 62 and 63 would be identical except that the colors of the exposing light would be changed from blue, green, and red to green, red, and infrared, respectively. The formation of the yellow, magenta, and cyan dyes and their addition into colors blue, green, and red would be identical as with the normal color film. The analysis of the step wedge with the microdensitometer tuned to blue, green, and red, would yield D-Log E curves for the green, red and infrared sensitive layers, respectively.

F. COMPUTER ANALYSIS EQUIPMENT

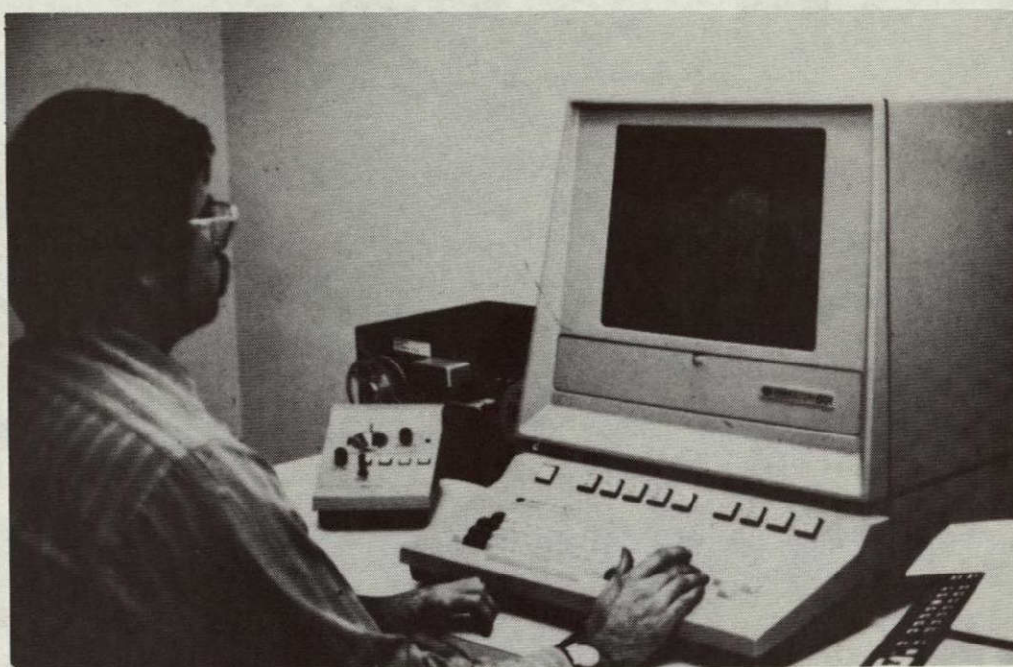
For LANDSAT data, a particular part of the earth is imaged by all four bands of the multispectral scanner. The smallest unit resolved on the ground (a pixel -- "picture element") is about 78 meters on a side. A pixel on the tape is recorded in all four bands. Therefore, the intensity of all four bands can be analyzed.

The data from the LANDSAT multispectral scanner are obtained either as photographic images* or as computer tapes. The computer tapes provide the most accurate data and the format most useful for analysis and classification of ground objects. For such analysis there must be some device that allows the operator to interact with the computer. Figures 64 and 65 show two such computer devices for this analysis, a PEP terminal and the Bendix MDAS terminal, respectively. The PEP terminal is a black and white display screen and a keyboard which allows the operator to interact with a conventional digital computer, view portions of the LANDSAT scene, and extract digital data at different locations in the scene from the different bands of the satellite scanner. Output from the PEP terminal is obtained by the computer digital printer or by copying data displayed on the black and white TV monitor screen.

The Bendix MDAS terminal and other special computer systems are designed just for multispectral tape analysis. Sophisticated computer software enables the enhancing and manipulating of the data by statistical techniques prior to classification of objects in a scene. The display is color coded -- a different color being assigned to each type of material classified. This color coded display can also be printed out on a color categorized map on photographic paper.

* LANDSAT photographic images are produced in essence by displaying LANDSAT tape data onto a TV screen and photographing the screen. These photographic images have film wedges on them to allow control over the photographic copy process.

FIGURE 64. PEP Terminal For Analyzing LANDSAT Tapes. This Terminal, Produced By Princeton Electronic Products, Inc. And Available At Most Computer Facilities, Makes It Possible For The Operator To Interact With The Computer Which Has The LANDSAT Tape On Its Tape Reader.



ORIGINAL PAGE IS
OF POOR QUALITY

FIGURE 65. Bendix MDAS Terminal For Multispectral Analysis Of LANDSAT Tapes. Such Special Computers Have Many Features Of The PEP Terminal But Have A Color TV Monitor And Are Specifically Designed To Analyze Multispectral Data By Sophisticated Statistical Techniques, Classify Different Features On The Earth, And Print Out Color Coded Classification Maps.



The MDAS system, like the PEP terminal, can also print out digital data. For statistical manipulation the MDAS signal is first multiplied by a factor of 4 or 2 depending on the band so the printout by the PEP or MDAS system will vary by a scale factor. Figure 66 shows the MDAS raw data so manipulated from the four bands of the LANDSAT scanner for three types of lakes -- a clear water lake, a humic lake, and an algal lake.

Note that in Figure 66, clear water which yields essentially a flat reflectance curve in the laboratory has much more green energy than infrared energy recorded on the LANDSAT data. This is because of the haze that causes a much greater scatter of the shorter wavelength light. Therefore there are more atmospheric effects and skylight reflection effects in the green than in the red and IR bands. The signals in the green and red bands are exceedingly high. This raw data is very difficult to relate to laboratory reflectance data.

G. OPERATIONAL LAKE ASSESSMENT PROGRAMS USING LANDSAT DATA

The Wisconsin Department of Natural Resources (DNR) was required to classify all the named lakes in the state as to their trophic level in response to federal legislation ("Federal Water Pollution Control Act Amendments of 1972," Section 314). In the spring of 1974, a cooperative project involving the Institute for Environmental Studies (UW-Madison) and the DNR was initiated to investigate the feasibility of using satellite imagery to satisfy the federal mandate to monitor lake water quality

Initially the project investigated using 9" by 9" and 70 mm positive transparencies from the LANDSAT satellite (Scarpace, Fisher, and Wade 1974). Difficulties with the radiometric fidelity of the 9" by 9" transparencies, and operational problems due to the extremely small image sizes of small lakes on the 70 mm images prompted the development of computer-assisted analysis of the imagery. A large interactive computer program was developed to provide highly versatile data extraction and analysis capabilities for LANDSAT or other multispectral data.

The computer program was designed for an interactive graphics terminal and the Madison Academic Computing Center's UNIVAC 1110 computer (Fisher and Scarpace 1975). The terminal chosen was the Princeton Electronic Products, PEP-801 because the Computing Center supported the development of the necessary software and the DNR owned such a terminal. Display information on the terminal (graphics and alphanumeric characters) is stored as an electronic pattern on a storage tube that is scanned to produce a high quality black and white television picture. Information can be retained with no computer action (or cost) for several hours.

Alphanumeric data can be entered into the computer via a standard keyboard. Position on the screen can be entered via a cursor control unit. A joystick on the control unit allows an operator to maneuver a small electronically generated cursor around the screen. Pressing a button on the control unit transmits the x and y coordinates of the cursor to the computer. This latter feature is used extensively to indicate the data pixel points to be extracted from the LANDSAT imagery for analysis.

Because of the limited data transfer rate between the 1110 computer and the PEP terminal, only 90 rows of 90 picture elements can be displayed at any one time.* Variable resolution allows the area on the screen to correspond to ground areas from 5.2 by 7.1 km to 46.3 by 64.1 km. This variability in resolution was sufficient to locate all the desired lakes in the state.

It was decided that to satisfy the federal law, a water quality assessment of all lakes greater than 10 acres was needed. There are approximately 4000 lakes that fit into this category in Wisconsin. It was also decided, for this first cut assessment, that the lakes would be ranked within each county in order of decreasing turbidity. No differentiation would be made at this time between water quality problems caused by algae, macrophytes, sediments, humic material, nor lakes where bottom signals were present. These problems were to be rectified in a later version of the classification program due to be released soon in a UW-Madison Water Resources Center Report, Use of Satellite Imagery for Lake Classification in Wisconsin.

* A full LANDSAT scene has approximately 3200 rows and 2400 picture elements/row.

Computer compatible tapes from 23 scenes were purchased from the EROS Data Center (Sioux Falls, South Dakota). These scenes were from the summers of 1973 and 1974. Each lake was imaged cloud free at least once on the 23 scenes. The data to be derived from the LANDSAT imagery for this project were the Band 5 brightness values in selected portions of each of the lakes in the state.

The desired locations of the data to be extracted were found by displaying a character representation of the Band 5 digital values on the screen of the PEP terminal. This was accomplished by the computer examining the Band 7 digital values and only displaying the Band 5 values when the Band 7 values were extremely low (less than 10 counts). This technique, known as bi-band masking, clearly outlined each of the lakes. The operators had numerous topographic quadrangles to check the shape and location of the lakes for positive identification.

Data are extracted by entering a lake name and then pointing the cursor at each desired point or at alternate corners of blocks of points. A one-digit area number is written at each selected point or block of points on the screen and adjacent to the extracted data. Data extraction continues as long as desired within the lake. It ends for a given lake with the entry of another lake name. At this time the Band 5 data is printed, punched, and filed by the computer for further analysis.

The data extracted by the program were sorted by county. Within each county, the lakes were ranked in order of decreasing average Band 5 brightness value. A computer-generated table for each of the 72 counties was produced in the spring of 1975 (e.g., Table 1). At the same time, a pictorial representation of the data points used for the classification was also made. This is a computer line printer rendition of the PEP terminal screen at the time of data extraction (e.g., Figure 67).

The Bendix MDAS system was also used to produce color-coded lake classification maps of two areas in Wisconsin. Figure 66 shows raw spectral signatures obtained by the Bendix MDAS system. Such spectral data were used in arriving at the automatic lake classification scheme further described in Chapter VII.

TABLE 1 Typical Output For One County Relating To Lake Turbidity Derived From Bands 5 And 7 Of LANDSAT Analysis. Lakes Are Ranked In Order Of Decreasing Turbidity. Some Lakes May Have Noise From Bottom Effects.

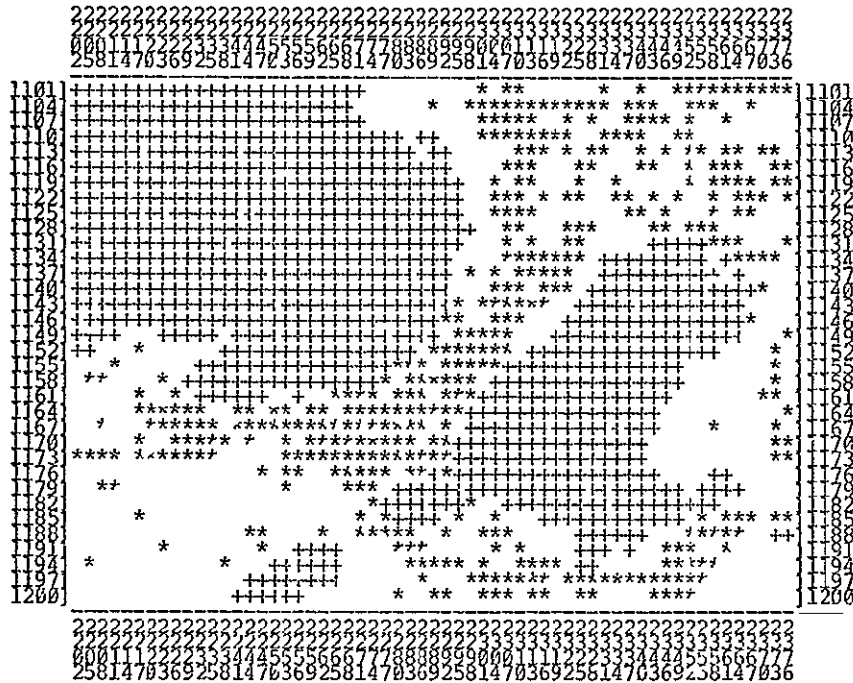
DNR District No. 1

Name. Southern Columbia County

<u>Rank</u>	<u>Lake Name</u>	<u>Number of Points</u>	<u>Band 5 Average</u>	<u>Band 5 Range</u>	<u>Scene Identification</u>
1	Swan	4	16.50	16-18	1378-16151003
2	Long	2	15.50	14-17	1378-16151003
3	Lazy	3	14.67	14-15	1378-16151004
4	Park	4	14.50	14-15	1378-16151003
5	Spring	3	14.00	14-14	1378-16151003
6	Lake Wisconsin	9	14 00	13-15	1378-16151003
7	Becker	2	13 50	13-14	1378-16151003
8	Silver	2	13.50	13-14	1378-16151003
9	George	2	13 50	13-14	1378-16151003
10	Wyona	2	13.50	13-14	1378-16151003
11	Crystal	1	13 00	13-13	1378-16151003

FIGURE 67. Image Scene As Viewed On The PEP Terminal. LANDSAT Image Of Madison, Wisconsin. The Operator Can Choose Any Spot In This Scene And Obtain The Intensity Readings At That Spot For A Particular Band Or Bands Of The LANDSAT Scanner

TITLE LANDSAT SCENE 1720-16073 FILE 3 OF 4 13JUL74 MADISON AREA
TAPE READ RESOLUTION: 1 PRINT RESOLUTION: 3
START ROW: 1101 END ROW: 1200 START COLUMN: 2202 END COLUMN: 2376



TITLE LANDSAT SCENE 1720-16073 FILE 3 OF 4 13JUL74 MADISON AREA
TAPE READ RESOLUTION: 1 PRINT RESOLUTION: 3

CHARACTER	RESOURCE	BAND	LOW	UP	BAND	LOW	UP
+	WATER	5	30	80	7	10	63
*	STREETS						

NUMBER OF PIXELS FOR WATER	898
NUMBER OF PIXELS FOR STREETS	438
NUMBER OF PIXELS UNCLASSIFIED	670

READY

ORIGINAL PAGE IS
OF POOR QUALITY

VII. APPLICATION

This chapter outlines four examples of applying remote sensing theory to water quality monitoring. The first example is a case where an \$8,000,000 intake for drinking water was located in turbid, unusable water. This could have been avoided had aerial photos (which clearly show the location of the turbid water) been adequately utilized. The second example involves mapping macrophytes by low altitude photography. The third example illustrates the unique laboratory spectral reflectance fingerprints of different types of algae, and the translation of these laboratory fingerprints to satellite fingerprints. The fourth example shows how lakes in a large region (10,000 square miles) were categorized and mapped by multispectral analysis of LANDSAT data, and how the lake with the heaviest algal concentration was found (Prairie Lake in Barron County, Wisconsin).

It is felt that these four examples demonstrate that remote sensing, properly used, can be a powerful tool for water quality monitoring and control.

A. EXAMPLE 1: TURBID WATER LOCATED BY AERIAL IMAGES

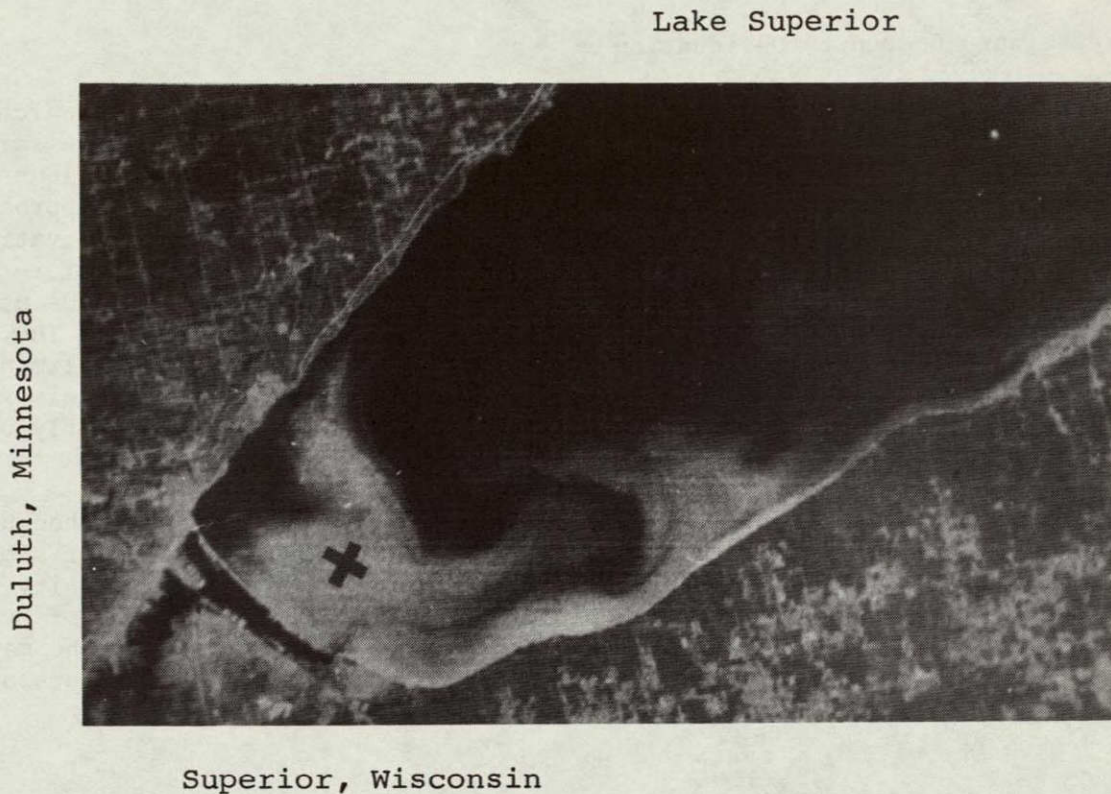
Lake Superior is one of the clearest lakes in the world. Early explorers remarked on its clarity and their ability to see rocks on the bottom and fish at great depths. Today anyone boating on or flying over Lake Superior will probably be amazed at its clarity, in many cases it is clearer than drinking water. Along the north shore of the lake, north of Duluth, Minnesota, this clear water is piped inland. Only chlorination is necessary to make it usable for drinking.

On the other hand, river and bank erosion near Superior, Wisconsin, cause suspended red clay particles to be mixed with the clear Lake Superior water. In Figure 68 this turbid water can be clearly seen in LANDSAT images. Careful analysis of LANDSAT images since 1972 and aerial photos since 1938 show the turbid water in an eddy that stays near Superior, Wisconsin over 50% of the time. After strong southwest winds, the turbid water moves eastward along the south shore of Lake Superior.

Evidently proper use was not made of the aerial photos on file in Superior, and it was proposed to construct a water intake in the center of the area where the turbid water eddy is located. This spot is marked by an "X" in Figure 68. Some water samples were collected in the area on a clear day when the wind was not too strong. On that day the water was clear. Plans were made and \$8,000,000 was spent constructing the intake and the pipe line to pump the water inland. However, after the intake was constructed, the water pumped for drinking purposes exceeded the turbidity limits for drinking water over 50% of the time.

Although aerial photos were evidently not used in the location of the intake, they were very useful in the lawsuit that resulted (Scherz and Van Domelen 1973).

FIGURE 68. LANDSAT Satellite Image Taken 12 August 1972 Showing The Southwest End Of Lake Superior Near Duluth. Note The Turbid Water. An X Marks The Spot Where An \$8,000,000 Water Intake Was Located (modified from Scherz and Van Domelen 1973).



B. EXAMPLE 2: MACROPHYTE MAPPING

The traditional method of mapping aquatic macrophytes is an expensive and time-consuming process. The following techniques illustrate how remote sensing can be a very effective tool in increasing the efficiency and accuracy of macrophyte mapping.

1. Macrophyte Community Mapping By Photo Interpretation

Determining aquatic macrophyte standing crop, total plant biomass (weight of above-ground, root, and rhizome plant parts per unit area), or plant density can be a difficult, time consuming, and expensive procedure in most studies on lakes of any significant size. For example, on Lake Wingra (Dane County, Madison, Wisconsin) Nichols (1971) obtained almost 1,500 0.1 m² samples to characterize a littoral zone community about 40 to 50 hectares (ha)* in size. These data

* 1 hectare = 10,000 meters²

were obtained without the aid of remote sensing techniques. When used in conjunction with remote sensing, a smaller number of plant material samples can be taken, and the final estimate of total standing crop will be more accurate. Use of remote sensing with biomass sampling in the lake also provides more accuracy in preparing map areas dominated by different plant species or by different standing crops of the same species.

a. Preliminary Community Delineation

To approximate the biomass or standing crop of different plant species which dominate various areas of aquatic macrophyte communities in lakes, it is not necessary for the lake manager to use the more expensive photoanalytic research techniques such as microdensitometry. Instead, the manager may use a more simplified approach that combines aerial photointerpretation with a minimum of ground truth observations. The investigator should first obtain the proper photographic imagery before collecting any ground data. Suitable imagery would include a 35 mm slide using Kodak color infrared film taken from 1000 to 3000 feet on a clear day. The axis of the lens should be vertical to the ground with care being taken to eliminate sun glitter (specular reflection of sun from water's surface). If the camera axis is nearly vertical then the noise due to the skylight reflection is nearly uniform across the scene.

Different colors appearing on the slide in areas of the lake that are thought to contain macrophytes usually will represent zones of different species or simply indicate different plant densities or plant biomass. Preliminary community boundary estimates can be made by projecting the image against a sheet of Mylar laid over a map of the lake area of interest. The different zones of the macrophyte community can then be outlined on the Mylar from areas of different colors on the slide.

b. Obtaining Ground Truth

The next step is to obtain an estimate of ground truth within each of the colored areas of interest observed on the film. The stratified random sampling design was selected for this purpose because it provides statistically usable data and at the same time assures that samples will be taken throughout the study area. (See Chapter III for a detailed discussion of sampling designs.)

The investigator can stratify this sampling pattern by setting compass lines at regular intervals across the littoral zone area selected for analysis. Each area should be one that appeared as a different color or markedly different shade on the photograph. In most cases it will be reasonable to select about five or six differently colored or shaded areas. The more areas that are selected for analysis, the finer the discrimination. The degree of discrimination must depend ultimately on the objective of the analysis.

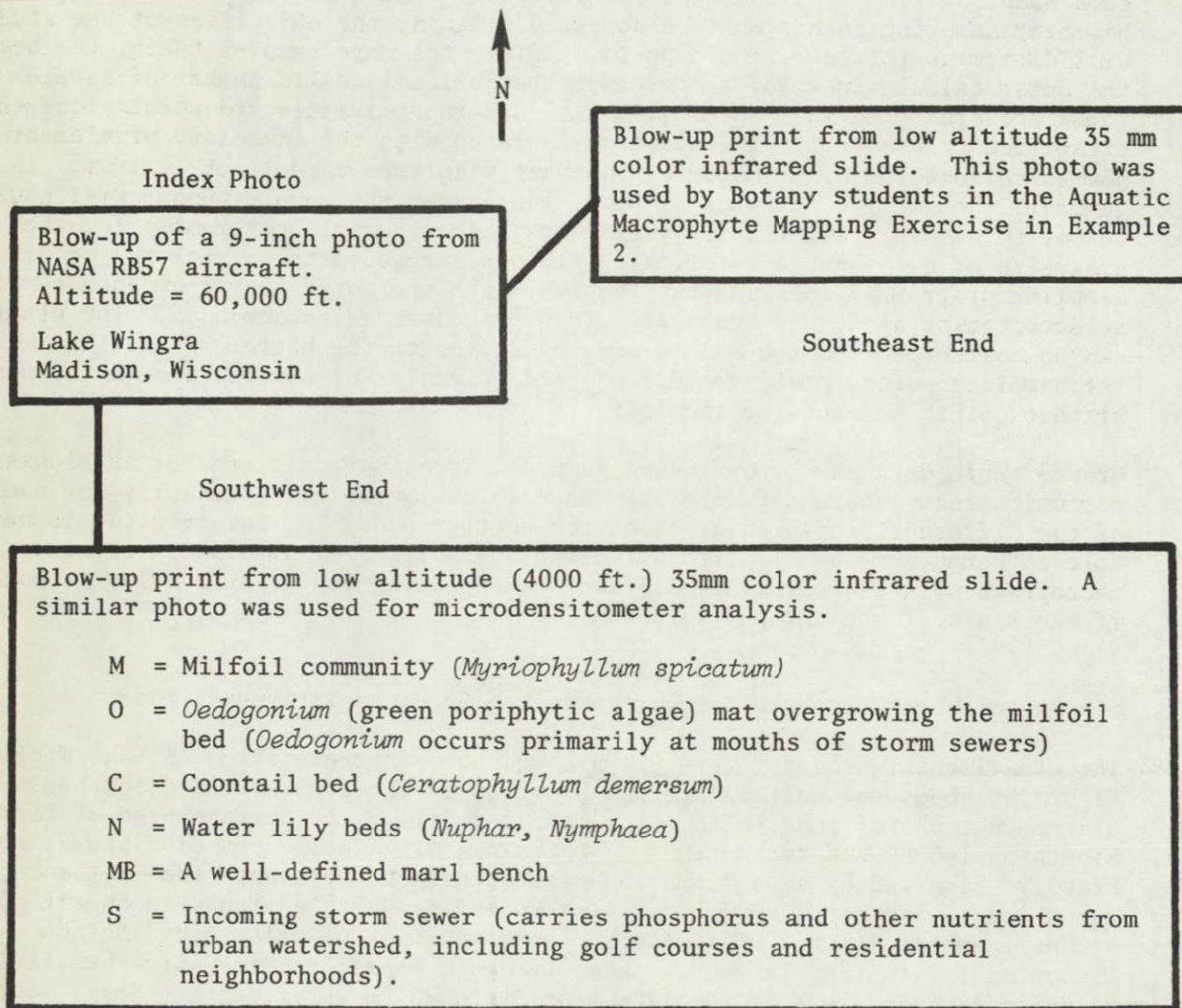
After setting out compass lines on the map and lake within each area to be investigated, sampling points should be selected from a random numbers table and designated along each sampling line to be followed. Designation of sampling points should be in distance units (meters or feet) from the starting point of each sampling line or transect to be followed. The question now arises as to how many sampling points must be selected. Again, the objectives of the study will determine this decision. Up to a point, the more samples taken, the better the data; calculations for the minimum statistically valid number of samples taken are presented in Chapter III. At each randomly selected point along the stratified transects the investigator is faced with the immediate problem of how to collect the plant material and what size area to collect it from. In general, the smaller the area sampled, the larger the sample number will have to be, to obtain statistically valid data. A reasonable compromise for the area size of each sample is 0.1 m^2 . Nichols increased the efficiency of his sampling program by locating two samples, each one meter away from each randomly selected point along his transect. This procedure is recommended. The plants can be collected from the sample area by diving to the bottom of the lake at the sampling point, placing a 0.1 m^2 grid (circular or square) around the plants at that point, and cutting them off.

Ground truth data may be expressed as plant stems per unit area or as biomass per unit area. These data are then used to designate plant quantity for each of the differently colored areas of the photographs. The investigator is now able to compute areas of different plant communities by planimetry of zones on photograph prints or from areas drawn on maps using the Mylar overlay method if the scale of photography is known.

c. Example Of Macrophyte Community Mapping By Photo Interpretation

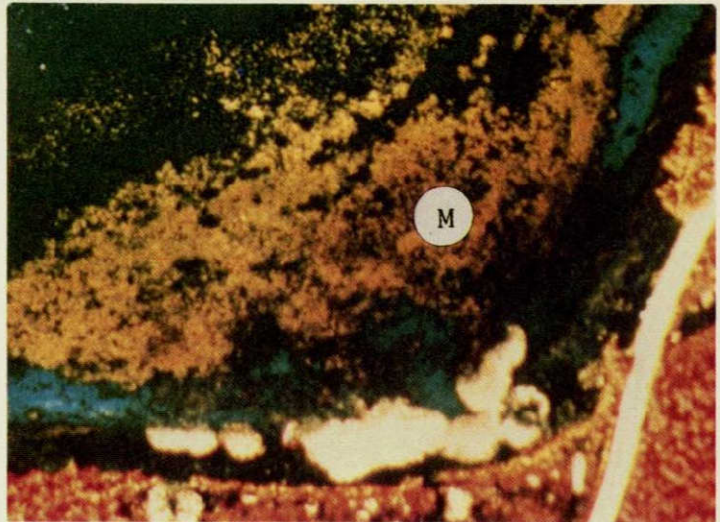
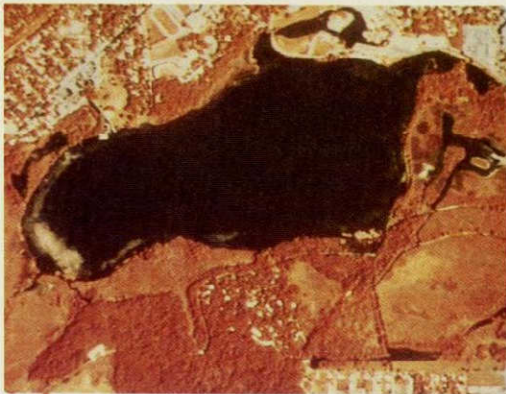
The experimental area for this example of photo interpretation is Lake Wingra. Figure 69 shows the entire lake and blow ups of the southeast and southwest ends of the lake photographed with color infrared film. The surface area of Lake Wingra is 140 ha and the maximum depth is 6.4 m. A well defined littoral zone heavily colonized by aquatic macrophytes occurs in the lake. The littoral community is dominated by *Myriophyllum spicatum*, which is found in nearly pure stands in water 80 to 270 cm deep. Other important plant species include *Nuphar variegatum* Engelm and *Nymphaea tuberosa* Paine, species which heavily colonize certain areas of the lake from 35 to 80 cm water depth. Small scattered stands of *Ceratophyllum demersum* L. occur at the shallow and deep water edges of the *Myriophyllum* beds. A well developed *Oedogonium* mat is usually found by midsummer overgrowing part of the *Myriophyllum*. The *Oedogonium* usually occurs at the mouth of storm sewers that provide heavy concentrations of phosphorus and other nutrients from urban runoff (lawn fertilizers, leaves, etc.). The most shallow areas typically have a scattering of *Myriophyllum* plants and various *Potamogeton* species (Nichols and Mori 1971). A few shallow areas of coarse marl substrate are conspicuous by their almost complete lack of vegetation.

Index Key For Figure 69 Color Infrared Photos Of Lake Wingra



ORIGINAL PAGE IS
OF POOR QUALITY

Index photo



Southwest end

Southeast end

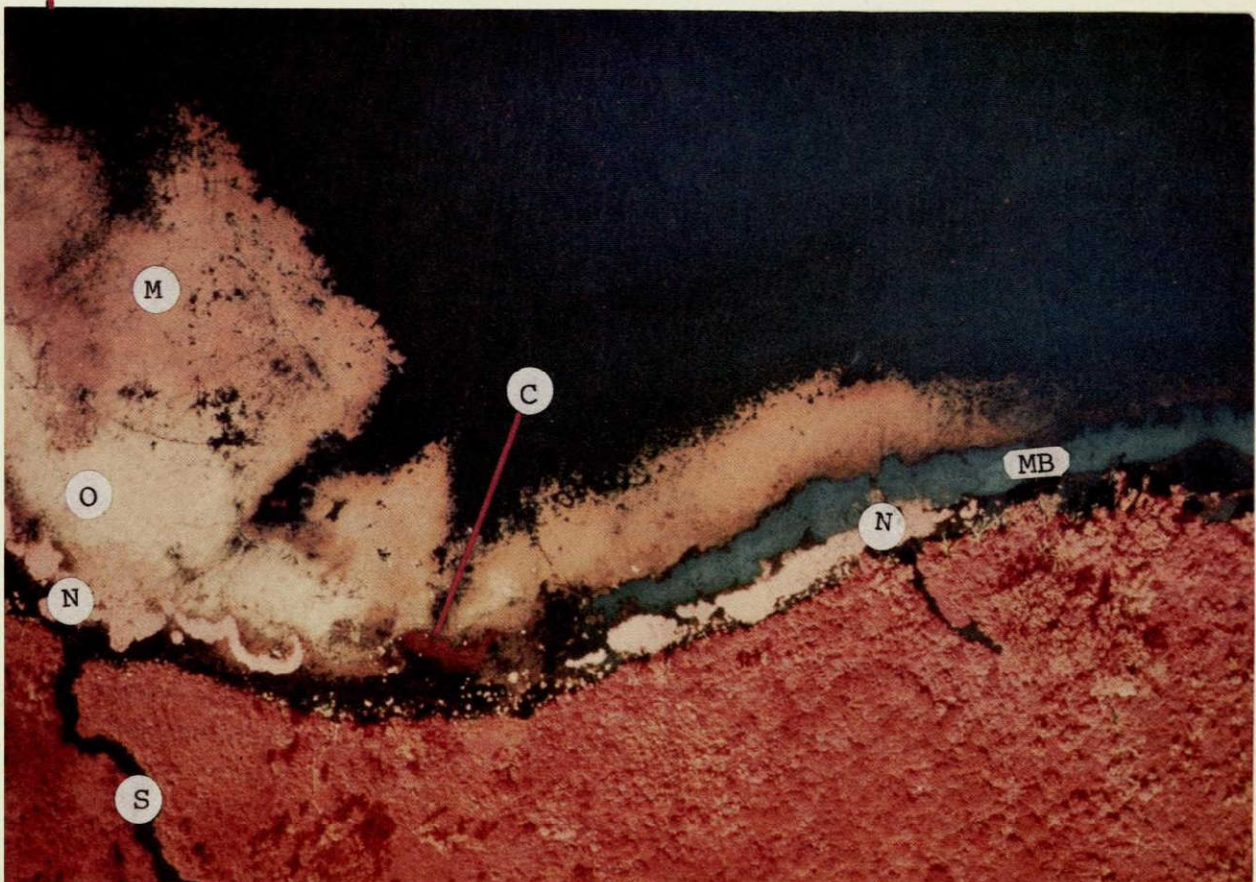


Figure 69. Color infrared photographs of Lake Wingra, Madison, WI.
Photos taken in late summer 1973.

a. Macrophyte Community Differentiation

A two-camera 35 mm aerial photographic system (Rinehardt and Scherz 1972) with color and color infrared film was used to obtain imagery on a scale of 1:34,000 and 1:17,000. Overlapping exposures were oriented so that the shoreline and littoral zone areas would lie near the center of the format. Flights were scheduled whenever possible on clear days and at times of low sun angle to avoid glitter.

Orientation of ground truth with photographic imagery was facilitated by using white plywood panels that were easily visible in the photographs. These panels were placed at selected vegetational boundaries to see if the boundaries could be seen on the photos. Color infrared film, Kodak Aerochrome 2443, was found to be excellent for identifying vegetation and was used exclusively for interpretation and analysis of the aquatic plant communities.

Standard methods of visual interpretation (Avery 1968) were used to characterize important image features. Ground truth data were then used to classify these image types according to their vegetational attributes (Table 2). Munsell colors were also determined when possible.

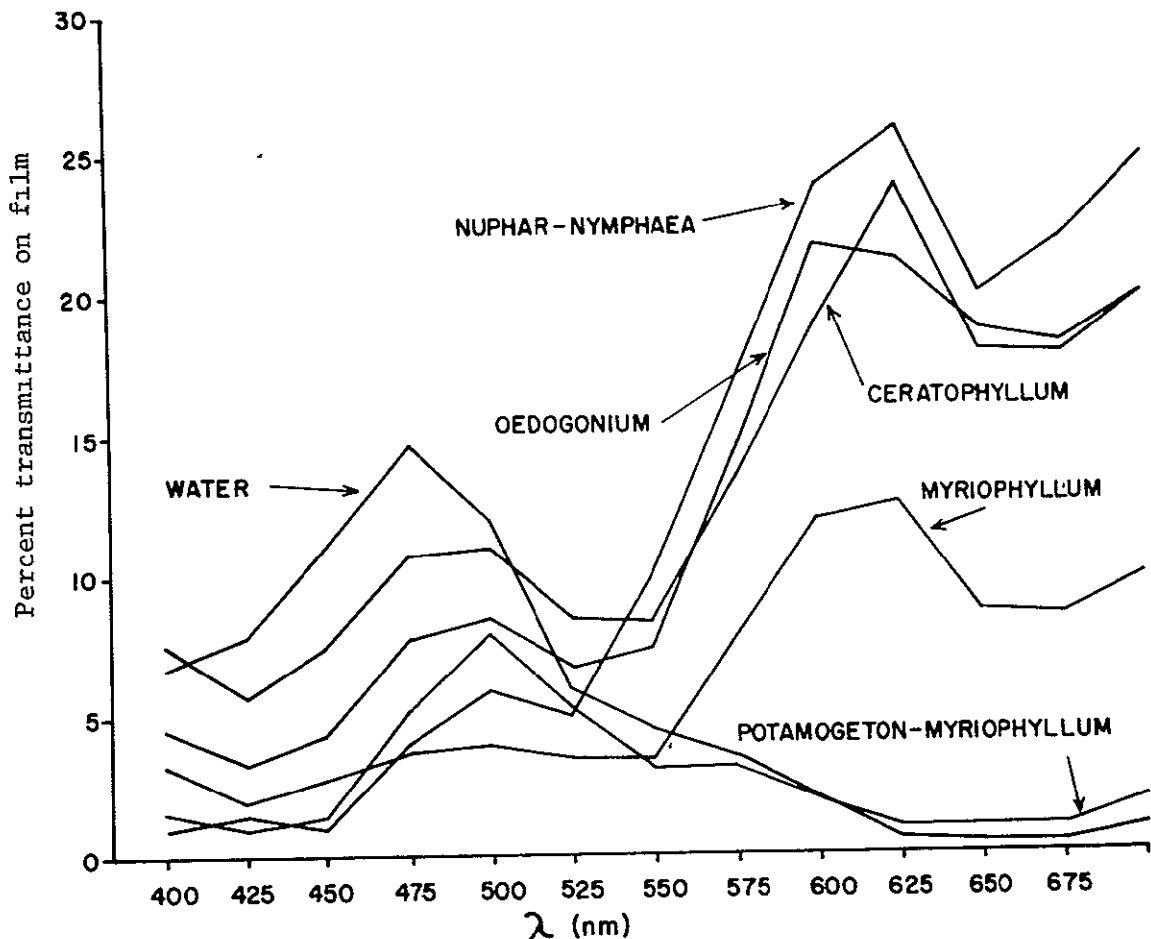
TABLE 2 Identification Key For Lake Wingra Image Types. Results Are For Color Infrared Film (Kodak Aerochrome 2443). Density Ratios Are 600 625 nm Except Values In Brackets Which Are 450.600 nm (Gustafson and Adams 1973)

TYPE	TOPE	TEXTURE	LOCATION	SHAPE	MUNSELL COLOR	DENSITY RATIO
MYRIOPHYLLUM	DEEP ORANGE	MOTTLED	MID TO DEEP LITTORAL (70-270 cm)	VARIABLE, BOUNDARIES DISTINCT	7.5R7/10	0.9306
NYMPHAEA	BRIGHT PINK	FINELY TEXTURED	PROTECTED AREAS SHALLOW TO MID LITTORAL (35-80 cm)	ROUND TO ELONGATE	2.5RP8/6	0.8843
OEDOGONIUM MAT	VERY LIGHT TAN	VERY SMOOTH	OVERGROWTH ON MYRIOPHYLLUM	AMORPHOUS, BOUNDARY INDISTINCT	7.5R9/12	1.0416
CERATOPHYLLUM	DEEP RED	UNIFORM TO ROUGH	EDGES OF MYRIOPHYLLUM BEDS	VARIABLE	7.5R3/12	0.8027
POTAMOGETON-MYRIOPHYLLUM	DARK GREEN	UNIFORM	NEAR SHORE LITTORAL	VARIABLE	-	1.8470 (0.728)
FLOATING-LEAVED POTAMOGETON	MEDIUM PINK	COARSE	MID LITTORAL (100-200 cm)	ROUND	7.5R8/6	-
DEEP WATER	DEEP BLUE	UNIFORM	AREAS MORE THAN 3 m DEPTH	-	2.5PB6/8	2.1620 (6.646)
SHALLOW WATER MARL	LIGHT TURQUOISE	UNIFORM	SHALLOW TO MID LITTORAL	ELONGATE WITH SHARP BOUNDARY	2.5PB8/4	-

Microdensitometer analysis of the various image types was conducted to develop an objective method for identification. The instrument employed was the Gamma Scientific microdensitometer described by Klooster and Scherz (1974). A spot size was selected that was equivalent to an area at the water surface of 0.7 m^2 in the photographs of the larger scale. This system is able to determine the transmittance characteristic of a film image at any wavelength from 0.35 to 0.8 microns.

Percent film transmittance for the various image types (Figure 70) was examined for wavelengths that could be used to form ratios characteristic of the respective images. Selected ratios were exposed to rigorous testing by lumping data from different times of the season and from different years. Ninety-five percent confidence intervals were calculated and means tested for actual differences by Duncan's new multiple range test (Steel and Torrie 1960).

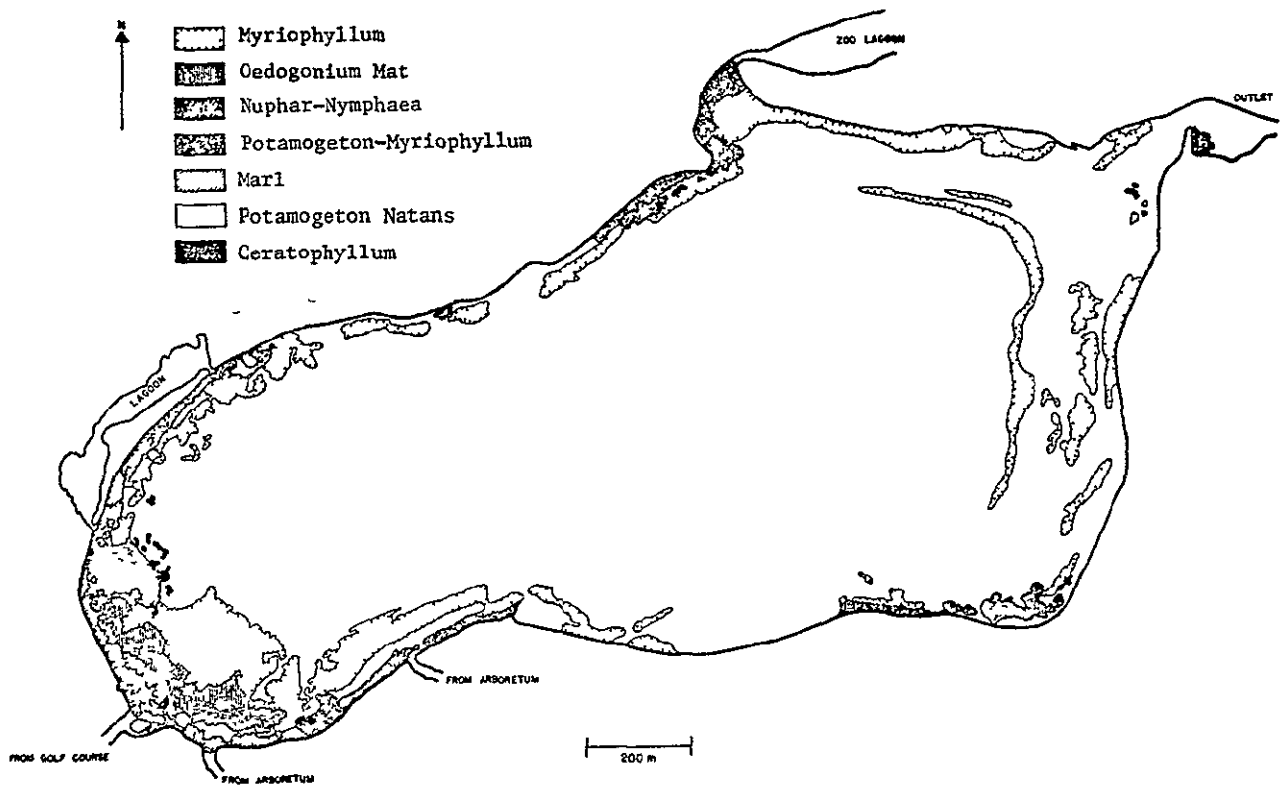
FIGURE 70. Spectral Signatures Of Some Of The Lake Wingra Image Types Of Macrophytes. Data From Microdensitometer-Spectrophotometer Analysis Of 35 mm Aerial Color Infrared Photographs (Kodak Aerochrome 2443) (modified from Gustafson and Adams 1973).



ORIGINAL PAGE IS
OF POOR QUALITY

The color infrared images were projected from standard equipment onto shoreline maps (1:1200 or 1:2400 scales) drawn on sheets of Mylar drawing plastic. Good results were obtained even with low precision equipment by using the shoreline as a control for correcting lens distortion and a slight deviation of the photography from the vertical. Features were identified and boundaries traced in with pencil. The maps were then inked and working blue line copies were produced directly from the original (Figure 71).

FIGURE 71. Lake Wingra Vegetation Map of 14 July 1971. Map Was Constructed From Aerial Color Infrared Photographs By Using Projection Techniques (from Gustafson and Adams 1973).



Most of the littoral zone vegetation of Lake Wingra appears red in the color infrared photography (Figure 69). This is expected for the floating leaved water lily or pondweed communities, but the submergent (*Myriophyllum* and *Ceratophyllum*) community also produces a red tone. The latter may be the result of these species growing with leafy stems very near the surface. The observation that a darkened image is produced by those areas of *Myriophyllum* growth that lacked sufficient vigor to approach the surface supports this hypothesis.

The *Oedogonium* and *Potamogeton-Myriophyllum* image types did not show the characteristic red tones of vegetation. The very light image of the algal mat may be the result of greater reflectance in the red region and less efficient absorption of photosynthetically active radiation because of marl accumulation on these plants. The absorption of IR energy by but a few inches of water may be another factor. In contrast to the algal mat, the *Potamogeton-Myriophyllum* community appears very dark. These shallow areas contain relatively few plants, and the resultant image is probably strongly affected by the reflective properties of the bottom material.

Some of the factors that can affect photographic image and make interpretation difficult are differing photographic exposures, processing, sun angle and possible sun glitter, sky conditions, water turbidity, and wave state. In photography taken over a period of two years certain interpretive criteria (especially tone contrasts between plant types) were quite variable. Microdensitometry was used to try to increase precision in the interpretive process.

In a single exposure the percent film transmittance value by microdensitometer analyses of the image types is quite characteristic (Figure 70). But this value was found to be ineffective when comparing photographs from different flights or even from several frames of the same flight.

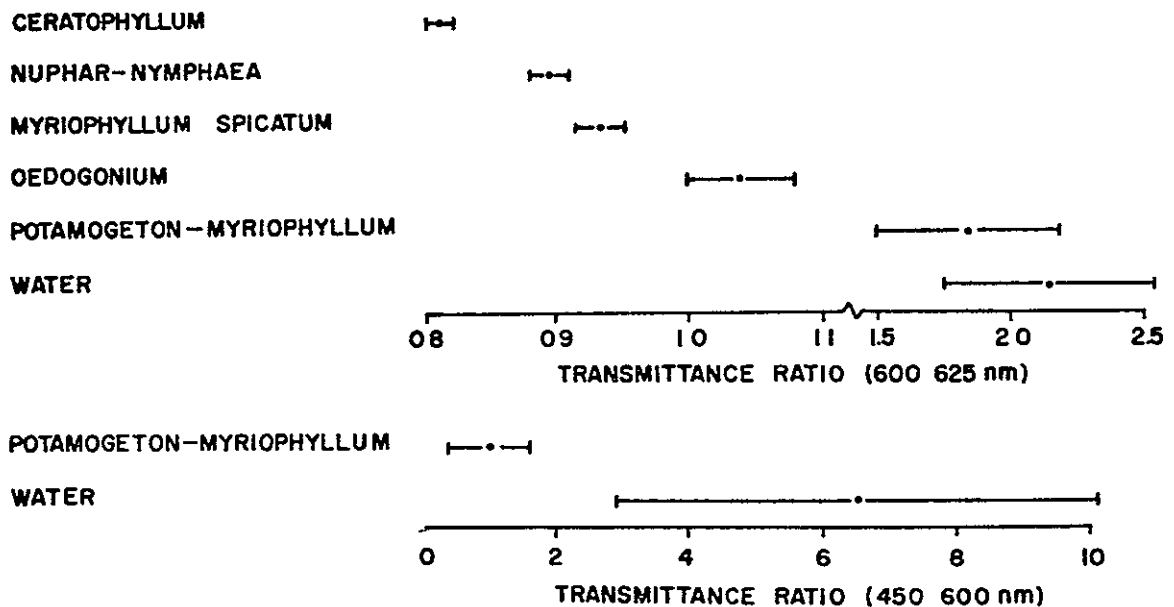
Satisfactory results were achieved only by using transmittance ratios at selected wavelengths (mostly the 600/625 nm* ratio). The ratio values for four of the plant types (*Nuphar-Nymphaea*, *Oedogonium*, *Ceratophyllum*, *Myriophyllum*) (Table 2) are quite similar, but the differences were significant at the 1% level. The use of an additional ratio of 450 600 nm was required for separation of the *Nuphar-Nymphaea* from the *Potamogeton natans* (Figure 72). These floating-leaf types have very similar tone but usually can be easily differentiated visually on the basis of texture.

Successful application of the densitometer analysis required care. The results were quite sensitive to exact calibration and alignment of equipment.

Detailed vegetation maps similar to Figure 71 were prepared for selected times during 1971-1972, and have been used to examine seasonal and annual change in the growth areas of *Myriophyllum spicatum*. The information has been used to refine harvest sampling procedures. The data have been correlated with nutrient and climatological factors. They could also be used to assess the effectiveness of harvesting or applications of chemicals for weed control and to measure the results of watershed management efforts. An anticipated use of the Wingra data is for ecosystem model verification and testing. The distribution and phenology of the various communities can also be followed through the season or compared from year to year. An annual photographic record for several lakes through a period of years could be easily obtained and would provide a good source of information for studies of lake succession.

* nm = nanometer = 10^{-3} microns = 10^{-9} meters

FIGURE 72 Mean Values And 95% Confidence Intervals For Film Transmittance Ratios Used For Differentiation Of The Lake Wingra Image Types Of Macrophytes. The First Four Types Are Separated On The Basis Of Film Transmittance Of 600 and 625 nm. The Additional Ratio Of 450:600 nm Is Required For The Separation Of The *Potamogeton-Myriophyllum* Type From The Open Water. Values Are From Microdensitometer-Spectrophotometer Analysis Of Images On Color Infrared Photography (from Gustafson and Adams 1973).



Some disadvantages of using the 35 mm format are image distortion due to the lens and nonprecise resolution. The low cost per frame (15¢ vs \$15 for the 9 x 9 inch mapping camera photo) and the availability of high quality 35 mm equipment were strong points in favor of its use. The results indicate that 35 mm photography is adequate for the methods used in this study. However, recent investigations requiring more precise quantitative information from the imagery have shown an advantage with using a larger format if cost is not a factor.

b Macrophyte Quantity Estimation By Microdensitometer Analysis Of Aerial Images

Optical density measurements of color infrared slide film images were used to estimate the standing crops of the *Oedogonium* mats and the *Myriophyllum* community. A Gamma Scientific spectrophotometer was used to sample the respective images using a spot size equal to 2.5 m² at the water surface. That is, a beam of light of a certain wavelength was passed through the film. It covered an area on the film that was equivalent to 2.5 m² on the lake surface. The film could be moved on the microdensitometer stand so that the beam effectively traversed the film, covering all areas of interest. The amount of light that could pass through the film at any given point depended both on the kind and amount of plant life represented on the film, as well as the wavelength of light chosen. Thus, the percent transmittance of different areas on the film was measured to certain wavelengths of light.

The wavelength 600 nm was used for *Myriophyllum* because of good separation of the transmittance characteristic for milfoil at that wavelength as contrasted with film transmittance for open (macrophyte-free) water. The wavelength 555 nm was chosen for study of the mat-forming filamentous alga *Oedogonium* because at 555 nm the percent transmittance characteristics for open water and milfoil overlap (Figure 70). This is a necessary prerequisite in that the *Oedogonium* is attached to milfoil which in turn is in water, so both the water and the milfoil are represented in the background of the image type representing the *Oedogonium*.

Several methods of photographic standardization were tested for their usefulness in correcting for such variables as sun angle, sky condition, wave state, and water turbidity. One method uses a ratio of plant community film density to open water film density. The second method uses a ratio of the image density of the plant community to the image density of a standard reflectance panel. The third method uses a ratio of two film densities at different wavelengths located at the same point in the plant community.

For Lake Wingra with its open water background, better results were obtained when the ratio of the readings from the plant communities to the open water was used than when a standard reflectance panel was used. This is apparently because open water readings have the same specular skylight reflection values as readings from the macrophyte communities, while the panel has no corresponding specular skylight reflection.

Harvest data were compared with data from film analysis by linear regression with good results (Figures 73 and 74). Biomass or stem density was obtained using the appropriate regression formula and multiplying that by the standard area obtained by photogrammetry

Certain features of the growth of *Oedogonium* and *Myriophyllum* in Lake Wingra facilitate the successful application of quantitative methods using aerial photography. Using 555 nm provides a uniform background while 600 nm provides a contrasting background on color infrared film (Figure 70). Both vegetation types are found in nearly pure stands with good correlation between cover, plant density, and standing crop.

FIGURE 73. Regression Analysis Of *Myriophyllum* Harvest Data And Film Densities That Were Standardized By Using Readings From Open Water Areas.

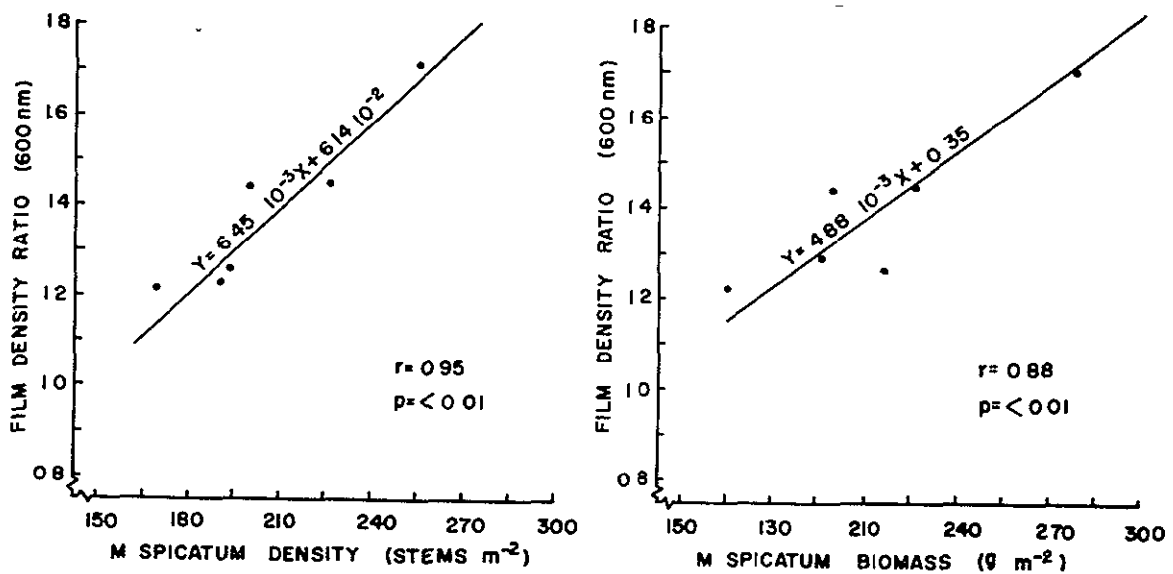
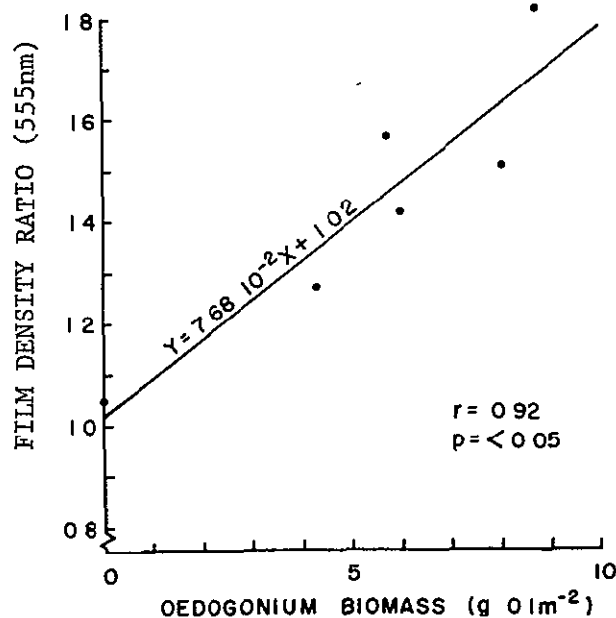


FIGURE 74. Regression Analysis Of *Oedogonium* Harvest Data And Film Densities. Note Film Density Ratios Here Mean The Value Obtained At A Wavelength When The Signal From The Plant Community Is Divided By The Signal From The Open Water In Lake Wingra For That Day (Gustafson and Adams 1973).



Further investigation has shown that for lakes with dramatically changing phytoplankton populations in the open water (and consequent fluctuating open water brightness), the open water calibration method* is of limited usefulness. In these lakes photoanalytic work should probably be done with standard reflectance panels to calibrate imagery.

The advantages of photographic methods are their efficiency and accuracy. When compared with estimates made using harvest procedures alone, the photographic methods were found to provide data of greater statistical reliability. The large sample size possible with photoanalysis resulted in standard errors with much less than 10% of \bar{x} . Those obtained by the harvest method were as high as 40% of \bar{x} . Total biomass estimates using the harvest method were much different than those of the photographic methods. Difficulties in estimating the exact area sampled while using the harvest method are suspected to result in substantial overestimation of *Myriophyllum* standing crop. Harvesting and sample processing required about 250 hours of work per estimate, while photographic analysis can be accomplished in as few as 10-15 hours. Short-term changes that would be completely obscured in the days or weeks required to collect the necessary number of samples can be monitored by photography. The photographic methods also have the advantage of being nondestructive.

C. EXAMPLE 3. REFLECTANCE FINGERPRINTS FROM DIFFERENT ALGAL TYPES AND THEIR LABORATORY-TO-SATELLITE TRANSLATION

Free-floating algae of the open water zone (phytoplankton) are well-known indicators of a lake's trophic status. The more eutrophic lakes generally have larger standing crops of algae than oligotrophic lakes. Excessive concentrations of blue-green algae are especially prevalent with eutrophic conditions. Seasonally, blue-green algae are more common in late summer, whereas diatoms are more often found in lake waters in the spring and fall. Green algae are commonly present at any point in the seasonal cycle of lakes. Preliminary evidence by Thorne (1977) indicates that to draw a relationship between narrow-band remote sensing image brightness and algal biomass (chlorophyll *a* concentrations), it may be necessary to know the class of algae present in the lake. Also, different taxonomic classes represent different lake trophic conditions.

Theoretically, by determining reflectance fingerprints in the laboratory a remote sensing system can be constructed to classify and quantify algae. The classification of algal types depends on the ability to recognize differences in reflectance fingerprints of different types of algae. Increasing concentrations of algae should be associated with increased scene brightness. The following discussion traces the remote sensing of algae from theoretical laboratory studies through low altitude photography to the application of LANDSAT satellite imagery for classifying and quantifying phytoplankton.

* Open water calibration means that a reading is taken on the open water and another reading is taken on the plant community in question. The ratio of the two is then correlated to the plants in the community.

1. Laboratory Fingerprints For Different Algal Types

Gramms and Boyle (1971) demonstrated that blue-green and green algae can be differentiated from their laboratory reflectance fingerprints. Further work by Thorne (1977) shows indeed that green algae, blue-green algae, and possibly diatoms have unique laboratory reflectance fingerprints. Thorne obtained reflectance curves for different concentrations of pure and mixed suspensions of algae representative of the three above mentioned types. Figures 75, 76, and 77 show the laboratory reflectance difference fingerprints, (D_i), and the visible absorption spectra for three different concentrations of green alga, a diatom, and a blue-green alga, respectively.

FIGURE 75. Laboratory Reflectance Differences And Energy Absorption Data For A Green Alga (*Scenedesmus quadricauda*).

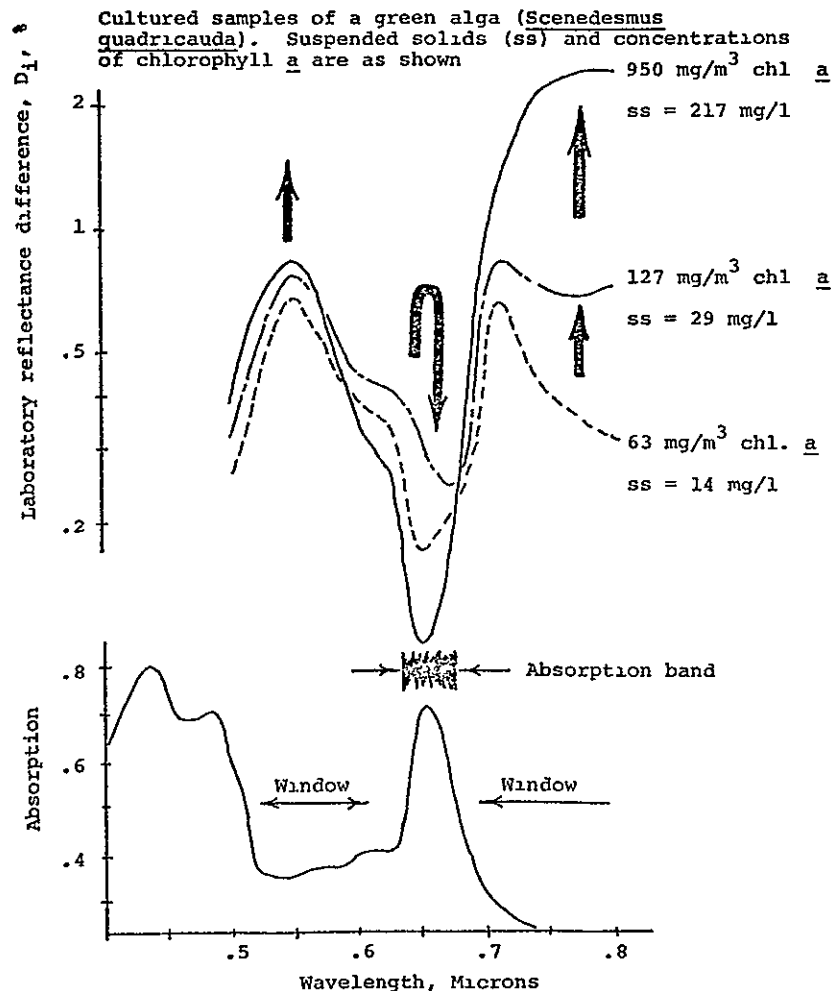
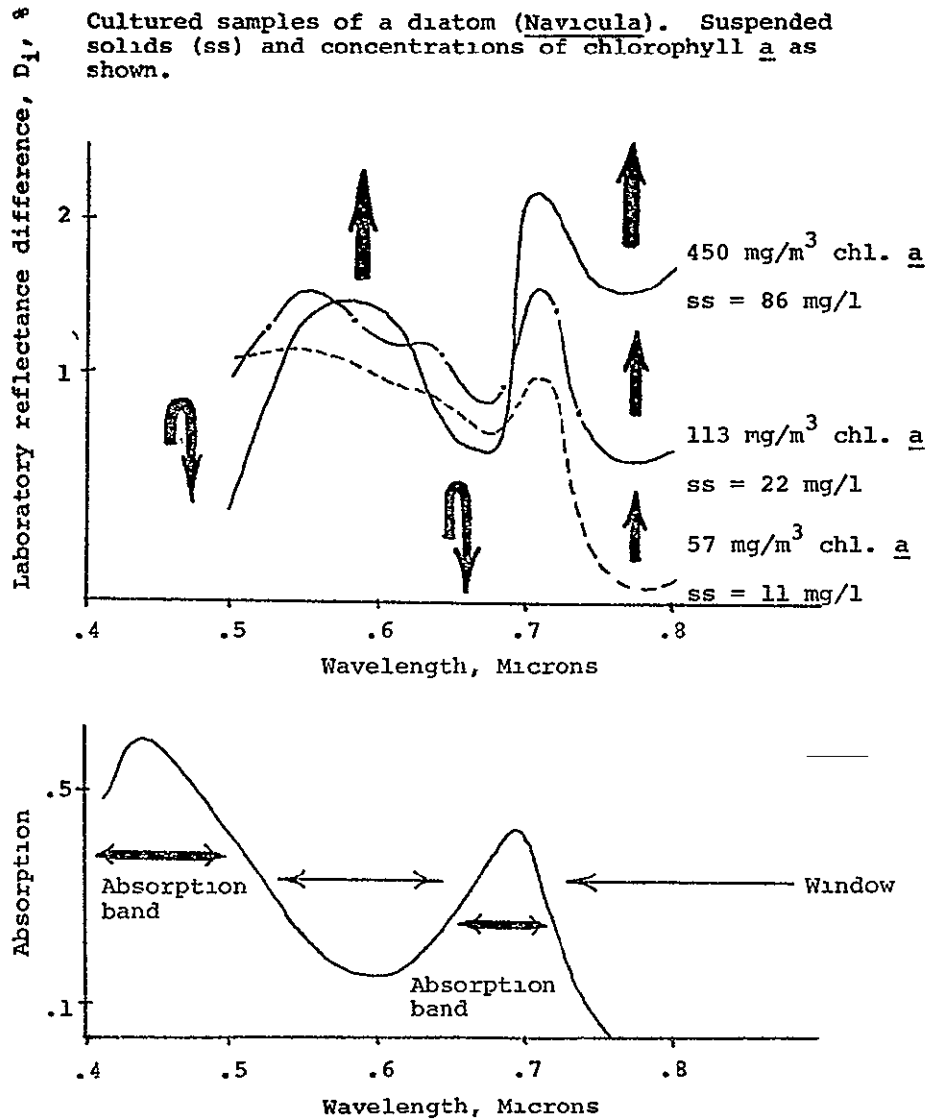
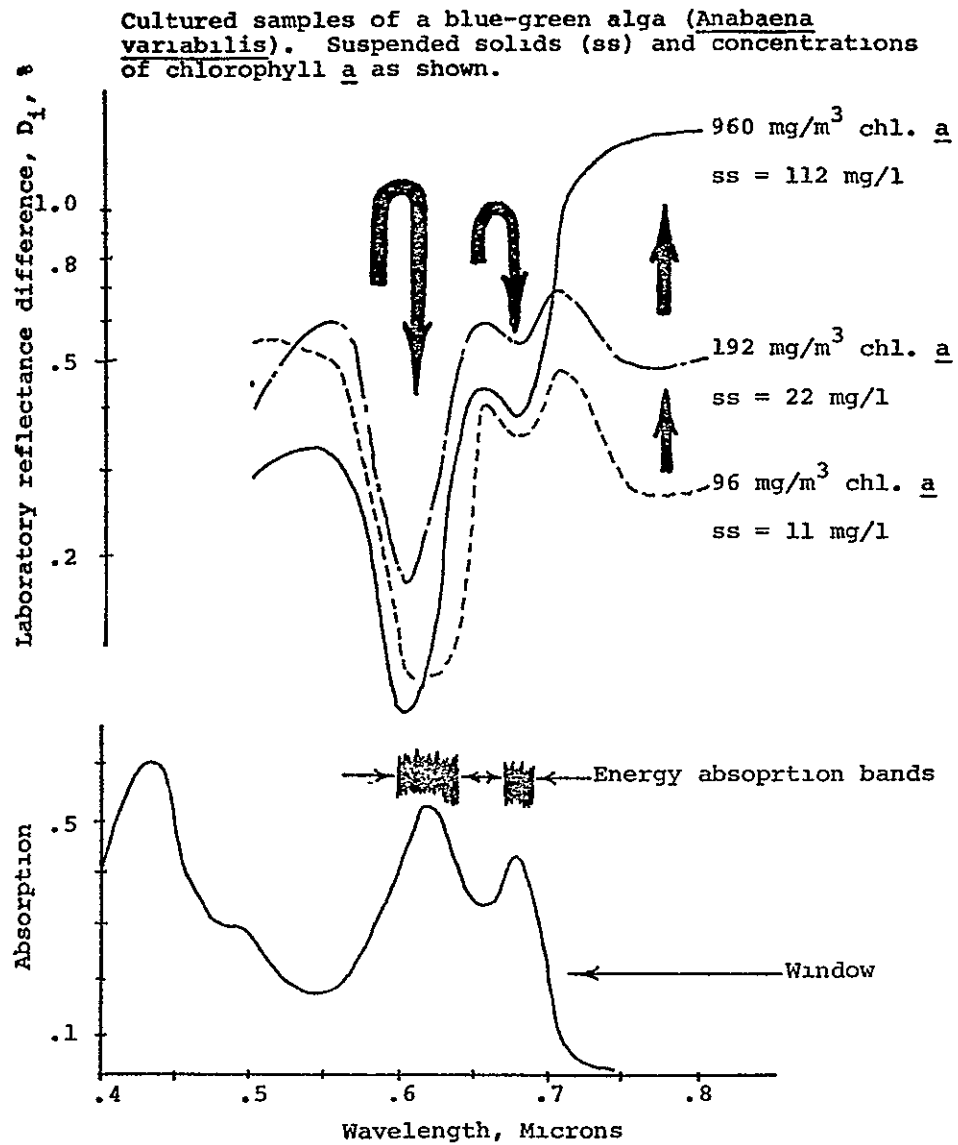


Figure 76 Laboratory Reflectance Differences And Energy Absorption Data For A Diatom (*Navicula*).



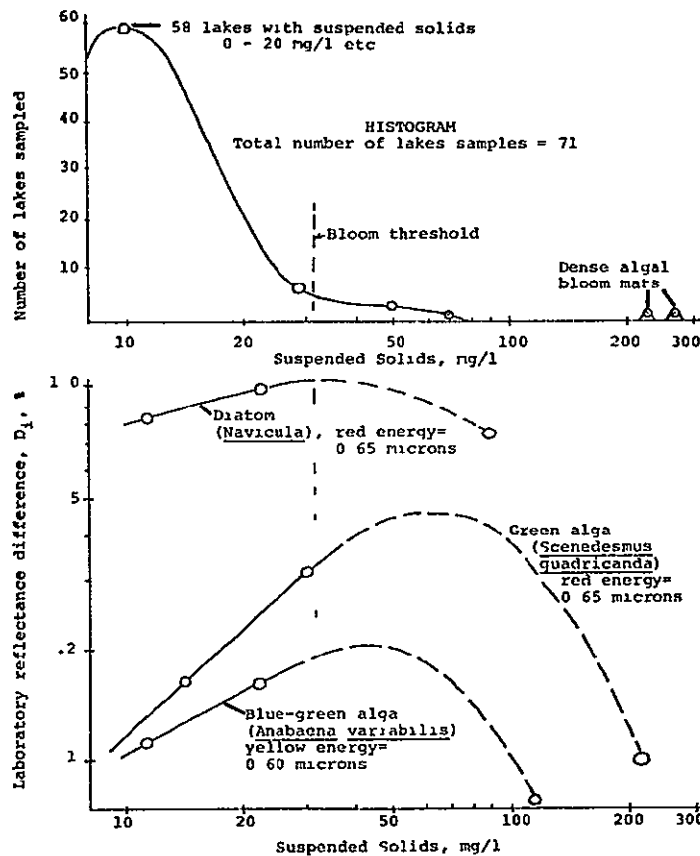
ORIGINAL PAGE ₁₅₁
OF POOR QUALITY

FIGURE 77 Laboratory Reflectance Difference And Energy Absorption Data For A Blue-Green Alga (*Anabaena variabilis*).



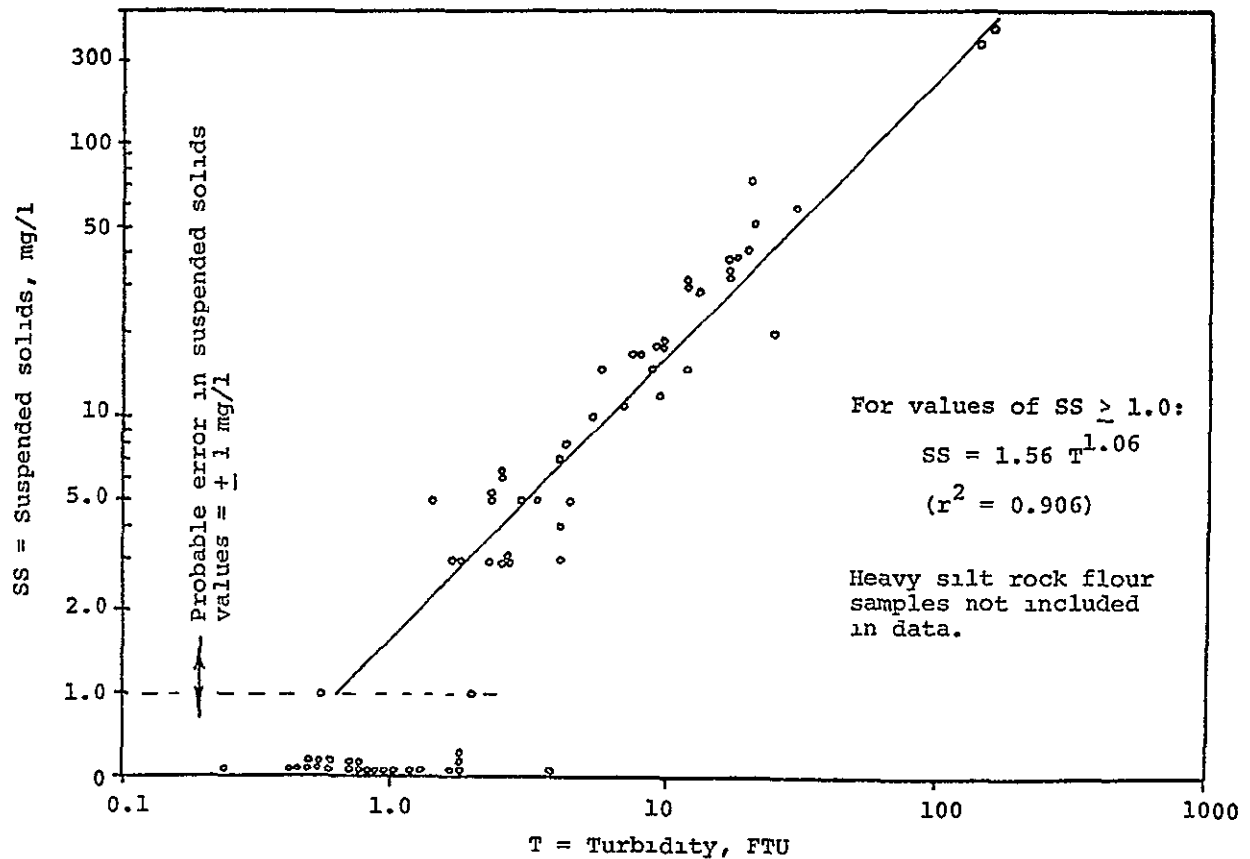
Note that with increased concentration a reflectance reversal occurs in areas of pigment absorption and that this reversal is most pronounced in areas where absorption by pigments is relatively high. In areas of the spectrum where little to no pigment absorption occurs, the reflectance behaves similarly to most other materials found suspended in water, i.e., the signal increases with increased concentration of material. These phenomena were observed in the field by Wrigley et al. (1975), working with high concentrations of *Aphanizomenon flosaquae* (L) Ralfs measured by a scanning spectrometer. However, Figure 78 illustrates that this nonlinearity of scene brightness with respect to algal biomass does not apply to the vast majority of natural waters. The histogram of surface suspended solids concentrations shows that only those lakes with algal bloom conditions fall within the region of this reflectance reversal. This reflectance reversal begins to appear with surface algal suspended solids concentrations in the range of 30-100 mg/l. For most lakes that remote sensing might be used to monitor and classify, algal reflectance reversal is no real problem, especially if the relatively broad band LANDSAT sensors are used.

FIGURE 78. Suspended Solids Versus Reflectance In The Absorption Bands Of Three Types Of Algae. Reflectance Reversals Caused By Absorption Of Dense Algae Mat Blooms Occur At Concentrations Higher Than Most Well-Mixed Lake Samples (As Shown By Histogram Of 71 Lakes Sampled In 1974).



Turbidity is a very broad band reflectance measurement (across the entire visible spectrum) and there seems to be no reversal or decrease of turbidity with higher concentrations of algal solids associated with blooms. Figure 79 shows the plot of turbidity versus suspended solids for lakes that have various amounts of algae and humic material present (no mud or silt lakes are present). The laboratory analysis for the samples in Figure 79 was done by standard methods. The plot of Figure 79 clearly shows that for very high concentrations of algae (even algal blooms) there is a consistent increase of broad band backscatter (turbidity) with increased weight of algae present (expressed as suspended solids).

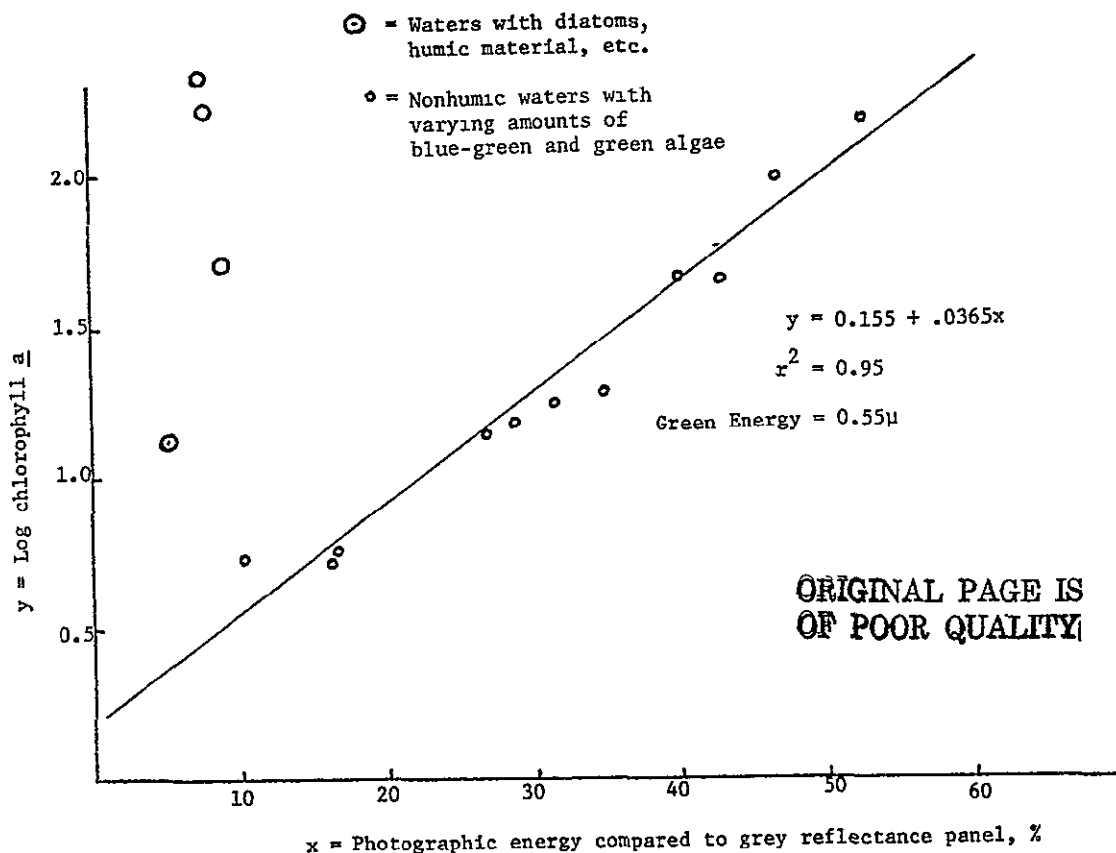
FIGURE 79. Suspended Solids Versus Turbidity For 71 Water Samples Collected In 1974. Various Wisconsin Lakes With Different Algal Content.



2 Phytoplankton Quantity and Low Altitude Photography

Although low altitude photography is a relatively expensive technique for lake classification (about 4-5 times as expensive as LANDSAT classification, (Thorne 1976), it potentially provides more information due to the smaller amount of atmospheric interference and better ground resolution. Data from laboratory reflectance studies of algae suggest that for natural concentrations of algae (usually less than 100 mg/m^3 chlorophyll a), green energy is probably the most useful wavelength region for estimating algal quantity. Figure 80 illustrates the relationship between green reflected energy and chlorophyll a concentration (in mg/m^3) as measured by aerial photography with high speed black-and-white film (Kodak 2485) through a .55 micron narrow band filter (.02 micron wide). The film brightness measured was corrected for surface reflectance of skylight using a plot constructed by Van Domelen (1974) similar to Figure 33. Differences in cloud conditions were accounted for. Variations in photo exposures were corrected by using standard field reflectance panels present in each photo scene analyzed. The resulting data (Figure 80) show a good correlation between image brightness and chlorophyll a for the lakes with mixtures of blue-green and green algae.

FIGURE 80. Plot Of Green Reflected Energy As Measured By Aerial Photography Versus Chlorophyll a Concentration For Blue-Green Algae In Nonhumic Waters Data For Diatom Lakes Fell From The Curve (Thorne 1976)



3. Translating From Laboratory To Satellite Fingerprints

The reflectance fingerprints in Figures 75, 76, and 77 were obtained with a reflectance spectrophotometer that was capable of sensing very narrow bands of energy in the range between 0.35 and 0.8 microns. Nine data points (0.500, 0.550, 0.600, 0.625, 0.650, 0.675, 0.700, 0.750, 0.800 microns) were taken in areas of the fingerprint curves thought to be necessary to give a full impression of the detail of each fingerprint. LANDSAT satellite data, however, have only three bands covering the same region of the spectrum (Band 4 = 0.5-0.6 micron, Band 5 = 0.6-0.7 micron, and Band 6 = 0.7-0.8 micron).

If the area under the laboratory curve between 0.5-0.6 microns is integrated, the signal strength is proportional to Band 4 of the LANDSAT satellite. A similar integration between 0.6-0.7 and from 0.7-0.8 microns would yield signals proportional to LANDSAT Bands 5 and 6.

The upper portion of Figure 81 shows the laboratory reflectance fingerprints for pure cultures of a diatom, a green, and a blue-green alga. The lower portion of this figure illustrates the integration of these curves to produce laboratory reflectance differences proportional to the signals expected from Bands 4, 5, and 6 of LANDSAT. Figure 82 shows a similar set of fingerprints and their analogous reduction to LANDSAT type data from mixtures of blue-green algae and diatoms as well as blue-green and green algae. The concentrations of these pure cultures and the mixtures were selected to approximate those found in lakes rich in algae but still below bloom threshold. The upper portion of Figure 83 depicts a summary of laboratory data integrated to provide curves analogous to those expected from LANDSAT data for the three pure cultures as well as the two mixed cultures. The lower half of Figure 83 shows the actual shape of LANDSAT fingerprints from four different algal lakes. Because the results from analyzing satellite data first became apparent after the satellite overpass, simultaneous ground truth samples were not collected for all lakes whose satellite fingerprints are shown in Figure 83. However, for Prairie Lake, the phytoplankton are known to be a mixture of blue-green and green algae, consistently heavy from year to year. The actual satellite fingerprints for the green and blue-green algae in Prairie Lake compare very well to the expected satellite signal for a lake containing a mixture of blue-green and green algae.*

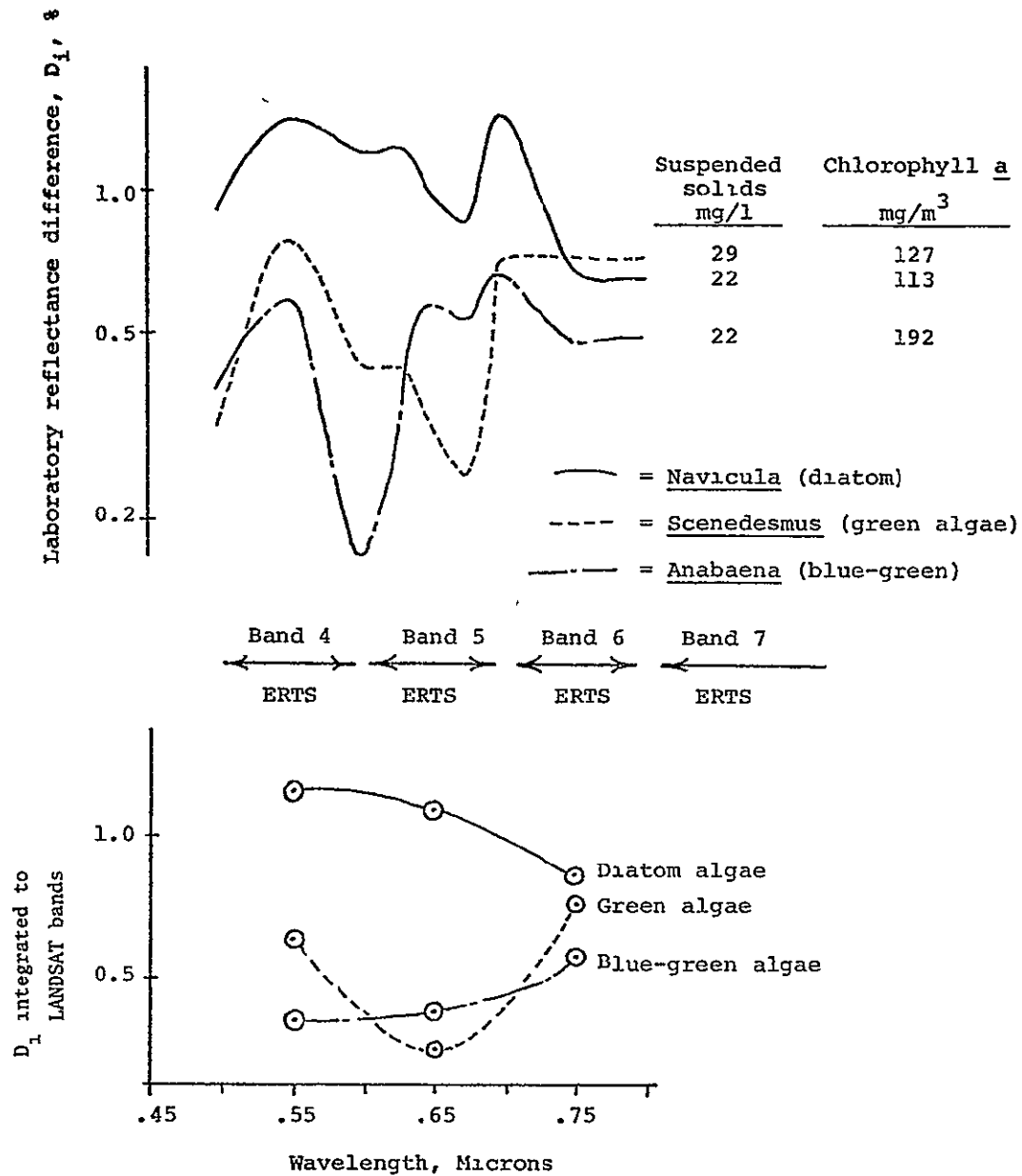
D EXAMPLE 4. THE CASE OF PRAIRIE LAKE FROM SATELLITE TO GROUND

1. Locating Problem Lakes From Color Coded Satellite Maps

When the first water quality color categorized map for this project was produced by the Bendix-MDAS system in the winter of 1975 it was apparent that the quality of water was associated with the type of landcover in the watersheds of the lakes.

* Appendix F gives a correlation between MDAS color coded maps and standard water quality parameters for 55 lakes which contain different amounts of algae in clear and tannin (humic) water.

FIGURE 81. Laboratory Reflectance Differences For Three Types Of Cultured Algae. Lower Curves Are Lab Values Integrated To Sensitivity Of Bands 4, 5, And 6 Of LANDSAT.



ORIGINAL PAGE IS
 OF POOR QUALITY

FIGURE 82. Laboratory Reflectance Differences, D_1 , For Two Types Of Cultured Algal Mixtures. Lower Curves Are Lab Values Integrated To Sensitivity Of Bands 4, 5, and 6 Of LANDSAT.

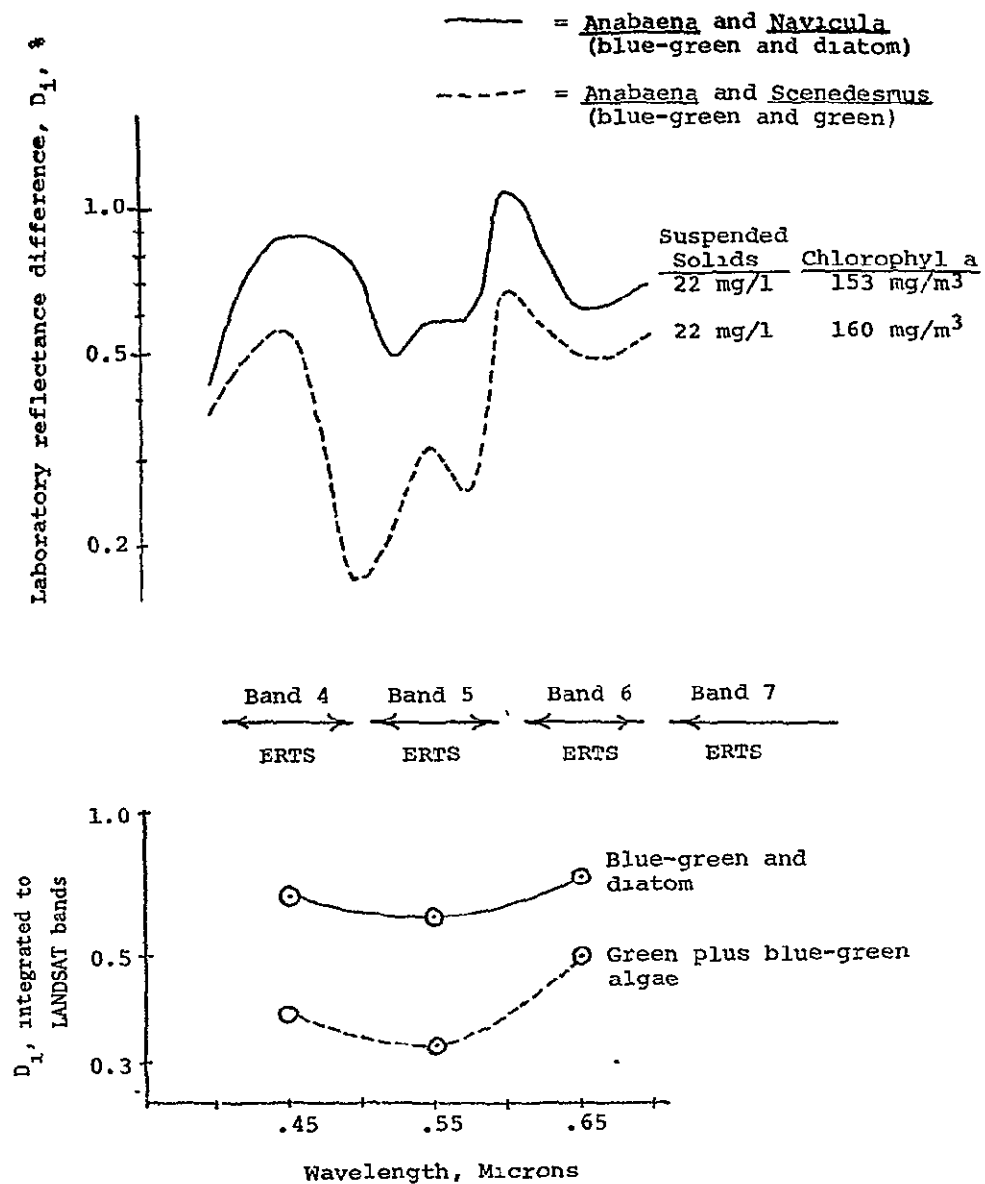
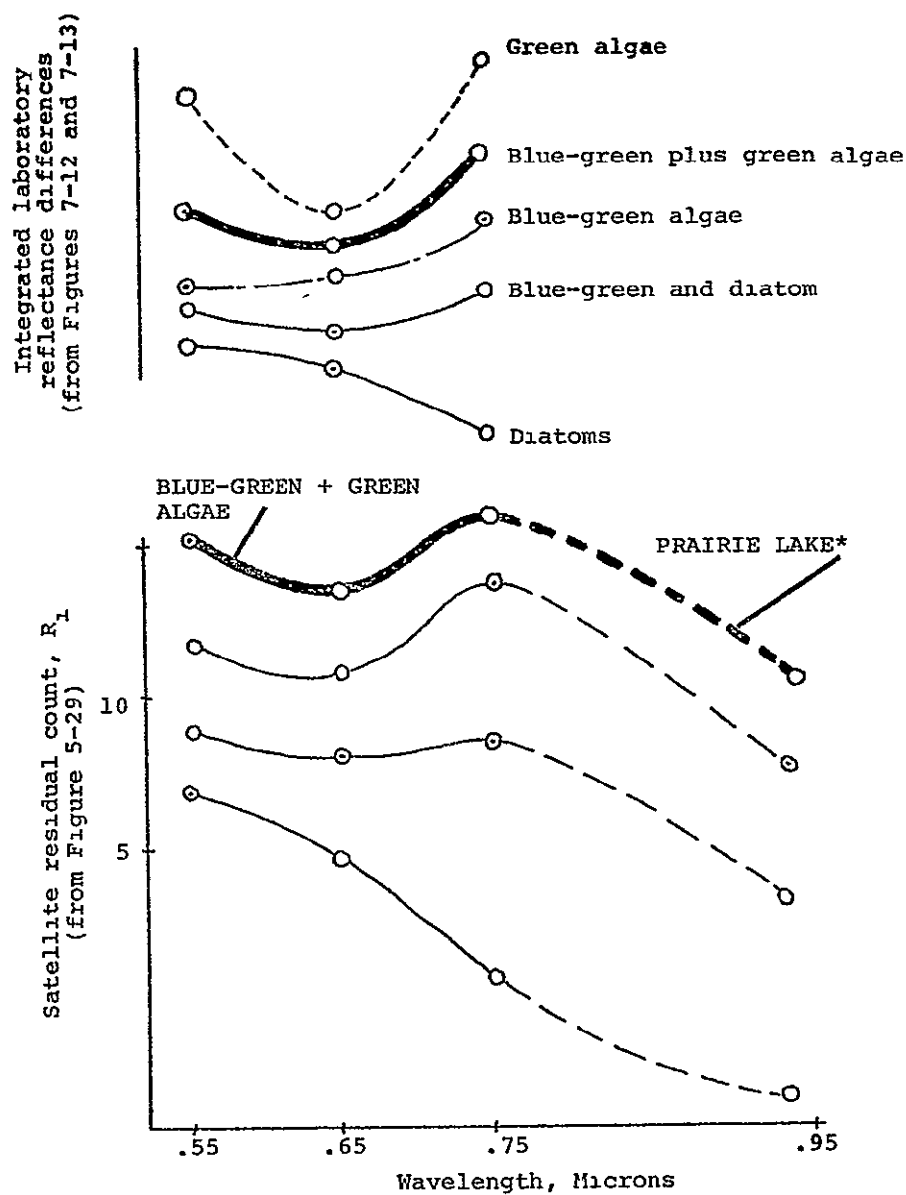


FIGURE 83. Integrated Laboratory Reflectance Differences For Algal Types Compared To LANDSAT Signal For Different Algal Lakes.



*Lake with heaviest algal concentration in northwestern Wisconsin as indicated by analysis of LANDSAT data

The clearest lakes in the area shown in Figure 84 appear dark and are on or near the Chippewa Indian Reservation, such as Lac Court Oreilles. This is probably because the watersheds of these lakes are essentially all forestland and nutrient runoff is low.

However, in the farmland beginning about 30 miles to the southwest near Rice Lake and Prairie Lake, most of the lakes contain medium to heavy algae. This is probably due to the agricultural runoff in this area. Animal manure and commercial fertilizers on watersheds of these lakes provide greater amounts of phosphorus and nitrogen for generous growth of algae and lake weeds. Such mesotrophic and eutrophic lakes appear light in Figure 84.

Prairie Lake appears very light because it has extremely heavy concentrations of algae — significantly higher than any of the other lakes. There were some medium algal pixels indicated on the south end of Prairie Lake but most of the lake was indicated as heavy algae. In fact, the algal concentration was so high on the north end of the lake that the computer failed to classify it as water and it was printed out as black (Figure 85). Skylab color and color IR photographs also confirmed that the green-colored algal concentration was much higher on the north end.

2. Low Altitude Photography and Observations

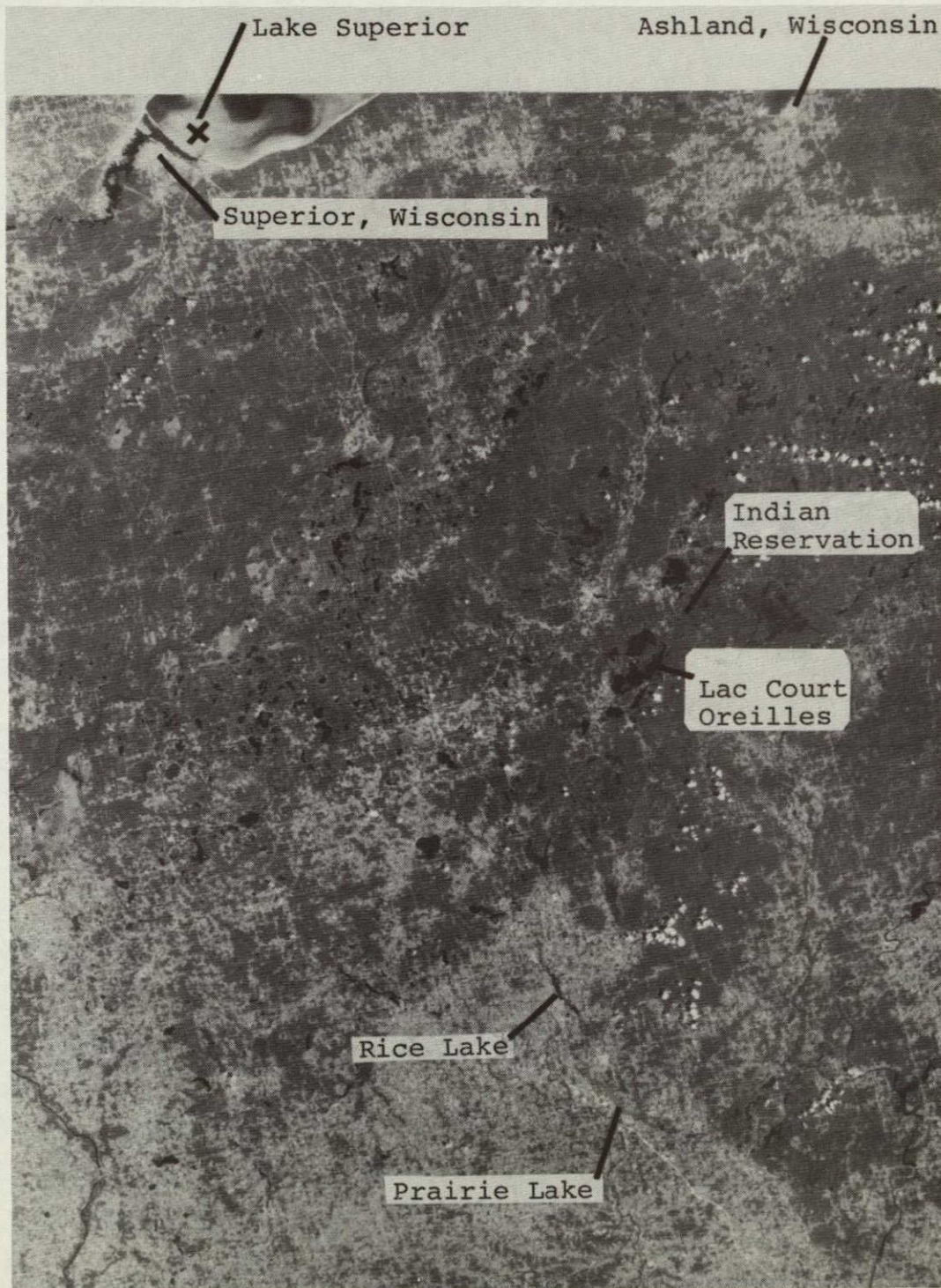
With Prairie Lake being thus pinpointed as a lake meriting intensive study, aerial observations were made; color and color IR photos of the lake were obtained in August 1975 during peak algal growth and in the spring of 1976 during maximum water clarity.

This lower altitude aerial work revealed that the heaviest algal concentrations occurred at the mouth of a short but relatively large-volume stream, Rice Creek, that flowed into the north end of the lake. Historical research revealed that the wild rice that once grew in this creek was well known, and was fought over by the Sioux and Chippewa Indians. Then the white man built a dam (which killed the wild rice) and began grazing cattle in and along the banks of the creek.

Still lower level aerial observations and 35 mm photos taken from the aircraft window in the spring of 1976 revealed that most of the water from Rice Creek apparently originates in a geological depression at the base of a rather high hill. This depression contains a swamp. On the west side of the swamp is the hill where cattle could be seen among the trees. Cattle paths showed that cattle crossed from the west bank to a large feeding area with barns and silos located on the east bank of Rice Creek.

The cattle yard around this feeding area drained into the adjacent swamp and a large cattle herd could be seen in the feeding area, in the swamp, and on the opposite side of the swamp (Figure 86). Some cows were seen wading in the shallow water of the creek. With the clear water of early spring, well defined cow paths were visible crossing Rice Creek and in some cases going several hundred feet down the center of the stream (Figure 87). The cows evidently ate the tons of fodder in the feed area on the east bank of the stream and deposited the resulting waste into the swamp and stream and onto the east and west bank that drained directly into Rice Creek.

FIGURE 84. LANDSAT Scene Of Northern Wisconsin Taken In August 1972. Red Energy — Band 5.



ORIGINAL PAGE IS
OF POOR QUALITY

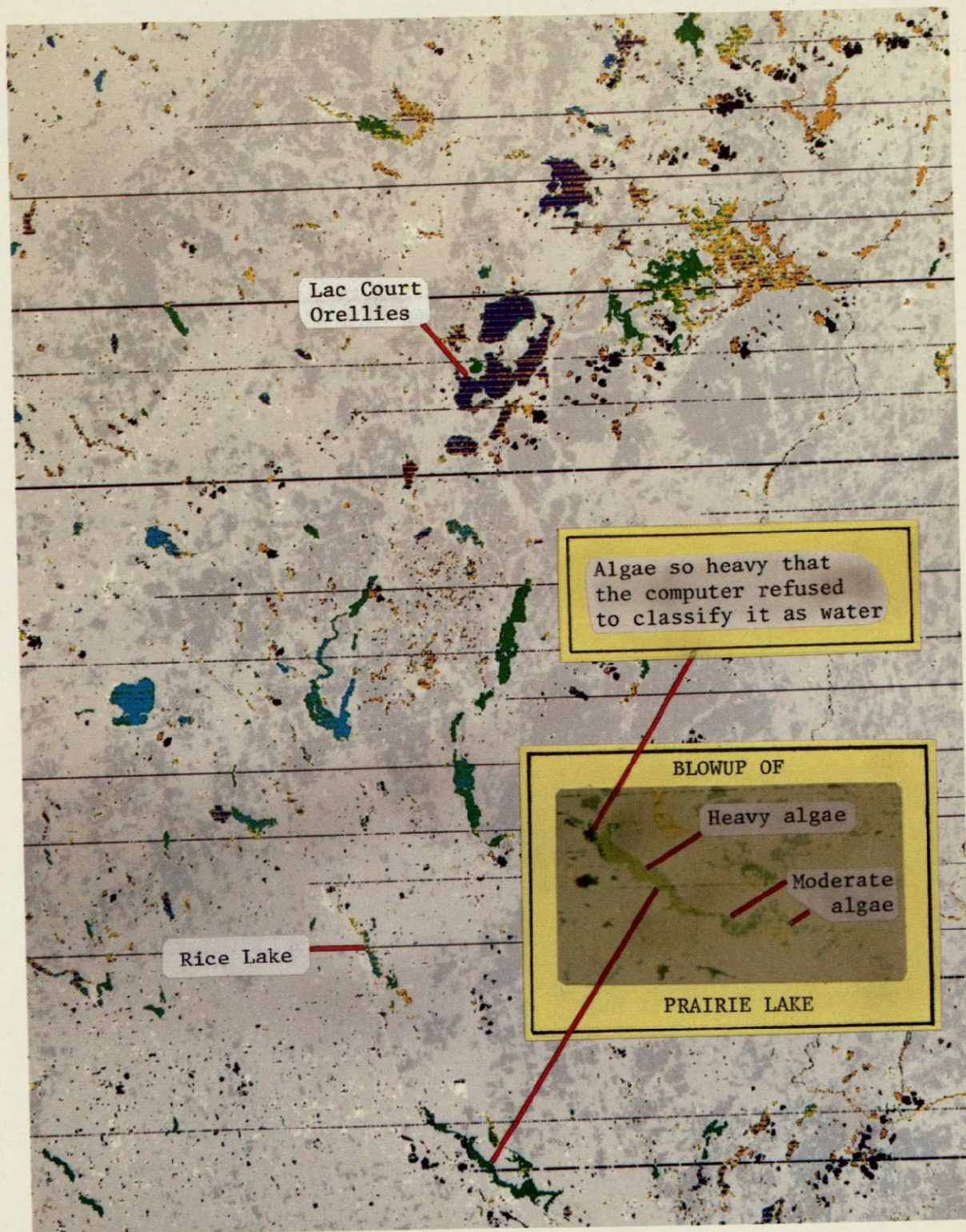


FIGURE 85. Bendix MDAS computer color categorized printout from multispectral analysis of LANDSAT data for a portion of northern Wisconsin. Note Prairie Lake. Date of imagery, 28 August 1973.

PRECEDING PAGE BLANK NOT FILMED

Color code for Figure 85—Bendix MDAS color categorized printout from analysis of multispectral LANDSAT data for a portion of northern Wisconsin.

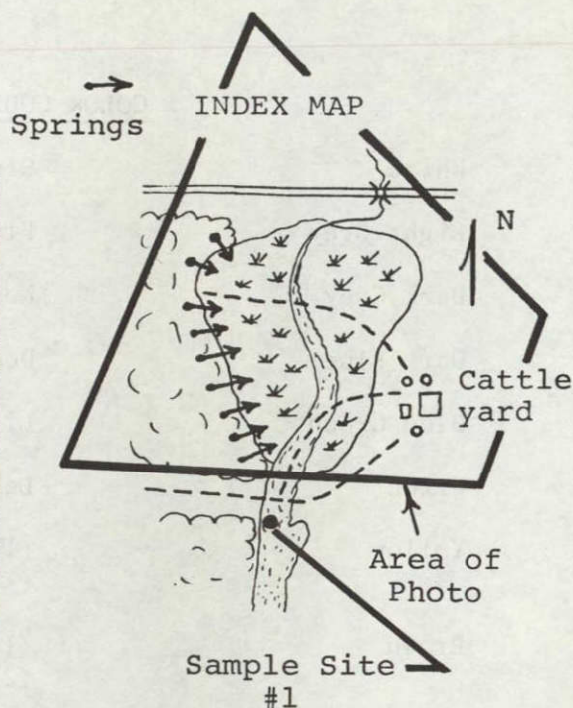
COLOR CODE

White	Cleared man-made features—towns, roads, etc.
Light Grey	Fields
Dark Grey	Woods
Dark Blue	Deep, clear water
Blue Green	Light to moderate algae in deep nonhumic water
Green	Lakes with moderate to heavy algae
Yellow	(1) Bottom showing in lakes (2) Silt in water
Brown	(1) Humic lakes (2) Mud bottom and grass in shallow humic lakes (i.e., rice beds) (3) shadows of clouds
Black	Unclassified: clouds, etc.

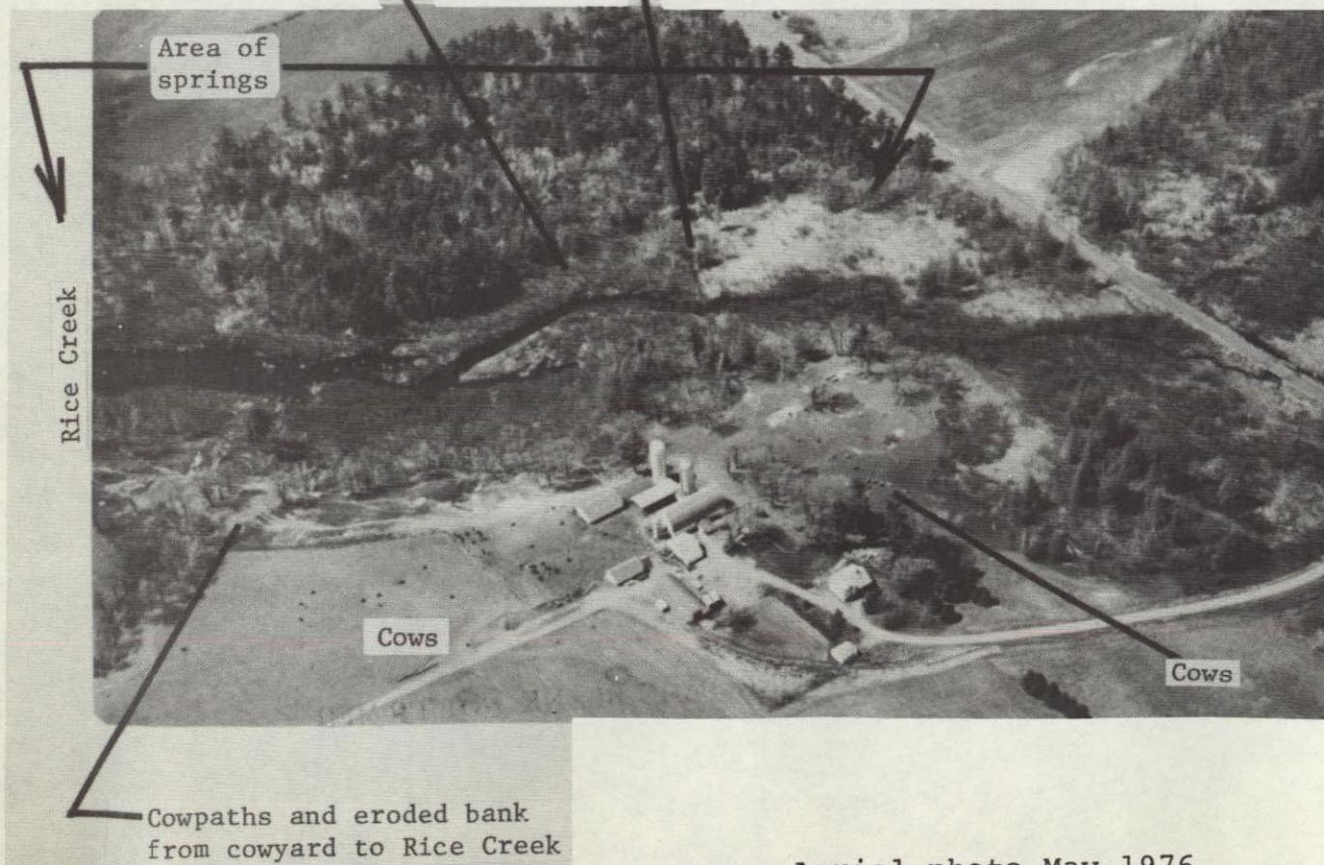
PRECEDING PAGE BLANK NOT FILMED

FIGURE 86. Cattle Yard Encompassing The Springs Of Rice Creek That Runs Into The North End Of Prairie Lake.

Cow in springhole
August, 1976

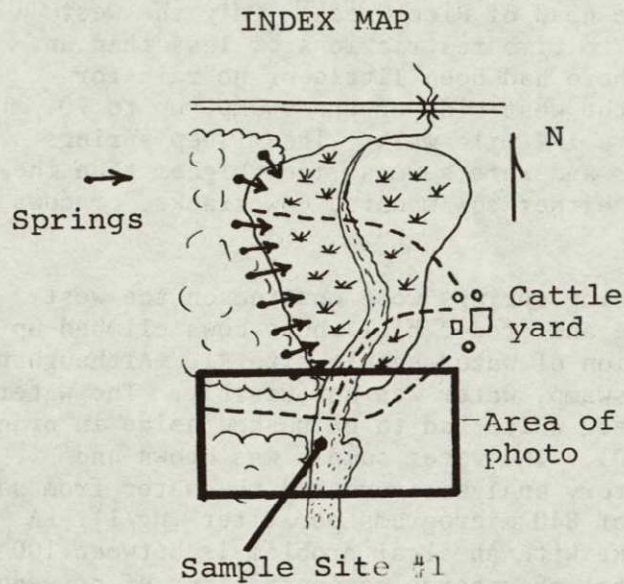


Corduroy road
and cowpath across
Rice Creek



Aerial photo May 1976
- 35mm handheld -

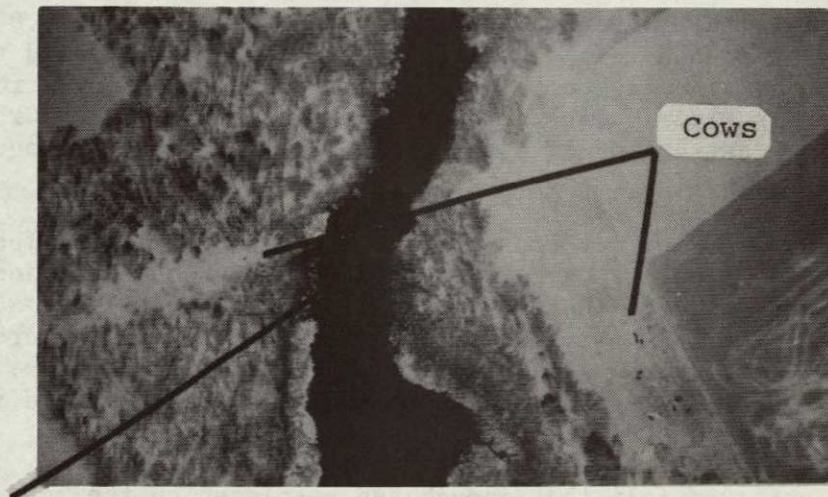
FIGURE 87. Use Of Green Energy In May To Penetrate Water And Show Cow Paths In Rice Creek.



Color infrared aerial slide taken in May 1976 and copied with black and white film using red and blue filters to show images formed by IR and green energy respectively.

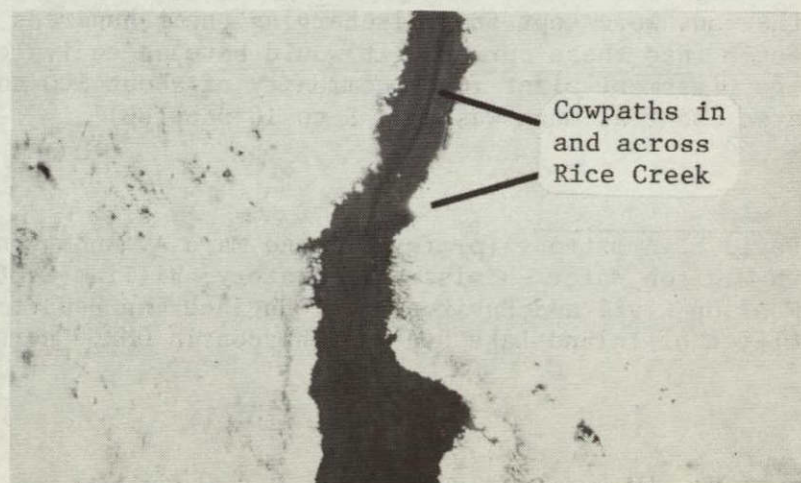
ORIGINAL PAGE IS
OF POOR QUALITY

Color IR photo copied with red filter (i.e., infrared energy in field)



SAMPLE SITE #1

Color IR photo copied with blue filter (i.e., green energy in field)



3. Collecting Ground Truth at Prairie Lake and Rice Creek

In late August 1976 when maximum algal and other biomass were expected, James P. Scherz visited the swamp at the head of Rice Creek. Only the west bank of the swamp was field-checked due to time restrictions of less than an hour. The weather had been very dry, there had been little or no rain for weeks. Yet at the base of the hill on the west side of the swamp, up to 70 seep spring holes were counted in about a 1/4 mile walk. These seep springs were about 5 to 10 feet or larger across and were several feet higher than the water level of the swamp. They all had either cow manure, cow tracks, or cows and horses wading in them (Figure 88).

In addition to the seep springs, 12 running springs were counted on the west bank. South of the tree area was a bare and eroded hill where cows climbed up and down. This area was near the location of water sample site #1. Although the creek is quite wide where it meets the swamp, water was not visible. The water surface was covered with a mat of duckweed which had to be pushed aside in order to get a water sample (Figures 89 and 90). The water sample was brown and smelled like decaying cow dung. Laboratory analysis revealed the water from sample site #1 had a total phosphorus content of 840 micrograms per liter ($\mu\text{g/l}$). A high level of total phosphorus for a lake with an algal problem is between 100 and 200 $\mu\text{g/l}$. Most eutrophic lakes have total phosphorus concentrations of between 30-100 $\mu\text{g/l}$.

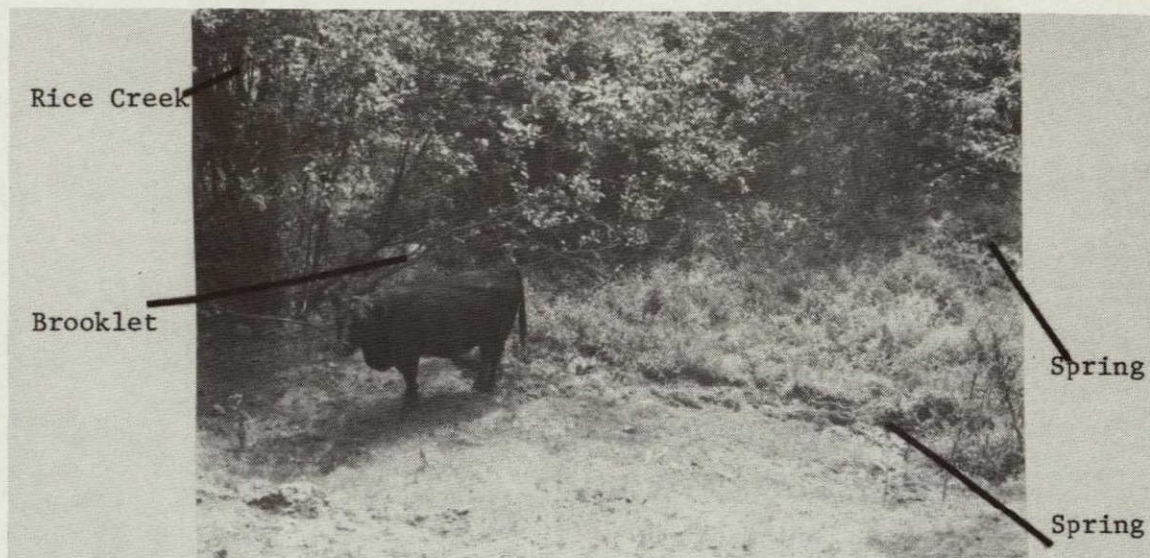
The total nitrogen content from sample site #1 was 16.8 mg/l. The total nitrogen content for untreated municipal sewage can be expected to vary between 20 and 40 mg/l. The high concentration of phosphorus and nitrogen decreased further south in Prairie Lake at greater distances from Rice Creek (Figure 91). However, the concentrations of total phosphorus and total nitrogen anywhere in Prairie Lake was called "exceedingly high."*

Time did not permit crossing the swamp to the cattle feed area on the east side of Rice Creek, but a corduroy road was sighted that aided the cows in crossing from one side of the muddy swamp to the other (Figure 86). Sixty cows were counted on the west side of Rice Creek alone. More were seen on the east side near the feeding area. Since the ground truthing trip, local people have said that springs are also on the east side of Rice Creek directly below the eroded bank where the cattle feed.

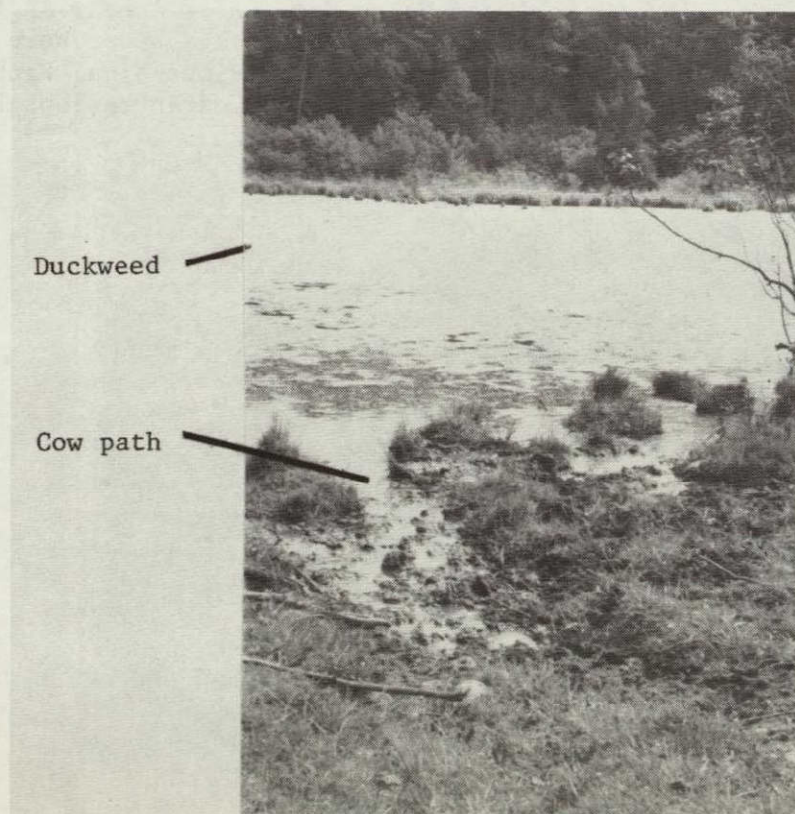
The observer felt that enough had been seen on the west side alone to indicate the effect that this cattle yard had on the water of Rice Creek and Prairie Lake. If the cows were kept from discharging their hundreds of pounds of waste a day directly into these springs, it would have an equivalent effect of building a sewage treatment plant for a community of about 500 to 1,000 people. (One cow creates about as much waste as 5 to 10 people.)

* David E. Armstrong (professor) and Marc A. Anderson (assistant professor), UW-Madison Water Chemistry Laboratory; William C. Boyle (professor), UW-Madison Civil and Environmental Engineering Department; and Donald R. Winter, Office of Inland Lake Renewal, Wisconsin DNR: personal communication.

FIGURE 88. Some Effects Of Cows Near And In Rice Creek. August 1976.



Cow by spring hole which runs into Rice Creek near Sample Site #1. Rice Creek is on top of photo through trees.



Cow path into Rice Creek near Sample Site #1

FIGURE 89. Cows On West Bank Of Rice Creek Near Sample Site #1. Duckweed Mat Shown On Surface Of Water. August 1976.



FIGURE 90. A View Of Rice Creek From Sample Site #1 Looking South Toward Prairie Lake. A Dense Mat Of Duckweed Makes Rice Creek Appear As A Green Field. Total Phosphorus Concentrations From This Water Were Several Times Higher Than Expected From Other Lakes With Serious Algal Problems. Water From Beneath The Duckweed Had Total Nitrogen Concentrations Between 50% and 75% As High As Expected From Municipal Sewers.

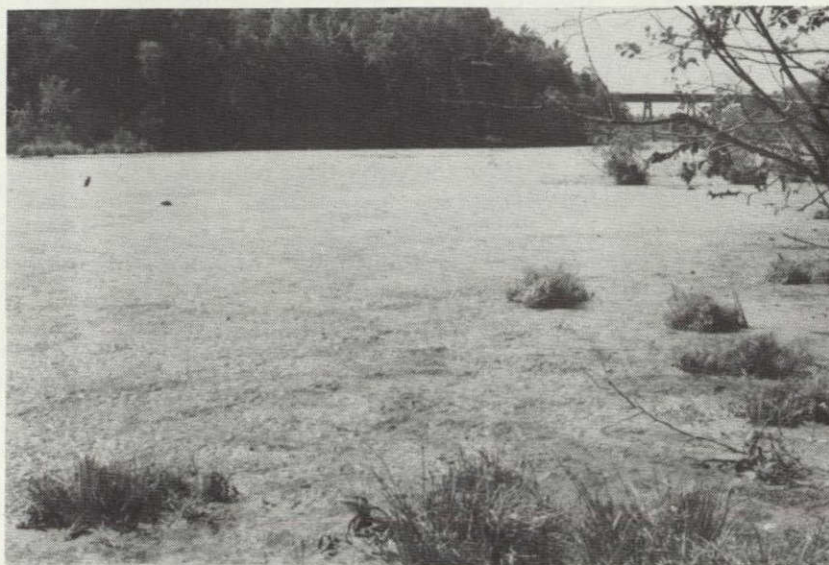
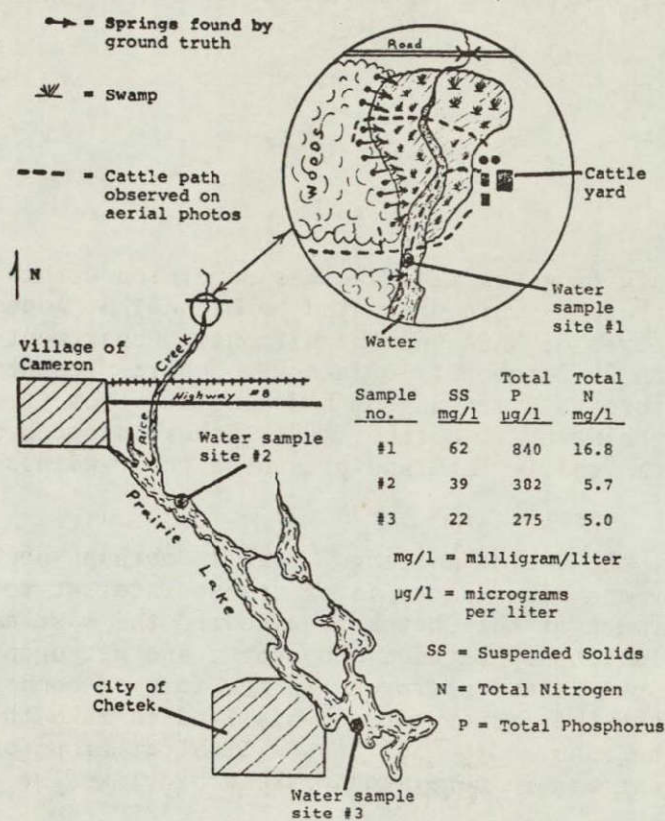
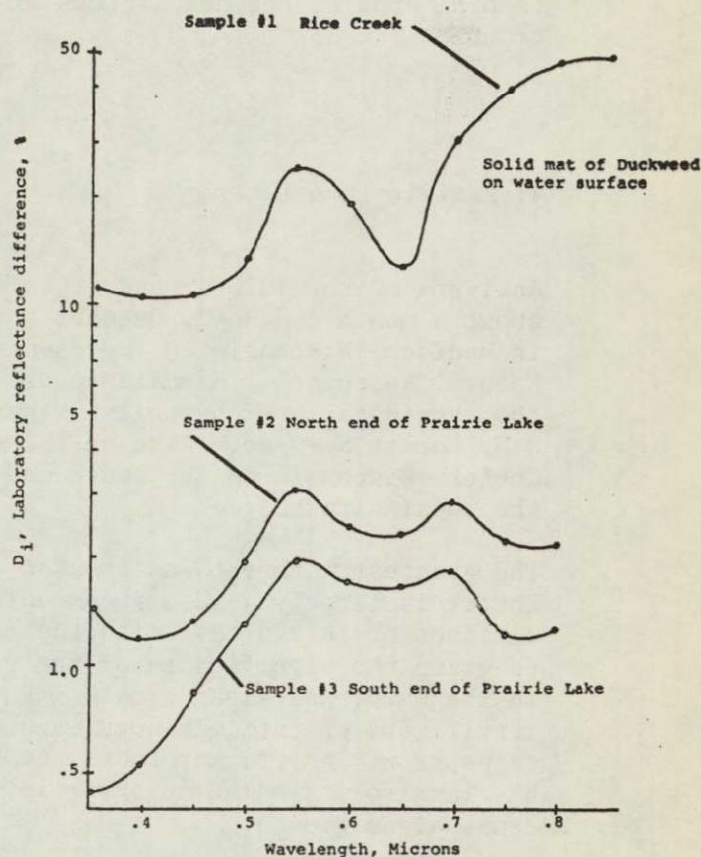


FIGURE 91. Map And Lab Data Relating To Water Samples Collected From Prairie Lake On 17 August 1976.



Sketch showing Prairie Lake, and cattle yard on Rice Creek.



Laboratory reflectance differences for water samples from Prairie Lake and Rice Creek.

The Prairie Lake area has been well known for recreation over the past 100 years; fishing and resort-related activities contribute a large part of the income to the area. In efforts to improve the water quality, the residents in years past had treated the lake with chemicals. This was discontinued in recent years because it apparently did no good. Chemicals treat only the symptoms of the problem. Regardless of the chemical treatment in any one year, unless the source of pollution is cleared up, the algae will come back the following year. Preventing nutrient pollution from entering Prairie Lake at places like Rice Creek would treat the cause of the problem.

ORIGINAL PAGE IS
OF POOR QUALITY

The case of Prairie Lake illustrates that remote sensing, used correctly, can be a tremendously powerful tool for those charged with managing water resources. From a Bendix MDAS color categorized map of an area 100 miles on a side, several lakes (out of hundreds) were pinpointed as having bad algae problems. Prairie Lake had the worst problem and remote sensing revealed the north end of the lake to be worse than the south. Low altitude remote sensing showed that a cow feeding area at the head waters of Rice Creek was an important source of the trouble.

4. Prairie Lake Later

Analysis of the 1976 ground truth data from Prairie Lake was completed within about a month and on 20 October the results were presented by Michael S. Adams in Madison, Wisconsin to representatives of NASA and the Wisconsin Department of Natural Resources. Simultaneously on 20 October 1976 James P. Scherz presented the same data in Minneapolis, Minnesota to a meeting of hydrologists from the U.S. Forest Service. Also on the evening of 20 October 1976, Scherz stopped at Chetek, Wisconsin on the south end of Prairie Lake and presented the findings to the local citizens.

The greatest interest was created at the Chetek meeting. This is perhaps because Chetek is largely a resort community and clear water is of utmost interest to citizens of this area. Also the farmers of the Chetek area seemed the most able to grasp the significance of the relationship between phosphorus and nitrogen in the water and algae growth. Phosphorus and nitrogen, in the form of commercial fertilizers or cattle manure, are what the farmer puts on his land to make the crops grow. Any farmer knows how the manure from 100 cows will alter crops on his land so it seemed no surprise that manure put into a lake would likewise cause algae growth.

The farmers seemed to have no trouble comprehending that trophic classification of lakes by satellite data must be done in late summer just as the weather begins to cool. If a farmer wished to determine which farm field had the most nutrients and could produce the most biomass (say, corn) he would not measure the height of the corn in May, June, or July while it was still growing nor in late September or October after it had died. The height of the corn should be measured in late August or early September after it had grown as much as possible and just before it begins to die.

By the end of the October 20 meeting at Chetek many people, after seeing the LANDSAT, SKYLAB, and aircraft images of the heavy algae at the north end of their lake, and the slides of cows in the springs flowing into the north end of the lake, seemed satisfied as to the probable cause of a major portion of their problem and were already talking of how to remedy the situation.

ORIGINAL FILED
OF POOR QUALITY

Leaders in this work to improve the lake were Reg. P. Nelson (realtor from Chetek), Gilbert Hagin (businessman in Chetek), James Dennis (biology teacher at Chetek High School), and the Chetek Lions Club.

Contact was also soon made with Roland H. Brownlee, Associate Professor of Business and Economics at the University of Wisconsin Center in Barron County. Professor Brownlee is Executive Director of a citizens' organization known as OASIS 2000, which sponsored meetings and radio programs concerning the cows in the springs of Prairie Lake and what to do about them.*

During the spring and summer of 1977, local citizen groups, in conjunction with the Wisconsin Department of Natural Resources and the Soil Conservation Service, and with the cooperation of the farmer who owned the cows, constructed fences to keep the cows out of the springs. The farmer was very cooperative and with the assistance of Gene Hausner of the Soil Conservation Service, Barron County, diversion ditches were constructed near the feedlot to help keep the cattle manure from draining into Rice Creek.

Roland Brownlee then asked Scherz to exactly repeat the sampling one year later and to analyze the samples in an identical manner to see if there was any change in water quality.

On 17 August 1977, one year and one day after the 1976 samples were collected, Scherz revisited the springs of Rice Creek and the water sample sites on Prairie Lake.

a. Sample Site #1

At first the walk from the road through the white pine woods to the springs seemed much as it had in August 1976. But upon close inspection the cattle paths seemed less pronounced than the year before. As the first spring was approached cow manure was still seen on the hillside near the spring and to a certain extent in the spring itself; but this was old and not fresh manure. Tracks were still found in the spring but they were made by deer and racoons and not cows. As other springs were visited it was obvious that the entire area was beginning to take on the appearance of a park rather than a cow yard. Freshwater brooklets from the springs ran between orange and green jewelweeds where a year before they ran through cow wallows.

Near Sample Site #1 where in 1976 there had been a sandy and eroded bank leading down to Rice Creek, in 1977 there was grass almost knee high. It was sparse grass but it was grass nevertheless (see Figure 92).

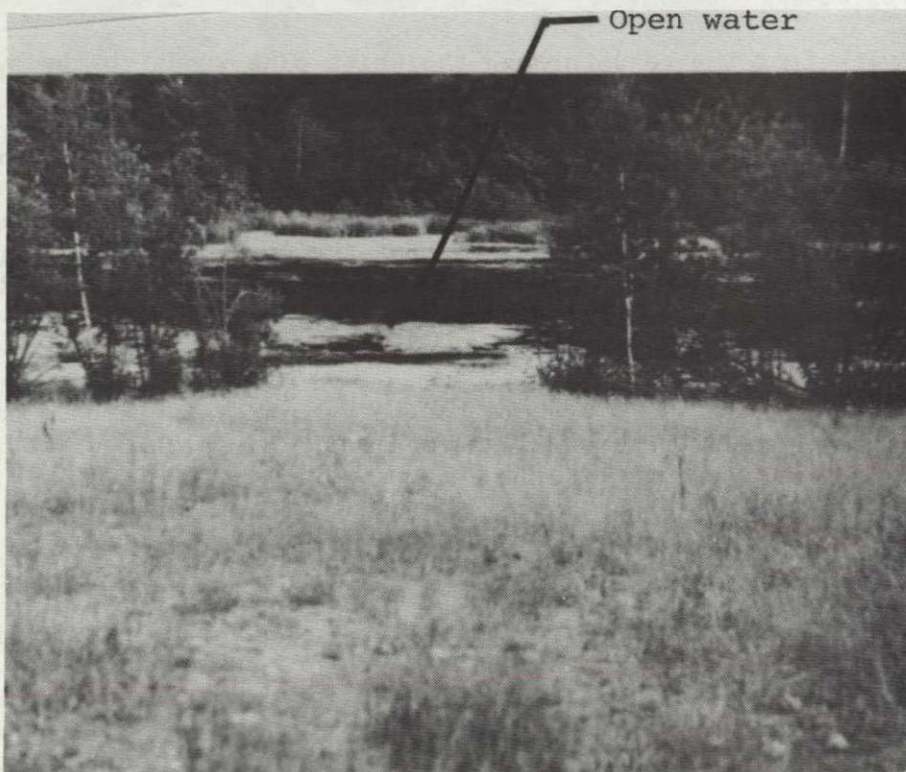
* OASIS 2000 is a nonprofit citizens' organization dedicated to preserving and enhancing the quality of life in northwest and north-central Wisconsin toward the year 2000. This organization sponsors radio broadcasts each Saturday morning on the Rice Lake radio station WJMC. These programs are produced jointly by Roland Brownlee and Wayne Arntson, Associate Professor of Chemistry who have also collaborated for several years on the production of methane from cattle manure.

FIGURE 92. Looking East To Sample Site #1 On Rice Creek. Note The Change From 1976 To 1977.



Filamentous algae
and duckweed

17 August 1976



Open water

18 August 1977

In 1976 the water in Rice Creek was completely covered with filamentous algae and duckweed. Then almost no open water was visible and the water below the algal mat was chocolate-brown in color and stank of cow dung. But a year later on 18 August 1977 duckweed covered only about 50% of the creek surface (see Figure 93). Wading was required to obtain the water sample. This stirred up much brown sediment in the bottom muds of Rice Creek. The nutrients in these bottom muds have accumulated over many years and will take years to leach out. Yet where the bottom was not stirred up the water was quite clear. Analysis of the water sample collected on 18 August 1977 at Site #1 revealed the following:

Total Suspended Solids:	3 mg/l in 1977 compared to 62 mg/l in 1976
Total Phosphorus:	50 μ g/l in 1977 compared to 840 μ g/l in 1976*
Total Nitrogen:	1.4 mg/l in 1977 compared to 16.8 mg/l in 1976.

In 1977 the values of suspended solids, phosphorus, and nitrogen were 5%, 6%, and 8%, respectively, of the 1976 values. The situation in 1977 was obviously greatly improved over 1976.

In one of the open patches of water in Rice Creek near Sample Site #1, there were even 30 to 40 stalks of wild rice growing. None had been seen in 1976. Wild rice requires sunlight to reach the bottom of the water and the mat of filamentous algae and duckweed that was present in 1976 would not allow such rice to grow. Much more improvement is necessary before Rice Creek will again produce rice beds of the type fought over by the Chippewa and Sioux Indians for more than 150 years before the White settlers came; but 30 to 40 stalks of wild rice in 1977 is a great improvement over none in 1976.

b. Sample Site #2

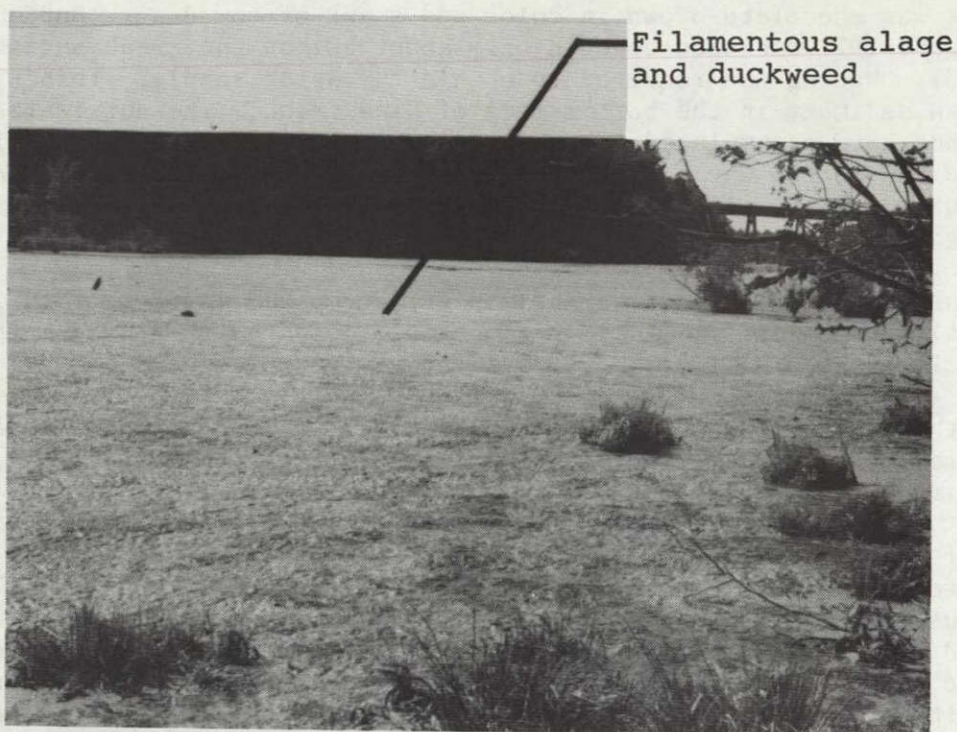
At Sample Site #2 on the north end of Prairie Lake significant algae was present but considerably less than in 1976, and no worse than one would expect in numerous other lakes in Wisconsin that are surrounded by farmland and cottages. Analysis of the water sample collected on 18 August 1977 at Site #2 revealed the following:

Total Suspended Solids:	28 mg/l in 1977 compared to 39 mg/l in 1976
Total Phosphorus:	250 μ g/l in 1977 compared to 382 μ g/l in 1976
Total Nitrogen:	2.8 mg/l in 1977 compared to 5.7 mg/l in 1976.

In 1977 the values for suspended solids, phosphorus, and nitrogen were 72%, 65%, and 49%, respectively, of the 1976 values.

* μ g/l = microgram per liter; 1000 μ g/l = 1 mg/l.

FIGURE 93. Looking South On Rice Creek From Sample Site #1. Note Change From 1976 To 1977.



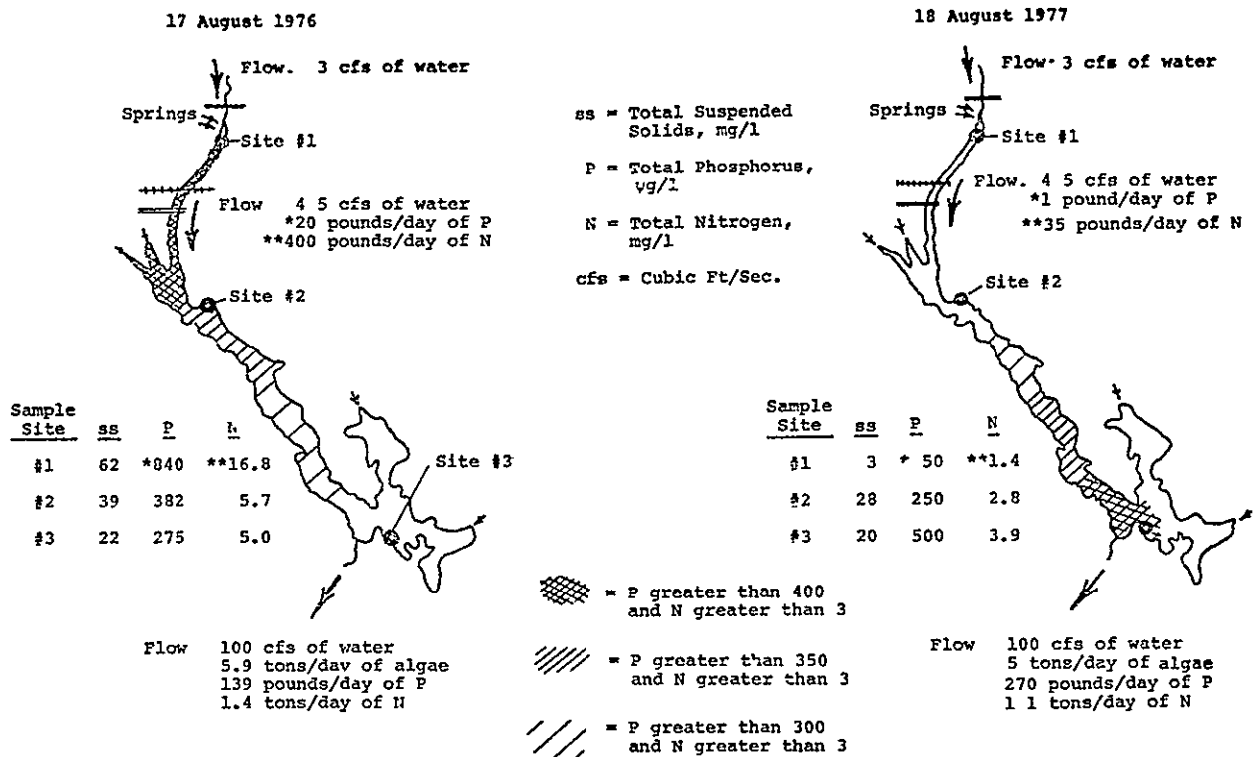
17 August 1976, P = 840 $\mu\text{g/l}$, N = 16.8 mg/l



18 August 1977, P = 50 $\mu\text{g/l}$, N = 1.4 mg/l

Corresponding calculations for 1976 are 5.9 tons/day, 139 pounds/day, and 1.4 tons/day, respectively, (see Figure 94). Therefore it seems that the discharges of algae and nutrients out of the lake in 1977 were approximately the same as in 1976, except for an increased discharge of phosphorus

FIGURE 94. Comparison Of 1976 And 1977 Water Quality Data And Approximate Flow Calculations.



In early September 1977, several days after a period of heavy rain, Scherz measured the flow of Rice Creek emptying into the north end of Prairie Lake as varying from 4 to 6 cubic feet/second. The flow of Rice Creek above the springs was 3.0 to 3.3 cubic feet/second.* There was about 1 pound/day of phosphorus, and 35 pounds/day of nitrogen going into the north end of Prairie Lake due to Rice Creek on 18 August 1977. This compares to an estimate of 20 pounds/day and 400 pounds/day, respectively, for 17 August 1976 (see Figure 94).

From the rough analysis of the sample data we can see that in 1977 the water on the north end of the lake has less nutrients than the south end. Also aerial observations in the late summer of 1977 indicated that the algae concentrations were heavier on the south end than on the north end. The high concentrations of phosphorus on the south end of the lake on 18 August 1977 at Sample Site #3 indicated that an even thicker algal bloom was possible there later into the period of optimum remote sensing for trophic classification (late August to early September). This algae bloom occurred in early September and water transparency as measured by the Secchi disc on 5 September 1977 was 8 inches on the south end of the lake as compared to 33 inches on the north end.

Once the heavy nutrient load from Rice Creek was removed, it appears that the water flow from the north end of the lake began flushing nutrients to the south. Such nutrients have accumulated over many years and, of course, will take years to flush out.

If there are less nutrients running into the lake than run out then the water quality naturally will improve. And in the north end of Prairie Lake, this is what appears to be happening. Certain stagnant bays on the north end of the lake still have heavy concentrations of algae but in the open lake there was much less algae in 1977 than in 1976. In addition to this being indicated by the water sample data and Secchi disc readings, one can observe the improvement by looking at the water from a boat, dock, or from an aircraft, and presumably from LANDSAT images, although no images from late summer 1977 had been acquired at the time of this report.

We must point out, however, that the cows in the springs of Prairie Lake were just one of the several possible sources of nutrients to the lake and that the data from one year are not enough. But if the present trend continues the water in Prairie Lake should continue to improve at least to a state where other sources of nutrients prevent further improvement. What appears to be a fantastic improvement in the water at the far north end of Prairie Lake in one year is primarily due to the interest and positive action of citizens and officials around the Prairie Lake area. LANDSAT imagery and aerial photography helped in presenting compelling evidence as to the nature of the problem.

* Terry Moe, Department of Natural Resources, Eau Claire, Wisconsin, also reports that 1973/1974 data gives the flow above the springs as 2.4 to 3.2 cubic feet/second.

ACKNOWLEDGMENTS

In the preparation of this report, Michael S. Adams, Associate Professor of Botany, was assisted by Todd D. Gustafson, David L. Haselow, and Billie Lofland.

Frank L. Scarpace, Assistant Professor of Civil and Environmental Engineering/Environmental Studies, specialized in equipment development and the use of the Princeton Electronic Products, Inc. (PEP) terminal for the analysis of aerial photos and satellite data. He was assisted by David L. Haselow and Kenneth W. Holmquist.

James P. Scherz, Professor of Civil and Environmental Engineering, focused on the interactions of energy with water, the atmosphere, and remote sensing detectors. He extrapolated this knowledge from the laboratory and boat level analysis to satellite data analysis and to the Multispectral Data Analysis System (MDAS) mapping system. Scherz was assisted in this work by Douglas R. Crane, William L. Johnson, Steven A. Klooster, Gregory L. Rinehardt, Alan R. Stevens, and John F. Van Domelen. Scherz also supervised the preparation of the final report with assistance from James F. Thorne.

William J. Woelkerling, former Assistant Professor of Botany, specialized in work with algal detection in lakes and was assisted by Ronald R. Rassner, James F. Thorne, and Christine R. Visser. Woelkerling was in charge of the organization and planning of this report until he moved to Australia in July 1976.

Others who contributed to this report are as follows:

Francis H. Schraufnagel, Deputy Director of Bureau of Water Quality, Wisconsin Department of Natural Resources (DNR) and many other persons from Wisconsin state agencies helped gather and analyze water samples. Some DNR funds contributed to maintenance of airplanes used for data gathering.

James L. Clapp, Professor of Civil and Environmental Engineering and Director of the IES Environmental Monitoring and Data Acquisition Group (EMDAG) and his staff gave administrative support throughout the project. Lawrence T. Fisher, Program Coordinator, and Scarpace jointly developed the PEP computer software for the LANDSAT image analysis and coordinated work between the state agencies and the University of Wisconsin-Madison.

Robert Rogers of the Bendix Corporation, Ann Arbor, Michigan, was principal investigator for National Aeronautics and Space Administration (NASA) Grant NAS 5-20942 involving the adaptation of the MDAS image analysis equipment for lake trophic classification. Woelkerling, Adams, and Scherz helped bridge the gap between the UW-Madison work and the operation of the MDAS equipment.

Kenneth Holtje of the U. S. Forest Service contributed aircraft and water analysis support for work on special humic lakes near Ely, Minnesota. Especially vital for the success of this research was the help given by the experts from the State Laboratory of Hygiene, UW-Madison Department of Civil and Environmental Engineering (Sanitary Section), and the UW-Madison Water Chemistry Laboratories for their analysis of water samples.

The investigators are also grateful to Donald Graff, formerly Professor of Civil Engineering, and William C. Boyle, Professor of Civil and Environmental Engineering, for their early work on the project and to Boyle's student, Lorne C. Gramms, for his laboratory work on algal reflectance. Michael Sydor, Associate Professor of Physics at the University of Minnesota at Duluth, helped by sharing his data on the red clay problem in Lake Superior. This help greatly facilitated the Wisconsin team's field work in relating laboratory data to satellite data. This collaboration also saved money that otherwise would have been spent on duplicate field trips and water analysis.

APPENDIX A

SOURCES FOR METHODS OF WATER QUALITY ANALYSIS USED AT THE
UNIVERSITY OF WISCONSIN-MADISON ON WORK DESCRIBED IN THIS REPORT

<u>Method</u>	<u>Source</u>
Turbidity	APHA* (1971)
Secchi disc depth	Hutchinson (1957)
Color	APHA (1971)
Suspended solids (also called volatile and nonvolatile solids)	APHA (1971)
Dissolved solids	APHA (1971)
Particulate Organic Carbon (POC)	Menzel and Vacarro (1964)
Total Organic Carbon (TOC)	Menzel and Vacarro (1964)
Dry weight	Strickland and Parsons (1972)
Chlorophyll <u>a</u>	Strickland and Parsons (1972)
Macrophyte dry weight and ash-free dry weight	Jackson (1958)
Total Kjeldahl nitrogen**	APHA (1971)
Total Phosphorus** (persulfate digestion-ascorbic acid method)	APHA (1971)

* American Public Health Association, Standard Methods for the Examination of Water and Wastewater (13th Edition).

** Even though these water quality parameters cannot be detected by remote sensing, they are included for their use in assessing total nutrient availability for biomass production

APPENDIX B

GENERALIZATIONS OF DEVELOPMENT PROCESS FOR COLOR FILMS

With color negative film the three layers contain dyes of yellow, magenta, and cyan. The dyes are formed by the oxidized developer reacting with a color coupler mixed into the emulsion. Silver grains of the upper or blue-sensitive layer are replaced by a yellow dye. Yellow light is the complement of blue light (yellow light is composed of green and red wavelengths). The black silver grains in the second or green-sensitive layer are replaced with a magenta dye. Magenta light is the complement of green light and is composed of blue and red wavelengths. The silver salts in the third or red-sensitive layer are replaced with cyan dye. Cyan light is the complement of red light and is composed of blue and green wavelengths. Thus, the color negative is a true negative because, where a color sensitizes the film, the complement of that color is produced on the processed color negative.

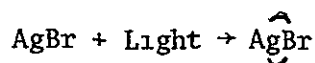
The film development process can be approximated by the following definitions and equations

Definitions

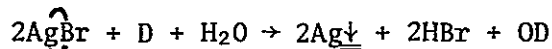
AgBr	=	Light sensitive silver salt (silver bromide)
$\widehat{\text{AgBr}}$	=	Weakened bond of silver bromide (latent image)
$\text{Ag}\downarrow$	=	Black silver image
HBr	=	Hydrogen Bromide
D	=	Developer
OD	=	Oxidized developer
Ye (color yellow)	=	Yellow color coupler
Ye (color magenta)	=	Magenta color coupler
Ye (color cyan)	=	Cyan color coupler
ODYe (color yellow)	=	Yellow dye
ODYe (color magenta)	=	Magenta dye
ODYe (color cyan)	=	Cyan dye

Reactions and Equations

The silver salt emulsion is exposed by light.



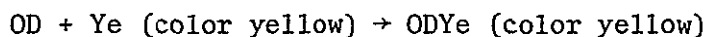
Upon development.



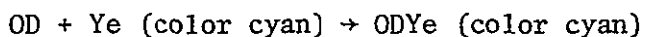
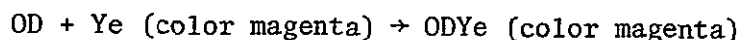
For a black and white image the 2HBr and the OD would be washed away, leaving the black Ag \downarrow to form the black and white image.

For color photography, however, the 2Ag \downarrow and 2HBr are washed away, leaving the oxidized developer, OD, which is used to make the three color dyes.

If a color yellow coupler had been mixed into the first layer when the emulsion was made, then this color coupler would combine with the oxidized developer to form a yellow dye:



Likewise for the other two layers



When white light is directed back through a finished normal color negative and exposes a similar three-layered printing emulsion, the color of the original object will result on the processed print. For example, where blue light struck the negative, a yellow dye is produced on the developed negative. When the yellow light from this negative is projected onto the print emulsion, the green and red sensitive layers of the print are energized. (Yellow light is composed of green and red wavelengths.) These layers change to magenta and cyan, respectively. The combination of magenta and cyan dyes produces the color blue which was the original color of the object (see Figures 95 and 96).

In summary, with color negative film, the silver salts of the appropriately exposed layers are developed and turn to a dye of the complementary color of the original object. The unused salts of the other layers are washed away. This negative is then used to expose a piece of color printing paper where the original colors of the object are formed. With the color reversal film, on the other hand, the partially developed film, itself, is reexposed to activate the complementary layers, and then the salts in the originally exposed layer are washed away. This is the same process as with a color negative and a color print except that both processes are done on the original film, the originally exposed salts being washed away, and the desired complementary colors being produced. This results in the original colors of the object on a color transparency.

FIGURE 95. Color Additive Process (Mixing Light). This Can Be Illustrated By Using Three Projectors Filtered Individually With Red, Green, And Blue Filters And Flashing Them On A Screen As Shown Below

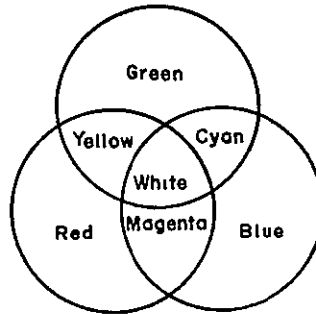
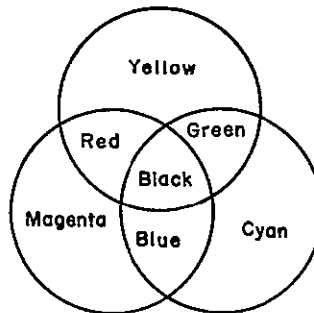


FIGURE 96. Color Subtractive Process (Mixing Pigments). This Can Be Illustrated By Taking Three Filters Of Yellow, Magenta, And Cyan And Overlapping Them, As Shown Below, Over A White Light



ORIGINAL PAGE IS
OF POOR QUALITY

APPENDIX C

CURVES FOR C_2 TO RELATE SATELLITE TO LABORATORY DATA

The laboratory spectral fingerprints for material in water are obtained from

$$D_1 = (\rho_{v_1} - \rho_{v_1})C_1 \text{ where } C_1 = \frac{1}{\rho_{PL}}$$

If the laboratory panel is BaSO_4 , ρ_{PL} is approximately 0.39 for all wavelengths and $C_1 = \frac{1}{0.39} = 2.56$.

The satellite spectral fingerprints for material in water are obtained from:

$$R_1'' = (\rho_{v_1} - \rho_{v_1})C_2 \text{ where } C_2 = H_0' \tau / \pi.$$

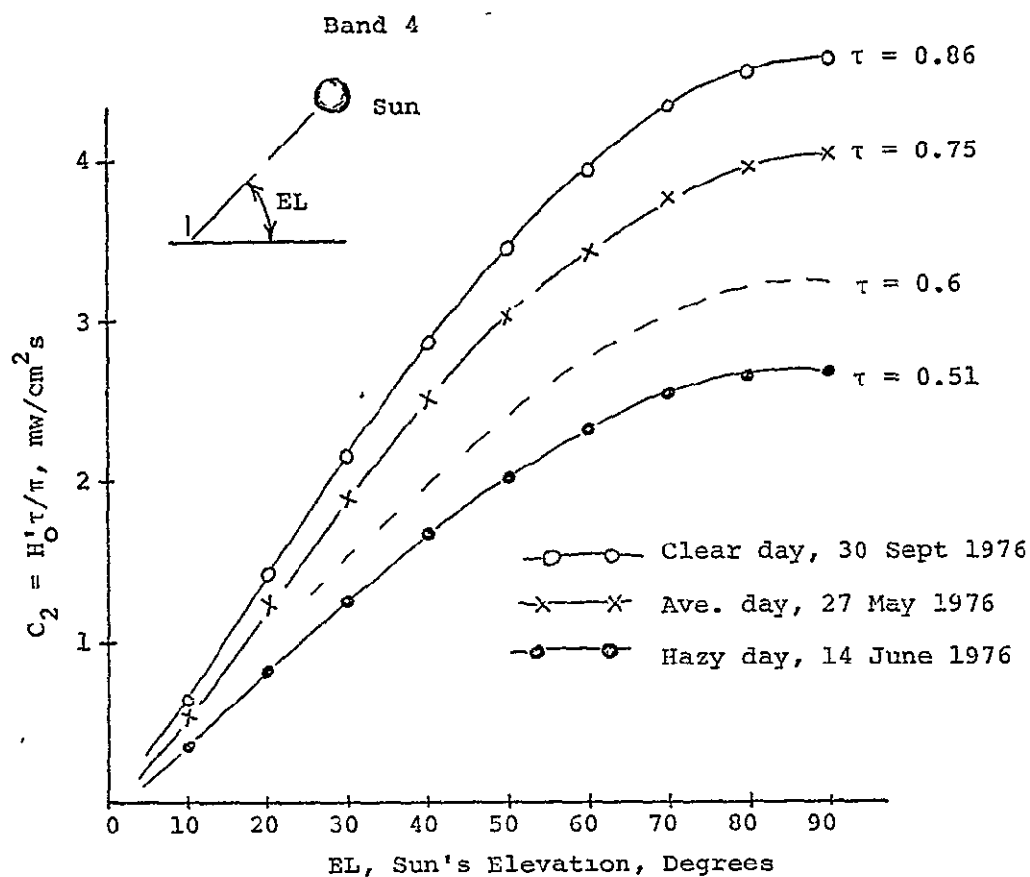
C_2 is therefore dependent on the total sun's irradiance horizontal to and at the earth's surface. This is H_0' which in turn is dependent on the elevation of the sun. C_2 is also dependent on the clarity of the air or τ .

Francis J Ahern along with others from the Canada Centre for Remote Sensing have been obtaining atmospheric parameters by observing LANDSAT radiance from clear lakes (Ahern et al. 1977). With observations of clear lakes near Ottawa and by use of the "Turner Model" they are able to calculate certain atmospheric parameters (Turner et al. 1971, Turner and Spencer 1972). From this work Ahern was able to extract data whereby the values of

$H_0' \tau / \pi$ (the theoretical value for C_2) could be calculated for three days in 1977. Data from a clear day, a hazy day, and an average day are given

Figures 97, 98, 99, and 100 show theoretical values of C_2 for LANDSAT bands 4, 5, 6, and 7. The values for C_2 are plotted against the sun's elevation, EL, which is contained in the data block for each LANDSAT scene (see Figure 30).

FIGURE 97 C_2 For Band 4. Data Supplied Courtesy Of Francis J. Ahern, Canada Centre For Remote Sensing, From Observations On McGregor Lake Near Ottawa And Calculations By The Turner Model.



ORIGINAL PAGE IS
OF POOR QUALITY

FIGURE 98. C_2 For Band 5 Data Supplied Courtesy Of Francis J. Ahern, Canada Centre For Remote Sensing, From Observations On McGregor Lake Near Ottawa And Calculations By The Turner Model.

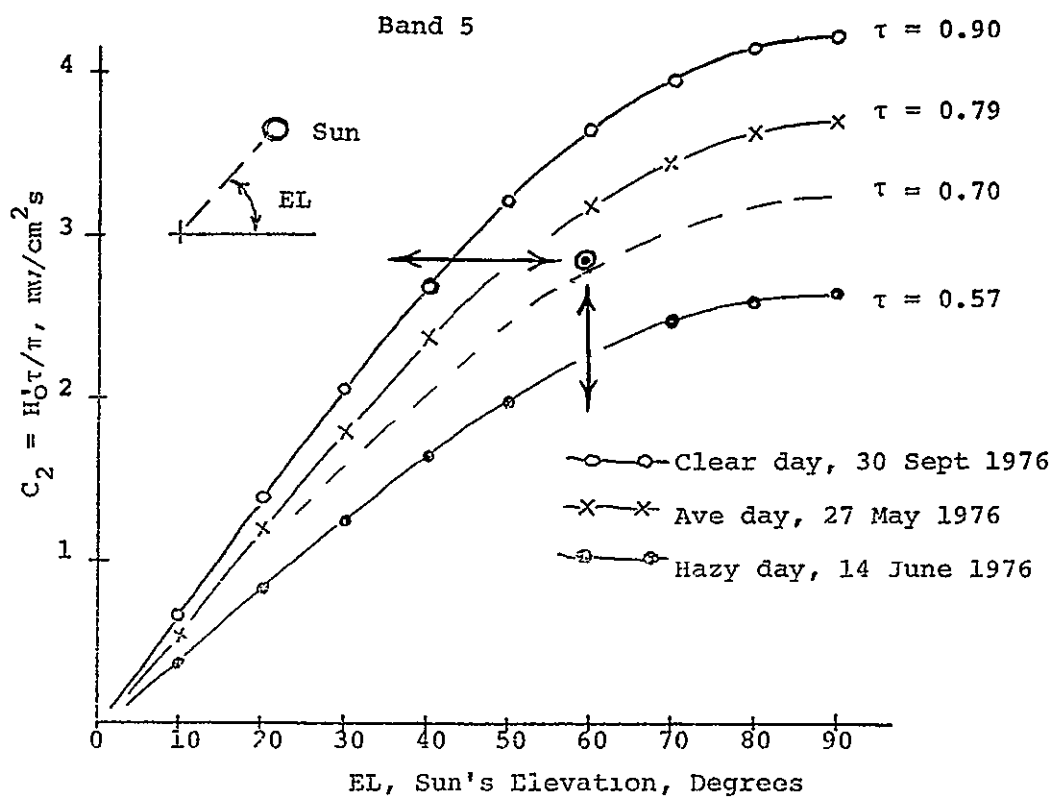
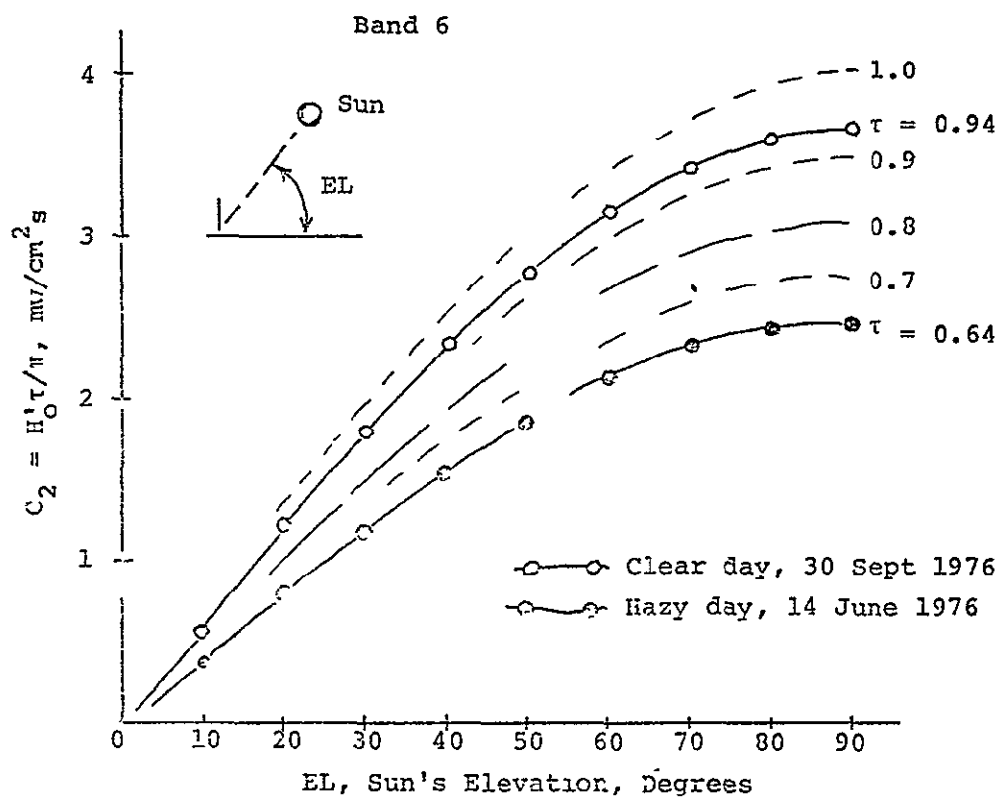
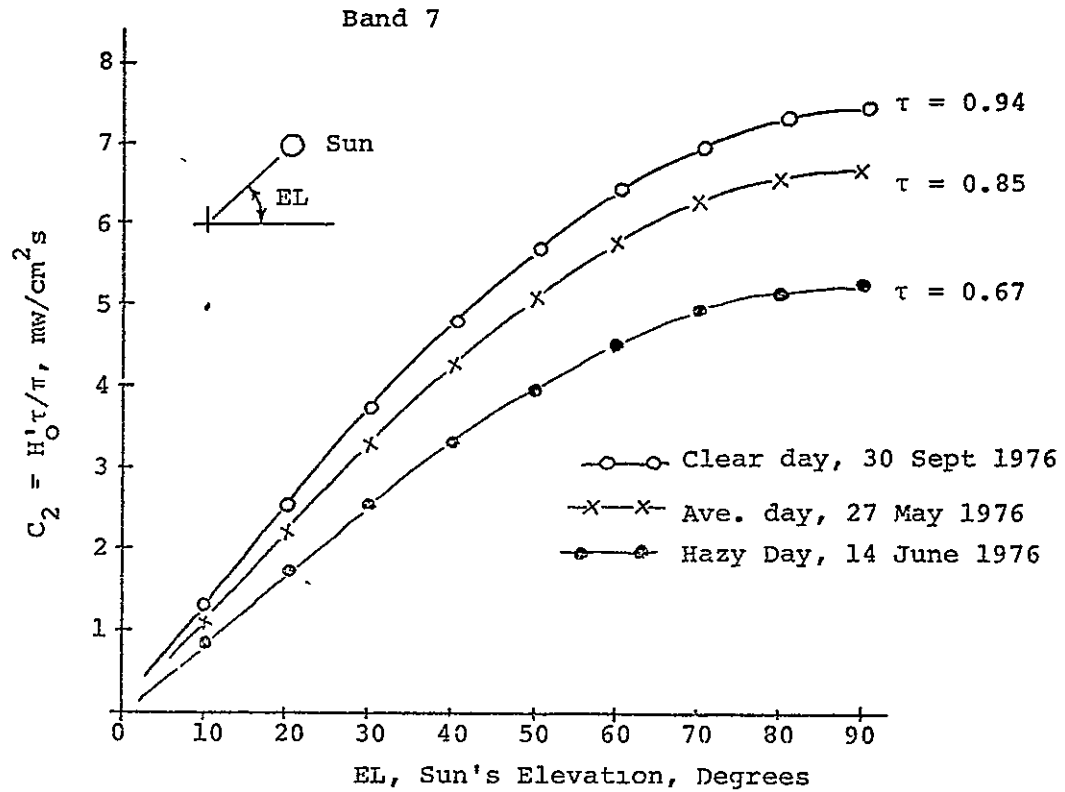


FIGURE 99 C_2 For Band 6. Data Supplied Courtesy of Francis J. Ahern, Canada Centre For Remote Sensing, From Observations On McGregor Lake Near Ottawa And Calculations By The Turner Model.



ORIGINAL PAGE IS
OF POOR QUALITY

FIGURE 100. C_2 For Band 7. Data Supplied Courtesy Of Francis J. Ahern, Canada Centre For Remote Sensing, From Observations On McGregor Lake Near Ottawa And Calculations By The Turner Model.



Dr Ahern's curves show the magnitude and change in the factor C_2 with different physical conditions. However, the curves cannot be used directly to correlate magnitudes of observed satellite reflectance values to laboratory values. This is because the theoretical model developed in Chapter 5 assumes that reflectance behaves in a linear manner while in reality it behaves as do other photometry relations — in a logarithmic manner. The simplifying linear assumption is entirely adequate for showing that the general shape of the laboratory fingerprints can be reproduced from satellite data, but if one wishes to correlate absolute magnitudes of laboratory and satellite data some correction factors are necessary.

In Chapter V the assumption is made that the ratio of R_1''/D_1 is constant for all values of turbidity. Yet the curves in Figure 31 show that both the laboratory and satellite reflectance depend on turbidity in a logarithmic manner and it can be shown that their ratio changes considerably with the turbidity of the water being analyzed

In Figure 31 the plots of log-reflectance versus log-turbidity are straight line curves which have many similarities with the plot of density versus log-exposure (D-Log E curve) for silver deposited on a photographic film (Figure 58). The curves in both figures are log-log plots describing the sensing and measurement of light. Absolute correlations from curves on both figures would be handled in a similar fashion.

For two lakes in Wisconsin an example follows for making an absolute correlation between laboratory and satellite radiance data of Figure 31 and Dr. Ahern's curves.

From Figure 31 the satellite reflectance for an average day can be expressed by

$$\text{Log } R_{(\text{sat})} = (.3)\text{Log } T + \text{Log } 9^* \quad \text{Eq. } E_1$$

where $R_{(\text{sat})}$ = percent satellite reflectance and
 T = turbidity

Reducing we have

$$R_{(\text{sat})} = T^{.3} (9)$$

and differentiating we have

$$dR_{(\text{sat})} = 9(.3)T^{-.7} dT = \frac{2.7dT}{T^{.7}} \quad \text{Eq. } E_2$$

*Standard notation for the plot of a straight line of form $y = mx + b$

For the laboratory reflectance we have:

$$\text{Log } AP_{(\text{lab})} = (5) \text{Log } T + \text{Log } 7 \quad \text{Eq. } E_3$$

where $AP_{(\text{lab})}$ is the percent lab reflectance compared to a BaSO_4 reflectance standard. From Equation E_3 :

$$AP_{(\text{lab})} = T^{.5}(.7) \quad \text{Eq. } E_4$$

and differentiating we have:

$$dAP_{(\text{lab})} = 5(.7)T^{-.5}dT = \frac{.35dT}{T^{.5}} \quad \text{Eq. } E_5$$

From Equations E_2 and E_5 we have:

$$dT = \frac{dR_{(\text{sat})} T^{.7}}{2.7}$$

and

$$dT = \frac{dAP_{(\text{lab})} T^{.5}}{.35}$$

And since the differences in turbidity between the two lakes will be the same in the lab as in the field we have:

$dT = dT$ and:

$$\frac{dR_{(\text{sat})} T^{.7}}{2.7} = \frac{dAP_{(\text{lab})} T^{.5}}{.35} \quad \text{or}$$

$$\frac{dR_{(\text{sat})}}{dAP_{(\text{lab})}} = \frac{7.7}{T^{.2}} \quad \text{Eq. } E_6$$

If one of the lakes being investigated is a clear-water lake (lake 1) and the other is more turbid (lake 2) then

$$dR_{(\text{sat})} = R_1'', \text{ and } dAP_{(\text{lab})} = D_1, \text{ and}$$

$$\frac{R_1''}{D_1} = \frac{7.7}{T} \quad \text{or} \quad \text{Eq. } E_7$$

$$R_1'' = D_1 (7.7)/T^{.2} \text{ and}$$

$$R_1'' = D_1(C_c) \text{ where}$$

$$C_c = 7.7/T^2$$

Thus we see that the ratio R_1''/D_1 is not constant but varies considerably with T. Therefore the observed value for R_1'' (the change in reflectance as observed from the satellite) will be C_c times higher than the change predicted from laboratory data and the theoretical model developed in Chapter V.

VARIOUS VALUES OF C_c
(dependent on T)

<u>T</u>	<u>C_c</u>
.1	12.2
.5	8.8
1	7.7
3.4	6.0
5	5.3
10	4.9
50	3.5
100	3.1

On 31 July 1974 the satellite went over southern Wisconsin and water samples from various lakes were gathered and analyzed.* One lake was a clear water lake (Devil's Lake). Another lake was moderately turbid (Lake Mendota). Laboratory and satellite values for these lakes are as follows.

* Data provided by Kenneth W. Holmquist, Research Assistant, Institute for Environmental Studies, University of Wisconsin-Madison.

Lake	T (FTU)	Band 5 Satellite Signal Counts	Band 5 Radiance, mw/cm ² s	R _i ["]	(.65μ) AP (lab) %	D ₁ %
Devil's	.25	11.7	.184	0	.27	0
Mendota	3.4	14.5	.228*	.044**	.92	65

For Lake Mendota the observed values for (observed) $R_1''/D_1 = .044/.0065 = 6.77$.

The approximate correction factor, C_c , for a lake with a turbidity of 3.4 (Mendota) is 6.0.

Therefore the theoretical value of R_1''/D_1 corrected for logarithmic relations, etc., is

$$\text{(theoretical)} \quad \frac{R_1''}{D_1} = 6.77 \div 6 = 1.23$$

Then the theoretical value for C_2 is:

$$C_2 = \text{(theoretical)} \quad \frac{R_1}{D_1} \times 2.56 = 1.23 \times 2.56 = 2.88***$$

From Dr. Ahern's curves for C_2 in Figure 98 for a sun elevation of 60° (Madison, Wisconsin, 31 July 1974) and a C_2 of 2.88 the corresponding value of τ is .72 (an average clear day)

A phone call to the National Weather Service at Madison, Wisconsin revealed at 10 AM on 31 July 1974 (the time of the satellite overpass) the sky was essentially clear with a visibility of 12 miles, i.e., an average clear day

* The maximum count possible on this satellite tape is 127, so

$$14.5/127 = 11.4\%$$

For Band 5 a count of 127 equals a radiance of 2.00 mw/cm²s (ERTS Users Handbook), so 11.4% x 2.00 mw/cm²sr = .228 mw/cm²s.

$$** \quad R_1'' = 228 - .184 = .044 \text{ mw/cm}^2\text{s}.$$

$$*** \quad C_2 = C_1 R_1/D_1$$

APPENDIX D

CONSTRUCTING A D-LOG E CURVE FOR COLOR REVERSAL FILM

Here is an example of how a D-Log E curve can be constructed for a normal color film processed to a color reversal slide. Prior to development of the film a standard step wedge was exposed on the film using standard laboratory techniques

Obtaining the x axis value

Assume that the intensity of the exposing light E_0 was constant at all visible wavelengths. The step wedge had six steps with densities of .1, .5, 1.0, 1.5, 2.0, and 2.5, respectively. From the following equation

$$D = \log_{10} \left(\frac{1}{T} \right)$$

the transmittance for each of the steps of the step wedge can be calculated. The corresponding transmittances for the six steps of the step wedge are .79, .32, .10, .032, .010, and .0032, respectively. Once the transmittance of the step wedge is known it is then possible to obtain the amount of energy that passed through the step wedge and exposed the film

$$T = \frac{E}{E_0}$$

where E = energy that passed through the step wedge
 E_0 = the energy of the exposing light

The corresponding amounts of energy (E) passing through the step wedge and exposing the film from the six steps are .79, .32, .10, .032, .010, and .0032 E_0 , respectively. These six values thus give the x coordinates for the D-Log E curve (exposure values)

Obtaining the y axis value

The y axis values for the D-Log E curve for this color film are determined by tuning the spectral microdensitometer to the color blue (.45 μ), green (.55 μ), and red (.65 μ) and obtaining readings for the colored light that passes through the different steps of the image of this film wedge

Assume that the spectral microdensitometer is tuned to the color blue (.45 μ) Furthermore, assume that I_0 is the energy that is read from the microdensitometer when no film is in the path of the small pencil of light illuminating the film. Furthermore assume that I_5 is the reading when this light I_0 is passed through step 5 of the film wedge. The density of that step on the image for the color blue (.45 μ) is:

$$D_5 = \log_{10} \frac{1}{T_5} \quad \text{where } T_5 = \frac{I_5}{I_0}$$

D_5 = Film wedge density for step 5 (blue light)

T_5 = Film wedge transmittance for step 5 (blue light)

I_5 = Intensity of light passing step 5 of film wedge (for blue light).

This value of density for step 5 (for the blue sensitive layer) can be plotted on the y axis of the D-Log E curve corresponding to the exposing energy E_5 (which is 1.0% E_0). In this manner all the y data points for the three layers of the film can be plotted.

Once the D-Log E curves are constructed, then the relative exposing intensities in the blue, green, and red parts of the visible spectrum can be obtained for any target.

Assume that a target on a normal color reversal film was analyzed with a spectral microdensitometer. Also assume that the film densities of the target obtained with the microdensitometer set at 0.45, 0.55, and 0.65 μ (which corresponds to film layers A, B, and C) were as follows (see Figure 101)

$D'_A = 1.9$, D'_A = Density of target on layer A (blue-sensitive)

$D'_B = 1.2$, D'_B = Density of target on layer B (green-sensitive)

$D'_C = 0.75$, D'_C = Density of target on layer C (red-sensitive).

By taking these values and entering the curves in Figure 101, it is possible to obtain the three values of energy exposing the blue, green, and red sensitive layers

$E'_A = 0.05$, E'_O = exposing energy (blue)

$E'_B = 0.11$, E'_O = exposing energy (green)

$E'_C = 0.50$, E'_O = exposing energy (red).

These values of exposing intensities can be plotted up versus wavelength to show an approximate spectral energy signature of energy coming from the target. For photography work the exact values of energy (E on D-Log E curves) are not very meaningful because the aperture and shutter speed setting of the camera make it practically impossible to relate the energy striking the film to that striking the front of the lens. Therefore the values of E'_A , E'_B , and E'_C are left on a relative scale.

The relative intensities of blue, green, and red energies ($E'_A = .05$, $E'_B = .11$, $E'_C = .50$) make it possible to construct a plot of energy versus wavelength (spectral energy signature) for the target analyzed.

If there are panels in the scene with known reflectance values, then it is possible to obtain percent reflectance signatures for diffuse objects. This can be done for different wavelengths to get a percent reflectance signature curve.

As can be seen, obtaining reflectance versus wavelength curves from photographic data becomes quite involved. Also, geometric and spectral corrections for the camera lens have not yet been considered. These corrections can become rather significant (Scherz 1972). One of the advantages of using LANDSAT satellite data is that they are taken by a multispectral scanner which has a linear relationship between radiance and raw data. There are no D-Log E curves for the multispectral scanner because the energy is not captured directly on film.* Also there are no lens corrections. Scanner data is ideal for multispectral analysis.

* The scanner does however have an instrument response curve (voltage versus radiance) which is the analogue of the D-Log E curve.

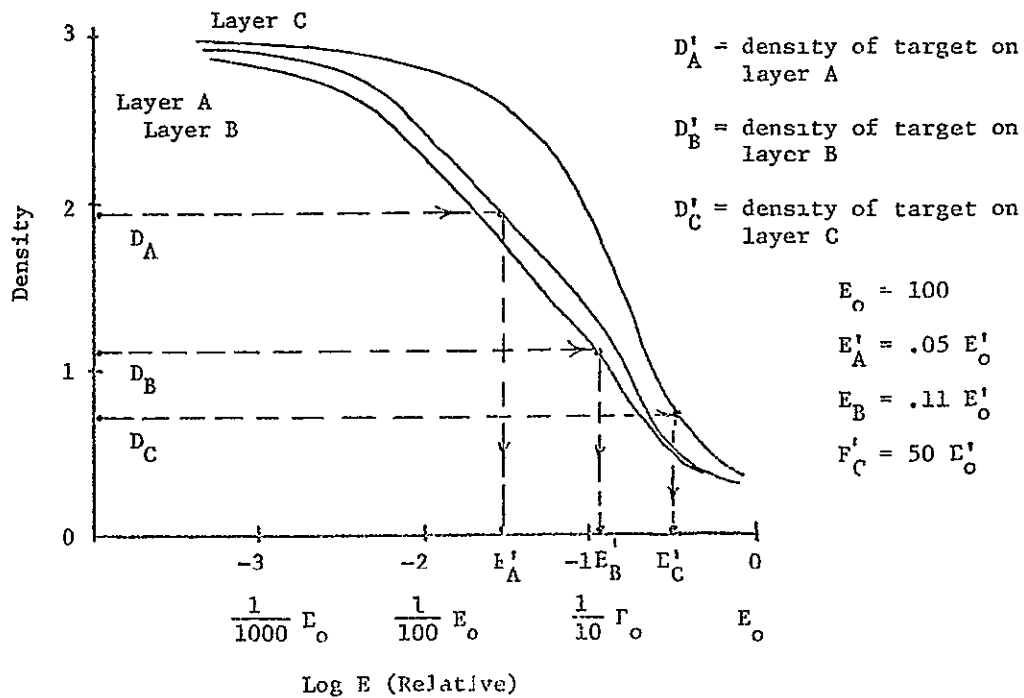
FIGURE 101. Constructing A D-Log E Curve For Color Reversal Film.

Densities of different steps on film wedge obtained with a color microdensitometer.

x axis		y axis			<div style="border: 1px solid black; padding: 5px; margin-bottom: 5px;">Layer A (blue sensitive)</div> <div style="border: 1px solid black; padding: 5px; margin-bottom: 5px;">Layer B (green sensitive)</div> <div style="border: 1px solid black; padding: 5px;">Layer C (red sensitive)</div> <div style="text-align: center; margin-top: 10px;">Color film</div>
% E_0	Step	D_A	D_B	D_C	
79	1	.3	.3	.35	
32	2	.5	.5	.75	
10	3	1.3	1.2	1.9	
3.2	4	1.9	1.7	2.6	
1.0	5	2.4	2.3	2.8	
0.32	6	2.8	2.7	2.9	

D_A = Density for layer A, etc.

The characteristic curves would then be plotted as below. Also densities of a target on the film can be obtained with a spectral microdensitometer D'_A , D'_B and D'_C and the exposing energies from that target determined E'_A , E'_B , E'_C .



APPENDIX E

REFLECTANCE FINGERPRINTS FOR MARL LAKES AND LAKES
CONTAINING SUSPENDED GLACIAL ROCK FLOUR

Water running from melting glaciers has a characteristic blue-green or turquoise color. This color is caused by fine suspended particles of ground-up rock called glacial rock flour. These fine particles cause blue-green wavelengths of light to be highly backscattered.

Lake Louise in Alberta, Canada is at the foot of a melting glacier and has this characteristic blue color. Here the water is very clear allowing one to see the bottom of the lake to a great depth (at least 20 to 30 feet). But in addition to the bottom signal, a strong blue-green color is visible coming from the water itself. Bow River, which Lake Louise empties into, also has this characteristic blue-green color. Many alpine lakes and rivers of Europe have a similar color for the same reason. Some lakes of northern Wisconsin and Minnesota are located in deposits of glacial till which because of erosion or springs keep the fine glacial rock flour suspended in them. This also causes a distinctive blue-green color.

Another class of lakes have a similar turquoise color yet with them the bright color is not caused by glacial rock flour but by rock particles being precipitated out. These are Marl lakes and the turquoise backscatter in them is caused by tiny particles of calcium carbonate (limestone) which deposit in the water but do not immediately settle out * One might liken this accumulation of fine rock particles in the water with the formation of ice in the air as snow. These fine white calcium carbonate particles reflect back light extremely well but because of their small size the blue-green wavelengths are backscattered the most.

Such Marl lakes have a very bright blue-green color easily recognized by anyone viewing them. These bright colors are often indicated in the lake names such as "Blue Water Lake" in northern Minnesota.

Such turquoise colored marl lakes of northern Minnesota can be identified by their characteristic residual satellite fingerprints. Figure 103 shows such fingerprints for marl and glacial rock flour lakes in northern Minnesota. These curves result from a project where lakes and land cover in three LANDSAT scenes were classified by the MDAS computer for the Minnesota Pollution Control Agency. On this project the marl lakes were given a bright turquoise color on the final computer printout map. Scherz conducted the mapping with help from Dale Trippler from the Minnesota Pollution Control Agency. The project was completed in September 1977. Accuracies on this project for both the water and land categories chosen were between 90 and 96 percent correct.

* Personal conversation with Dale J. Trippler, Division of Water Quality, Minnesota Pollution Control Agency, Roseville, Minnesota, September 1977

Figures 102 and 103 show laboratory fingerprints and satellite residual fingerprint for marl lakes and waters containing suspended glacial rock flour.

FIGURE 102 Reflectance Curves For Marl Lake And Water Containing Glacial Rock Flour — Laboratory Fingerprints And Expected Satellite Fingerprints.

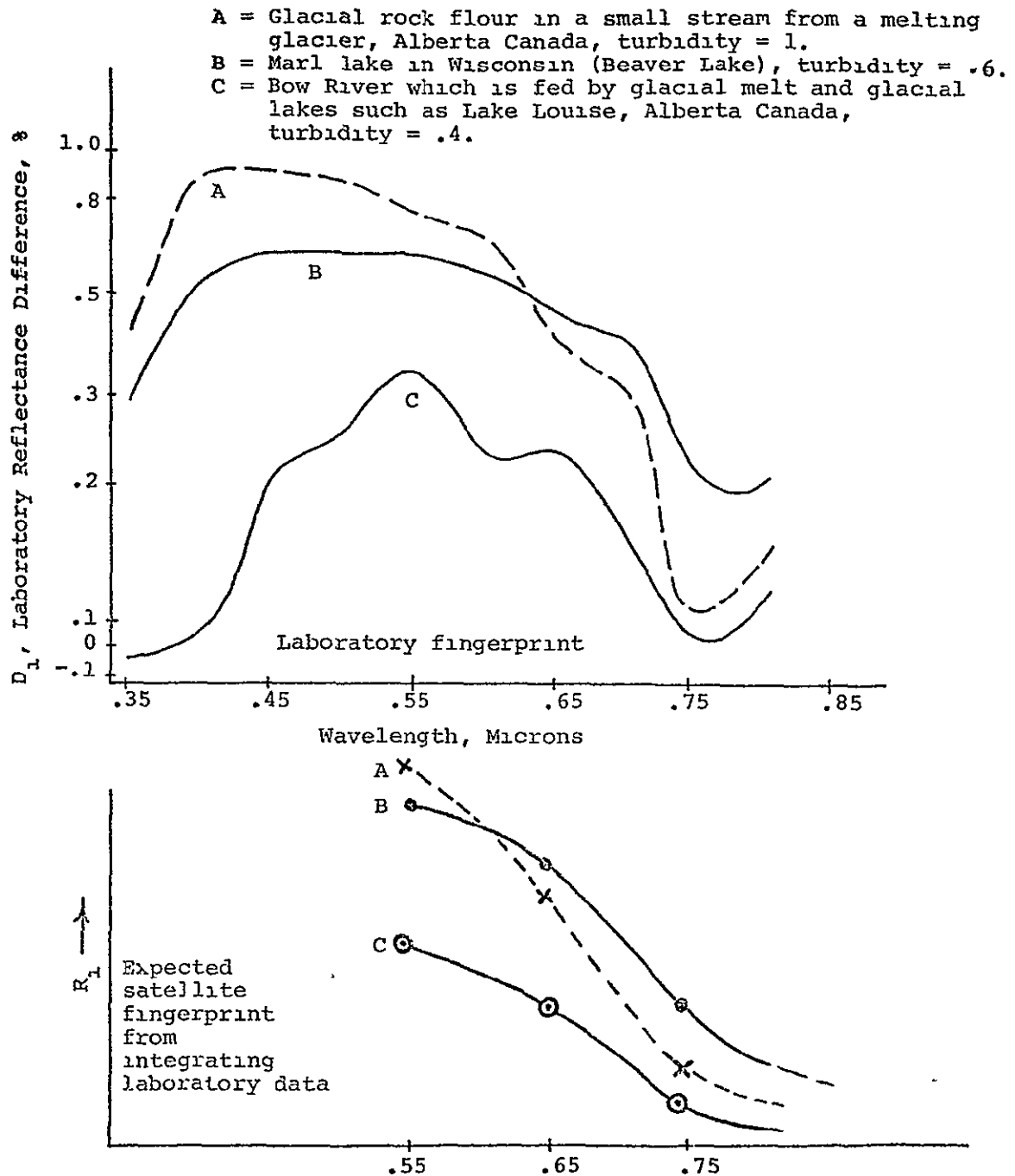
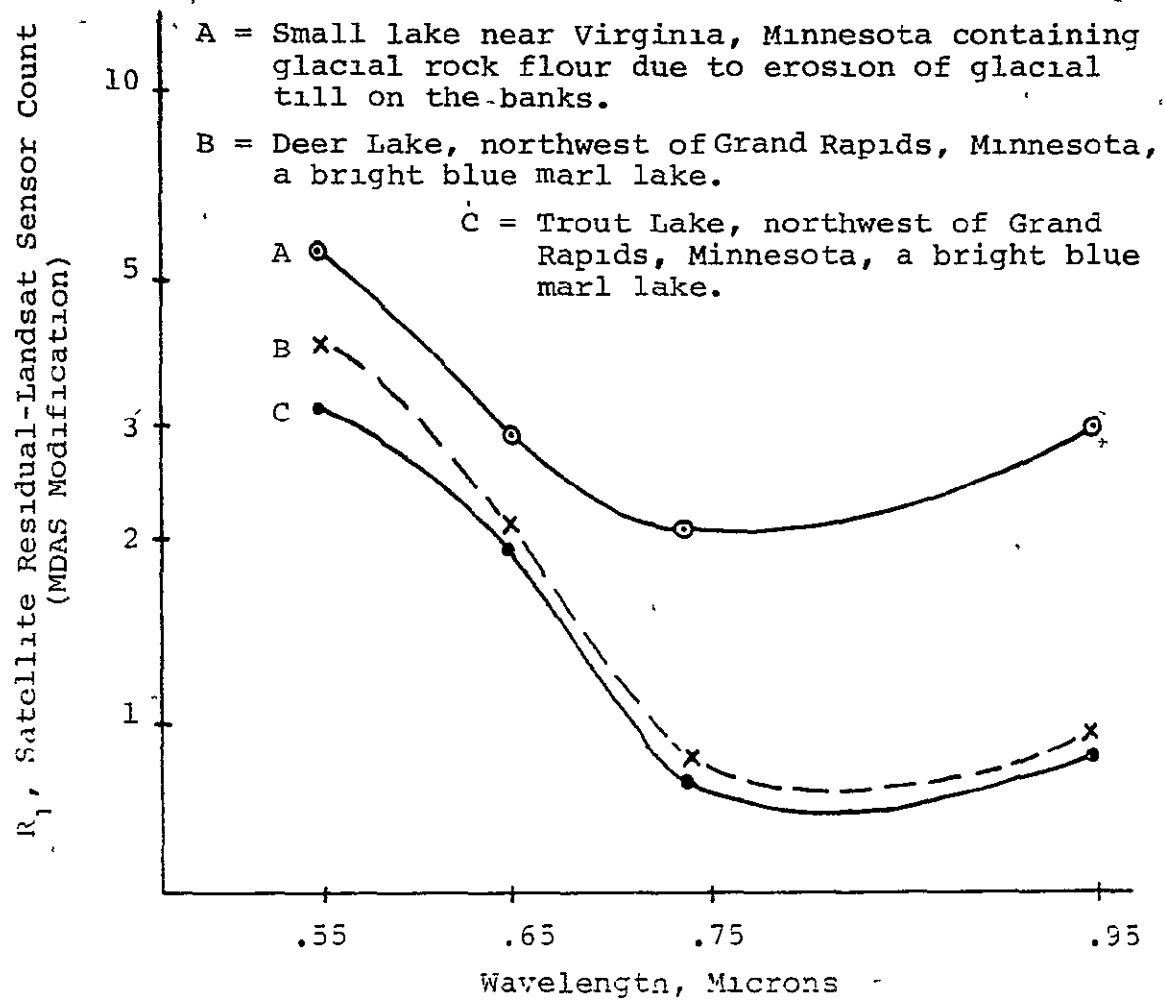


FIGURE 103. Satellite Residual Fingerprints For Marl Lakes And Lakes Containing Glacial Rock Flour Lakes In Northern Minnesota.



As can be seen in Figure 102, Samples A and C, although they both contain suspended glacial rock flour, have entirely different spectral reflectances. Sample A, which was collected at the base of a melting glacier, reflects mostly in the blue region, while the water from the Bow River (Sample C) reflects mostly in the green region.

There appears to be two possible explanations for this change in reflectance. One possible explanation is that the particles of material within the water have different colors. But since the rocks that the glacier rides over are neither green nor blue in color this explanation hardly seems plausible. The second possible explanation is that there are different sizes of particles in the different waters.

To check the second possible explanation research assistants Linda Kalman* and Kirk Morgan** analyzed both water samples with a Coulter Counter. The resulting data consisting of total volume of suspended particles as a function of particle diameter is shown in the curve in Figure 104.

One will note that Sample A which reflected most highly in the blue region has the majority of its particles in the size range of 0.6 to 6 microns. On the other hand, Sample C which reflected mostly in the green region has most particles of sizes 10 to 30 microns. Therefore it appears that the difference in reflectance between Sample A and Sample C, as indicated in Figure 102, is caused by different size distributions of particles of rock flour.

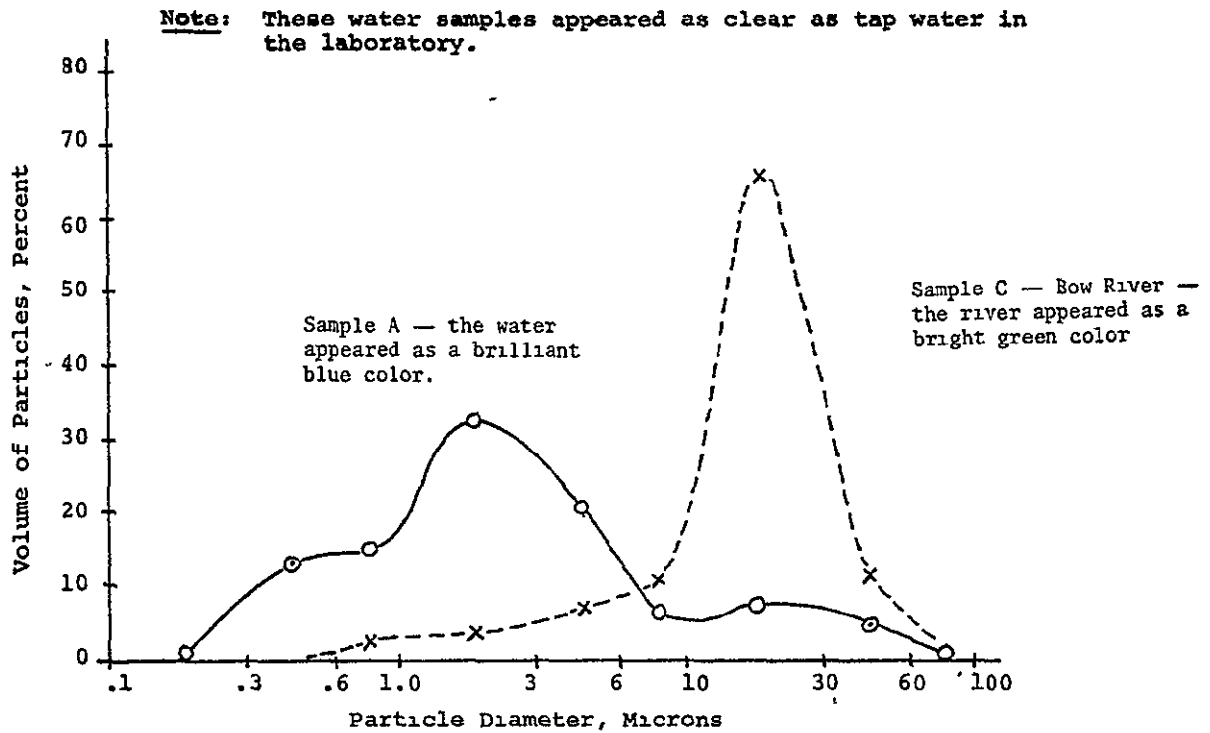
One will also note that with both samples the water was quite clear. In the laboratory both had the appearance of being as clear as tap water. Sample C which had a turbidity of 0.4 has a corresponding theoretical Secchi disc reading of 22 ft as indicated in Figure 4. Likewise Sample A has a theoretical Secchi disc reading of 6 ft. From the theoretical Secchi disc readings it is apparent that both waters are relatively clear, although the backscatter shows very discernable wavelengths of light.

The blue and green colors are apparently caused by very small rock particles distributed through the water which act like tiny reflectors. Marl lakes which have a bluish color perhaps have a size distribution of precipitating calcium carbonate particles similar to that for Sample A. As shown in Figure 102, Beaver Lake, a marl lake, has a laboratory reflectance fingerprint similar in shape and magnitude to that of Sample A.

* Research Assistant, Department of Civil and Environmental Engineering, University of Wisconsin-Madison

** Research Assistant, Department of Geology and Geophysics, University of Wisconsin-Madison.

FIGURE 104. Particle Size Distribution For Two Waters Containing Glacial Rock Flour. Color For The Light Backscattered From Those Relatively Clear Waters Is Apparently Caused By The Size Of The Fine Rock Particles Suspended In The Water.



APPENDIX F

CORRELATION OF STANDARD WATER QUALITY DATA
WITH THE LANDSAT COLOR CODED MAPS

In the summer of 1977 Mr. Dale Trippler of the Minnesota Pollution Control Agency provided voluminous amounts of water quality data associated with lakes that had been color coded by the MDAS system.

A. WATER QUALITY DATA

Fifty-five lakes were located on the color coded printout and the water quality data was correlated with the color coded maps. There was naturally much scatter in the data because the standard water quality data represents samples taken from throughout the year and not at the exact time of the LANDSAT overflight.

Nevertheless, care was taken to attempt to separate out water quality data collected closest to the optimum time - late August to early September. It was also thought that 55 lakes would provide a statistically sound set of data so that a comparison of the averages of parameters associated with each MDAS lake category would give meaningful results.

B. MIXTURES OF WATERS AND CATEGORY SELECTIONS

Most of the water in the lakes being classified is basically a mixture of 3 materials: (1) clear water; (2) dissolved tannin (humic) material which absorbs more of the short wavelengths of light as more of it is added; and (3) suspended material which increases the scatter of all wavelengths of light as more of this material is added to the water.

Figure 105 shows the schematic developed to handle all the possible mixtures of clear water, tannin and algae.

Inorganic material such as marl (calcium carbonate) particles, glacial rock flour, silt, and red clay, etc. also increases backscatter of all wavelengths of light as more of it is added. However, these inorganic materials have different reflectance fingerprints than tannin and algae and can be separated by analysis of their fingerprints by the MDAS system. Figure 105 shows how the marl lake category superimposes over the clear water category and can be color coded and separated if desired. One will notice in Figure 105 that each spot on the curve has a unique combination of clear water, tannin, and algae.

Profiles I and III represent mixtures of clear water (C10) to heavy tannin (T10), and clear water (C10) to heavy algae (A10), respectively.* Profile II represents water containing both algae and tannin.

* C10 means that water is 10/10 clear water. C5T5 means it is 5/10 clear 5/10 tannin, etc.

C. CORRELATION OF COLOR-CODED MAP TO FIGURE 105

In assigning a particular lake to a category for correlation, first the MDAS printout was viewed. If the pixels within the lakes were all brown it was given a T10 category (i.e., along Profile I). If the pixels in the lake were all green an A10 category was assigned, etc. If the lake had 50% brown and 50% blue pixels it would lie along Profile I midway between a clear water and a tannin water category.

Thus, each lake represented on the MDAS color-coded printout could also be located on the graph in Figure 105. Not only was it possible to determine what category the lake fell into but it was also possible to determine where the average water for that lake lies within that category (on the plot on Figure 105).

The next step was to correlate the different categories with corresponding water quality parameters for each lake. Then average water quality parameters could be summarized for all the lakes within each category represented on Figure 105.

D. SIGNIFICANT WATER QUALITY PARAMETERS

The most important parameter that relates to satellite signals is of course turbidity, which is indicated in the field by use of the Secchi disc. Clear water has very little suspended material and therefore low turbidity (measured by scattering of light) and a large Secchi disc reading. Any dissolved materials in clear water would be transparent material such as nonprecipitating calcium carbonate (measured by alkalinity) Tannic acid and humic material which is indicated by the water parameter of "color" would not be expected to be large in clear water lakes

When the alkalinity becomes so high that the calcium carbonate begins precipitating out and settling to the bottom these fine particles will increase the backscatter in the blue but because they are so small and fine they would not be expected to significantly effect the Secchi disc reading or turbidity values. Such lakes are called "marl" lakes and would have high values of Secchi disc readings and alkalinity.

If nutrient inflow of nitrogen and phosphorus are high enough so that algae begins to grow in the water the turbidity will rise and the Secchi disc readings will decrease. Concentration of living algae will also be indicated by measured values of chlorophyll a

Dead algae, tree roots and other nondecayed organic or "humic" material will act like tea leaves in tea or grape skins in old wine to produce a brown "tannin" color in the water. The tannin is dissolved into the water and cannot be removed by filtration. It is measured by the water quality parameter called color. However, in addition to the dissolved material, the tannin or humic waters often have brown undecomposed organic matter floating in them. This suspended brown organic matter increases turbidity and decreases Secchi disc readings

Therefore, for a very tannin lake one would expect an increased value for color, and a slightly decreased value of Secchi disc reading. The amount of chlorophyll a in a tannin lake can be large or small depending on the amount of nutrients (phosphorus and nitrogen) in the water and the resulting growth of biomass.

E. WATER CATEGORIES AND AVERAGE PARAMETER VALUES

Table 3 shows a plot of the water quality parameters of: Secchi disc reading, chlorophyll a color, and total alkalinity for the different water quality categories. There would be a slight variation in the average values given depending on the exact location of the water categories as plotted on the graph in Figure 105. The size and location of each category depends on the colors assigned to the different tannin lakes.

TABLE 3 Water Quality Parameters Associated with Different MDAS Lake Categories Shown in Figure 105

MDAS Lake Category	Profile	Water	Standard Water Quality Parameters			
			Secchi Disc Reading (inches)	Chlorophyll <u>a</u> ($\mu\text{g/l}$)	Color Pt-Co Units	Total Alkalinity CaCO_3 (mg/l)
1	III	Clear	60-200 Ave = 95*	4-8 Ave = 6*	5-130 Ave = 25	75-140 Ave = 116
2	III	Marl	80-140 Ave = 100*	5-10 Ave = 8	7-12 Ave = 10	80-150 Ave = 104
3	III	Light- medium algae	20-40 Ave = 35*	20-35 Ave = 30*	---	89-120 Ave = 104
4	III	Medium- heavy algae	20-40 Ave = 30*	35-60 Ave = 45*	---	89-107 Ave = 98
5	I	Tannin	19-74 Ave = 62*	0-14 Ave = 7.3*	35-320 Ave = 120*	15-100 Ave = 80

* Most significant correlation of parameters with water type.

The significant information shown in Table 3 is as follows

The categories of clear water (dark blue) and marl (turquoise when printed out) have large Secchi disc readings averaging from 95 to 100 inches

The parameters of color (a measure of tannin) and chlorophyll a (a measure of algae) are low for these lakes. The values of chlorophyll are 6 and 8, respectively. As can be expected, the marl lakes have the highest average value of alkalinity of any of the categories (128 mg/l). Both marl and alkalinity are caused by calcium carbonate.

The light-to-medium and medium-to-heavy algal categories have average Secchi disc readings of 35 and 30 inches, respectively and chlorophyll a values of 35 to 40.

Tannin water lakes have an average Secchi disc reading of 62 inches. The chlorophyll a and alkalinity readings are low (7.3 and 80, respectively). As would be expected, the tannin waters have the highest average value for color - an average of 120 (about 10 times higher than that for clear lakes).

F PARAMETERS CORRELATION CURVES

Table 3 gives the average water quality parameters associated with each water category shown in Figure 105. It is also possible to plot up the exact relation between different water quality parameters and values of clear water, C, tannin, T, and algae, A, as shown in Figure 105.

1. Secchi Disc Readings Versus Chlorophyll a and Color

Increased turbidity and the accompanying decreased Secchi disc readings are caused by suspended particles within the water. For clear water the turbidity is low (approaching zero) and the Secchi disc readings are high. Suspended silt and clay from erosion such as shown in the southwest end of Lake Superior cause increased turbidity and decreased Secchi disc readings. However, for naturally occurring waters of inland lakes in northern Wisconsin and Minnesota, the suspended material that decreases the Secchi disc reading is either living algae or dead humic matter which provides brown dissolved and suspended matter to the water. The brown suspended material decreases the Secchi disc reading. The absorption of light by the brown dissolved material also would tend to decrease the Secchi disc reading. This brown dissolved material is measured by the parameter of color.

Figure 106 shows the correlation between Secchi disc readings and color for all lakes with this data given. As can be seen, increased color corresponds to decreased Secchi disc readings. Living algae (indicated by chlorophyll a) cause increased turbidity and decreased Secchi disc readings as does the parameter of color. If there is a mixture of both chlorophyll a and tannin in the water it is not possible to directly correlate chlorophyll a with Secchi disc readings because the tannin water (indicated by color) causes noise in the correlation.

Figure 107 shows the results of plotting up the values of chlorophyll a versus Secchi disc readings for all the lakes. There is no apparent correlation. Similar curves for lakes lying along Profiles I and II of Figure 105 also have no apparent correlation (Figure 108). Only when lakes are selected which lie along Profile III (no tannin) does a correlation exist between chlorophyll a and Secchi disc readings (Figure 109).

From the MDAS color coded output the green color for a lake depends on the amount of algae present (as does chlorophyll *a* in the lab) Figures 109 and 110 show that the correlation of algae to Secchi disc readings can be done from both satellite data and laboratory data once the lakes are plotted on a graph as in Figure 105 and selected as lying along Profile III.

2. Secchi Disc Readings from MDAS Color Coded Output and Aerial Reconnaissance Observations

Figure 110 shows that by use of the MDAS color coded map and the graph in Figure 105 it is possible to obtain Secchi disc readings for algal lakes lying along Profile III. Similar correlation can be accomplished for the color brown along Profile I and for the summation of the colors brown and green along Profile II.

Figure 111 shows a curve relating the estimated content of the color brown on the MDAS printout to Secchi disc readings. The lakes chosen for the curve lie between Profiles I and II on Figure 105.

There is a problem, however, in the MDAS printout scheme being analyzed. For this run the bottom lakes, normally printed out as yellow, were printed out as brown - the same color as the tannin lakes. Therefore, some of the lakes indicated as brown on the MDAS output (Figure 111) are really clear lakes (with large Secchi disc readings) with bottom showing. The effect of these bottom lakes would be to scatter the plotted data and flatten the correlation curve for the MDAS data.

However, the aerial observations for these lakes (used in training the MDAS computer) do not have the bottom lakes confused with the tannin lakes. A plot of the tannin content (T) of lakes estimated by aerial reconnaissance is also shown in Figure 111. The curve from the aerial reconnaissance would be expected to be nearly identical to the curve for the MDAS color coded output if the clear bottom lakes had been given a separate color code.

Along Profile I it is possible to obtain Secchi disc readings from the strength of the color brown. Along Profile III it is possible to obtain Secchi disc readings from the strength of the color green. The Secchi disc reading is effected by both the green and the brown color (both algae and brown humic material decrease the Secchi disc readings). If one wishes to obtain the Secchi disc reading along Profile II, the correct correlation curve must contain values for the sum of green plus brown colors. Figure 112 shows such curves relating Secchi disc readings to the sum of green and brown colors along Profile II.

A new Profile IV was also created horizontally across the graph in Figure 105 at a tannin value of about 6. Figure 112 also shows the correlation along Profile IV for lakes containing only tannin and algae (no clear water).

As can be seen the correlation curve appears to be about the same as the one for Profile II.

3. Color and Chlorophyll a Directly from the MDAS Color Coded Map

The Secchi disc readings can be obtained from a MDAS color coded map and the curves in Figures 110 and 112. Then with the Secchi disc readings the curves on Figures 106 and 109 can be used to obtain color and chlorophyll a.

For these lakes which have no silt and clay, it is obviously also possible to eliminate the curves for Secchi disc readings and obtain color and chlorophyll a directly from the MDAS color coded output.* Figure 113 contains curves relating color to the observed amount of tannin content and brown color near Profiles I and II. Figure 114 contains curves relating chlorophyll a to amount of algal content and green color along Profile III. If MDAS data from all the lakes is plotted, the same curve results as in Figure 114, but there is more scatter to the data. This is probably due to the tannin water in the mixtures. Dark tannin water would naturally effect the sunlight's penetration into the water and the satellite's ability to detect algae.

4. Total Phosphorus

If enough phosphorus and nitrogen runs into a lake, interacts with sunlight, and remains there long enough, algae will form. Phosphorus is much more scarce than nitrogen. It is usually measured in micrograms/liter, while nitrogen is measured in milligrams/liter (a difference of 1000 times). The atmosphere is composed mostly of nitrogen while phosphorus is much less abundant. Therefore, phosphorus can be expected to usually be the limiting parameter for algal growth.

A correlation is then expected between the amount of chlorophyll a from algae in the water and the total phosphorus content. Figure 115 shows a plot of total phosphorus versus chlorophyll a from the Minnesota data (all lakes).

As can be seen in Figure 115, there is a correlation for water from the lakes. However, the plot of the water from the St. Louis River** lies far off the curve for the other data. This is expected because the river is moving water and the phosphorus picked up by the river and its tributaries would not yet be converted into algal biomass.

Since chlorophyll a can be correlated to the amount of green color in a lake as shown on the MDAS color coded output (Figure 114), one would also expect that a correlation could be made for total phosphorus. Figure 116 shows this correlation between observed green color and phosphorus for all the lakes analyzed which contained such data. Also on this curve the plot for water from the St. Louis River lies far above the average curve for the lake waters.

* If any lakes have turbidities caused by suspended material other than algae and brown humic material, the desired correlations of Secchi disc readings to chlorophyll a and color would not hold (i.e., red clay in Lake Superior and red iron mine waste suspended in water).

** The St. Louis River is a wide mouthed river which empties into Lake Superior between the cities of Duluth and Superior.

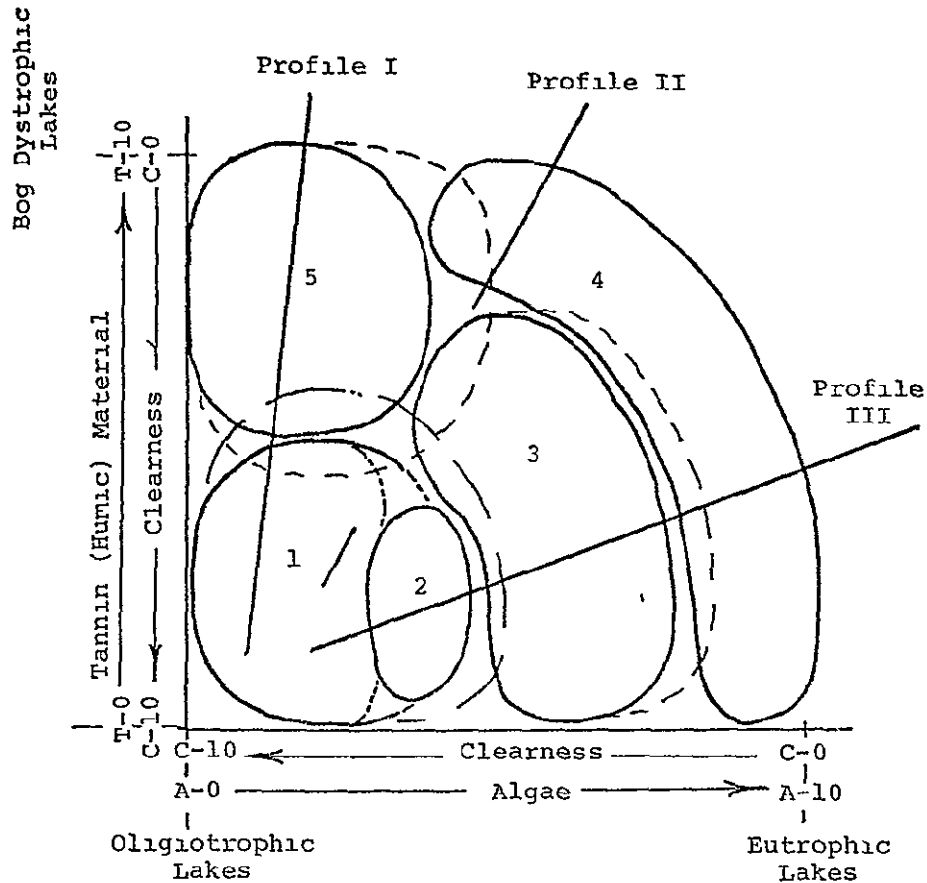
5 Marl Lakes

From Table 3 it can be seen that marl lakes have high average values of alkalinity and very clear water (or water with high Secchi disc readings). If such a clear lake were to receive high inputs of phosphorus and nitrogen, the resulting algae would scatter light which would override the characteristic blue-green color caused by the precipitating fine particles of CaCO_3 . Therefore not all lakes with high alkalinity appear as the blue-green marl lakes, but all blue-green marl lakes would be expected to have high values of alkalinity.

On the MDAS color coded map being analyzed the marl lakes were printed out as a turquoise color. Lakes containing MDAS pixels of turquoise color were compared to the corresponding values of alkalinity.

Figure 117 shows this data. Although the curve in Figure 117 is quite flat it does show that there is a correlation between the strength of the turquoise color and alkalinity. The correlation of pH of alkalinity for various lakes is also shown in Figure 117.

FIGURE 105. Trophic Classification Scheme for LANDSAT Water Categories as a Function of Dissolved Tannin and Suspended Algae Material. Size of Category Depends on Colors Assigned to Various Training Lakes.



Category	Type of Water	Color on Printout
1	Clear water	Dark blue
2	Marl	Turquoise or dark blue*
3	Light-medium algae	Light green
4	Medium-heavy algae	Dark green
5	Tannin water (humic)	Brown

*Dark blue on initial work - turquoise on later refinement work.

ORIGINAL PAGE IS
OF POOR QUALITY

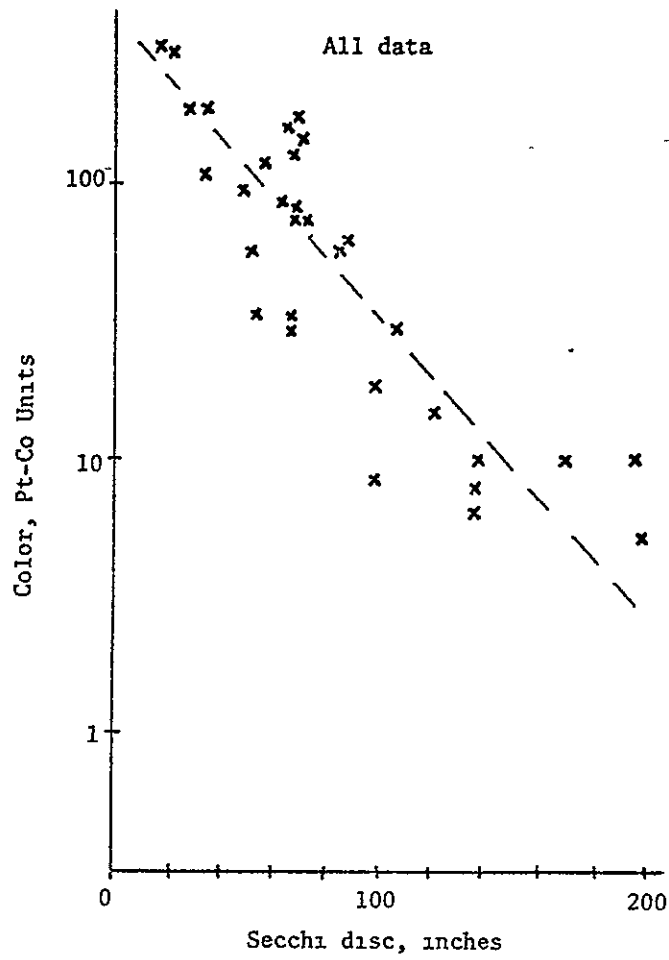


FIGURE 106. Color Versus Secchi Disc readings — Minnesota Water Depth.

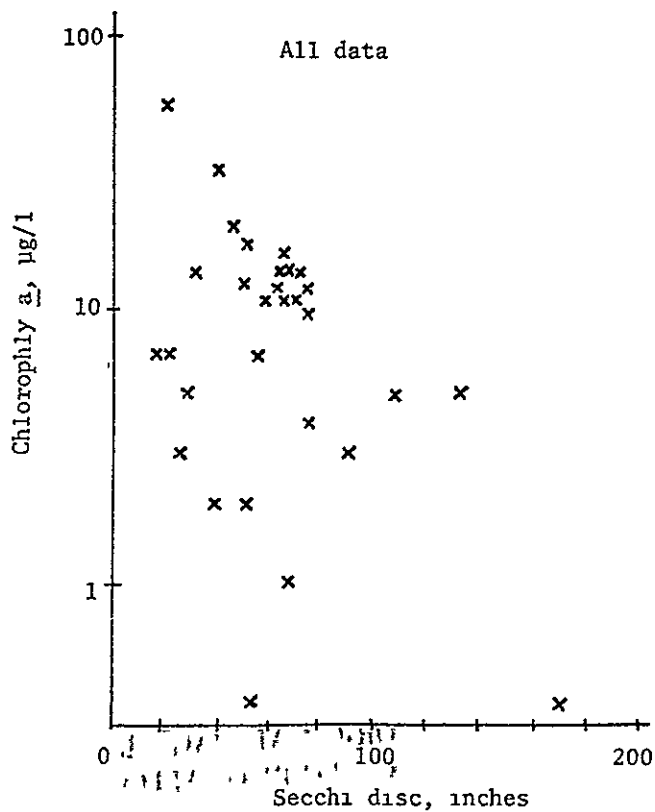
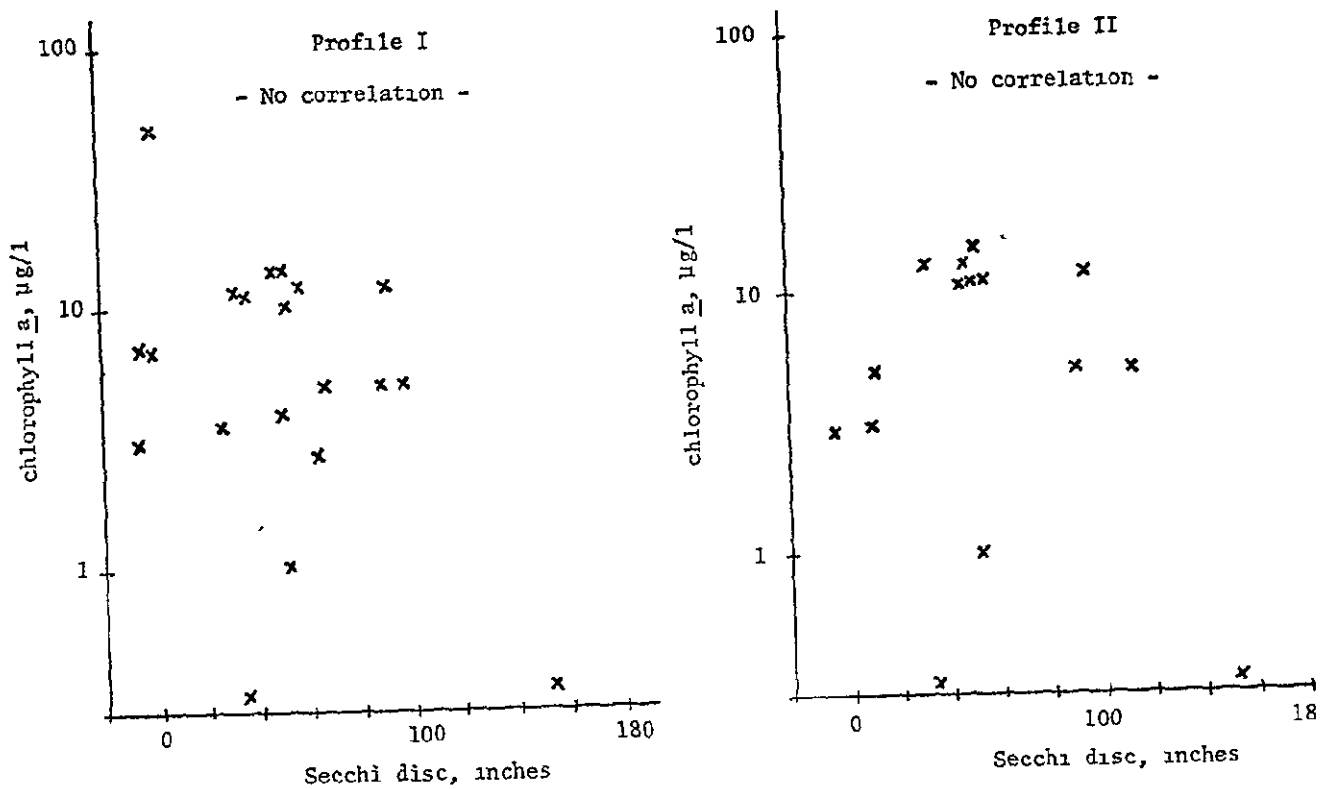


FIGURE 107 Chlorophyll *a* Versus Secchi Disc Readings — Minnesota Water Data

FIGURE 108. Plot of Secchi Disc Readings Versus Chlorophyll a For Lakes Lying Along Profiles I and II in Figure 105 — Minnesota Water Quality Data



ORIGINAL PAGE IS
OF POOR QUALITY

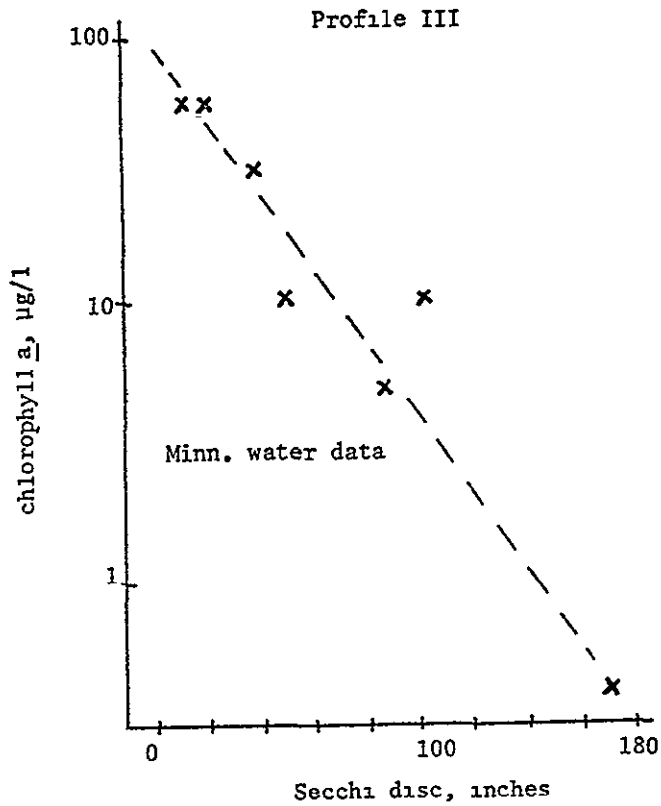


FIGURE 109. Secchi Disc Readings Versus Chlorophyll a — Along Profile III, Figure 105.

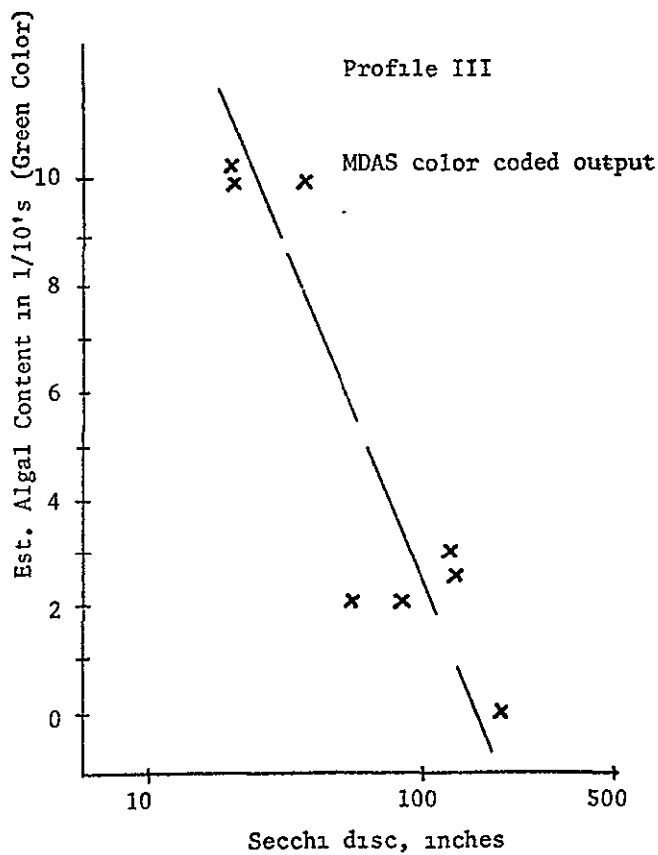


FIGURE 110. Secchi Disc Readings Versus Estimated Algae Content Along Profile III, Figure 105.

FIGURE 111. Secchi Disc Readings Versus Estimated Tannin Content - Along a Profile Between I and II in Figure 105.

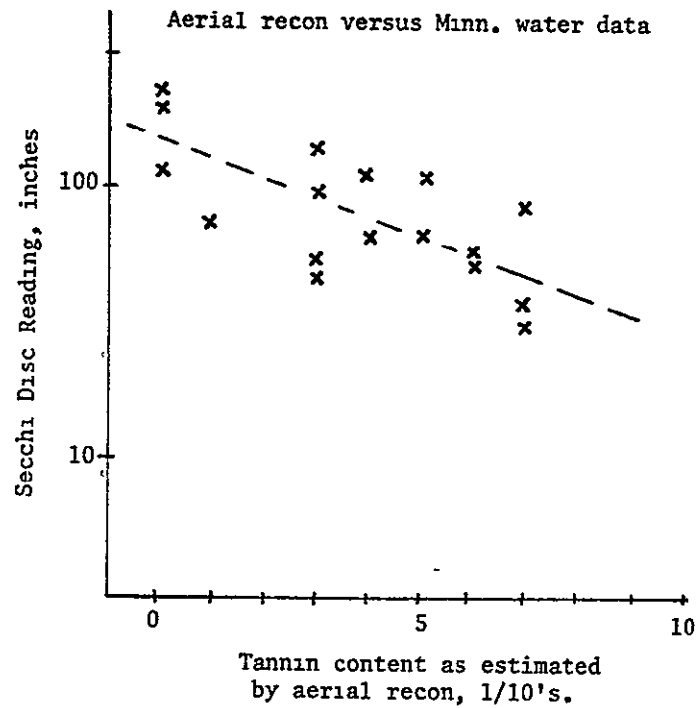
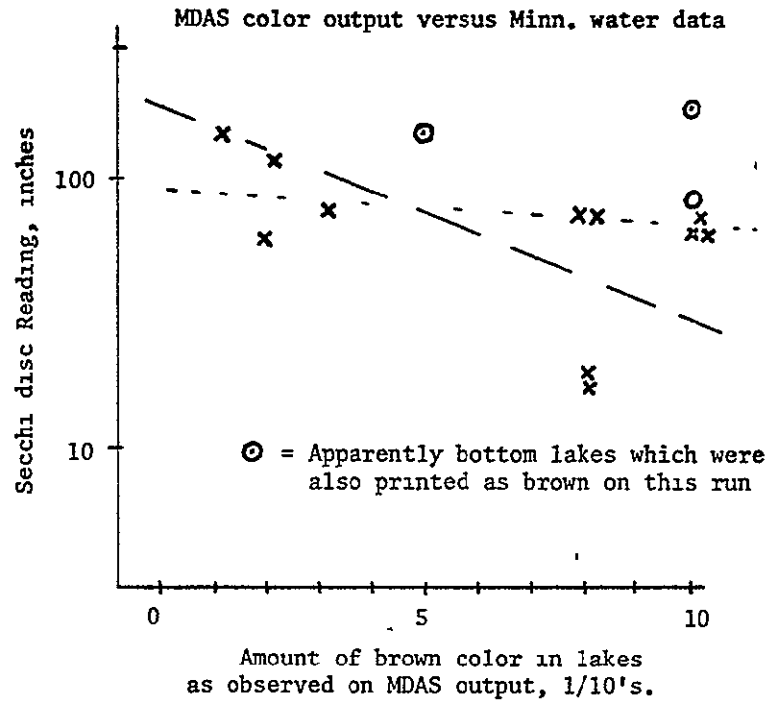


FIGURE 112. Secchi Disc Readings Versus the Sum of Green and Brown Colors in Lakes as Observed on MDAS Color Coded Output. Profiles II and IV as Shown.

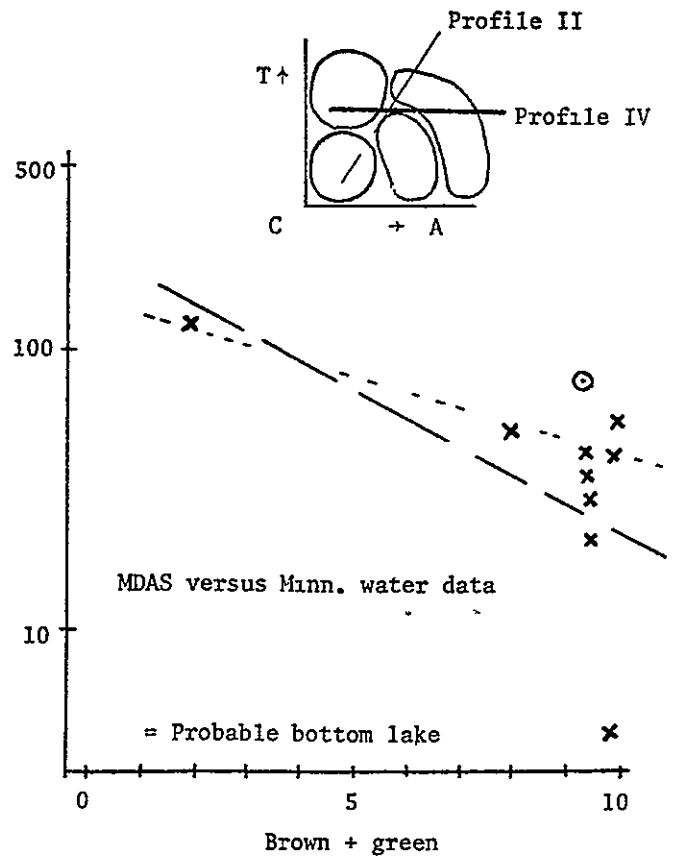
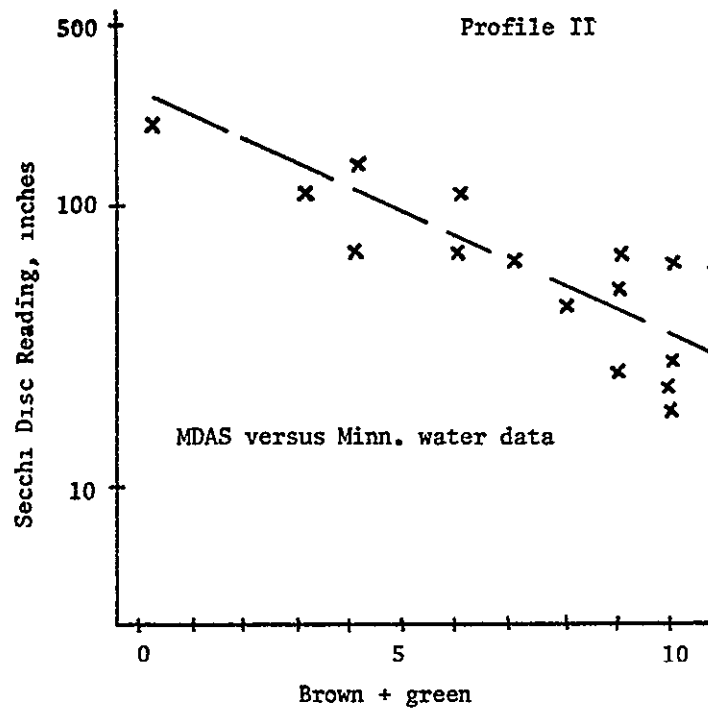
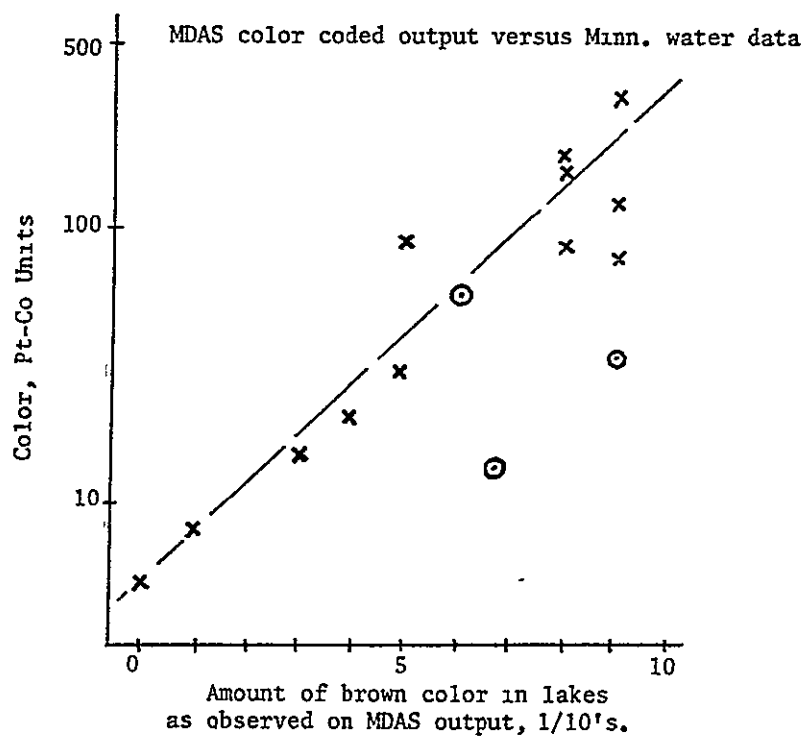
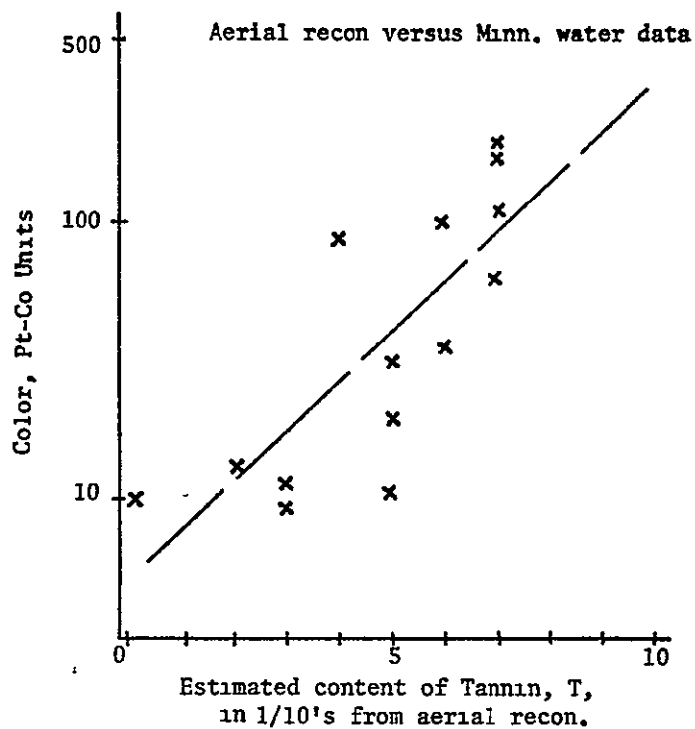


FIGURE 113. Color Versus Estimated Tannin Content - Along a Profile Between Profile I and II in Figure 105.



ORIGINAL PAGE IS
OF POOR QUALITY

FIGURE 114. Chlorophyll a Versus Estimated Algal Content, Profile III, Figure 105.

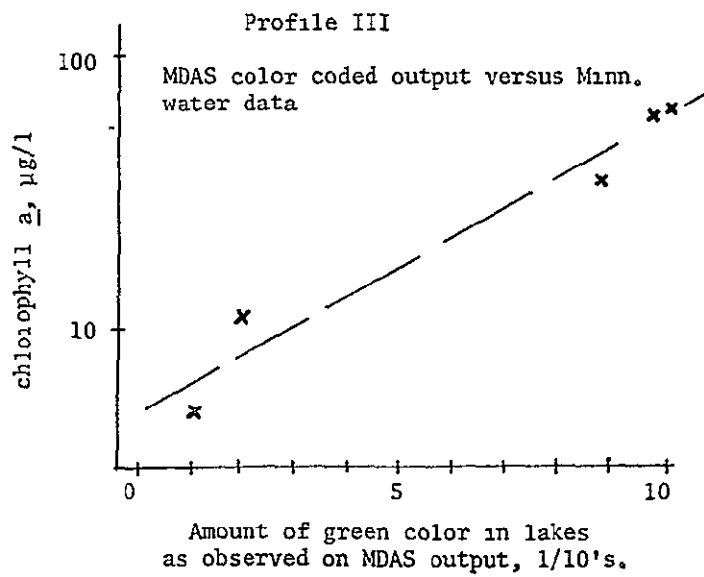
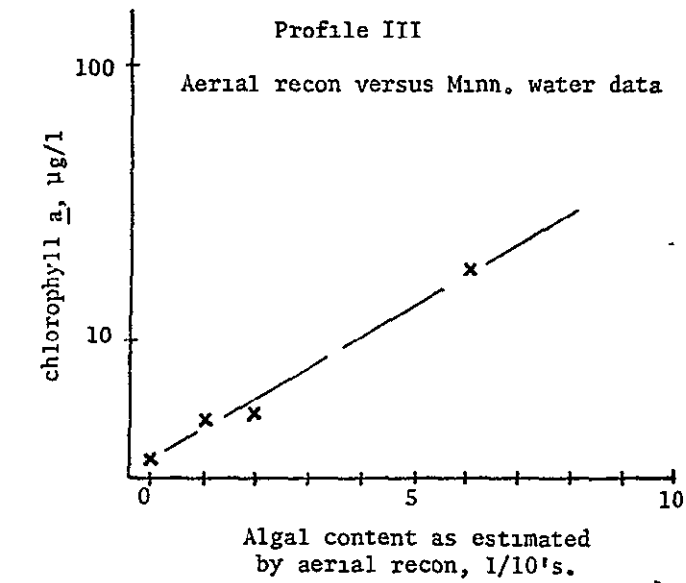
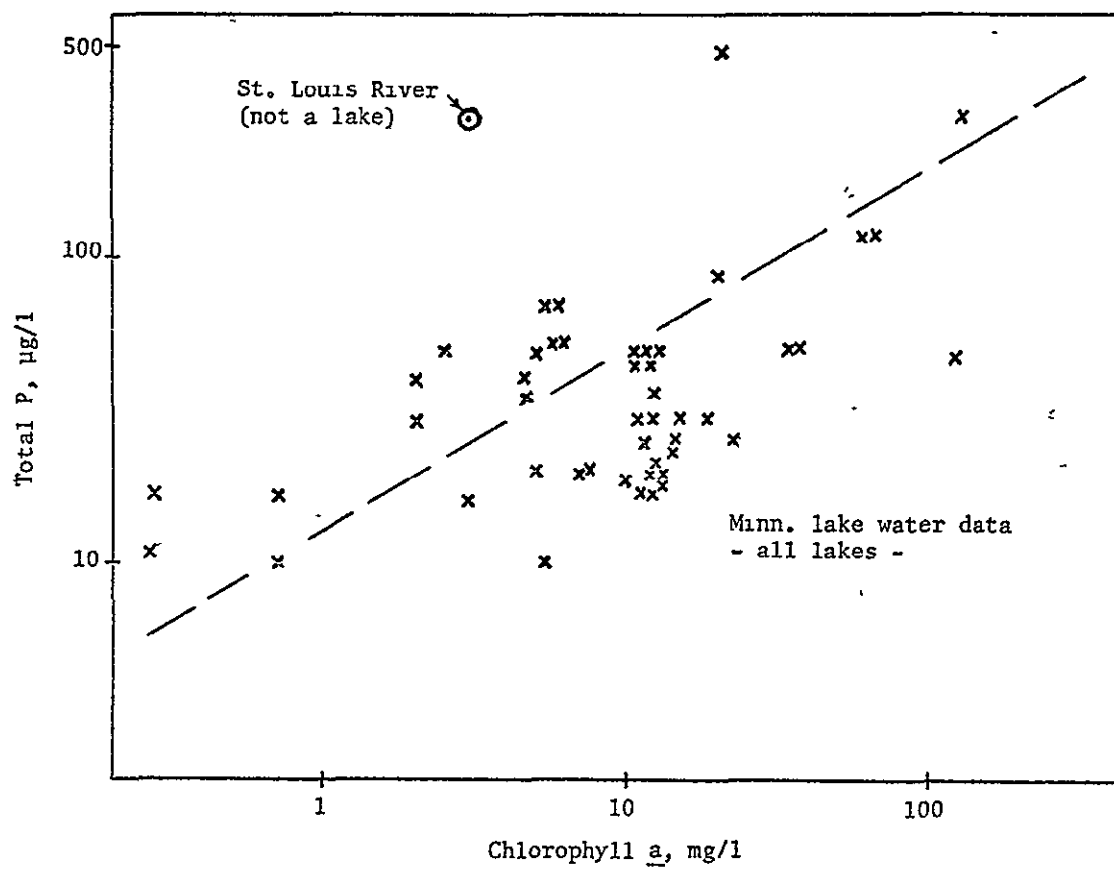


FIGURE 115. Chlorophyll a Versus Total Phosphorus

ORIGINAL PAGE IS
OF POOR QUALITY

FIGURE 116. Amount of Green Color Observed on MDAS Color Coded Printout in 1/10's.

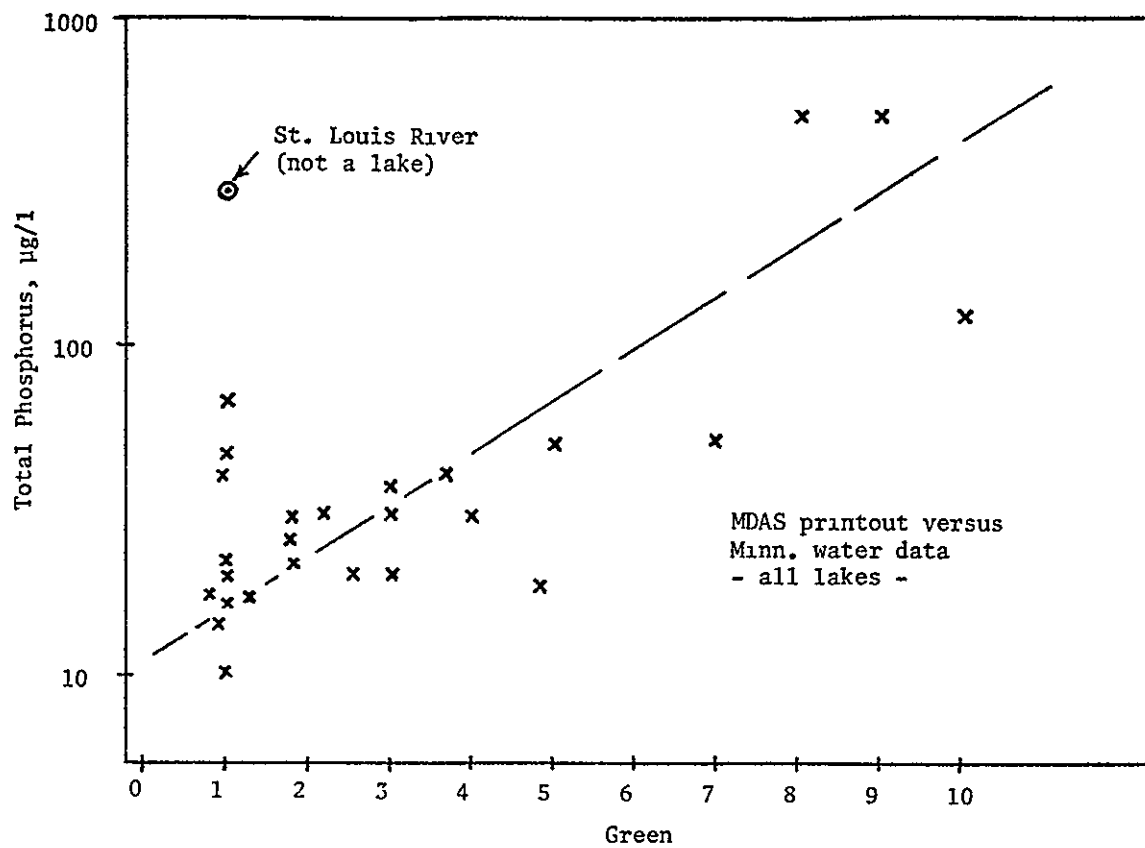
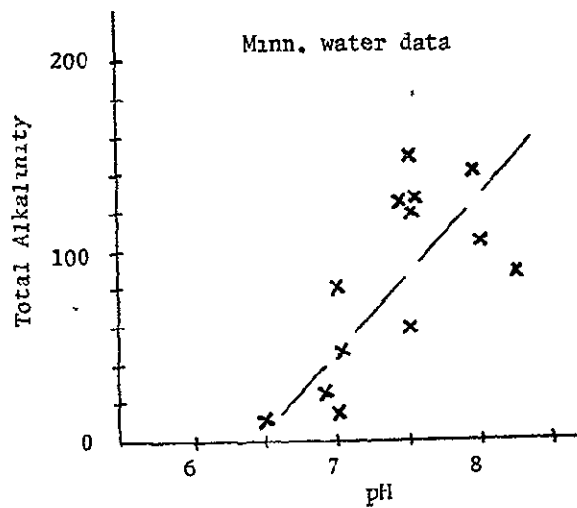
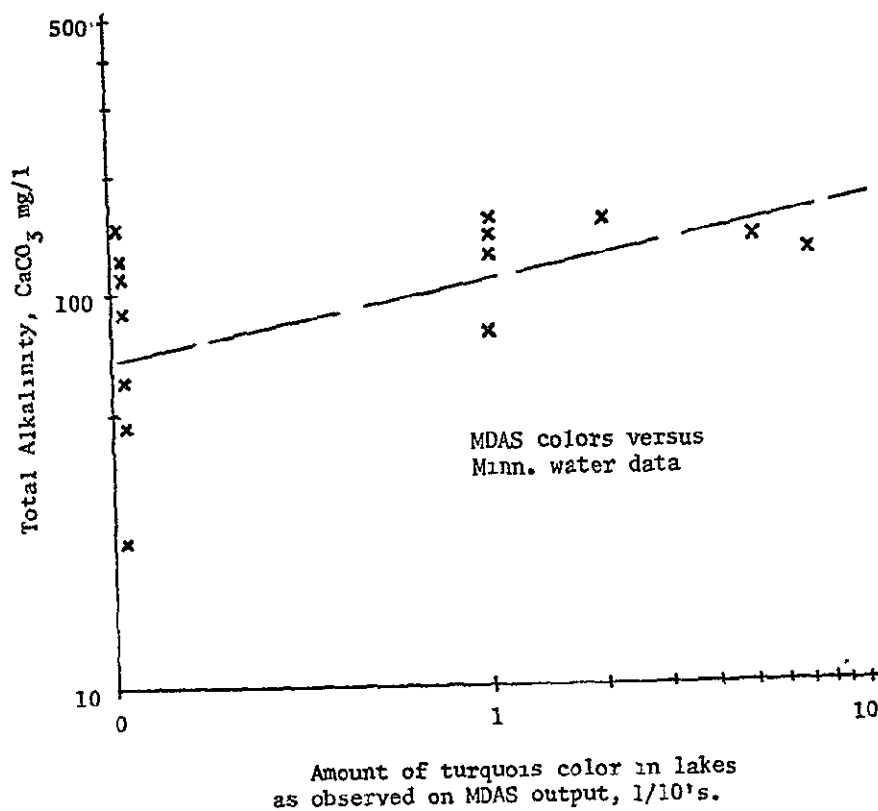


FIGURE 117. Data Pertaining to Marl Lakes when They were Printed Out as Turquoise by MDAS on the Color Coded Output Maps.



ORIGINAL PAGE IS
OF POOR QUALITY

REFERENCES

- Adams, M. S., and McCracken, M. D. 1974. Seasonal production of the *Myriophyllum* component of the littoral of Lake Wingra, Wisconsin. *Journal of Ecology* 62: 457-465.
- Ahern, F. J.; Goodenough, D. G.; Jain, S. C.; Rao, V. R.; and Rochon, G. 1977. Use of Clear Lakes as Standard Reflectors for Atmospheric Measurements. Proceedings of the Eleventh International Symposium on Remote Sensing of Environment, Environmental Research Institute of Michigan, Ann Arbor, Michigan.
- American Public Health Association, American Water Works Association, and Water Pollution Control Federation 1971. Standard Methods for the Examination of Water and Wastewater, Thirteenth Edition. 874 pp.
- American Society of Photogrammetry, Manual of Color Aerial Photography 1968 Falls Church, Virginia., 550 pp.
- Avery, T. E. 1968 Interpretation of aerial photographs. (2nd Edition). Burgess Publishing Company, Minneapolis, Minnesota. 324 pp.
- Baines, H. 1970. The Science of Photography Revised and edited by E. S. Bomback. Fountain Press, England (a division of John Wiley & Sons, Inc.) and Halsted Press, New York
- Birge, E. A., and Juday, C. 1927. The organic content of the water of small lakes Proceedings of the American Philosophical Society Philadelphia. 66 357-372
- Boland, D. H. P. 1975. An evaluation of the earth resources technology satellite (ERTS-1) the multispectral scanner as a tool for the determination of lacustrine trophic state. Ph D. thesis Oregon State University
- Boland, D. H. P. 1976. Trophic classification of lakes using LANDSAT-1 (ERTS-1) multispectral scanner data United States Environmental Protection Agency document EPA-600/3-76-037 245 pp. Available from National Technical Information Service, Springfield, Virginia, 22161.
- Campbell, R., (ed) 1970 Photographic Theory for the Motion Picture Cameraman. A. S. Barnes & Company New York. 160 pp
- Center for Remote Sensing Information and Analysis. 1971 Proceedings of the 7th International Symposium on Remote Sensing of Environment. Center for Remote Sensing Information and Analysis Institute of Science and Technology University of Michigan-Ann Arbor. Proc 7 (Vol. III) 1627-1650.

- Christman, R. F., and Ghassemi, M. 1966. Chemical Nature of Organic Color in Water. *Journal of the American Water Works Association*. 58(6): 723-741.
- Clegg, R. H., and Scherz, J. P. 1975. A comparison of 9 inch, 7 mm and 35 mm cameras. *Photogrammetric Engineering and Remote Sensing* 41(12) 1487-1500.
- Eastman Kodak Company. 1967. Kodak Black and White Films in Rolls. Kodak Publication No. AF-13. Rochester, New York.
- Edmundson, W. T. 1970. Phosphorus, nitrogen, and algae in Lake Washington after diversion of sewage. *Science* 169: 690-691.
- Fisher, L. T., and Scarpace, F. L. 1975. A versatile interactive graphics analysis program for multispectral data. *American Society of Photogrammetry* Washington, D.C. Proc. 41 601-612.
- Golterman, H. L., and Clymo, R. S. 1969. Methods for Chemical Analysis of Fresh Waters (Edited by H. L. Golterman with assistance of R. S. Clymo) International Biological Programme No. 8. Blackwell Scientific Publications. Oxford. 172 pp.
- Gramms, L. C. 1971. Reflectance and Transmittance Characteristics of Selected Green and Blue-Green Unialgae for Remote Sensing Applications. Ph.D. thesis University of Wisconsin-Madison.
- Gramms, L. C., and Boyle, W. C. 1971. Reflectance and Transmittance Characteristics of Selected Green and Blue-Green Unialgae. Remote Sensing Report No. 5, Institute for Environmental Studies, University of Wisconsin-Madison. 25 pp.
- Gustafson, T. D., and Adams, M. S. 1973a. Remote sensing of *Myriophyllum spicatum* L. in a shallow, eutrophic lake. American Water Resources Association. (Minneapolis, Minnesota). Remote Sensing and Water Resources Management Proc. 17 387-391.
- Gustafson, T. D., and Adams, M. S. 1973b. The Remote Sensing of Aquatic Macrophytes. Part I. Color-Infrared Aerial Photography as a Tool for Identification and Mapping of Littoral Vegetation. Part II. Aerial Photography as a Quantitative Tool for the Investigation of Aquatic Ecosystems. Institute for Environmental Studies Remote Sensing Program. University of Wisconsin-Madison. 25 pp.
- Hasler, A. D. 1947. Eutrophication of lakes by domestic drainage. *Ecology* 28 383-395.
- Holmes, R. W. 1970. The Secchi Disc. In *Martek Mariner*, Vol. 2, No. 1-2-3. Martek Instruments, Inc. Newport Beach, California.
- Hudson, R. D., Jr. 1969. Infrared System Engineering. Wiley-Interscience, John Wiley & Sons, Inc. New York. 642 pp.

- Hutchinson, G. E. 1957. A Treatise on Limnology, I. Geography, Physics, and Chemistry. John Wiley & Sons, Inc. New York. 1015 pp.
- Hutchinson, G. E. 1967. A Treatise on Limnology, Vol. II. Introduction to Lake Biology and the Limnoplankton. John Wiley & Sons, Inc. New York. 1115 pp.
- Hutchinson, G. E. 1973. Eutrophication: The scientific background of a contemporary practical problem. *American Scientist*. 61: 269-279.
- Jackson, M. L. 1958. Soil Chemistry Analysis. Prentice Hall Englewood Cliffs, New Jersey. 498 pp.
- Klooster, S. A., and Scherz, J. P. 1974. Water quality by photographic analysis. *Photogrammetric Engineering*. (No 8), 30. 927-935
- Likens, G. E. 1972. Eutrophication and aquatic ecosystems. In: G. E. Likens, ed., *Nutrients and Eutrophication. The Limiting Nutrient Controversy*. American Society of Limnology and Oceanography Special Symposia 1. 3-13.
- Margalef, R. 1968. *Perspectives in Ecological Theory*. University of Chicago Press. Chicago. 111 pp
- Melchiorri-Santolini, U., and Hopton, J. 1972. Detritus and its role in aquatic ecosystems. *Proceedings of an IBP-UNESCO Symposium. Memorie dell' Istituto Italiano di Idrobiologia*. (Suppl 29). 540 pp.
- Menzel, D. W., and Vaccaro, R. F. 1964. The measurement of dissolved organic and particulate carbon in seawater. *Limnology and Oceanography*. 9: 138-142.
- National Academy of Sciences 1969. *Eutrophication. Causes, Consequences, Correctives*. National Academy of Sciences. Washington, D.C. 661 pp.
- Naumann, E. 1919. Några synpunkter angående limnoplanktons ekologi med särskild hänsyn till fytoplankton. *Svensk Botanisk Tidskrift*. 13. 129-163.
- Nichols, S. A. 1971. The Distribution and Control of Macrophyte Biomass in Lake Wingra. Final Completion Report Project No. OWRR B-019-WIS. Water Resources Center, University of Wisconsin-Madison. 111 pp
- Nichols, S. A., and Mori, S. 1971. The littoral macrophyte vegetation of Lake Wingra. *Transactions of the Wisconsin Academy of Science, Arts and Letters*. 59. 107-119
- Oglesby, R. T. 1969. Effects of controlled nutrient dilution on the eutrophication of a lake. In: *Eutrophication Causes, Consequences, Correctives*. National Academy of Sciences. Washington, D. C. pp. 483-493.
- Piech, K. R., and Walker, J. E. 1971. Photographic Analyses of Water Resource Color and Quality. *American Society of Photogrammetry*. Falls Church, Virginia. Proc. 37. 258-279.

- Rogers, R. H.; Peacock, K., and Shah, N. J. 1973. A technique for correcting ERTS data for solar and atmospheric effects. Third Earth Resources Technology Satellite-1 Symposium sponsored by NASA/GSFC, Washington, D.C. pp. 1787-1804.
- Rodhe, W. 1969. Crystallization of eutrophication concepts in northern Europe. In: Eutrophication: Causes, Consequences, Correctives. National Academy of Sciences. Washington, D.C. pp 50-64.
- Rinehardt, G. L., and Scherz, J. P. 1972. A 35 mm aerial photographic system. American Society of Photogrammetry. Falls Church, Virginia. Proc. 38. 571-579.
- Ruttner, F. 1963. Fundamentals of Limnology (3rd Edition, translated by D. G. Frey and F. E. J. Fry) University of Toronto Press. Toronto. 295 pp.
- Scarpace, F.; Fisher, L. T., and Wade, R. 1974. The use of ERTS imagery for lake classification. Proceedings, Symposium on Remote Sensing and Photo Interpretation. Commission VII (ISP), Banff, Canada. pp. 259-271.
- Scherz, J. P., Graff, D. R., and Boyle, W. C. 1969. Photographic characteristics of water pollution. Photogrammetric Engineering. 25. 38-43.
- Scherz, J. P., and Stevens, A. R. 1970. An Introduction to Remote Sensing for Environmental Monitoring. Report No. 1, The University of Wisconsin Remote Sensing Program. Madison, Wisconsin.
- Scherz, J. P. 1971. Remote Sensing Considerations for Water Quality Monitoring. Proceedings, Seventh International Symposium on Remote Sensing of Environment Ann Arbor, Michigan pp. 1071-1087.
- Scherz, J. P. 1972. Final Report on Infrared Photography Applied Research Program. Report No. 12, Institute for Environmental Studies. University of Wisconsin-Madison
- Scherz, J. P.; Klooster, S. A., and Van Domelen, J. F. 1973. Aerial and Satellite Photography — A Valuable Tool for Water Quality Investigations. Proceedings, American Society of Photogrammetry — American Congress of Surveying and Mapping. Fall Convention, Orlando, Florida. pp. 883-905
- Scherz, J. P., Sydor, M.; and Van Domelen, J. F. 1973. Aircraft and Satellite Monitoring of Water Quality in Lake Superior near Duluth. Third Earth Resources Technology Satellite-1 Symposium sponsored by NASA/GSFC, Washington, D C pp 1619-1636.
- Scherz, J. P., and Van Domelen, J. F. 1973. Lake Superior Water Quality near Duluth from Analysis of Aerial Photos and ERTS imagery. Proceedings, International Symposium on Remote Sensing and Water Resources Management, Burlington, Ontario Also Proc No 17, Remote Sensing and Water Resources Management — American Water Resources Association pp 147-160.
- Scherz, J. P., Van Domelen, J. F., Holtze, K.; and Johnson, W. 1974. Lake Eutrophication as Indicated by ERTS Satellite Imagery. Proceedings, Symposium on Remote Sensing and Photo Interpretation. Commission VII (ISP), Banff, Canada pp 247-258.

- Scherz, J. P., Crane, D. R.; and Rogers, R. H. 1975. Classifying and Monitoring Water Quality by Use of Satellite Imagery. Proceedings, American Society of Photogrammetry — American Congress of Surveying and Mapping. Fall Convention, Phoenix, Arizona. pp. 320-343.
- Scherz, J. P., and Van Domelen, J. F. 1975. Water Quality Indication Obtainable from Aircraft and LANDSAT images and Their Use in Classifying Lakes. Proceedings, Tenth International Symposium on Remote Sensing of Environment Ann Arbor, Michigan. pp. 447-460.
- Scherz, J. P. 1977. Lake Water Quality Mapping from LANDSAT. Eleventh International Symposium on Remote Sensing of Environment Ann Arbor, Michigan.
- Schwoerbel, J. 1970. Methods of Hydrobiology. Pergamon Press, New York.
- Stauffer, R. E. 1974. Thermocline Migration — Algal Bloom Relationships in Stratified Lakes. Ph.D. thesis (Water Chemistry). University of Wisconsin-Madison.
- Steel, R. G. D., and Torrie, J. H. 1960. Principles and Procedures of Statistics McGraw-Hill Book Company, Inc. New York. 481 pp.
- Strandberg, C. H. 1963 35 mm Aerial Photography for Measurement Analysis Presentation, U.S. Public Health Service, Division of Water Supply and Pollution Control, Demonstration Grant WPD 20 01-1963.
- Strandberg, C. H. 1965. Aerial Photographic Interpretation Techniques for Water Quality Analysis, a paper presented at the 1965 Meeting of American Society of Photogrammetry at Washington, D C , March 30.
- Strandberg, C. H. 1967 Aerial Discovery Manual. John Wiley & Sons, Inc. New York.
- Strickland, J. D. H., and Parsons, T. R. 1972. A practical handbook of seawater analysis 2nd edition Bulls Fish. Res. Bd. Canada. 167, 310 pp.
- Sydor, M. 1973. A Study of Minnesota Forests and Lakes Using Data From Earth Resources Technology Satellites (12 month progress report). Space Science Center University of Minnesota-Minneapolis. 70 pp.
- Thienemann, A. 1918 Untersuchungen über die Beziehungen zwischen dem Sauerstoffgehalt des Wassers und der Zusammensetzung der Fauna in norddeutschen Seen. Archiv für Hydrobiologie. 12: 1-65
- Thorne, J. F. 1976 The Remote Sensing of Algae. M.S. thesis (Botany). University of Wisconsin-Madison.
- Thorne, J. F. 1977. The Remote Sensing of Algae. Sixth Annual Remote Sensing of Earth Resources Symposium University of Tennessee Space Institute Tullahoma, Tennessee.

- Turner, R. E., Malila, W. A., and Nalepka, R. F. 1971. Importance of Atmospheric Scattering in Remote Sensing. Proceedings of the Seventh International Symposium on Remote Sensing of Environment, Environmental Research Institute of Michigan. pp. 1651-1697.
- Turner, R. E., and Spencer, M. M. 1972. Atmospheric Model for Correction of Spacecraft Data. Proceedings of the Eighth International Symposium on Remote Sensing of Environment. Environmental Research Institute of Michigan, Ann Arbor, Michigan. pp. 895-934
- Vallentyne, J. R. 1974. The Algal Bowl, Lakes and Man. Department of Environment, Fisheries and Marine Service. Ottawa, Canada. Publ 22. 186 pp
- Van Domelen, J. F. 1974. Photographic Remote Sensing — A Water Quality Management Tool. Ph.D. thesis (Civil Engineering). University of Wisconsin-Madison.
- Vollenweider, R. A. 1971. Scientific Fundamentals of the Eutrophication of Lakes and Flowing Waters, with Particular Reference to Nitrogen and Phosphorus as Factors in Eutrophication. Tech Rep., Organization for Economic Cooperation and Development. Paris. 254 pp.
- Weber, C. A. 1907. Aufbau und Vegetation der Moore Norddeutschlands. Botanische Jahrbücher 40, Beibl. 90 19-34.
- Westlake, D. F. 1965. Some basic data for investigations of the production of aquatic macrophytes. Mem. Ist. Ital. Idrobiol. 18 (Supplement) 229-248.
- Wetzel, R. G. 1964. A comparative study of the primary productivity of higher aquatic plants, periphyton, and phytoplankton in a large shallow lake. Internationale Revue der Gesamten Hydrobiologie. 49. 1-61.
- Wetzel, R. G., and Allen, H. L. 1970. Functions and interactions of dissolved organic matter and the littoral zone in lake metabolism and eutrophication. In: Z. Kajak and A. Hillbricht-Ilkowska, eds., Productivity Problems of Freshwaters. PWN Polish Scientific Publishers. Warsaw. pp. 333-347.
- Wetzel, R. G. 1975. Limnology. W. B. Saunders Company. Philadelphia, Penn.
- Wrigley, R. C., Klooster, S. A.; LeRoy, M. J., Horne, A. J.; and Anderson, H. M. 1975. Field Measurements of Algal Biomass by Infrared Reflectance. NASA TMX-73, 107.

GLOSSARY

Airborne residual	the residual when the signal from a deep, clear lake is subtracted from the signal from another lake.
Allochthonous	refers to a source of organic matter production located outside of the lake.
Allotrophic.	see allotrophy.
Allotrophy.	the process of lake enrichment or nutrition from an external source.
Alphanumeric	letters, numbers, and other characters.
Anaerobic	refers to biological functions taking place in the absence of oxygen. Anaerobic conditions often prevail in mud or sediments causing the familiar gas bubbles of methane and hydrogen sulfide.
Aperture	opening in a camera lens that allows light to pass on to the film. The focal length of the lens, f , divided by its diameter, d , defines a number F which is called the aperture setting of the camera lens. $F = f/d$
Apparent laboratory reflectance:	percentage of radiance from a sample material being analyzed when compared to a standard reflectance panel in the laboratory
ASA	the speed of a film or its sensitivity to light as defined by the American Standards Association.
Atmospheric effects	remote sensing signal modification caused by the atmosphere
Autochthonous:	refers to a source of organic matter production located within a lake.
Autotrophic:	see autotrophy.
Autotrophy	the process of lake enrichment or nutrition from an internal source
Barium sulfate (BaSO_4).	a white material used in the laboratory as a reflectance standard.
Biomass	amount or mass of biological material.
Blue-green algae	a group of algae containing chlorophyll <u>a</u> plus phycocyanins

Bog dystrophic.	see dystrophic
Bottom reflectance.	signal returning from the bottom of a water body.
Chironomid.	type of aquatic insect whose larvae are associated with the low-oxygen sediments of enriched waters.
Colloidal	pertaining to a suspension of very small, fine material in water.
Color micro-densitometer.	see spectral microdensitometer.
Color negative film:	film that is processed to a color negative such that what was blue on the scene becomes yellow on the film, etc. The colors developed on the negative are complementary colors of the exposing light.
Color reversal film:	a color film that is processed to a positive so that what was blue on the scene becomes blue on the film, etc.
Depth of field:	distance within the scene being photographed (toward and away from the camera) where objects are in focus.
Diatom	a group of algae containing chlorophyll <u>a</u> and <u>c</u> plus fucoxanthins (yellow-brown in color).
Diffuse reflector	a rough surface which scatters incident light in various directions
DNR.	Department of Natural Resources.
Dystrophic:	pertaining to lakes which receive large inputs of decay-resistant humic substances Dystrophic lakes have also been called brown water lakes, tannin lakes or humic lakes
Ecosystem.	a system formed by the interrelationships between a community of organisms and its environment.
Electromagnetic energy spectrum	the continuum of x-rays, visible light, heat, and radio waves
EMDAG	Environmental Monitoring and Data Acquisition Group Part of the Institute for Environmental Studies, University of Wisconsin-Madison.
Epipellic	growing on mud or sand (soft bottom substrate).
Epiphyton	an organism which grows attached to a larger plant

ERTS:	Earth Resources Technology Satellite, more recently called LANDSAT.
Eutrophic.	a lake ecosystem of high primary productivity.
Filamentous algae:	algae that are comprised of long strings of cells.
Film wedge:	image of a step wedge as it appears on a developed film.
Fingerprint:	the difference in the volume reflectance of an experimental water sample and clear water expressed over a given wavelength range. This difference is due only to material present in the experimental water sample
Focal length:	distance in which parallel light rays reaching a lens are brought to focus at a point
FTU.	Formazin Turbidity Unit A method of measuring turbidity of water which uses an optical meter.
Green algae:	a group of algae containing chlorophyll <u>a</u> and <u>b</u> only.
Ground truth.	the results of field investigations to ascertain the ground conditions relating to some remote sensing investigation.
Halides	Bromide, Chloride, Iodide, etc.
Hectare	a metric unit of area equal to 10,000 square meters.
Humic lakes:	lakes containing large amounts of humic substances. Humic refers to a group of organic acids, humic acids. Such lakes are often associated with tamarack swamps and have a brown, tea color. They are also known as brown water or dystrophic lakes.
Hypereutrophic	extremely eutrophic.
Hypolimnetic.	pertains to the layer of a lake below the thermal stratification zone (i.e., the layer on the bottom of the lake below the zone of rapid temperature change).
Hypolimnion	the area of a lake below the zone of thermal stratification. (No significant amount of light penetrates this zone.)
IES:	Institute for Environmental Studies at the University of Wisconsin-Madison.
Irradiance	total energy incident on a unit area of some flat surface per unit time.
JTU.	Jackson Turbidity Unit. A candle method for determining turbidity of water

Labile compounds·	chemical compounds which can be easily biologically degraded or converted in form (e.g., a solid converted to a gas by the addition of heat or an organic chemical which can be converted easily from one form to another).
Laboratory apparent reflectance·	see apparent laboratory reflectance
Laboratory difference·	the difference resulting when the laboratory apparent reflectance for distilled water is subtracted from the laboratory apparent reflectance for another water sample.
Laboratory residual.	the residual signal in the laboratory when the signal backscattered from distilled water is subtracted from that backscattered from another water sample.
Lambert's Law	law that relates to radiance onto and from a perfect diffuse reflector For example, from a uniformly illuminated sky on an overcast day (when the sun is not visible) the total irradiance onto a flat panel is H'_O , $H'_O = \pi L'_C$ where L'_C is the radiance of the skylight Lambert's Law also states that the radiance returning upward from the panel (P') is as follows· $P' = H'_O \rho_p / \pi$ where ρ_p is the diffuse reflectance of the panel. L'_C and P' are radiance values, watts/cm ² s H'_O is irradiance in watts/cm ² .
LANDSAT	originally called ERTS. Earth monitoring satellite in polar orbit over the earth It is capable of taking an image of any point on the earth once every eighteen days. Images are recorded in the green, red, and infrared parts of the energy spectrum.
Laurentian	pertaining to hard Precambrian rocks exposed in Canada.
Limnology	the study of freshwater lakes, rivers, and streams
Littoral zone·	shallow zone at the edge of a lake where light penetrates to the bottom and rooted lake weeds can be found.
Macroflora	relatively large plants (visible to the unaided eye)
Macrophytes·	large aquatic plants. Some are often called lake weeds
Marl lakes	lakes where the chemistry and lake metabolism are primarily controlled by calcium and magnesium carbonates

MDAS.	Multispectral Data Analysis System. A computer system developed by the Bendix Corporation for analyzing LANDSAT tapes and classifying land cover types.
Mesotrophic:	a lake that is between eutrophic and oligotrophic in trophic status; i.e., having moderate algal and/or weed growth.
Metabolic:	pertaining to the life activities or processes of an organism.
Metabolism:	see metabolic.
Metric cameras:	cameras specifically designed to produce aerial photos of extreme positional accuracy.
Micron (μ).	also called micrometer; one millionth of a meter = 10^{-6} meters
Multiband photography:	photography where the energies in different parts of the photographic spectrum are photographed separately.
Multispectral scanner:	an optical scanner which records the energy received in several bands of the electromagnetic energy spectrum.
Munsell colors	a system of color specification developed by H. H. Munsell based on hue, saturation, and brilliance in terms of certain arbitrary scales presented in a series of charts.
Nanometer	one billionth of a meter = 1×10^{-9} meters.
NASA.	National Aeronautics and Space Administration.
Nonvolatile	substances not easily changed to gas by heat or chemical action.
Oligotrophic	low biological productivity in a lake. Usually refers to a very clear lake free from weeds and algae
Ontogeny.	in the context of this report, the developmental sequence of events of a lake (for example, the evolution of a lake from oligotrophy to eutrophy).
Organic	compounds of carbon, hydrogen, and oxygen derived from living organisms.
Organic carbon.	reduced carbon from living organisms.
Orthochromatic film	black and white photographic film sensitive to ultraviolet, blue, and green light.

Panchromatic film:	black and white film which is sensitive to all the colors that the human eye sees.
Particulates:	finely divided solid or liquid particles.
PEP terminal:	an interactive graphic computer terminal developed by Princeton Electronic Products, Inc.
Photic zone.	zone of sufficient light for photosynthesis.
Photogrammetry:	art or science of obtaining reliable distance and elevation measurements from photographs.
Photometer:	instrument for measuring light in the visible and near visible portion of the electromagnetic spectrum
Photometric:	pertaining to measurement of light.
Photometry.	measurement of light emitted or reflected from objects.
Photosynthate	organic product of photosynthesis.
Photosynthetic	the capability of a plant to make its organic nutrients from light and carbon dioxide.
Phytoplankton	algae that are suspended within the water (free-floating algae)
Planimetry	the measurement of map area by use of a planimeter, an instrument which traces the boundaries of map area and simultaneously performs an aerial integration.
Precambrian	a geological time prior to when easily found fossils were left in rocks or, a rock bed from this period.
Radiometry.	measurement of intensity of radiant energy.
Reflectance:	a fraction expressing the percentage of energy returned from an object.
Reflectance panel	panel of known and constant diffuse reflectance across the photographic spectrum.
Reflection.	the return of energy from any object
Refractory compounds	inorganic compounds which are not labile at high temperature i.e , not easily converted to gas by heating or converted from one chemical form to another,
Remote sensing:	determining the physical or chemical properties of an object without actually coming in contact with it.

Resolution cell:	the smallest ground dimension which can be discerned on imagery.
Rhizome	a stem which grows under the ground and sends up visible plant parts at intervals along its length.
RPMI	Radiant Power Measuring Instrument. A portable instrument developed by Bendix Corporation.
Satellite residual	see airborne residual
Scuba	underwater diving gear (self-contained underwater breathing apparatus).
Secchi disc:	a white or black and white disc about eight inches in diameter which is lowered into the water in order to measure the transparency of the water
Secchi disc reading:	a water transparency measure based on the depth at which the Secchi disc disappears from sight.
Sensitometry	techniques for measuring the sensitivity of different films
Sestonic	pertaining to material suspended in water,
Signature	the energy-wavelength curves for light returning from particular materials suspended in water.
Silver halides	Silver Bromide, Silver Chloride, Silver Iodide, etc.
Skylight.	energy originating in the sky Either from blue sky, haze, or clouds
Snell's Law	law that relates to specular reflection from and refraction into an interface between two materials.
Spectral microdensitometer:	a device used for analyzing color of a film transparency. Sometimes referred to as color microdensitometer.
Specular reflection	reflection from a smooth surface, as in the reflection from a mirror.
Steradian	unit measure of a solid angle (total sphere = 4π steradians).
Succession	the progressive development of vegetation toward its highest ecological expression, the climax; replacement of one plant community by another.
Surface reflection:	signal returning from the water surface.

Target or test area:	an area on the ground for which the investigators know the ground conditions.
Taxonomy	science of classification of organisms.
Total suspended solids:	weight of both volatile and nonvolatile suspended material in a water volume (usually expressed as mg/l).
Training set.	a small subset of the data from a remote sensing image that corresponds to the test area or training sites on the ground.
Training sites:	see target or test area
Trophic	relating to the processes of energy and nutrient transfer from one or more organisms to others in an ecosystem
Turbidity:	a measure of the amount of light backscattered from suspended particles within a water body
Volatile	substances easily changed to gas by heat or chemical action.
Volume reflectance.	signal returning from material in a volume of water.

APPENDIX III

Radiative Transfer Model Including Air-Water Interface

Radiative transfer models for turbid atmospheres have been developed in the Department of Meteorology. The radiative processes occurring in the water are essentially the same as those in the air. The model developed by Dr. James Weinman and Ms. Linda Kalman has been extended to the water, with appropriate changes made to account for the air-water interface.

The equation of transfer defining the diffuse irradiance, $I(\tau, \mu, \alpha)$, is

$$\{1\} \mu \frac{dI}{d\tau}(\tau, \mu, \alpha) = -I(\tau, \mu, \alpha) + \frac{\omega}{4\pi} \int_0^1 \int_{-1}^1 P(\mu, \alpha; \mu', \alpha') I(\tau, \mu', \alpha') d\mu' d\alpha'$$

where

$$\mu = \cos \theta$$

$$\theta = \text{zenith angle}$$

$$\alpha = \text{azimuth angle}$$

$$K(Z) = \text{extinction coefficient}$$

$$\tau = \int_0^Z K(Z') dZ' = \text{the optical depth}$$

$$\omega = \text{albedo for single scattering}$$

$$P(\mu, \alpha, \mu', \alpha') \text{ is the phase function for light incident at } (\mu', \alpha') \text{ and scattered in the direction } (\mu, \alpha)$$

Two iterations are performed to obtain an expression for the diffuse radiance arriving at the camera; The first iteration uses simple approximations to compute the radiance, $I(\tau, \mu)$, and the phase function $P(\mu, \alpha, \mu', \alpha')$. The equation is solved and an approximate analytical expression for the source term is derived in terms of measurable parameters (scattering and absorption coefficient in air and water).

The second iteration uses the approximate expression for $\hat{I}^*(\tau, \mu)$ obtained above, in the integral term only. Standard haze phase functions and measured sediment phase functions are used in terms involving single scattering events. Approximate phase functions are used to evaluate terms involving multiple scattering. The equation of transfer is resolved and an expression for the diffuse radiance is obtained.

1st Iteration

Expressions for $\hat{I}^*(\tau, \mu)$ and $P(\mu, \alpha, \mu', \alpha')$ can be determined using the Delta-Eddington approximation [1,2].

$$\{2\} \hat{I}^*(\tau, \mu, \alpha) = \hat{I}(\tau, \mu_0, \alpha_0) \delta(\mu - \mu_0) \delta(\alpha - \alpha_0) + \hat{I}(\tau, -\mu_0, \alpha_0) \delta(\mu + \mu_0) \delta(\alpha - \alpha_0)$$

(1)(2)

$$+ (I_0(\tau) + \mu I_1(\tau))$$

(3)

ORIGINAL PAGE
OF POOR QUALITY

- (1) represents the direct solar beam,
- (2) represents the solar beam after reflection off the water surface,
- (3) represents diffuse light

The phase functions for haze particles in the air, as well as sediment particles in the water are typically sharply peaked in the forward scattering angles. It has been found suitable and convenient for calculations to represent the phase function as shown below:

$$P(\mu, \alpha; \mu', \alpha') = 4\pi f \delta(\mu' - \mu) \delta(\alpha' - \alpha) + (1-f) \bar{P}(\mu, \alpha, \mu', \alpha')$$

The first term is the forward scattering peak represented by a delta function; f is the fraction of area under the phase function curve that is represented by the forward scattering, it is typically approximately 0.5. \bar{P} is a scaled phase function with the large forward scattering peak eliminated. It is approximated by

$$\bar{P} = \sum_{l=0}^L W_l P_l(\mu) P_l(\mu')$$

where P_l are Legendre polynomials. The approximate phase function used in the integral of equation (1) is truncated at $L=1$.

Using these approximations the integral term can be evaluated explicitly, and the equation solved for I_0 and I_1 , the diffuse intensity terms.

2nd Iteration

The equation of transfer is basically the same as in the 1st iteration

$$\{3\} \mu \frac{dI(\tau, \mu, \alpha)}{d\tau} = -I(\tau, \mu, \alpha) + \frac{\omega}{4\pi} \int_0^1 \int_0^{2\pi} P(\mu, \alpha, \mu', \alpha') \bar{I}^*(\tau, \mu', \alpha') d\mu' d\alpha'$$

The term $\bar{I}^*(\tau, \mu', \alpha')$ in the integral is represented as

$$\bar{I}^* = I_{\text{diffuse}} + \int_0^V \delta(\mu - \mu_0) \delta(\alpha_0) + \hat{I} \delta(\mu + \mu_0) \delta(\alpha_0)$$

where $I_{\text{diffuse}} = I_0 + I_1 \mu$ was obtained as the solution to the 1st iteration

The integral is evaluated using measured scattering phase functions for the sediment, and standard haze phase function for the terms involving single scattering events (1) and (2). The integral term is evaluated using Legendre Polynomials to represent $P(\mu, \alpha; \mu', \alpha')$.

The equation is then solved utilizing appropriate boundary conditions for the irradiance.

Various approximations appear in the model which may affect the accuracy of the derived radiances. The diffuse radiances derived in the first iterations are insensitive to changes in the azimuth. The radiances scattered by the atmosphere are quite sensitive to azimuth angle if the sun is at an appreciable zenith angle. We therefore intend to adapt a Doubling program which was previously developed by Hansen [3] to this part of the problem. This work will be based on the efforts of Davies and Weinman (1977) [4].

The existence of waves and large multiple scattering in the water will obliterate any α dependence in terms dealing with the water

Another problem arises as a result of waves on the water surface. The model, as it has thus far been developed, assumes a flat unrippled water surface which will produce familiar specular reflection terms. With waves and ripples present the problem becomes more complex (Preisendorfer [5]) To date, no attempt has been made to consider the effect of waves. Waves tentatively appear to be of little importance, since the imagery of the turbid water exhibits little or virtually no extended sunglint even when there is substantial specular reflection of the solar disc further out in the lake.

References

1. Joseph, J.H., W.J. Wiscombe and J.A. Weinman, 1976. "The Delta-Eddington Approximation for Radiative Flux Transfer." J. Atm. Sci., 33 2452-2459
2. Shettle, E.P., and J.A. Weinman, 1970. "The Transfer of Solar Irradiance through Inhomogeneous Turbid Atmospheres Evaluated by Eddington's Approximation." J. Atm. Sci., 27 1048-55.
3. Hansen, J.E., 1969. "Radiative Transfer by Doubling Very Thin Layers." Astrophys. J., 155: 565-573.
4. Davies, R. and J.A. Weinman, 1977. "Results from Two Models of the Three Dimensional Transfer of Solar Radiation in Finite Clouds." Proceedings, Symposium on Radiation in the Atmosphere, Garmisch-Partenkirchen, 19-28 August 1976. Science Press, Princeton, N.J., p. 630
5. Preisendorfer, R.W., 1976. Hydrologic Optics, Vol VI U.S. Dept. of Commerce, NOAA, Honolulu, Hawaii. p. 390.

ORIGINAL PAGE IS
OF POOR QUALITY

APPENDIX IV

ORIGINAL PAGE IS
OF POOR QUALITY

September 29, 1977

Mr. Marshall Johnston
Janesville Gazette
1 So. Parker Dr.
Janesville, Wis.

Dear Marsh:

An article in the September 22 edition of your newspaper reported on the results of a Beloit-area thermal scan research project jointly undertaken by Wisconsin Power and Light Company, the University of Wisconsin and the Wisconsin Department of Natural Resources. The story labeled the research as a failure because "the results of the tests were disappointing."

Research should not be termed a failure merely by calling its results disappointing. Quite the contrary is true, however. We learned much from this initial thermal scan project. We now know more about roof heat loss and thermal scan technology than we would had we not participated in this research.

One of the important byproducts of research, of course, is being able to determine what works and what doesn't work. We are greatly encouraged by what the scanning program accomplished. And we consider it highly successful in creating an awareness among our customers of what they can do to weatherize their homes.

We learned of the limitations of thermal scanning and the flyovers, limitations which will be beneficial in any future programs.

We learned that our customers are eager to learn more about insulation and how to conserve energy.

Through a customer survey, which was an integral part of the entire thermal scan project, we learned of the many problems and concerns that we must deal with in our future efforts to help customers conserve energy.

There are many more positive elements that resulted from this research program, none of which were brought out in the story.

Not only was I concerned by your reporting that the research program was a failure, but I was particularly disappointed when a wire service moved the story in a similar negative tone and it was then picked up by other papers in the state.

Wisconsin Power and Light is involved in many research projects, ranging from load management and solar heating experiments to the feasibility of turning coal into a liquid fuel. I shudder to think that their success or failure will be judged on whether the results of initial tests were disappointing. Rather, I think they should be judged on the

-2-

final results, accumulated from the benefits derived from each step along the way.

We will continue to participate in these various research projects in order to continue to provide our customers with adequate reliable energy supplies. In the meantime, we look upon our thermal scan project, not as a failure, but as a step towards helping our customers conserve energy at a time when it has become one of the necessities of life.

Sincerely,

DWT:bcs

David W. Thompson,
Division Manager

APPENDIX V

University of Wisconsin-Parkside
Kenosha Wisconsin 53140
Telephone AC 414 553 2228

Physical Plant

June 20, 1977

Mr. Richard F. Woroch
Central Administration
University of Wisconsin System
1930 Monroe Street, P.O. Box 8010
Madison, Wisconsin 53708

RECEIVED U ARC AND L G			
JUN 22 1977			
BTA		TES	
GGF		RT	
EGH		CE	✓
JJK		T	
WTK			I
EJQ		FILE	

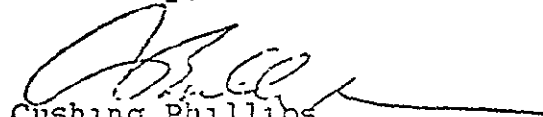
Dear Dick:

I am returning herewith your slide of the infra-red trace made last December of the UW-Parkside buildings. I also enclose my notes interpreting the slide.

Comparison of the slide to plans of the buildings made it possible to identify most of the "hot" areas quite accurately, I believe, although the scale distortion complicated the analysis. There is no question in my mind that the heat losses through the Classroom roof and the Physical Education pool roof are the result of defective insulation. The suggested theory that the heat loss indicated on the trace along the south side of Classroom Building is reflected solar heat from the windows doesn't stand up when you consider that the east half of the Classroom south face has large windows close together, but the west half has very small, widely spaced windows. Both areas are similar on the trace. Also, the south faces of other buildings with more glass do not show comparable heat loss.

I believe this information is worth forwarding to the Bureau in connection with the arguments over liability and loss on the Classroom roof. If it is possible to assign temperatures to the colors of the film a fair estimate of heat loss could probably be made and this, of course, has a price tag.

Sincerely,


Cushing Phillips
Director, Physical Plant

CP:ck
Enclosures
cc: Bert Anderson
Terry Steiger
J.E. Galbraith
G. Goetz

ARCHITECTURE AND ENGINEERING	FILE
UW-	
PROJ NAME	
CAT.	
PROJ. NO	

Notes - Infra-red (Heat Survey) Scan - UW-Parkside

(from slide made 12/15/76)

(1) Com Arts

Red areas at east and west end of Unit B (Classroom) are mechanical penthouse exhausts. Central yellow area of Unit B is skylight.

(2) WLLC

Central red area is skylight. Small red areas west of skylight and at NW, NE, and SE corners are exhausts from penthouses.

(3) Greenquist

Four central red areas (in N-S line) are skylights. Four yellow areas to west are mechanical penthouses. Red and yellow areas between the two north and two south pairs of penthouses are the result of exhausts from the penthouses. Red and yellow area at south side of auditorium, east of concourse is relief vent for auditorium ventilating system.

(4) Physical Education

Yellow and red area in NW corner is swimming pool roof. Small red areas in north and south center are exhausts. The swimming pool roof and low roof areas appear to have defective insulation.

(5) Classroom

Skylights along concourse show up as small red areas; also skylight south of north central penthouse (and exhaust) shows as red area. Entire roof area except for part of the roof over 105 and 107 shows yellow and red. This can only be the result of wet insulation (which is borne out by the recent inspections of the roof).

(6) Union

Exhausts show at NW corner and north central area as red spots. Skylights at south side of building and along north side of central part show yellow with small red areas. Other exhausts show as small red areas at north side of theatre and center of south side.

APPENDIX VI

DIGITAL ANALYSIS OF LANDSAT DATA IN THE
DETECTION AND MAPPING OF SPRUCE BUDWORM INFESTATION
IN NORTHERN WISCONSIN

H. E. Hogan

R. P. Madding

Institute for Environmental Studies

The University of Wisconsin-Madison

Research Report Prepared For

U.S. Department of Agriculture
Forest Service
St. Paul, Minnesota

State of Wisconsin
Department of Natural Resources
Madison, Wisconsin

October 1977

TABLE OF CONTENTS

	<u>Page</u>
SUMMARY	1
BACKGROUND	5
STUDY AREA DESCRIPTION AND INFESTATION CHARACTERISTICS	8
DATA COLLECTION AND ANALYSIS METHODS	11
RESULTS AND DISCUSSION	18
CONCLUSIONS AND RECOMMENDATIONS	39
REFERENCES	41
ACKNOWLEDGEMENTS	42

LIST OF TABLES AND FIGURES

	<u>Page</u>
Table 1. Visual Characteristics of Ground Resources on Color-Infrared Aerial Imagery from 12 July 1976	12
Table 2. Program CLSTRN Output	24
Table 3. Brightness Value Range	26
Figure 1. Summary of Project Activities	4
Figure 2 Site Location Map	9
Figure 3. Brightness Value Map - Band 7, and Final Training Set Locations	21
Figure 4 Box Classification	27
Figure 5 Forest Cover Type Map	31
Figure 6. Vegetation Classification Map	32
Figure 7. Vegetation Classification Map	35

ORIGINAL PAGE IS
OF POOR QUALITY

SUMMARY

The use of LANDSAT MSS digital data and computer-assisted analysis techniques was investigated in a study to detect and map areas of spruce budworm infestation in forest stands of balsam fir and white spruce. The approach is a potentially efficient method of monitoring vegetation conditions and conducting forest surveys. The objectives of the study were to utilize LANDSAT data (a) to identify and map areas of infestation, and (b) to determine the severity of infestation that is present.

A LANDSAT computer-compatible tape was obtained from 11 July 1976 when peak foliage browning of fir and spruce was visible. Computer analysis was accomplished by the use of the Remote Sensing Applications Programs of the Environmental Monitoring and Data Acquisition Group of the Institute for Environmental Studies at the University of Wisconsin-Madison. Color and color-infrared 70mm aerial imagery at scales of 1:78,900 and 1:46,800 provided a record of ground conditions.

Training sets for computer classification were identified from a forest cover type map that was produced by photo-interpretation. Local vegetation patterns made the selection of small-sized training sets necessary. However, the training sets could be well located on a computer printout map with respect to prominent geographic features. Training set performance was based on the results from the intermediate program analysis and from a comparison of preliminary computer classifications with the cover type map. Spectral differences between many of the training sets

representing different levels of defoliation could not be readily distinguished. The final training sets are those with distinct spectral differences which best qualified to represent appropriate resource classes.

Nine resource classes were identified including two levels of coniferous infestation. Extensive and moderate infestation categories were used as classification levels to distinguish between the interpretations made by ground and remote sensing survey methods. Overlap between the range of brightness values of various resource classes was present. Consequently, the initial results of a supervised box classification (BOXCLS) program were unsatisfactory, and further refinement of mutually exclusive class boundaries for this approach was not pursued. An unsupervised maximum likelihood classification (MAXLIK) program was used instead.

The classification printout maps from MAXLIK gave results that were mostly favorable. The location and spatial coverage of all resource classes was fairly accurate when the computer classification map was compared with the cover type map and checked with the color-infrared aerial imagery. Moderate Infestation represents an intermediate class such that its cover type boundaries were not always clearly defined. Its distribution by computer classification, however, is consistent with the photo-interpretation results. The class is mostly associated with a Mixed Swamp Conifer cover type, as well as other heterogenous composition types that do not qualify as Extensive Infestation.

The overall results of Extensive Infestation were also good, but there were classification errors. The spatial coverage of large, homogenous stands of fir and spruce with spruce budworm infestation compared well with the

cover type map. Numerous small patches of coniferous infestation were also located by the computer classification. However, the class was unable to distinguish between different species types that were exhibiting defoliation properties similar to the fir and spruce.

More adequate training sets of these conditions would permit better analysis, but the identification of different species by spectral response may be possible only by more sensitive satellite sensors. The results indicate that the LANDSAT system can be used to identify and map areas of coniferous infestation, but that supplementary methods are required to determine the type and severity of defoliation that is present. Further analysis techniques are recommended to remedy some of the problems.

The principal activities of the study are summarized by the flow chart (Figure 1). The organization and interaction of LANDSAT and photo-interpretation activities can be easily seen. Process components are identified by round-cornered boxes, and product components are identified by square-cornered boxes. Each component is the resultant of all entering components. Individual programs of the RS*AP program file are identified above the corresponding activities performed by the computer. Selection of the final training sets for computer classification is preceded by a feedback circuit where training set performance is evaluated by the intermediate program analysis and preliminary classifications. Reference to the flow chart may be made while reviewing the documentation of the study.

```

graph LR
    RSAP[RS*AP PROGRAM FILE] --> IDENTIFY_STUDY_AREA[IDENTIFY STUDY AREA]
    STUDY_AREA[STUDY AREA] --> LANDSAT_VEIPASS[LANDSAT VEIPASS]
    STUDY_AREA --> PHOTO_FLIGHT[AERIAL PHOTOGRAPHIC FLIGHT MISSION]
    LANDSAT_VEIPASS --> SELECT_SCENE(SELECT LANDSAT SCENE FROM FILM TRANSPARENCIES)
    SELECT_SCENE --> COMPATIBLE_TAPE[COMPUTER COMPATIBLE TAPE]
    COMPATIBLE_TAPE --> IDENTIFY_STUDY_AREA
    IDENTIFY_STUDY_AREA --> BRIGHTNESS_MAP[BRIGHTNESS VALUE MAP 1:27,500]
    BRIGHTNESS_MAP --> IDENTIFY_TRAINING_SETS[IDENTIFY TRAINING SETS]
    IDENTIFY_TRAINING_SETS --> TRAINING_ANALYSIS[TRAINING SET PROGRAM ANALYSIS]
    TRAINING_ANALYSIS --> FINAL_SELECTION[FINAL TRAINING SET SELECTION]
    FINAL_SELECTION --> VEGETATION_CLASS[VEGETATION CLASSIFICATION M-PC]
    PHOTO_FLIGHT --> FILM_PROCESSING[70mm FILM PROCESSING]
    FILM_PROCESSING --> COLOR_IMAGERY[COLOR & COLOR-INFRARED AERIAL IMAGERY 1:78,900 1:46,800]
    COLOR_IMAGERY --> PHOTO_INTERPRETATION[PHOTO INTERPRETATION]
    PHOTO_INTERPRETATION --> BASE_MAP[BASE MAP OF FOREST CONDITIONS 1:24,000]
    BASE_MAP --> FOREST_OVERLAY[FOREST COVER TYPE MAP OVERLAY 1:27,500]
    FOREST_OVERLAY --> IDENTIFY_TRAINING_SETS
    FOREST_OVERLAY --> TRAINING_EVAL[TRAINING SET PERFORMANCE EVALUATION]
    TRAINING_EVAL --> PRELIMINARY_MAPS[PRELIMINARY CLASSIFICATION MAPS]
    PRELIMINARY_MAPS --> IDENTIFY_TRAINING_SETS
    EXISTING_MAPS[EXISTING COVER TYPE MAPS] --> FOREST_OVERLAY
    ZOOM_SCOPE[ZOOM TRANSFER SCOPE] --> BASE_MAP
    ZOOM_SCOPE --> FOREST_OVERLAY
    FILM_CATALOG[FILM CATALOG FILE] --> COLOR_IMAGERY
    USGS_MAP[USGS MAP 1:24,000] --> PHOTO_INTERPRETATION
    GROUND_CHECK[GROUND CHECK] --> BASE_MAP
    TRAINING_ANALYSIS --> BOA_CLS[BOA CLS ANALYSIS]
    BOA_CLS --> PRELIMINARY_MAPS
    
```

The flow chart summarizes the project activities that were used to determine LANDSAT capabilities in the detection and mapping of spruce budworm infestation. A similar procedure would be followed in an operational program to monitor and inventory forest conditions by satellite-computer methods.

BACKGROUND

The composition and structure of the forest community is determined by the dynamic interaction of both physical and biological influences. Vegetation change is a continuous process in community development as a result of the inherent properties of plant populations, fluctuations in the environment, and the presence of disturbance conditions. Disturbance often has the most immediate and pronounced effects on vegetation and it is an important concern in natural resource management.

Vegetation change due to disturbance may result from a variety of causes including fire, windthrow, drought, flooding, disease, insect infestation, animal browsing, pollution, and land use practices. Biological causes account for the greatest indigenous change in forest vegetation. Infestation from disease or insects is a recurring problem that is pervasive in the landscape. The initial effects of an epidemic outbreak typically result in morphological change and physiological stress which will kill individual trees and spread throughout the population. The more subtle and prolonged effects of disturbance on ecosystem energetics and evolutionary development are not clearly understood. Effective management planning depends on the ability to locate infestation areas, and determine the type and severity of infestation that is present. Therefore, regular monitoring is necessary to inventory forest conditions and update the changes that have occurred.

Ground and aerial cruising methods have limited application in locating new outbreaks and determining the geographic extent of infestation that is present. Low-level aerial photography has proven reliable in damage evaluations (Ashley, Rea and Wright, 1976). However, the expense of covering

large regions at frequent intervals is costly, and the manual effort for interpretation would be laborious.

Satellite systems offer the potential for the efficient collection of ground cover data (Dodge and Bryant, 1976). Information may be compiled over a broad region and spatially related to a geographic mapping base. Frequent monitoring is possible with the regular orbital intervals of the land resources satellites. Remote sensing information can also be readily analyzed by automated data processing techniques. Thus, the effort of conducting forest surveys may be significantly reduced, and the cartographic content of the information may be greatly enhanced.

However, various operational difficulties do exist, and the utility of satellite-computer survey methods is conditional to the kind of problem under study. The capability of the system for detecting vegetation stress depends on (a) the resolution of data gathering equipment, (b) the refinement of data analysis methods, (c) the ecological characteristics of regional vegetation, and (d) the physical disturbance that is evident from stress conditions. If the system is capable of providing suitable information for management decisions, and it is feasible, then an operational program may be implemented.

A recent study has indicated that photo-interpretation of LANDSAT Multi-Spectral Scanner (MSS) data is capable of distinguishing between healthy vegetation and disturbed vegetation from insect infestation (Moore and Rohde, 1975). Differences in tonal characteristics were evident on film transparencies, and two levels of defoliation (moderate and heavy) were identified. The study suggested that the analysis of computer-compatible tapes would increase the resolution of the data, and might

permit the identification of areas with light defoliation. Computer processing would provide an easy method of quantifying spatial information as well.

Other studies have compared standard photo-interpretation and computer-assisted techniques to classify forest and rangelands, and to detect vegetation stress (Heller, 1975). Success in classifying cover types was possible by both methods, but the results in detecting stress were not satisfactory. A conclusion of the study was that the usefulness of LANDSAT remote sensing data appeared to be limited in its application to management planning. The information could not be directly applied to the preparation of unit management plans or impact statements, although it did give a regional perspective to natural resource conditions.

The purpose of this study is to determine LANDSAT capabilities in a survey of eastern spruce budworm (Choristoneura funiferana Clem) infestation in stands of Balsam Fir (Abies balsamea) and White Spruce (Picea glauca) in northern Wisconsin. The study is a preliminary investigation into the potential use of LANDSAT and computer-assisted techniques in forest infestation surveys. A more comprehensive study using a greater range of analysis methods would be warranted if initial results appear favorable. The present study is concerned with the application of basic techniques to a small test area. The primary objectives of the study are to utilize LANDSAT data (a) to identify and map areas of infestation, and (b) to determine the severity of infestation that is present.

STUDY AREA DESCRIPTION AND INFESTATION CHARACTERISTICS

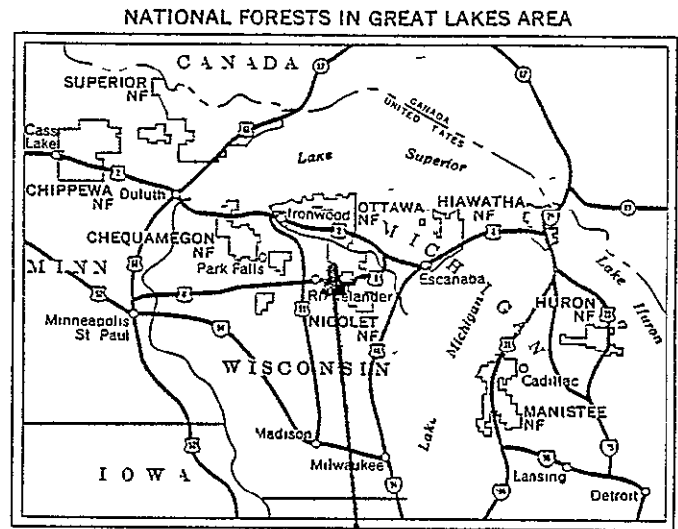
The study area is located 15 miles east of Rhineland, Wisconsin, in Oneida and Forest counties (Figure 2). It includes approximately 130 square miles of land, most of which is part of the Nicolet National Forest or owned by the Consolidated Paper Company of Wisconsin Rapids. As a result of glaciation, the regional physiography is characterized by rolling landscape with many small lakes and wetlands interspersed with drumlin formations. The drumlins are typically aligned in a NE-SW direction with a change in elevation of less than 200 feet above lowland areas. Upland vegetation is mostly hardwoods consisting of maple, yellow birch, basswood, elm, white ash, paper birch, and aspen. Jack pine, red pine, white pine, and hemlock are also found. Lowland vegetation is predominantly coniferous species such as white cedar, tamarack, black spruce, white spruce and balsam fir. Tagalder and black ash are also present.

Spruce budworm infestation occurs in stands of balsam fir and white spruce which grow locally at the edge of lowland sites intermediate to upland areas. Consequently, the pattern of fir-spruce stands is generally restricted in shape and size. Larger stands occasionally occur in flat areas where ground water is maintained at a suitable level.

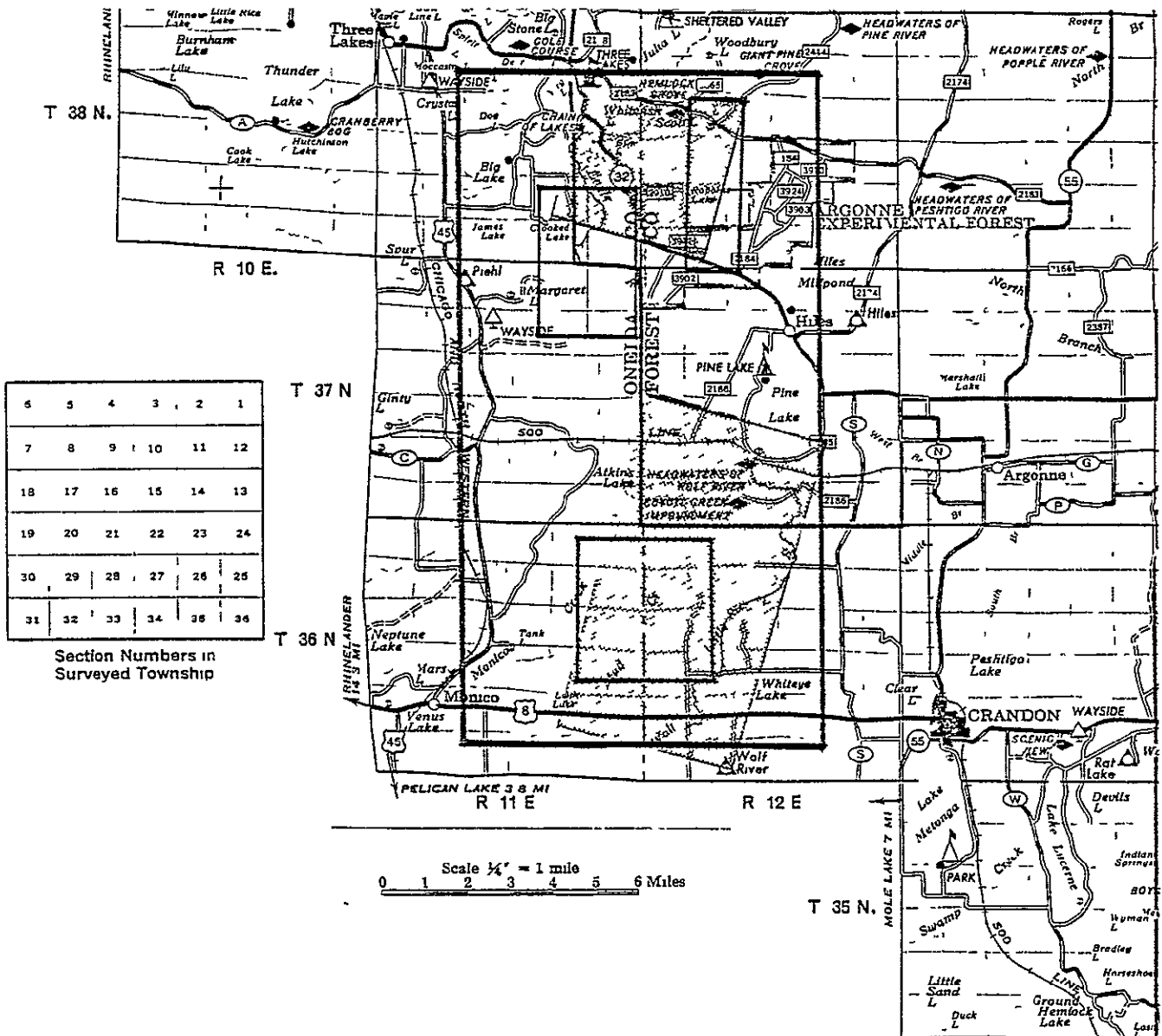
Spruce budworm has had a long and complex history in Canada and the United States. It has persisted in the northern and western conifer forests despite extensive control programs. The presence of epidemic spruce budworm in the western Great Lakes region is fairly recent, with the present outbreak in Wisconsin dating to the late 1960's. The outbreak and spread of an infestation has a periodic frequency that is related to the conditions which affect the life cycle of the insect. Life cycle development is

FIGURE 2. Site Location Map.

Aerial imagery at a scale of 1:78,900 was flown for the large area outlined below. Coverage was also obtained for the three smaller areas at a scale of 1:46,800. The small shaded area is the training area used for computer classification (Figures 3 & 6). The final training sets from the training area were used to classify the area indicated by the large shaded area (Figure 7).



STUDY SITE



influenced by (a) the condition of the host vegetation, (b) seasonal weather, (c) predators and parasites, (d) fire, and (e) forest management practices.

The characteristics used to determine the severity of defoliation by ground survey are based on distinct visible features. The categories for a four-level classification are

0-20% foliage loss	-	Light Defoliation	
20-40%	"	" - Moderate	"
40-60%	"	" - Heavy	"
60%+	"	" - Severe	"

Light defoliation occurs during the initial outbreak of an infestation, and it is characterized by a slight change in the color of the foliage from green to a dull green-grey cast. Moderate defoliation represents the condition where browning during mid-summer is significant, and the dull foliage cast after the dead needles drop is more perceptible. Heavy defoliation is characterized by a pronounced change in foliage cast with complete foliage loss in the top five feet of the crown. Heavy defoliation generally occurs in the second or third year after repeated infestation. Severe defoliation is where overall foliage loss exposes much of the branching underneath. This condition will result in mortality the following year. The severity of defoliation will vary with the number of insect larvae present, the degree of activity, and the number of repeated occurrences. The differences that are apparent on the ground between different classification levels may be discretely identified by visual observation.

DATA COLLECTION AND ANALYSIS METHODS

Aerial photographic coverage of the study site was completed on 12 July 1976 when peak browning of the foliage of fir and spruce was visible due to feeding by spruce budworm larvae. Dual Hasselblad cameras were used with 70mm color (Kodak 2448) and color-infrared (Kodak 2443) film to provide a record of ground conditions. The entire study area was flown at an altitude of 10,000 feet (1:78,900) in four north-south flight lines (Figure 2). Three priority areas were also flown at an altitude of 5,000 feet (1:46,800). All imagery was catalogued, and individual frames were keyed to a USGS topographic map for easy reference.

The color-infrared (CIR) imagery was used for photo-interpretation. The wide variation in spectral response evident on the imagery allowed different cover types to be determined (Table 1). Tone, texture, and spatial characteristics were used to distinguish one type from another. Identification of most cover types was confirmed by ground check.

Vegetation patterns were delineated from the aerial imagery on a base map at a scale of 1:24,000. A Bausch & Lomb zoom transfer scope was used for the interpretation and mapping of general forest conditions. Three conditions were identified including healthy vegetation (red CIR response), vegetation under stress (green CIR response), and vegetation experiencing partial stress (green-red CIR response). The intermediate category predominantly consisted of areas of a heterogeneous composition such as mixed species types or vegetation that contained small patches of infested areas mixed with healthy vegetation. Identification of specific cover types was not made on the base map until after the general forest conditions had been delineated, and a ground check could be made.

TABLE 1. Visual Characteristics of Ground Resources
on Color-Infrared Aerial Imagery from 12 July 1976.

GROUND FEATURES	TONE/TEXTURE CHARACTERISTICS	COMMENTS
Non-Forest Resources: Roadways Cultivated Land Exposed Land (Clearcut) Open Field Water Macrophyte Vegetation Marsh Lowland Herbs & Shrubs	white/smooth white-pink-blue / fine very light pink / fine light pink-blue / fine black / smooth purple / fine, broken blue-white / medium pink / fine-medium	regular pattern; streaked irregular boundaries, variable uniformity may vary tone varies with turbidity forms island patches in water tone varies with moisture species coarser texture with trees
Deciduous Forest: Aspen Maple-Basswood-Birch Yellow Birch Black Ash	pink-light red / fine red / medium dark red / coarse red / medium	small areas at forest periphery broken texture mixed with maple; mottled uniform texture
Coniferous Forest: Hemlock Jack-Red-White Pine Balsam Fir-White Spruce White Cedar Tamarack	dark blue-green / medium very dark red / coarse dark green-blue / medium blue / medium-coarse brown / medium	mixed with diciduous species mottled generally uniform, small stands near water near water

A preliminary ground check was made in October 1976 to become familiar with the study area and the general conditions that were present. A more complete check was made in June 1977 by ground and low-level aerial reconnaissance to identify specific conditions on the photo-interpreted base map. Both ground and aerial perspectives were necessary to obtain a thorough knowledge of cover conditions. The base map was used to identify training areas for computer classification, and to prepare a cover type map overlay at the scale of the computer printout maps.

The computer classifications were evaluated by comparing the results of the printout maps with the Forest Cover Type Map (Figure 5). The zoom transfer scope was used to rescale the vegetation patterns from the base map to a computer printout map. Identification of the cover types was made primarily by ground survey. Existing cover type maps from 1948 and 1964 were also consulted for much of the training area. Many areas on the Forest Cover Type Map were designated according to the U S Forest Service classification. These were areas that could be readily identified, and were important locations for the training sets. The areas that were not designated by a cover type class either were not adequately ground checked or were heterogenous in composition. More refined delineation of cover types was prohibited by the poor lighting of the imagery from the zoom transfer scope, and by the large scale of the computer printout maps. Better photo-interpretation would result with the use of other optical equipment.

Selection of the LANDSAT scene was made by examining the film transparencies on the dates that closely coincided with the date of the aerial imagery and determining cloud-free coverage. This was done by using MSS Band 5 and 7 which clearly distinguish areas of cloud cover. Scenes from

2 July, 11 July, 20 July and 29 July were examined. A computer-compatible tape containing the digital spectral data was obtained from an overpass on 11 July 1976 for LANDSAT Scene 2536-15561. Cloud cover obscured about 50% of the entire scene, but the study area was mostly cloud-free.

The necessity of ordering film products from the EROS Data Center to determine suitable coverage caused additional delay in analysis. Approximately 5 months time was necessary to receive the digital tapes after the satellite overpass. The time delay could be reduced by a month if it were known beforehand that the scene was cloud-free. Changes at the EROS Data Center in cataloging, processing, and accessing LANDSAT information could significantly reduce turnaround time in the future.

The LANDSAT data is collected from a multi-spectral scanner (MSS) which detects electromagnetic energy in four separate wavelength bands reflected from the earth's surface. Band 4 is sensitive to energy between the wavelengths 0.5-0.6 microns (green light), Band 5 between 0.6-0.7 microns (red light), Band 6 between 0.7-0.8 microns (infrared light), and Band 7 between 0.8-1.1 microns (infrared light). The energy is recorded as brightness values on each of the four bands. Brightness values range between 0-127 on Bands 4, 5 and 6, and between 0-63 on Band 7. Ground resources reflect a certain amount of energy depending on their morphological and physiological characteristics. Different resources can be identified by a spectral response that is unique to each resource type.

The LANDSAT scanner collects spectral information from individual picture elements or pixels. Each pixel represents a ground area of 1.15 acres in size with the rectangular dimensions of 185 feet horizontal by 260 feet vertical. An entire LANDSAT scene covers a ground area of 100 x 100 nautical miles.

Computer analysis of the digital LANDSAT data was accomplished by use of the Remote Sensing Applications Programs (RS*AP) of the Institute for Environmental Studies at the University of Wisconsin. RS*AP is a computer program package designed for the analysis of remote sensing information (Fisher, 1976). Program development was primarily funded by the NASA Office of University Affairs as part of the ongoing water quality and remote sensing research of the Environmental Monitoring and Data Acquisition Group at the University of Wisconsin-Madison. The program library is periodically updated and expanded to provide greater capabilities in analysis methods

Two principal programs were used in this study to classify spectral information from the LANDSAT scene and produce printout maps of the results. Each program operates in a different manner, and offers a different approach towards the method of analysis.

BOXCLS is a box classification program that classifies individual pixels by determining whether they are contained within certain class boundaries. A class boundary is established by the upper and lower limits of brightness values in each of the four bands. The boundary limits can be either manually entered into the program, or they can be automatically calculated from statistical information filed by programs TRAIN and STATS. The boundary limits for manual operation are determined by using programs TRAIN and HSGRAM or SCATTER which give the brightness value distributions. The upper and lower boundary limits may then be selected to represent the spectral characteristics of a particular resource

MAXLIK is a maximum likelihood classification program that uses Bayesian theory to statistically determine the class in which a pixel belongs. Unlike BOXCLS, MAXLIK does not require boundary limits set by a range of brightness values. Instead, each pixel is compared to the

probability density function that describes each training set, and assigns the pixel to the class where its probability is maximal. Program STATS provides the statistical information necessary for the operation of MAXLIK. A threshold option in the program serves as a control mode, such that more stringent probability requirements are present with an increasing threshold. When the threshold value is 0, and the collection of training sets fully represents the range of possible spectral responses, each pixel will be assigned to one of the classes. A higher threshold value requires each pixel to be more similar to a particular class, and it will be unclassified if it does not qualify.

The operation of the classification programs, BOXCLS and MAXLIK, is based on information obtained from the training sets. Suitable training sets can be determined by the use of various intermediate programs including SLICE, TRAIN, HSGRAM, SCATTER and STATS. A printout of the raw LANDSAT data stored on computer tape is obtained by using program SLICE which assigns an alpha-numeric character to represent an equally divided range of brightness values for a single band. The printout map is a density slice of the spectral data containing unclassified brightness values. The brightness value map may be used to geographically locate resource areas and identify training sets. A zoom transfer scope was used to superimpose vegetation patterns from the aerial imagery over the computer printout map, and delineate the boundaries with respect to prominent natural and cultural features. The training sets were then identified on the composite map.

Program TRAIN is used to extract selected data points from the LANDSAT scene, and load them into a file. The data file may then be used with additional programs to give output information about the training sets. HSGRAM produces a histogram which plots the number of data points in the

training set with the brightness values in each band. Program SCATTER plots the brightness values of one band against the brightness values of another band. This gives the spatial area in the matrix that is occupied by the spectral response of each training set. STATS gives statistical information about the training set by calculating the mean vector, covariance matrix, inverses, determinants, eigenvalues and eigenvectors. This information is filed in a statistics file to be used with MAXLIK or the automatic mode of BOXCLS. These programs provide the basic analysis techniques of RS*AP.

RESULTS AND DISCUSSION

Much of the success of the classifier programs is determined by the reliability of the training sets. Good training sets are those which best represent ground resources. Training set performance is affected by the conditions on the ground and by the resolution of the satellite sensors. Some observations on the selection and suitability of the training sets should be discussed before evaluating the classification results.

The collection of training sets should include the complete range of resource cover types so as to distinguish each resource by a known spectral response. Cover types should be a homogenous unit that can be distinctly identified. Cover type areas greater than 80 acres in size are preferable to accommodate a training set of 35-40 pixels which is large enough for a valid statistical sample. A buffer area between the training set and the boundary of the resource is necessary, because the satellite scanner does not clearly distinguish between the borders of different resource types. A minimum of 20 acres may be sufficient when the location and boundaries of the resource area can be pinpointed on the computer printout map, and when the resource type is significantly different from surrounding areas. Non-vegetated ground resources such as lakes and exposed lands are more easily identified under restrictive conditions than vegetated resources. However, this will also result in a small statistical sample which will affect the use of the classifier programs.

Ground conditions in the study area made selection of suitable training sets somewhat difficult. The landscape mosaic is comprised of vegetation patterns that are relatively small in size due to ecological and historical conditions. Consequently, the training sets contain only 9-21 pixels each.

The presence of lakes as distinct ground features enabled the resource types to be accurately delineated on the computer printout map, and the training sets could be well located. Thus, the content of the training sets is representative of the resource types, although the sample size is small.

A final selection of 12 training sets (Figure 3) was made from a total of nearly thirty. Each training set was identified by a sequential number according to the following decimal system:

10-19	Natural Landscape Features
20-29	Cultural Landscape Features
30-39	Non-Forest Vegetation
40-49	Upland Deciduous Forest
50-59	Lowland Deciduous Forest
60-69	Upland Coniferous Forest
70-79	Lowland Coniferous Forest
80-89	Special Vegetation Conditions
90-99	Non-Resource Features

The final training sets were used to identify nine resource classes including 2 levels of coniferous infestation. Greater attention was given to the identification of infestation areas than to other resource types. This was because of the emphasis of the study and the greater difficulty in distinguishing between these cover conditions.

Several training sets representing coniferous infestation were evaluated. Most of the training sets selected by ground survey to represent different defoliation conditions gave spectral responses that were very similar. The variation in brightness values that was present was mostly attributed to differences other than vegetative conditions such as the appearance of background features. A clear distinction between different levels of defoliation was not readily apparent. Adequate training sets for this approach could not be obtained because the ground areas were too small or they lacked homogenous cover type conditions as viewed by the satellite-sensor.

FIGURE 3. Brightness Value Map - Band 7, and Final Training Set Locations.

The output from program SLICE shows the brightness values in a single spectral band for a defined area, and represents the raw LANDSAT MSS data. Refer to Figures 5 & 6 for geographic orientation.

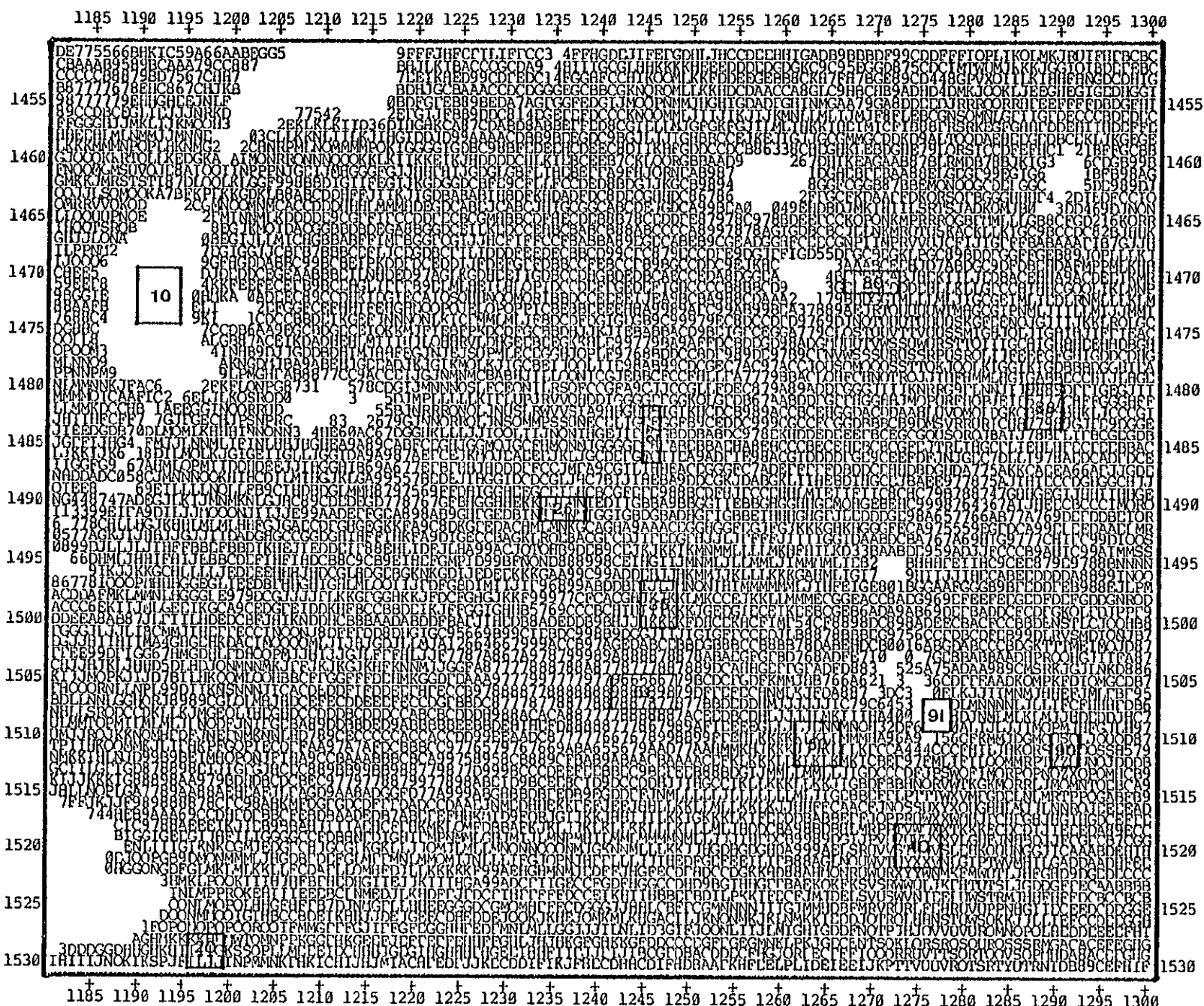
VALUES BELOW 10 ARE BLANK

10	11	12	13	14	15	16	17	18	19	20	21	22	23	24
TO	TO	TO	TO	TO	TO	TO	TO	TO	TO	TO	TO	TO	TO	TO
000	111	222	333	444	555	666	777	888	999	AAA	BBB	CCC	DDD	EEE
000	111	222	333	444	555	666	777	888	999	AAA	BBB	CCC	DDD	EEE
000	111	222	333	444	555	666	777	888	999	AAA	BBB	CCC	DDD	EEE
25	26	27	28	29	30	31	32	33	34	35	36	37	38	39
TO	TO	TO	TO	TO	TO	TO	TO	TO	TO	TO	TO	TO	TO	TO
FFF	GGG	HHH	III	JJJ	KKK	LLL	MMM	NNN	OOO	PPP	QQQ	RRR	SSS	TTT
FFF	GGG	HHH	III	JJJ	KKK	LLL	MMM	NNN	OOO	PPP	QQQ	RRR	SSS	TTT
FFF	GGG	HHH	III	JJJ	KKK	LLL	MMM	NNN	OOO	PPP	QQQ	RRR	SSS	TTT
40	41	42	43	44	45									
TO	TO	TO	TO	TO	AND									
000	VVV	WWW	XXX	YYY	ZZZ									
000	VVV	WWW	XXX	YYY	ZZZ									
000	VVV	WWW	XXX	YYY	ZZZ									

Training Set			
Identification Number		Resource Class	
10	(1)	Water	
20	(2)	Cultivated Land	
25	(2)	Exposed Land	
27		Exposed Land	
35	(3)	Lowland Herbs & Shrubs	
50	(4)	Lowland Deciduous	
40	(5)	Upland Deciduous	
61	(6)	Upland Coniferous	
80	(7)	Mixed Dec-Con - Mod.Inf.	
88	(8)	Lowland Conif - Ext.Inf.	
90	(9)	Cloud	
91		Cloud Shadow	

ROWS---1451 TO 1530 COLUMNS---1181 TO 1300
EVERY ROW AND COLUMN IS SHOWN
SLICED ON BAND 7

BRIGHTNESS VALUE MAP



ORIGINAL PAGE IS
OF POOR QUALITY

The procedure of directly correlating a known level of defoliation for a specific ground site with a distinctly identifiable training set could not be thoroughly tested. Therefore, it was necessary to modify this approach somewhat by selecting those training sets that have distinguishable spectral differences to represent appropriate class levels.

Different levels of infestation were detected from the LANDSAT MSS data by the modified method, and the results of the classification maps were generally good. A classification system which differs from the system used by ground survey was chosen to distinguish between the interpretations that are made by ground and remote sensing sources. Extensive and moderate levels of infestation were used in the study as general classification categories.

Selection of the final training set for Class (8) - Extensive Infestation was based on the results from the classification printouts in the training area. Training set #88 gave the best overall results, although it had not been initially regarded as a primary candidate because of its location. The site was satisfactorily identified on the imagery and checked by aerial reconnaissance, but it was inaccessible to ground visitation. The training set contains a better sample content than any of the others representing spruce budworm infestation of fir-spruce stands.

It was more difficult to identify suitable training sets for resource classes with infestation conditions that were less extensive. This was primarily due to the inability to distinguish spectral differences between many of the training sets representing coniferous infestation. Training set #80 was selected to represent Class (7) - Moderate Infestation from a site that is less homogenous in composition than those of Class (8) training

sets, but one that was ground checked and best qualified as an intermediate level class. Class (7) represents a broader range of brightness values between Class (8) and the other vegetation classes (Table 3). No suitable training set could be identified for a third class that would represent light infestation.

Training set performance was based on the results from the intermediate program analysis and from a comparison of preliminary computer classifications with the cover type map overlay. Reference to the color-infrared aerial photos was made in conjunction with the classification comparison to check the results of specific conditions

An evaluation of the training sets was also made for the MAXLIK classification by using program CLSTRN. CLSTRN classifies the pixels within each training set by the maximum likelihood algorithm, and produces a table which shows the number and percentage of pixels that were identified in each class (Table 2). From a training set sample of 21 pixels for Class (6) - Upland Coniferous, 19 pixels were classified as Class (6) and 2 pixels or 9.5% were classified as Class (8) - Extensive Infestation. Other classification disagreements occurred between (4) and (3), (7) and (8), and (8) and (6). Eight of the twelve training sets showed that 100% of the sample were in classification agreement, and the remaining four training sets showed better than 90% agreement. Non-forest resource classes showed better results in the CLSTRN analysis than forest classes. CLSTRN gives an indication of the quality of the training sets for MAXLIK classification, and the possibility of where misidentification may occur. The results do not show how correct or incorrect the classification was, and the results are not a statistically valid indication of the amount of misidentification when applied to a larger classification area

The brightness value range of the final training sets shows the spectral separation that occurs between different resource classes (Table 3). A distinction between the values obtained strictly from the training sets and the values obtained from within the boundary of the resource area may be noted. Class (3) through Class (8) utilize Bands 6 and 7 more fully than Bands 4 and 5. Overlap of the brightness value range is apparent, particularly with Classes (6), (7) and (8). The separation of brightness values into mutually exclusive classes was not possible from representative training sets. This can be done manually by assigning some arbitrary cut-off level between classes.

The procedure of manually assigning brightness value boundaries to resource classes in a supervised classification was done for the BOXCLS program. The initial results of the classification were not very encouraging. The printout maps appeared with only about 50% of the pixels classified. This meant that the values of the pixels which remained unclassified did not lie within any of the designated class boundaries.

The requirement for classification by BOXCLS is such that a pixel is either included within a class boundary or it is excluded. Expanding the range of the brightness value boundaries to include more pixels would result in greater misidentification due to overlap. When there is an overlap between different class boundaries, certain resource classes are favored over others in the classification process. When the values of a particular pixel are within the brightness value range of more than one class, the program will classify that pixel as a member of the class that is ordered first in the routine.

The class boundaries established by the brightness value range occupy a certain spatial area in a matrix formed by the spectral bands (Figure 4).

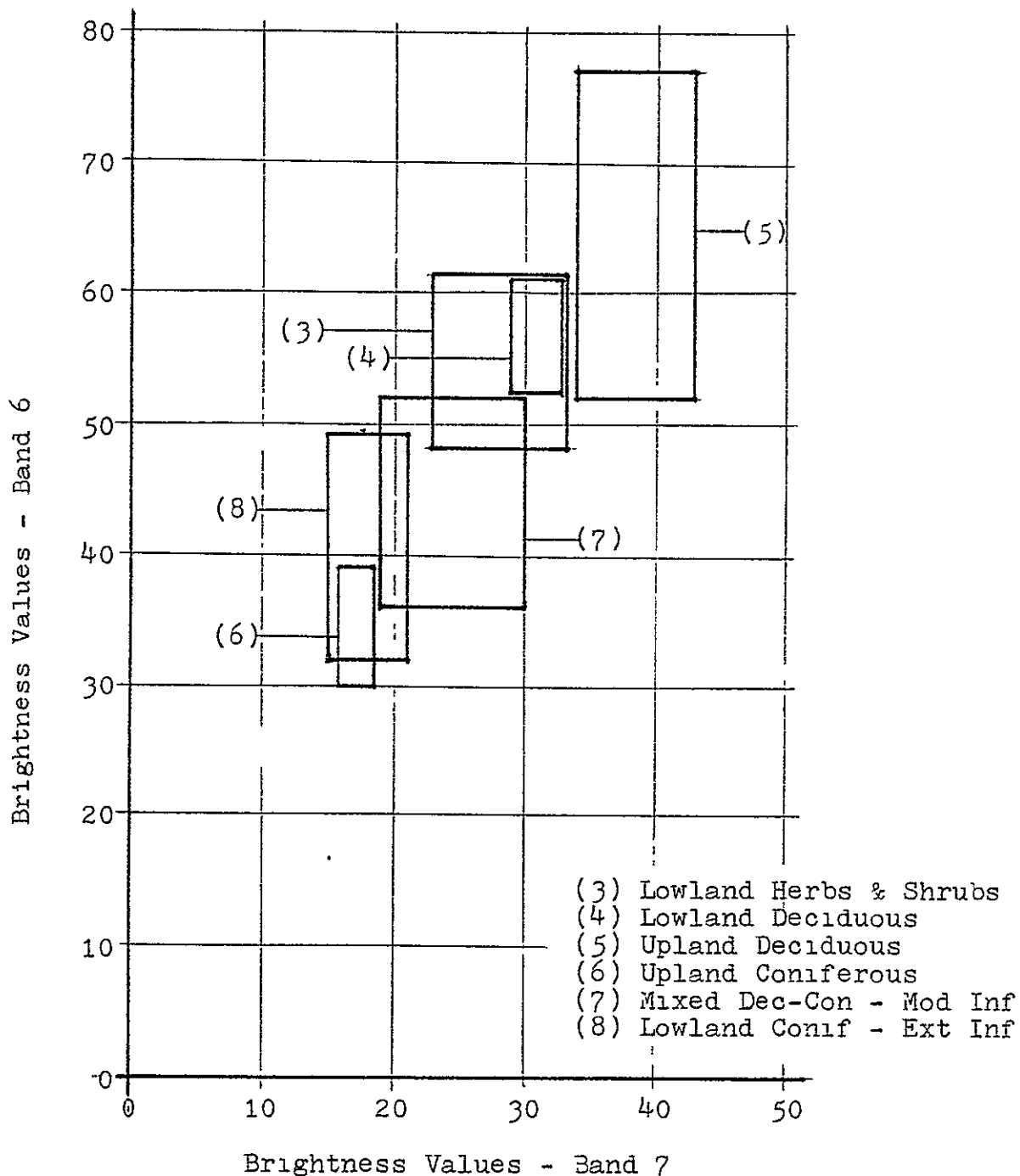
TABLE 3. Brightness Value Range.

The range of brightness values for the training set of each class is given in all four spectral bands. The values in parenthesis () represent the brightness value range determined by examining the area of each class irrespective of the training set.

		Band 4	Band 5	Band 6	Band 7
10	(1) Water	-12 (-16)	-09 (-14)	-09 (-28)	-09 (-11)
20	(2) Cultivated Land	26-28 (15-28)	33-41 (26-41)	48-65 (50-67)	25-30 (25-30)
25 27	(2) Exposed Land	17-18 18-21 (15-21)	15-19 19-24 (13-25)	54-61 48-55 (44-73)	28-33 24-27 (20-35)
35	(3) Lowland Herbs & Shrubs	13-16 (15-17)	12-14 (12-15)	52-59 (48-61)	28-31 (23-33)
50	(4) Lowland Deciduous	12-16 (13-14)	11-12 (10-12)	52-57 (52-61)	29-33 (29-33)
40	(5) Upland Deciduous	13-16 (12-17)	11-13 (11-13)	58-77 (52-77)	38-44 (34-43)
61	(6) Upland Coniferous	12-15 (12-15)	10-13 (10-13)	30-37 (30-39)	16-19 (16-19)
80	(7) Mixed Dec-Con - Mod.Inf.	12-15 (12-16)	11-12 (11-13)	38-53 (36-52)	20-26 (19-30)
88	(8) Lowland Conif - Ext.Inf.	12-15 (12-17)	11-13 (11-14)	32-43 (32-49)	15-21 (15-21)
90	(9) Cloud	31- (18-)	31- (18-)	66- (56-)	34- (29-)
91	Cloud Shadow	-11 (-13)	-09 (-11)	10-19 (10-23)	-09 (-18)

FIGURE 4. Box Classification.

The range of brightness values defines the class boundaries that can be used for classification by program BOXCLS. The brightness values from 2 of the 4 spectral bands (Table 2) were used to delineate the spatial areas illustrated in the matrix below. Boundary overlap occurs between many of the classes. Figure 4 may be compared with Table 3 to denote possible misidentification.



ORIGINAL PAGE IS
OF POOR QUALITY

The areas are dimensioned by the upper and lower limits for each of the four LANDSAT bands. Each class is distinguished by its position in the matrix, and by the size of its area of occupancy. The extent of class independence can be seen from the illustration showing the areas defined by only two of the spectral bands. Classes (1), (2) and (9) are distinct from the other classes in Bands 4 and 5, and are not shown. Reference to Table 3 should be made so that the values in all four bands are consulted.

Recognizing the problem created by the overlap of brightness values, the attempt to better define suitable class boundaries for the BOXCLS classifier program was not pursued further. Improved results would be expected with greater refinement. This kind of problem, however, is better handled by the unsupervised maximum likelihood classifier because it is not necessary to have mutually exclusive classes.

The classification printout maps from MAXLIK gave results that were mostly favorable. The location and spatial coverage of every resource class was fairly accurate when the computer classification map (Figure 6) was compared with the cover type map overlay (Figure 5) in the training area. A check with the color infrared imagery gave further support to the results.

It was easier to assess the results of some classes than of others, because their cover type boundaries were better defined. These included: Class (1) - Water, Class (6) - Upland Coniferous, Class (5) - Upland Deciduous, and Class (8) - Lowland Coniferous - Extensive Infestation. All of these classes showed good results. Class (2) - Cultivated and Exposed Land was well classified in upland areas, but it became mixed with Class (3) - Lowland Herbs and Shrubs and Class (4) - Lowland Deciduous. The non-forest lowland areas were less homogenous in cover conditions which










FIGURE 5, Forest Cover Type Map.

The Forest Cover Type Map overlay was delineated by generalized photo-interpretation of the 1:78,900 color infrared aerial imagery. Selected areas have been designated according to the forest type classification of the U.S. Forest Service outlined below. An asterisk (*) indicates which cover types were identified. Prominent geographic features and section lines are also identified on the map overlay. The scale of the original computer printout map is 1:27,500 which has been reduced to 1:38,800 for documentation.

- | | |
|------------------------------|---------------------------|
| *A - Aspen | N - Pin Oak |
| B - Paper Birch | *O - Open |
| C - E. Red or N. White Cedar | P - Southern Pine |
| D - Black Cherry | *Q - Mixed Swamp Conifers |
| *E - Swamp Hardwoods | *R - Red Pine |
| *F - Spruce-Fir | *S - Black or Red Spruce |
| G - White Spruce | *T - Tamarack |
| H - Hemlock | U - Upland Brush |
| I - Local Use | V - Cove Hardwoods |
| *J - Jack Pine | W - White Pine |
| K - Oak-Hickory | X - Post or Blackjack Oak |
| *L - Lowland Brush | Y - Oak-Pine |
| *M - Maple-Basswood-Birch | Z - Local Use |

FIGURE 6. Vegetation Classification Map.

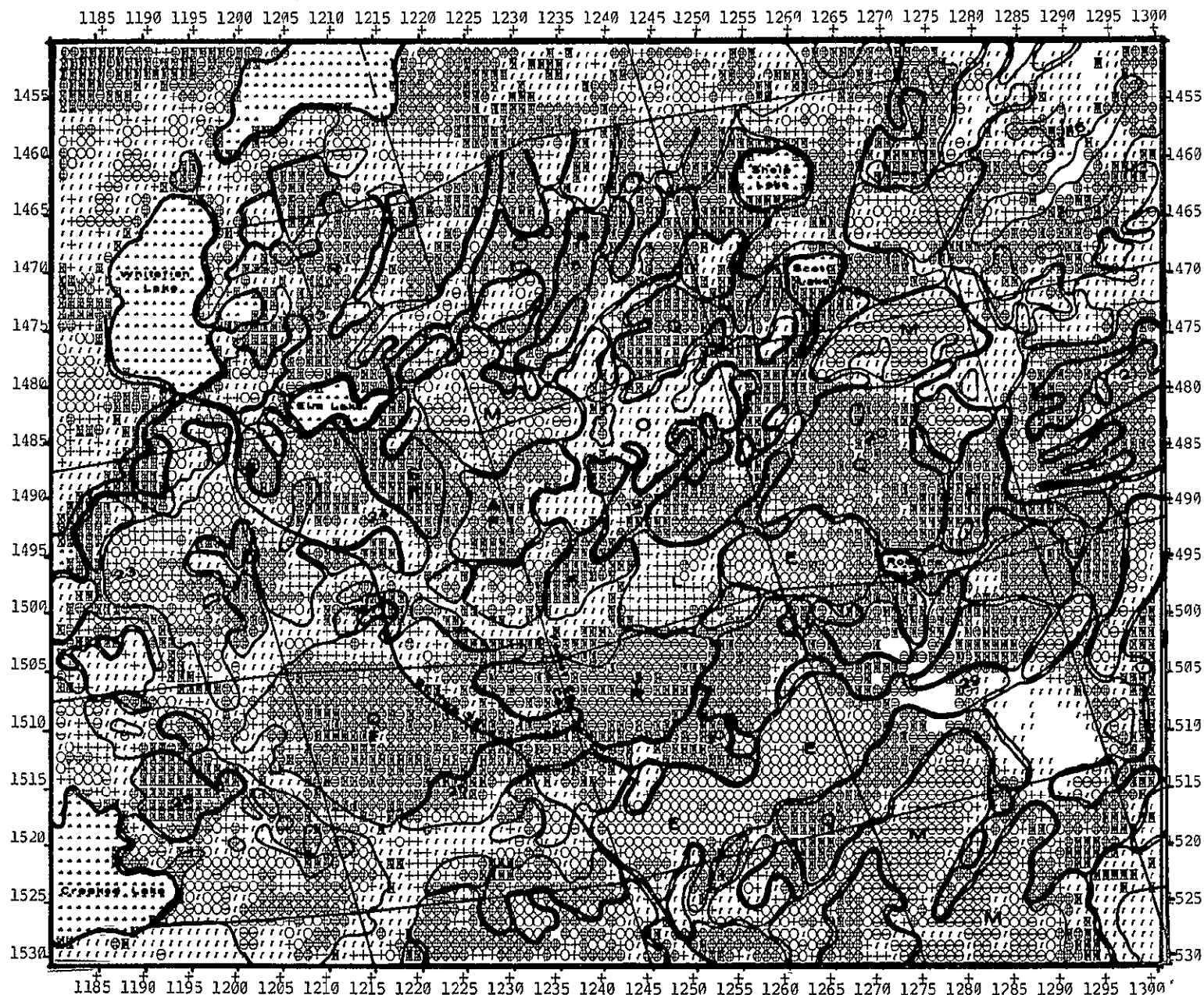
Computer classification of the LANDSAT MSS data was performed by program MAXLIK. The results of the classification in the training area shown below may be compared with the Forest Cover Type Map overlay. The scale of the original computer printout map is 1:27,500 which has been reduced to 1:38,800.

- | | |
|---|--|
|  | (1) Water |
|  | (2) Cultivated Land
Exposed Land |
|  | (3) Lowland Herbs & Shrubs |
|  | (4) Lowland Deciduous |
|  | (5) Upland Deciduous |
|  | (6) Upland Coniferous |
|  | (7) Mixed Deciduous-Coniferous -
Moderate Infestation |
|  | (8) Lowland Coniferous -
Extensive Infestation |
|  | (9) Cloud
Cloud Shadow |

LANDSAT SCENE 2536-15561 FILE 2 OF 4 11JUL76
 ROWS--1451 TO 1530 COLUMNS--1181 TO 1300
 EVERY ROW AND COLUMN IS SHOWN
 CLASSIFIED BY MAXLIK ROUTINE.
 BANDS USED -- 4 5 6 7

SPRUCE BUDWORM DEFOLIATION

FOREST COVER TYPE MAP VEGETATION CLASSIFICATION MAP



PRECEDING PAGE BLANK NOT FILMED

ORIGINAL PAGE IS
 OF POOR QUALITY

accounted for much of the class mixing. Class (9) - Cloud and Cloud Shadow indicates where spectral interference with ground resources is occurring. The results of its location were good, although there is no way to clearly determine the extent of its coverage.



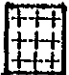


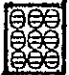



Class (7) - Mixed Deciduous/Coniferous - Moderate Infestation represents an intermediate class, such that its cover type boundaries were not always clearly defined. Its distribution from computer classification was consistent with that of the color infrared photos. The class is mostly associated with the Mixed Swamp Conifer cover type (Sections 20, 29, 25) on the Forest Cover Type Map (Figure 5). It also represents other heterogeneous areas that do not qualify as Class (8). The results of Class (7) in the test area were also good (Figure 7). A large area (Coord. 1640, 1345) comprised of mixed cover conditions which is located south of Pine Lake was properly classified as Class (7). Its distribution in outlying areas (Coord. 1630, 1310, and 1675, 1330, and 1725, 1335) showed that the class was also able to identify intermediate conditions on small sites.

Class (8) - Lowland Coniferous - Extensive Infestation did quite well overall in the classification results, but there were classification errors. The class represents the areas on the color-infrared imagery with a solid, dark green-blue appearance which is characteristic of coniferous defoliation. The location and spatial coverage of the areas can be easily determined. Both of these performance measures helped to evaluate the classification results.

The spatial coverage of Class (8) on the computer printout map (Figure 6) coincides nicely with the infestation areas identified on the cover type map and the aerial imagery. The larger, homogeneous stands (Coord. 1490, 1280,

FIGURE 7. Vegetation Classification Map.

The final training sets from the training area were used to classify a different area of the LANDSAT scene shown below (see Figure 2). The scale of the original computer printout map is 1:27,500 which has been reduced to 1:38,800.

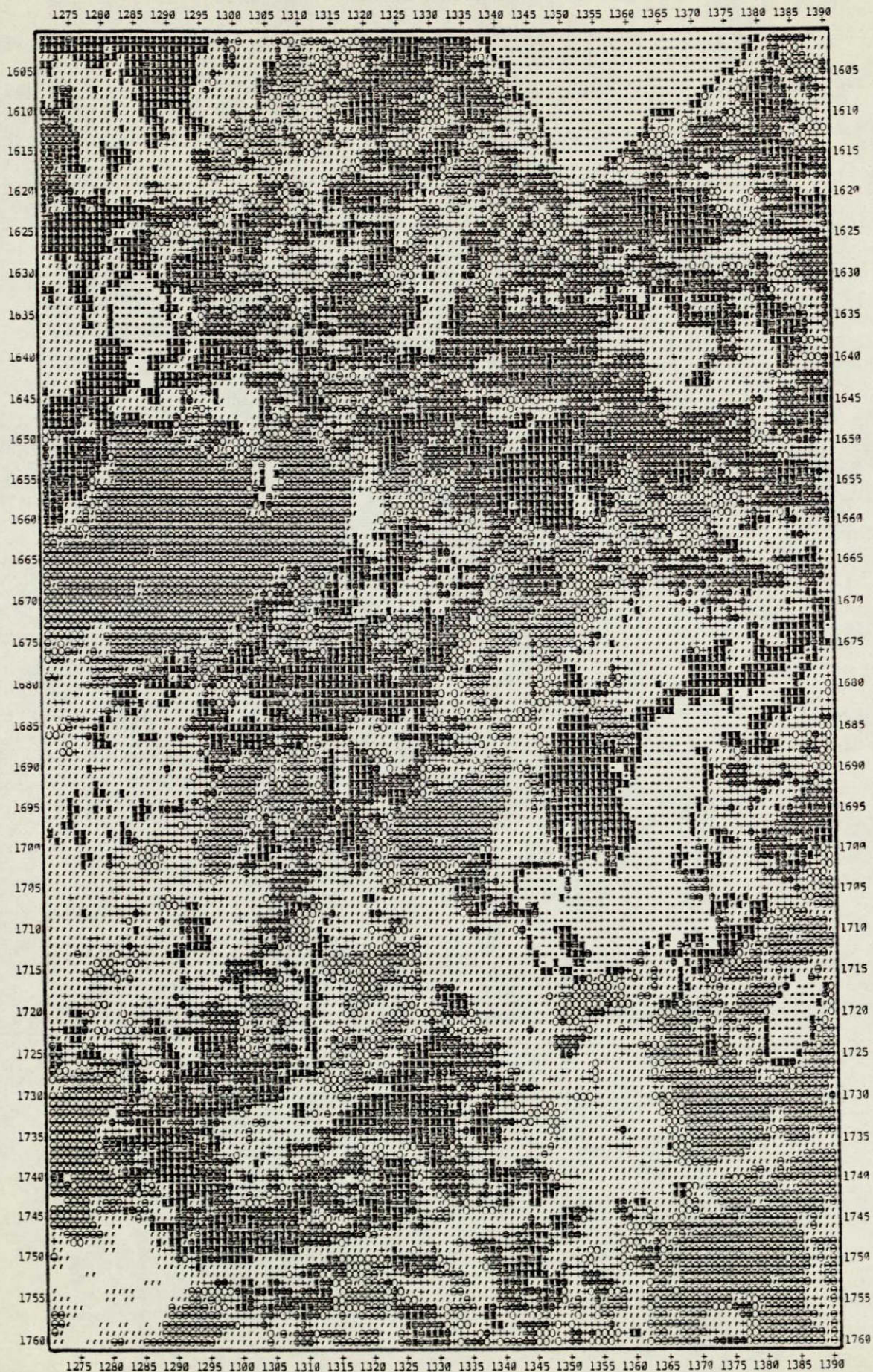
- | | |
|---|--|
|  | (1) Water |
|  | (2) Cultivated Land
Exposed Land |
|  | (3) Lowland Herbs & Shrubs |
|  | (4) Lowland Deciduous |
|  | (5) Upland Deciduous |
|  | (6) Upland Coniferous |
|  | (7) Mixed Deciduous-Coniferous -
Moderate Infestation |
|  | (8) Lowland Coniferous -
Extensive Infestation |
|  | (9) Cloud
Cloud Shadow |

LANDSAT SCENE 2536-15561 FILE 2 OF 4 11JUL76
ROWS--1601 TO 1760 COLUMNS--1271 TO 1390
EVERY ROW AND COLUMN IS SHOWN
CLASSIFIED BY MAXLIK ROUTINE.
BANDS USED -- 4 5 6 7

SPRUCE BUDWORM DEFOLIATION

ORIGINAL PAGE IS
OF POOR QUALITY

VEGETATION CLASSIFICATION MAP



and 1500, 1240; and 1520, 1265; and 1490, 1215; and 1515, 1195) compare well with the Forest Cover Type Map (Figure 5). The areas delineated on the cover type map, however, do not adequately show the numerous, small patches of coniferous infestation that are present. The computer classification did well in locating these areas (Coord. 1515, 1215; and 1515, 1230) when they were checked with the aerial imagery. The results indicate that the classification did not over-classify ground coverage by extending beyond the cover type boundaries, nor did it under-classify by failing to locate the smaller, outlying areas.

Although the MAXLIK classification program performed well in locating and spatially defining areas of infestation, there was some misclassification. Class (8) was unable to distinguish between different species types that were exhibiting defoliation properties similar to the stands of balsam fir and white spruce.

Tamarack was experiencing a sawfly infestation that was causing a browning of foliage and loss of needles (Coord. 1500, 1273). White cedar was displaying brown seed capsules which gave the same appearance as foliage browning (Coord. 1475, 1263). Defoliation of lowland conifer species was also caused by high water (Coord. 1503, 1228).

Herbaceous wetland vegetation with dark tonal characteristics on the color-infrared imagery was misclassified in some areas (Coord. 1488, 1190; and 1493, 1183). The large wetland (Coord. 1690, 1355) on the west side of Little Rice Lake was incorrectly identified as Class (8) (Figure 7). Other marsh vegetation with different tonal characteristics (Coord. 1675, 1360; and 1690, 1285) was classified as Class (2). A narrow band around the boundary of some lakes was misclassified as Class (8). This may be attributed

The classification results, therefore, have been restricted to a descriptive evaluation.

The results indicate both attributes and limitations of the LANDSAT system in conducting forest surveys. The suitability of the method is not only determined by its information capabilities, but also by the information requirements which are necessary for effective natural resource management. Some inventory and analysis methods can address certain resource questions better than others. Similarly, no single method can provide complete information to all questions. The evaluation of new and developing methods is too often based on the improvement that can be made over traditional methods. An incongruity will result by solely attempting to resolve the set of questions that had been dealt with previously. Instead, the set of questions may be expanded towards a more comprehensive and insightful management approach. As such, different analysis techniques are best employed as complementary methods, each capable of providing information that address particular resource questions.

CONCLUSIONS AND RECOMMENDATIONS

The study was a stringent test of LANDSAT capabilities for forest infestation surveys. As previously discussed, four principal factors influence the capability of the system for detecting vegetation stress. Various aspects of these factors were evident in the outcome of the results. First, regional landscape conditions restricted the selection and suitability of the training sets for computer classification. Second, data from only one LANDSAT scene was examined which showed the physical disturbance due to infestation during a single period of seasonal change. Third, data analysis was restricted to the application of basic classification programs to identify ground resources. Nevertheless, the results of the study were encouraging.

The following conclusions may be inferred from the results of the digital analysis of LANDSAT data

1. Areas of coniferous infestation can be identified and accurately mapped by the use of the MAXLIK classification program
2. Two levels of infestation can be distinguished by distinct spectral responses.
3. A direct correlation between the levels of infestation determined by computer analysis and the severity of defoliation determined by ground survey could not be adequately tested.
4. Different species types exhibiting defoliation properties similar to forest stands of balsam fir and white spruce could not be distinguished by computer classification.

Further analysis became apparent from the results of the study to resolve some of the problems that were encountered, and to improve the

application potential of satellite-computer methods to natural resource management. The following recommendations are suggested

1. Locate additional training areas with cover types that
 - (a) represent a complete range of ground conditions,
 - (b) can be well located by prominent geographic features, and
 - (c) have a homogenous composition which is suitable in size to accommodate training sets.
2. Analyze LANDSAT scenes from different times of the year when ground conditions have changed to determine what additional kinds of cover type information can be obtained.
- 3 Utilize other computer programs which can offer further refinement of the LANDSAT data.
4. Establish a close cooperative effort between the investigators and resource management personnel to identify and integrate the information capabilities of the LANDSAT system in a comprehensive management framework, and to re-define the information requirements for resource management accordingly.

REFERENCES

- Aldrich, R.C. (Tech Coord.), 1976. Evaluation of Skylab data for forest and rangeland surveys. Forest Service Res. Pap. PSW-113 Pac. SW Forest and Range Exp. Sta., Berkeley.
- Aldrich, R.C., 1975. Detecting disturbances in a forest environment. Photogr. Engr. 41: 39-48.
- Ashley, M.D., J. Rea, and L. Wright, 1976. Spruce Budworm damage evaluations using aerial photography. Photogr. Engr. 42. 1265-1272.
- Beaubien, J., 1976. La photographie a'eriennne couleur infrarouge 'a petite 'echelle et l'inventaire des d'egats caus'es par la tordeuse des bourgeons de l'epinette. For. Chron. 52: 137-141.
- Dodge, A G. and E.S. Bryant, 1976. Forest type mapping with satellite data. Jour. For. 74. 526-531.
- Fisher, L.T., 1976 RS*AP: a program package for remote sensing data analysis. Inst. Env. St. Publ., Univ. of Wisconsin, Madison.
- Heath, G.R., 1974 Earth resources satellites - their potential in forestry. Jour. For. 72: 573-575.
- Heller, R.C. (Tech. Coord.), 1975. Evaluation of ERTS-1 data for forest and rangeland surveys Forest Service Res. Pap. PSW-112. Pac. SW Forest and Range Exp. Sta., Berkeley.
- Heller, R.C. and R V Bega, 1973. Detection of forest diseases by remote sensing. Jour. For. 71. 18-21.
- Moore, H.J. and W.G. Rohde, 1975. Gypsy Moth defoliation assessment forest defoliation is detectable from satellite imagery. NASA CR-146626, MF #N76-20601. NASA, Houston.
- Morris, R.F. (Ed.), 1963. The dynamics of epidemic spruce budworm populations. Mem. Ent. Soc. Canada. Rep. No. 131.
- Rohde, W.G., T. Gregg and H.J. Moore, 1975. Detection of Gypsy Moth damage with high altitude aircraft and satellite data. Proc. 4th Remote Sensing Earth Res. Conf.

ACKNOWLEDGEMENTS

Grateful appreciation is expressed to Don Renlund, Supervisor, Forest Pest Control, Al Prey, Forest Pathologist, and Stan Banash, District Forest Entomologist of the Wisconsin Department of Natural Resources; Bob Doerner, Field Representative, and Art Hastings, Entomologist of the U.S. Forest Service, Northeastern Area State and Private Forestry; and Larry Fisher, Project Coordinator, Environmental Monitoring and Data Acquisition Group, and Frank Scarpace, Assistant Professor, Institute for Environmental Studies, of the University of Wisconsin, for their personal assistance in helping to make this study possible. The cooperation of the EROS Data Center, Sioux Falls, South Dakota, and the Consolidated Paper Company of Wisconsin Rapids, Wisconsin is acknowledged. Ken Beghin, Chief Pilot, Wisconsin Department of Natural Resources, and his crew were responsible for the acquisition of the aerial photography. The development of the computer programs used in the study was made possible by research support from the NASA Office of University Affairs. Funding for the project was provided by the U.S. Forest Service.